REVERSE MICELLES IN SUPERCRITICAL CARBON DIOXIDE FOR PHARMACOLOGICAL APPLICATIONS: A SPECTROSCOPIC CHARACTERIZATION

by

Eliana Jara Morante

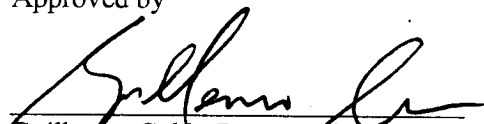A thesis submitted in partial fulfillment of the requirements for the degree of
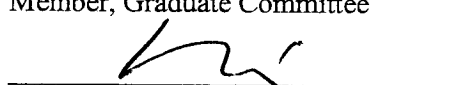
DOCTOR OF PHILOSOPHY
in
Chemical Engineering

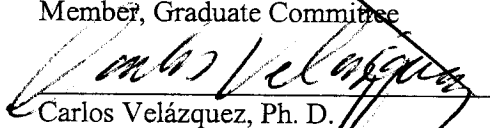UNIVERSITY OF PUERTO RICO-MAYAGÜEZ CAMPUS
2004

Approved by
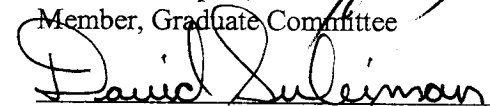
_____
Guillermo Colón Burgos, Ph. D.
Member, Graduate Committee

_____ Oct. 18, 2004
Date

_____
L. Antonio Estévez, Ph. D.
Member, Graduate Committee
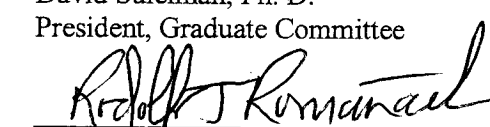
_____ October 18, 2004
Date

_____
Carlos Velázquez, Ph. D.
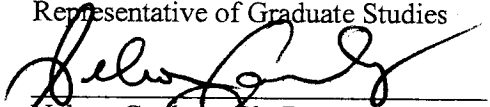Member, Graduate Committee

_____ Oct. 18, 2004
Date

_____
David Suleiman, Ph. D.
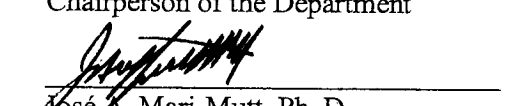President, Graduate Committee

_____ Oct. 18, 2004
Date

_____
Rodolfo Romañach, Ph. D.
Representative of Graduate Studies

_____ Oct 18, 2004
Date

_____
Nelson Cardona, Ph. D.
Chairperson of the Department

_____ Oct 18, 2004
Date

_____
José A. Mari-Mutt, Ph. D.
Director of Graduate Studies

_____ OCTOBER 25, 2004
Date

ABSTRACT

The aim of this research is to characterize microemulsions in supercritical (sc) CO_2 using two spectroscopic techniques (UV-Vis and FT-IR) and apply the microemulsion approach to extract impurities from a pharmacological drug, hydroxy ethyl starch (HES).

Nonionic pluronic (PL92, PL31, and P17R2), perfluorinated (Zonyl) and polyethylene glycols ethers (Gele) surfactants with known solubility in $scCO_2$ have been used to form microemulsions. Aqueous solutions of pharmacological drugs (acetaminophen and imipramine HCl) have been added to the systems in an attempt to capture the polar solute in the core of the microemulsion formed in $scCO_2$.

The indicator (N,N,-dimethyl-4-nitroaniline) was used to characterize microemulsions with UV-Vis spectroscopy, due to its large solvatochromic shift. The maximum absorbance shifted to lower energy (red shift) due to the specific hydrogen bonding interactions when the polarizability/dipolarity (π^*) of the solvent increased. The π^* values for the five indicator-H_2O-surfactant-$scCO_2$ systems indicated the formation of a changing microenvironment as pressure increased, achieving values comparable to those of linear hydrocarbons. The higher π^* values corresponded to P17R2-Indicator-H_2O-$scCO_2$ (from -0.22 to 0.05) at pressures and temperatures ranging 91-221 bar and 313-323 K, respectively. Compared to the other surfactants, P17R2 has demonstrated to be more stable, perhaps due to its structure (PPO-EO-PPO), which gives it more ability to trap H_2O through stronger hydrogen-bonding interactions. The systems evaluated have shown to be solute sensitive. Even though the π^* values suggested a constant water-like surrounding, different behaviors were observed for acetaminophen and imipramine HCl. This suggested different intermolecular interactions among the components that compromised the stability and performance of the surfactants. Data taken with this technique also provided the possibility to evaluate the systems through other parameters used to characterize the supercritical state, such as the local density augmentation, dielectric constant, and second virial coefficient.

FT-IR spectroscopy was used to study the intermolecular interactions of microemulsions in $scCO_2$. The effect of pressure and H_2O addition to the systems was evaluated at 313 K. This effect was analyzed through the inspection of characteristic peaks that have been proven to be sensitive to micellization (e.g., the variation of the ratio CH_2 asymmetric to CH_3 symmetric stretching vibration, deformation around the CH_3 asymmetric bending vibration, the C–O stretching, and the C=O region) and gave evidence of hydrogen bonding interactions. The formation of different hydration states was also used to characterize the microemulsions. The four (OH) regions evaluated (free, hydrogen bonded, non-hydrogen bonded, and monomeric H_2O) denote the interactions with the hydrophilic portion of the surfactants. P17R2-Acetaminophen-H_2O-$scCO_2$ system showed the best performance with H_2O loaded up to 4% prior to phase separation or destabilization. However, I can not assure a one-phase micellar system because the cloud point was only verified by visual inspection through the high-pressure cell. The values of water-to-surfactant molar ratio (W_0) calculated showed variation with pressure and H_2O addition. According to the low W_0 values (<15), it can be concluded that with

Gele reverse micelles have been formed. Again, the performance of the surfactants was affected by the pharmacological drugs used in this study, which agrees with the UV-Vis spectroscopic conclusions.

Microemulsions and other extraction strategies (pure $scCO_2$ and cosolvents-$scCO_2$) were applied in the extraction of ethylene glycol from HES. Two HES lots with different amounts of impurities were treated with $scCO_2$, obtaining a 48% and 96% extraction. The 3-5 hours supercritical extraction processes were performed at 200 bar and 313 K. Based on extraction percentage, the performance of the cosolvent-$scCO_2$ agrees with its dielectric constants. Since the extraction process is H_2O-composition dependent, the formation of reverse micelles to trap the polar compounds (e.g., ethylene glycol, H_2O) in the micelles core seemed to be adequate. With 75% extraction, Gele-$scCO_2$ showed a solvent capacity comparable to polar modified acetonitrile-$scCO_2$ system (87%) and higher than acetone-$scCO_2$ (65%). Zonyl was able to trap H_2O and hence the ethylene glycol. This was verified through the detection of the broad band situated around 3300 cm^{-1} assigned to hydrogen bonded (OH). The low level composition did not destabilize the microemulsions formed in $scCO_2$. This leads to the conclusion that these surfactants can be used to extract organic compounds in a ppm-level composition, through the formation of reverse micelles or microemulsion. This can be a useful application of commercial and non expensive surfactants and an attempt to replace the use of environmentally undesirable and expensive organic solvents.

RESUMEN

El propósito de esta investigación es caracterizar microemulsiones en CO_2 supercrítico (sc) usando dos técnicas espectroscópicas (UV-Vis y FT-IR) y aplicar el método de microemulsiones para extraer impurezas de la droga farmacológica "hydroxyl ethyl starch" (HES).

Surfactantes no iónicos plurónicos (PL92, PL31 y P17R2), perfluorinados (Zonyl) y éteres de glicol de polietileno (Gele), de solubilidad en scCO_2 conocida se usaron para formar microemulsiones. Se agregaron soluciones acuosas de drogas farmacológicas (acetaminofen e imipramina HCl) al sistema para capturar el soluto polar en el núcleo de la microemulsión formada en CO_2-sc.

Se usó el indicador (N,N,-dimetil-4-nitroanilina) para caracterizar microemulsiones con espectroscopia UV-Vis por su gran desplazamiento solvatocrómico. La absorbancia máxima se desplazó a bajos niveles de energía ('red shift'), debido a las interacciones de puente de hidrógeno, al aumentar la polarizabilidad/dipolaridad (π^*) del disolvente. Los valores de π^* obtenidos para los cinco sistemas indicador-H_2O-surfactante-scCO_2 indican la formación de un micro-ambiente cambiante con el aumento de presión, alcanzando valores comparables a los de hidrocarburos lineales. Los valores de π^* más altos corresponden al sistema P17R2-indicador-H_2O-scCO_2 (de -0,22 a 0,05) a presiones y temperaturas variando de 91-221 bar y 313-323 K, respectivamente. Comparado con los otros surfactantes, el P17R2 demostró ser más estable, quizás debido a su estructura (PPO-EO-PPO) que le confiere mayor habilidad de atrapar H_2O a través de interacciones fuertes tipo puente de hidrógeno. Los sistemas evaluados mostraron ser sensibles al soluto. Aunque los valores de π^* sugieren entornos polares similares al H_2O, se observaron comportamientos diferentes para acetaminofen e imipramina HCl, sugiriendo interacciones intermoleculares diferentes entre los compuestos que comprometen la estabilidad y el desempeño de los surfactantes. Los datos obtenidos con esta técnica permitieron evaluar los sistemas formados mediante otros parámetros usados para caracterizar el estado supercrítico, tales como el aumento en la densidad local, la constante dieléctrica y el segundo coeficiente de virial.

Se usó espectroscopia infra-roja (FT-IR) para estudiar las interacciones intermoleculares de microemulsiones en scCO_2. Se estudió el efecto de la presión y de la adición de H_2O a los sistemas a una temperatura de 313 K. Se analizó mediante la inspección de picos característicos que son sensibles a la micelización (i.e., la relación de los modos de vibración asimétrica-simétrica de los grupos CH_2 y CH_3, la deformación alrededor de la vibración asimétrica CH_3, la vibración de elongación C–O y la región de C=O), y dan evidencia de interacciones de puente de hidrógeno. La formación de diferentes estados de hidratación también se usó para caracterizar las microemulsiones. Las cuatro regiones evaluadas (H_2O libre, H_2O sin enlaces tipo puente de hidrógeno, con enlaces de puente de hidrógeno y H_2O monomérica) denotan la interacción con la parte hidrofílica de los surfactantes. El sistema P17R2-acetaminofen-H_2O-scCO_2 tuvo el mejor comportamiento con cantidades de H_2O de hasta un 4% antes que ocurra la separación de fases o desestabilización. Sin embargo, no se puede asegurar que se consiguió un sistema

de una fase micelar, ya que la inspección de la transparencia del sistema fue en forma visual a través de las ventanas de la celda de alta presión. Los valores de la relación molar de H_2O a surfactante (W_0) calculados, mostraron variación con la presión y la adición de H_2O. De acuerdo a los pequeños valores W_0 (<15) alcanzados se puede considerar que solo con Gele se formaron micelas inversas. Nuevamente, el desempeño de los surfactantes fue afectado por la presencia de las drogas farmacológicas usadas en el estudio, lo cual concuerda con las conclusiones de la técnica UV-Vis.

Las microemulsiones y otras estrategias de extracción ($scCO_2$ puro y con cosolventes) se usaron en la extracción de glicol de etileno de HES. Dos lotes de HES con diferentes contenidos de impurezas se trataron con $scCO_2$, obteniéndose un 48% y un 96% de extracción. El proceso de extracción supercrítica se llevó a cabo a 200 bar y 313 K por 3-5 horas. En base al porcentaje de extracción, la eficacia de los solventes varía de acuerdo con sus constantes dieléctricas. Debido a que el proceso de extracción depende del contenido de H_2O, la formación de micelas inversas para atrapar compuestos polares (glicol de etileno y H_2O) en el centro de las micelas parece ser un proceso adecuado. Con un 75% de extracción, el sistema Gele-$scCO_2$ demostró tener una capacidad solvente comparable al sistema polar acetonitrilo-$scCO_2$ (87%) y más alto que acetona-$scCO_2$ (65%). El surfactante Zonyl fue capaz de capturar agua y por lo tanto glicol de etileno. Esto se verificó por detección de la amplia banda situada alrededor de 3300 cm^{-1} asignada a (OH). El bajo nivel de composición de H_2O o compuesto orgánico no desestabiliza las microemulsiones formadas en CO_2-sc. Esto lleva a la conclusión que estos surfactantes pueden ser usados para extraer compuestos orgánicos en una composición a nivel de ppm, mediante la formación de micelas inversas o microemulsiones. Esta puede ser una aplicación útil de surfactantes comerciales y baratos en un intento de reemplazar los solventes orgánicos tóxicos y costosos.

FOREWORDS

A los grandes ausentes…

A los sueños que quedaron en el camino

A las intenciones frustradas

A los silencios justificados por la falta de inspiración

A lo que falta porque hace que lo que sobra sea determinante

Al fabuloso origen que no tendrá continuidad…

ACKNOWLEDGMENTS

The awareness of the beginning is not as clear as that of the end, because the fulfillment of a goal makes the difference. It is in oneself's hands to build the path, to find out the answer, and during that process, life reveals itself through the people who become important to us and make these experiences even more worthy. I would like to thank everyone who helped me through this journey. To my advisor Prof. David Suleiman for his guidance, support, and for those days when everything was an opportunity to create, learn, and understand. To my graduate committee for their advices and considerations

Excellent persons whom I met in this adventure: Prof. Francisco Medina, for his support during my unforgettable sojourn in Tarragona, Spain. Prof. Charles Eckert for receiving me in his academic and research world, because his words have their own meaning. Dr. Jie Lu, and Dr. Josh Brown for their help and useful advices during my days in GeorgiaTech. The moon's light reveals wonderful inspirations if only we have the attitude, thanks for teaching me that Prof. Alex Leyderman.

With my deepest gratitude to Carmen, my mother, and my family, for always reminding me who I am. Helga, because our lives are a rendezvous where to enjoy and grow. Antonio, for opening my heart in a way that I barely understood but made me realize what I am made of, and just letting me be.

Adalis, neither distance nor time was an apology for both not to be friends. Leo, my friend, because we both know how worthy are the minutes we shared. Mrs. Celia all the faith you have is an inspiring learning. There are eyes that can go beyond the evident, to you, Vanessa.

Mr. Angel Zapata for his help and advices during the technical and laboratory work. To the Faculty and staff of the department and to the Chemical Engineering Department, University of Puerto Rico for giving me the opportunity and financial assistance.

TABLE OF CONTENTS

LIST OF FIGURES

LIST OF TABLES

CHAPTER 1

Introduction and Background

1.1 Introduction

Rapid technological advances have presented many complex ecological and energy efficiency issues. As a result, pollution prevention, waste management, and energy uses represent the most profound challenges of the 21st century. Environmental concerns over the extensive use of volatile organic compounds (VOC), halogenated solvents, and inordinate amounts of water by processing industries (e.g., electronics, pharmaceuticals, dyes, and coatings) throughout the world have led to an extensive search for harmless solvents. The need to develop a more environmentally responsible and energy-efficient solvent technology platform is paramount, and the leading candidate is liquid and supercritical carbon dioxide ($scCO_2$). Technological breakthroughs in the past decade indicate that $scCO_2$ could be the most commonly used solvent in this century. The major incentives to use $scCO_2$ as a solvent in many commercial processes are the elimination of environmentally harmful organic solvents, reduction of waste streams, and decrease of the residual contamination. Neither the poor solvent capacity of $scCO_2$ for polar molecules or for many other compounds of commercial interest has hindered the development of $scCO_2$-based processes. To meet these challenges, the design of surfactants for the $scCO_2$ phase and the behavior of these compounds (e.g., solute, reactant, products) in the supercritical phase are key considerations that will enable a sustainable $scCO_2$ technology platform with a positive impact in the society.

This research studied the molecular interactions in micro-domains formed in supercritical fluids (e.g., microemulsions). Although the spectroscopic study gives information at molecular level, this knowledge can be used in any practical and industrial application (e.g., extraction, purification and separation of pharmacological drugs).

This document introduces the research developed during the last years. The strategies of analysis and results obtained from the two spectroscopic studies are

explained in separate chapters. Every chapter lists the principal literature reviews cited in the chapter in the section named as reference. The motivation of this investigation is widely explained in section 1.2. The section explains the criteria under the surfactants and solutes were chosen, their importance and principal conclusions of previous investigations performed in our laboratory. Section 1.3 gives a general background of supercritical fluids, pointing out the state of the art of the UV-Vis and FT-IR spectroscopic techniques and their applications in supercritical fluids. Those specially dealing with the characterizations of microenvironments formed in scCO$_2$. The main parameters used for this characterization are also described to have a global understanding of the richness of the technique and usefulness in the supercritical fluid area. In the same way the literature concerned to emulsion, microemulsions and the variety of surfactants used in supercritical fluids are presented.

The principal spectroscopic techniques used in this investigation (e.g., UV-Vis, and FT-IR) are briefly described in Chapter 2. This chapter also deals with the physicochemical properties and characteristics of the materials, (e.g., pharmacological drugs, CO$_2$, and surfactants) under investigation. In this chapter, the experimental set-up employed along the investigations are shown and described. The particular procedures corresponding to every particular scenario are described as well.

Chapter 3 deals with the characterization of the microemulsions in supercritical fluids by the UV-Vis spectroscopic technique. The solvatochromic parameters (e.g., α, β, π^*) used to characterize the micro-domains are widely described as well as the fundamental theory upon the results are analyzed. Several approaches were used in order to analyze and characterize the microemulsions in scCO$_2$.

Chapter 4 presents the FT-IR spectroscopy studies and its uses in the characterization of microemulsions in scCO$_2$. The first sections of the chapter describe the principal characteristics of the IR spectrum of the pure compounds (e.g., scCO$_2$, H$_2$O, surfactants) used in the investigation. The spectrums were characterized throughout the recognition of the principal vibration modes. The next sections, deal with the FT-IR analysis of the

complete systems (pharmacological drug-surfactant-H_2O-scCO_2) to verify the formation of microemulsions in the fluid phase. This is done throughout an in-depth analysis of characteristic regions which are known to give reference of microemulsion formation; specifically the ν(OH) stretching region. Also, the shifts of the characteristic vibration modes, sensitive to intermolecular interactions, are analyzed as well as the reasons of their behavior.

Chapter 5 presents the removal of the impurity ethylene glycol from a pharmacological drug. Many extraction strategies were used (e.g., pure scCO_2, scCO_2 with cosolvents, and scCO_2 with surfactant) to accomplish the low concentration required by the manufacturer (e.g., ppbs). The microemulsion formation of organic compound in scCO_2 approach was explored to accomplish the removal of impurities from the drug. This was an example of a practical application of the microemulsion approach.

Finally, in chapter 6 is point out the principal conclusions of our results, trying to establish the common conclusions attained from the two spectroscopic techniques and the practical separation performed in the investigation. Recommendations for future studies are also presented.

1.2 Motivation

The study of the fluid properties near the critical point is critical for the development of supercritical (sc) technologies and for further understanding of the features of supercritical fluids (SCF's). Researchers are giving more attention to these sc technologies to become very attractive in practical applications (59).

A supercritical fluid (SCF) (substance heated past its critical temperature and pressurized past its critical pressure) has gas-like mass-transport properties (e.g., diffusion, viscosity) and liquid-like solvating properties (e.g., density) (Table 1-1). These properties are very sensitive to changes in pressure and temperature, and may be tuned by them. Thus, little changes in pressure and temperature will produce large changes in density and therefore the solvency capacity will increase various orders of magnitude. To gain insight into the process taking place in SCF's, one should first know the

characteristics of them. Thus, much of the research is directed to understand the molecular characteristics of the fluids and the intermolecular interactions.

Table 1-1: Comparison properties of gas, SCF and liquid (88)

	Density [kg/m^3]	Viscosity [mPa•s]	Difusivity$\times 10^4$ [m^2/s]
Gas			
30°C, 1 atm	0.60 – 2.0	$(1-3)\times 10^2$	0.1– 0.4
Supercritical Fluid			
Near T$_c$, P$_c$	200 – 500	$(1-3)\times 10^{-2}$	0.7×10^{-3}
Near T$_c$, 4P$_c$	400 – 900	$(3-9)\times 10^{-2}$	0.2×10^{-3}
Liquid			
30°C, 1 atm	600 – 1600	0.2 – 3	$(0.2-2)\times 10^{-5}$

The ubiquitous feature about SCF's is their macroscopic inhomogeneities, the most known is the long range density fluctuations that occurs near the critical point (97). However, due to the lack of accurate properties for the solutes used, and their very low volatilities, it has not been possible to determine the inhomogenieties and non-idealities of the supercritical phase. In general, the strength of specific interactions between a solute and a supercritical fluid has been inferred from its solubility. But the limitation of the solubility approach is the difficulty in break up the van der Waals, polar and hydrogen-bonding interactions.

Due to the solvent density inhomogeneities manifested by solvent-solvent and solute-solvent clustering, the spectroscopic approach has been adequate to determine solvent parameters (e.g., α, β, π*). These parameters have given a more complete picture of the intermolecular interactions in solution occurring on the molecular scale, and constitute the more comprehensive measure of the polarity of the solvent than any other single physical constant (71).

In many of these SCF's systems of practical interest, the molecules used (solute and solvent) differs greatly in size, shape, structure and polarity. Thus, their solute-solute, solute-solvent, and solvent-solvent intermolecular interactions are different from each other and exhibit versatile forms of these characteristic energies (97). Traditionally most

investigations of these molecules have involved macroscopic phenomena (e.g., phase changes, thermodynamic, etc), but the complexity of these mixtures has led to the need for more detailed information on a molecular level. Therefore, vibrational techniques can help out to explore the phenomena occurring in these complex microenvironments and enhance the understanding of multi component supercritical systems.

Table 1-2: Properties of SCF's (arranged according pressure) (74)

Substance	Molecular Weight	Temperature [K]	Pressure [MPa]	Density [g/cm^3]	Dielectric Constant
C_2F_6	138.012	293.0	3.06	0.622	
$CClF_3$	104.459	302.0	3.87	0.579	
CH_4	16.043	190.5	4.61	0.162	1.261
CHF_3	70.014	299.3	4.86	0.528	2.564
C_2H_6	30.070	305.4	4.88	0.203	1.283
C_2H_4	28.054	282.3	5.04	0.214	1.331
N_2O	44.013	309.6	7.25	0.452	
CO_2	44.010	304.1	7.38	0.468	1.322
NH_3	17.031	405.6	11.28	0.234	
H_2O	18.015	647.1	22.06	0.322	48.426

There are many SCF's that exhibit interesting physicochemical properties (Table 1-2); CO_2 has a dielectric constant similar to ethylene (C_2H_4) and ethane (C_2H_6), hence similar solvation power. The CO_2's large quadrupole moment gives it a high critical pressure which is comparable to N_2O (polar compound). The unusual and interesting physicochemical properties of CO_2, which will be presented in detail in chapter 2 section 2.5.3, has ascribed specific interest in CO_2 which are magnified by its green properties. CO_2 is a natural occurring gas that can be found in natural reservoirs, or as a by-product from the production of ammonia, natural gas, ethanol, and hydrogen. Using CO_2 does not contribute to the enhancement of the greenhouse effect (global warming), because most of the CO_2 that is sold today (82%) is a by-product from these processes rather than a

product of combustion of fossil fuels (87).

CO_2 is non-flammable gas and benign solvent. It has a TLV[1] of 5000 ppm, thus is less toxic than many other organic solvents (i.e., acetone has a TLV of 750 ppm, pentane 600 ppm, and chloroform 10 ppm) (4). In addition to the environmental benefits, using CO_2 can be more energetically efficient than using conventional solvents. Due to its low heat of vaporization, CO_2 requires lower processing temperatures. Hence, significantly reduces the energy costs associated with H_2O-intensive processing and also eliminates the inevitable contamination problems associated with the pollution of H_2O effluent streams. Ultimately, in order to adequately judge the sustainability of a CO_2-based process, one should consider the source of CO_2 used in a process and how we can ride of it from the product without increasing pollution. Thus, in a typical process CO_2 is easily recycled. CO_2 can be widely used specially in the food, and pharmacological drugs industry due to its high TLV and non VOC designation. Also, the recent commercialization of fabric cleaning using CO_2 benefits both form CO_2's advantages in human-contact applications and situation where emissions appear unavoidable.

The main disadvantage is the need of high pressure to employ in $scCO_2$-based process that increases the operating costs. Obviously, additional safety concerns should be addresses vs. the analogous process at atmospheric conditions. However, these issues would not impede the commercialization of these processes nor they will in the future, especially because no further purification or separation stages are required. CO_2 is still under the scope of many investigations. According the reports, the numbers of CO_2 based processing plants operating worldwide are 100 and steadily growing. Its main uses are in the food processing (e.g., extraction or fractionation), fluoropolymers synthesis by Dupont, hydrogenations by Thomas Swan, coating by Union Carbide, polyethane processing by Crain industries, Micell in dry cleaning and Global technologies (4).

One way to reduce the cost of a $scCO_2$-based processes is to minimize the size of the

---

[1] Threshold limit value, airborne concentration at 298 K to which it is believe that nearly all workers may be repeatedly exposed day after day without adverse effect.

equipment, given that CO_2 is typically proposed as a solvent rather than a reactant, the most important issue is to minimize the amount of solvent flowing through the process. Consequently, one should choose to design substrates that exhibit high solubility in $scCO_2$, and thus lower the need of operating at high pressures.

Generally, depending on the process, the rate, yield and economy of any process are greatly defined by solute solubility. The solubility in $scCO_2$ is correlated with the ability of a solute to participate in electrostatic interactions or the acidity/basicity of CO_2 (14). To date it has been demonstrated the high solubility of lipophilic compounds (e.g., cholesterol), perfluorinated and some hydrocarbons in $scCO_2$. Most notably $scCO_2$ can solubilize non-volatiles compounds at near ambient temperature.

Even at its supercritical conditions, CO_2 shows low solvency capacity for high molecular weight or hydrophilic compounds due to its low dielectric constant and polarizability per volume. One strategy to increase the solvent power of CO_2 is through the increase of its polarizability and to modify this property, cosolvents are commonly used. They are small polar organic compounds that modify the fluid phase generating hydrogen-bonding acceptor or hydrogen-bonding donor capabilities in the non polar CO_2.

Because of $scCO_2$ is different from either lipophilic organic phases or hydrophilic solvents it may be considered a third type of condensed phase. This fact opens up many interesting new possibilities in combination with interfaces. That is the possibility of create reverse micelles or microemulsions using surfactants, and make $scCO_2$ suitable for dissolving more polar molecules. The formation of aggregates of surfactants in dense fluids, found out by Gale et al. (26), overcomes the natural hindrance of using $scCO_2$ as a solvent for non polar molecules only. The microemulsion approach overcomes the limitations of cosolvents which can only be added in small concentrations, (due to phase equilibria considerations) and with limited choice of hydrogen-bonding donor or acceptor capacity. Formation of microemulsions in $scCO_2$ was one of the most amazing discoveries especially when they were able to trap water in the inner core of the reverse micelle (47).

Since then, many applications for $scCO_2$ have been addressed, several for industrial scale and other still at laboratory scale. Water-$scCO_2$ microemulsions and other emulsions are appealing substitutes for traditional organic solvents in material processing solvent-free coatings, heterogeneous reactions (polymerization), biological processes, and separation processes (purification and extraction of heavy metals).

Even though the breakthrough of forming $scCO_2$ microemulsions, several issues concerning the surfactants need to be addressed yet. To design surfactants with tailored solubility in $scCO_2$, the knowledge of the intermolecular amphiphile-solvent interactions is essential. Since, aggregation is brought about by a balance between the lateral interactions among surfactants molecules at the surfactant interface and the interactions between the surfactant and the solvent. It is very important to precise the driving forces that take account in the formation of the microstructures (e.g., Lewis acidity/basicity, van der Waals forces, polarizability, dipole-induced dipole interactions). The surfactant must be relatively inexpensive and be able to form microemulsions at reasonable pressure.

This research focused in commercially known surfactants, inexpensive and chemically versatile. These surfactants were chosen based on their solubility in $scCO_2$ (71), but the study did not restrict to perfluorinated surfactants, in spite of their high solubility. Since, if the use of fluorinated compounds (e.g., perfluorooctanesulfonic acid and closely related compounds) will be restricted in the future, this could limit the use of $scCO_2$ in certain areas. Obviously, polar surfactants would interact more successfully with polar solutes, but the pressures to solubilize them in $scCO_2$ are higher, and then unpractical for an industrial approach. Therefore, in this study were used nonionic surfactants, with similar characteristics (e.g., linear), with different structural ordering, different polar heads (e.g., ethylene oxide, carboxylic groups, etc), and different skeletal backbone (e.g., perfluorinated, propylene oxide).

Surfactants have widespread industrial applications in detergency, dispersion stabilization, foaming, emulsification, cosmetic formulations, along with more specialized applications in pharmaceuticals (e.g., drug solubilization and control drug

release), bio-processing (i.e., protection microorganism from mechanical damage) and separations (i.e., solubilization of organic in aqueous solutions).

It is well known that conventional pharmaceutical processing involves extensive use of organic solvents as antisolvent for recrystallizing drugs from solutions, reaction media in the synthesis of drugs or extracting agents for selectively isolating drugs from solid matrices. Health concerns caused by some of these solvents (e.g., methylene chloride) due to either environmental emissions and/or traces residues in the product have propelled research to develop 'environmentally benign' processing techniques that eliminate or reduce the pollution. And one of the alternative solvents is $scCO_2$ in which the major research is focused. The manufacture of pharmacological drugs involves many batch operations (e.g., reaction, separation, purification, crystallization, etc.) and these operations are time-consuming, energy-intensive, and have a large risk of contamination of the drug. Many of these processes can be unified in just one process using $scCO_2$, making them safer, faster and more cost effective. Even though high pressure is needed, appropriate commercial equipment with successful performance in supercritical processes can be found in today's market with good laboratory practices (GLP) and good manufacturing practices (GMP) at competitive prices.

The replacement of environmentally undesirable solvents is an important issue in the pharmaceutical and specialty chemical areas. In order to use $scCO_2$ one must know the key parameters in the interaction of $scCO_2$ with pharmaceuticals or intermediates. The solubility of pharmacological drugs has been study by several researchers. Even though their solubility is in the range of 10^{-3} to 10^{-7} [mol solute/mol $scCO_2$] it has not dissuaded to continue the investigation in this area. The laboratory has obtained solubility data for pharmacological drugs by conventional dynamic gravimetric and chromatographic methods. Those drugs studied includes: anti-inflammatory drugs (e.g. naproxen, ibuprofen, acetaminophen) (27), anti-aids (e.g., azodicarbonamide, and 2-phenyl-4H-3, 1-benzoxazin-4-one), anticancer (e.g., taxol, thymidine, and s-fluorouracil) (76), antidepressant (e.g., imipramine HCl) (45), and plasma volume expander (e.g., hydroxyl

ethyl starch) (85). The drugs showed particular intermolecular interactions with $scCO_2$, although they belong to the same family. For this investigation two pharmacological drugs were selected: acetaminophen and imipramine HCl.

Acetaminophen belongs to the nonsteroidal anti-inflamatory drugs, with very low solubility in $scCO_2$ (e.g., ppms) (6). Comparing with naproxen and ibuprofen, which belong to the same family of drugs, acetaminophen has a carbonyl group and an amino group that confers polarity to the drug. The carbonyl compound and the saturated $-C-N-$ are the responsible of the $n \rightarrow \pi^*$ transition bands that provoke the hypsochromic shift[2] of the molecule.

Imipramine HCl is a tricycle antidepressant drug its solubility in $scCO_2$ is of a 10^{-7} mole fraction order of magnitude (45). According to our results it does not present any shift in UV when it is dissolved in different solvents, and because of its complex structure, it is difficult to precise which of the chromophore groups is responsible for the UV maximum absorption. The presence of the adduct HCl, obviously makes it soluble in H_2O. Previous studies in $scCO_2$ have demonstrated that imipramine HCl is stable, but the presence of H_2O would modify it. At the same time it is worth mention that the ionic form of the drug will affect the pH of the microemulsion, and hence the formation and stability of it. Acetaminophen and imipramine HCl has unique characteristics and each one is representative of a family of pharmacological drugs. The finding of this research concerning to intermolecular interactions, may or may not establish a generalization among the related drugs.

Finally, it was important to use the microemulsion approach to solve a real process problem. That is why the plasma volume expander pharmacological drug called Hydroxy Ethyl Starch (HES) was selected, which possesses impurities that must be removed. This approach will be applicable as an alternative to solve this problem due to the low concentration (i.e., ppm level) in which the ethylene glycol and ethylene chlorohydrine are present in the drug.

---

[2] Shift of the maximum wavelength to shorter wavelengths, also called blue shift.

1.3 Background

The inability of the solvent macroscopic properties (e.g., dielectric constant, refractive index, and dipole moment), to describe the complexity of solute-solvent interactions on a molecular level has lead to the introduction of various empirical solvent polarity scales, such as Dimroth's (E_T), Kosover's (Z), and Dubois's (Φ) single polarity scale or Brooker's (χ_A and χ_B), and Kamlet and Taft's multi-parameter scales from spectroscopic measurements (48).

The most used parameters to characterize solvent properties are the Kamlet-Taft parameters, which give information about the interactions occurring at the molecular level. Kamlet and Taft reported the α, β, and π^* parameter for 250 liquid organic solvents, measured by UV-Vis spectroscopic method (48). They correlated those parameters in a linear solvation relationship, demonstrating that the solvatochromic comparison method may be used to unravel, quantify, correlate and rationalize multiple interacting solvent effects on many types of physicochemical properties and reactivity parameters. Latter, in an attempt to provide a quantitative empirical measure of the non-specific van der Waals interaction (e.g., contributions other than hydrogen bonding), Laurence et al. (56), built the π^* scale in a variety of 229 solvents using two different indicators one of them N,N-dimethyl-p-nitroaniline. These parameters have been applied to supercritical fluids, and most of the commonly used supercritical solvents have been characterized using this technique. Abbott et al., determined the hydrogen bonding interaction in liquid and supercritical hydrocarbons (e.g., HFC-32, and HFC 134a) (1). Sigman et al. (82), determined the β and π^* solvatochromic indicators in $scCO_2$ over a wide range of densities. Using the same technique, Yonker et al. (94), characterized four supercritical solvents (e.g. NH_3, N_2O, Freon-13 and CO_2). They concluded that the π^* scale behaves the same as the Hildebrand solubility parameter (δ) ($NH_3 > CO_2 \approx N_2O$ > Freon-13) and this behavior can be tuned by changes in pressure. Furthermore, these results were correlated with the McRae-Bayliss model of solvatochromism, which is based on the Onsager's reaction field theory (96). The extensive application of the

solvatochromic approach was proved to be effective to characterize binary supercritical fluids to determine the dependency of the local composition with the temperature, pressure and concentration (95).

Other useful parameter for SCF's characterization is the Dimroth's parameter (E_T). E_T is based on the phenyl blue transitional energy (Figure 1-1), and it helps to determine the solvent strength of the supercritical fluids as well as the local density in the vicinity of the solute. Data taken with the E_T suggested that liquid and $scCO_2$ have polarities close to those of hydrocarbons, but have polarizabilities which are even lower than those of fluorocarbon solvents (54). The $E_T(30)$ scale refers to the energy of intramolecular charge-transfer $\pi \rightarrow \pi^*$ transition of pyridium-N-phenoxide betaine dye (Figure 1-1).

Phenol blue (E_T)   Pyridium-N-phenoxide betaine ($E_T(30)$)
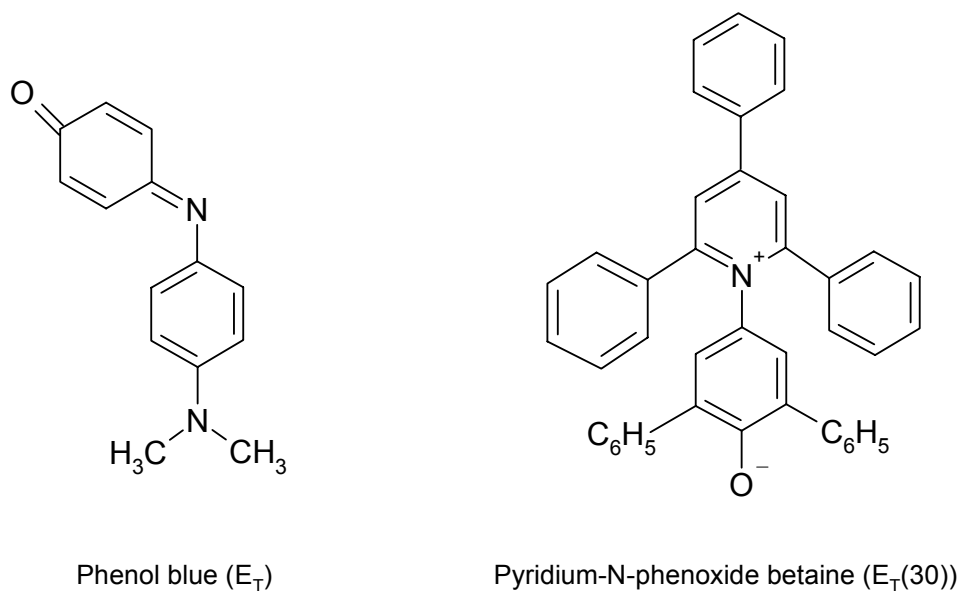
Figure 1-1: Solvatochromic dyes.

Extensive studies (56) have shown that in the absence of hydrogen bonding (HB) interactions, the main physical difference between π^* and $E_T(30)$ values lies in different responses to solvent polarizability effects. Because of this value provides a measure of the local density augmentation, it was used to correlate reaction rates involving a reactant and the transition state polarity change in SCF solvents (7, 56). Bekârek et al. (41),

correlated the $E_T(30)$ value for the bulk region with the solvent dielectric constant (ε) and refractive index (n) for non-hydrogen bond solvents, and can be used for scCO$_2$.

Because of the chemical nature of the solvatochromic probes used to obtain the parameters defined above, the UV-Vis spectroscopic became an eligible technique to characterize the SCF's. Although UV-Vis is an important tool to provide useful information at a molecular level, it does not completely provide information about intermolecular interaction, and hydrogen bonding. Thus, it is necessary a complementary technique like infrared spectroscopy.

Fourier Transform Infrared spectroscopic (FT-IR) is another useful technique to study the supercritical solutions. This approach overcomes the inherent limitations of the UV-Vis spectroscopy, related to the use of solute probes that may introduce uncertainties concerning to possible probe-solvent interactions. FT-IR spectroscopic studies were used to characterize pure and binary supercritical CO$_2$ through the study of frequency shifts in supercritical fluids (5). This vibrational technique is also useful to determine the intermolecular interactions arising from the solvent-solute interactions monitoring the shift of specific chemical groups provoked by the surrounding media.

Much of the investigation using this technique has focused in the understanding and identification of molecules that have favorable intermolecular interactions with scCO$_2$. Based on the Lewis acidity of scCO$_2$ in presence of Brønstead and Lewis based (e.g., H$_2$O, amines, amides, and basic polymers) it was possible to quantify the equilibrium constant among those substances and proved the existence of an electron donor-acceptor structure (67). This work also suggested that Lewis basic groups can add important specific interactions that raise solubility in scCO$_2$.

In spectroscopic studies Kazarian et al. (51), demonstrated that polymers possessing electron-donating functional groups (e.g. carbonyl groups) exhibit specific interactions with scCO$_2$, with a slightly stronger strength than dispersion interactions. This conclusion was assessed upon observing the splitting of the bending mode of CO$_2$. O'Shea et al. (72), with the UV-Vis technique, studied polar and hydrogen-bonding interaction in

binary mixtures with scCO$_2$, and argued that the complex formation is most probably of a Lewis-acid base nature, where the carbon atom of the CO$_2$ molecule acts as an electron acceptor and the carbonyl oxygen in the polymer as an electron donor. With this knowledge, it was important to relate these intermolecular interactions in terms of adequate macroscopic properties (e.g., solubility, superficial tension, etc) that describe the solute-solute interactions, and be able to predict their behavior.

In that sense, the solubility of many polymers in scCO$_2$ were studied, and results demonstrate how creative, polymer synthetic chemistry can be used to improve polymer solubility in scCO$_2$ (71). The wide variety of compounds evaluated, only provided limited insight into why most polymers do not dissolve in scCO$_2$ regardless of pressure and temperature. It was seen that although fluorinating side groups or copolymers blocks enhance solubility several fold in scCO$_2$, fluorination alone does not ensure that the polymer will be soluble in scCO$_2$ (68).

FT-IR was proven to be a useful technique in the understanding of the hydrogen bonding (HB) interactions. This was the key factor to understand the action of so-called modifiers or cosolvents, monitoring the specific ν(OH) and ν(C=O) bands that were able to interact with the supercritical phase. These results indicate that the difference in the free alcohol concentration varies significantly among the fluids ethanol, CO$_2$, and heptane. The degree of HB of nonionic surfactants has been measured in scCO$_2$ and ethane, the average number of mers in a hydrogen-bonded aggregate varies from 2.5 to 5.0 on the basis of interpretation of the spectra with a simple mass action model (92). Experiments performed in non-hydrogen bonding solvents (i.e., SF$_6$) have demonstrated that the degree of hydrogen bonding varies substantially between the gas, supercritical fluid, and liquid states (31)

Kazarian et al. (50), studied and modeled the interaction between a proton donor and acceptor from the gas phase to supercritical state. Most of the extensive work in hydrogen bonding has been focused in methanol (25). They found that most of the methanol in scCO$_2$ is predominantly hydrogen bonded alcohol and this behavior varies on the

supercritical fluid used. Gupta et al. (31), avoided this problem of self association by using a base. Yee et al. (93), examined the solubility of a fluorinated alcohol in $scCO_2$, where no evidence of a special attractive interaction between CO_2 and perfluorinated portion of the molecule was found, but the highly repulsive nature of neighboring alkanes minimizes the solute-solute interactions and improves the solubility of perfluorocarbons. Lalanne et al. (55), found that the strongly attractive interactions between ethanol and $scCO_2$ are predominantly due to dispersion forces that dominate the stabilization energy between these molecules.

1.3.1. Emulsions and Microemulsions

Emulsions (droplets from 100 nm to several micrometers in diameter) are thermodynamically unstable entities, but may be kinetically stable. The emulsions are inherently unstable because of the large interfacial free energy. This thermodynamic instability is manifested in the various mechanisms of emulsion destabilization, like aggregation, coalescence, sedimentation, and Oswald ripening.

Microemulsions are entities thermodynamically stable and apparently homogeneous. They form spontaneously as a response of the system to diminish the high entropic content in a mixture of two immiscible substances. They contain particles that are extremely small, (i.e. droplet diameters in microemulsions typically range from 2-50 nm (58). Microemulsions are usually transparent/translucent as opposed to emulsions which are turbid (dirty, muddy). Generally, this structure arises when the concentration of surfactant is high. Microemulsions have properties that have been proven to be useful over other structures such as, their thermodynamic stability, their spontaneous formation, the possibility of near uniform size of droplets of the suspension formed, and the possibility of nearly homogeneous mix of oil and water soluble substances.

When placed in a solvent, the surfactant tends to aggregate in such a way that different structures can be formed. The hydrophilic head and the hydrophobic tails behave in different ways. This is understood by what is called hydrophobic and hydrophilic interactions. If the fluid phase is hydrophilic, the interaction between the polar heads and the solvent is strong relative to the interaction between the non-polar parts that try to stay away from the solvent and form a non-polar core. Then the molecules tend to form *micelles* (from the Latin 'micella' - meaning small bit) (Figure 1-2).
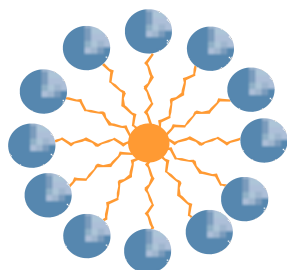
Figure 1-2: Micelles.

When the fluid phase is of hydrophobic nature, the entity formed is called a reverse micelle. In this system, the hydrophilic head tends to get closer in order to stay away from the solvent to minimize the contact, with the hydrophilic head group forming a core and the hydrophobic tails interacting with oily phase (Figure 1-3).

The stability of the micelles depends upon whether the concentration of molecules is greater than or less than a critical micelle concentration (CMC). This is the minimum concentration (number of molecules per unit
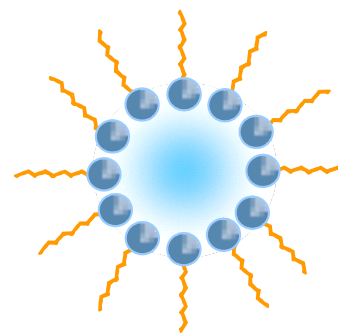
Figure 1-3: Reverse micelles.

volume) needed for the resultant micelle to be stable. On changing the temperature, or the concentration of the surfactants or additives in the continuous phase the resultant structures formed change in size, shape and aggregation number of the micelle with the structure varying from spherical through rod-or dislike to lamellar shape. At high

concentrations, reverse micelles are generally non-spherical (the lamellar phase) (77).

The size gap between emulsions and microemulsions, are called miniemulsions, also referred to as nanoemulsions. These are composed of droplets in the 50-500 nm range, the interfacial area per volume is 20 times less for a 100 nm miniemulsion droplet than for a 5 nm microemulsion droplet. Thus, for a given amount of surfactant a larger volume of water may be emulsified in miniemulsions. Because of the less stringent requirements for the surfactant in lowering the interfacial tension, a much wider range of surfactants may be utilized. Relative to macroemulsion droplets, smaller miniemulsion droplets are more stable due to lower gravitational settling and Hamaker[3] interactions between the smaller water cores (15).

1.3.2. Surfactants

Amphiphiles are molecules that possess both hydrophilic and hydrophobic segments. Since they adsorb to surfaces and interfaces to change the interfacial tension, they are also referred to as surfactants (surface active agents). The property of surfactants that invariably plays a role in all applications is their ability to reduce the interfacial tension of the interfaces. Many types of surfactants were evaluated with $scCO_2$ by Consani et al. (11) in 1990. Based in their observations and subsequent studies, many authors concluded that there are certain groups that are solubilized by $scCO_2$ as shown in Table 1-3.

In general the CO_2-philicity part of a surfactant has to have certain characteristics to design the proper surfactant (83). The tails are expected to have low cohesive energy density, low solubility parameter, low polarizability, and electron-donor capability (CO_2 is a weak Lewis acid). Not only the surfactant must be interfacially active (this can be achieved by varying the chemical makeup of both the head group and the tail), but must be able to lower the interfacial tension near to zero (this can be achieved through the replacement of the CO_2/H_2O interface with a H_2O/head and a CO_2/tail interface).

---

[3] Van der Waals attractive forces arising from polarizabilities of the particles that produce flocculation.

Table 1-3: Groups used for increasing solubility of surfactants in CO_2

Name	Chemical Structure
Acetylenic groups	$HO-CH_2-C\equiv C-H$
Poly (propylene oxide)	$*-[O-CH_2-CH(CH_3)-]_n$
Poly(hexafluoro-propylene oxide)	$*-[O-CF_2-CF(CF_3)-]_n-$
Poly(1,1-dihydroperfluoro-octylacrylate)	$*-[CH_2-CH(C(=O)-(CF_2)_6-CF_3)]_n$
Siloxane	$*-[Si(CH_3)_2-O-]_n-*$

Finally, the surfactant must be compatible with the curvature of the microemulsion droplets. In the case of H_2O in CO_2 microemulsions, this requires that the repulsion between hydrophilic headgroups be weaker than the tail-tail repulsion (78).

With these criteria, the design of perfluorinated surfactants has been the tendency of many investigators. However, the high cost of these surfactants can render the economics of a $scCO_2$ process unfavorable unless the surfactant can be recycled. Other alternatives are being studied to design CO_2-philic, composed of only carbon, oxygen, and hydrogen that is the so called functionalized polyethers and copolymers of cyclic ethers (79).

The phase behavior of the emulsions of water in oil was characterized by Winsor in 1948 (89), this same classification has been accepted for various phenomenon exhibited in a ternary oil-H_2O-amphiphile system. These phases are Winsor I, Winsor II, and Winsor III. In Winsor I, the surfactant resides primarily in the aqueous phase, normal micelles in equilibrium with excess oil. In Winsor II the surfactant resides primarily in the oil phase; reverse micelles in equilibrium with excess oil. And in Winsor III the

surfactant resides primarily in a middle phase in a middle phase in equilibrium with the aqueous and oil phases. The effect of pressure on multiphase microemulsions have been throughout investigated by many researchers, Bartscherer et al. (3) summarized these works. Much of their results indicate that molecular interactions at the surfactant interface may be controlled by simply adjusting pressure. The key factor in the solubilization of surfactant in $scCO_2$ is the determination of the cloud point. The cloud point is the point (temperature and pressure) where a new phase precipitates with a decrease of pressure (it is also called a haze point). Due to polydispersity of the system, the cloud point is only an approximate measure of the solubility, but this approximation has been shown to be accurate enough to determine the trends in solubility.

The formation of microemulsions and emulsions in $scCO_2$ has been verified by visual inspection of phase behavior (23, 35, 84, 91), spectroscopic techniques like small-angle-X-ray spectroscopy (SAXS) (24) and small-angle-neutron-scattering (SANS) (18). They are adequate techniques for quantitative investigations of structure and interactions in reverse micelles. Such techniques have shown that the reverse micelles have a spherical droplet structure (17, 18). Furthermore, the microstructure of the micro-emulsions were studied by electric conductivity suggesting that water in $scCO_2$ microemulsions forms discrete droplets rather than bicontinuous structures (57). In order to understand the emulsion behavior, the effect of multiple formulation variables such as CO_2 density, temperature, salinity, added alcohol, and surfactant tail length, as well as the volume fraction of water, in the formation and stability of emulsions was evaluated (58). Those results showed the tendency of their behavior and how complex and versatile those systems can be. Organic-in-CO_2 microemulsions have also been formed with poly(ethylene glycol) (PEG600) (32), which is interesting and useful for designing and developing surfactants system for practical applications (i.e., inexpensive and vastly available) in supercritical fluid science and technology .

One potential method for solubilizing hydrophilic species in $scCO_2$ was developing surfactants that support water in $scCO_2$ microemulsions. The existence of a water core

has been proven by many researchers. This opens up the alternative to use reverse micelles in $scCO_2$ to solubilize heavy polar molecules including proteins, the most polar substances of biological interest and other pharmacological drugs with low solubility in $scCO_2$ and water-insoluble drugs.

In that sense, Ayala et al. (2), solubilized a protease and other proteins of relevance importance in propane-based microemulsions. Surfactants can be employed to extract proteins from a buffer to an organic phase, through manipulation of the physicochemical properties of the aqueous phase (e.g., pH, ionic strength, etc.). Holmes et al. (39), and Niemeyer et al. (70), studied the effect of buffering of aqueous solutions and pH in supercritical environment respectively. Ikushima (40), besides to use $scCO_2$ in the synthesis stereoselective of an enzyme-catalyzed ester, he characterized reverse micelles with H_2O-AOT[4] in ethane, clarifying the rotational isomerism of AOT and identifying the diverse H_2O microenviroments in the reverse micelles by FT-IR technique.

Therefore, it has been demonstrated that microemulsions may be used to dissolve a wide range of ionic and polar molecules, also crystallize organic compounds (90). Microemulsions are considered a new environment for inorganic reactions (10), catalytic reactions (44), organics reactions (42, 43) enzyme-induced reactions (38, 49), and produce metallic nanoparticles (8, 9, 46, 69).

The ability to design surfactants for the aqueous-$scCO_2$ interface based upon knowledge of the relationship between colloid formation, stability phase behavior and interfacial tension is of interest for a wide variety of heterogeneous reactions and separation processes in $scCO_2$. Much work has focused on the design of surfactants capable of supporting water in $scCO_2$ taking account CO_2-tail interaction properties that affect the curvature of the micellar interface and surfactant volatility (13, 18, 22, 34, 36, 37, 79, 83).

Many attempts have been done to understand the mechanism of microemulsions formation and their stability through surfactant properties like, surface tension and relate

---

[4] Sodium bis(2-ethylhexyl)sulfosuccinate

it to the design of novel surfactants (12, 20, 32, 71). Those results found a clear correlation between the limiting surface tension of a surfactant and its performance in water/CO_2 microemulsions as measured by the phase transition pressure. Therefore, potential surfactants can be identified before making time-consuming phase stability measurements in high pressure CO_2.

The fluorinated surfactants are considered the most CO_2-philic active surfactants a summary of them can be found in Eastoe et al. (19). Among them the most studied surfactant is the perfluoropolyether (PFPE) carboxylate. For PFPECOO$^-$NH$_4^+$ water in CO_2 microemulsions, the existence of an aqueous domain in CO_2 with a polarity approaching that of the bulk water, has been demonstrated by many techniques such as FT-IR (64), UV-visible absorbance (10), fluorescence, electron paramagnetic resonance (EPR) (33) and SANS (98). The commercial surfactant ammonium carboxylate salt of Krytox FSL (2500 molar mass) is capable of supporting water in a scCO$_2$ emulsion (10%), which has been used in the extraction of biomolecules (28, 29, 47, 86, 91). Variations of the perfluoro-surfactants are the phosphate-based fluoro-surfactants (52, 80), where the phosphate head increases the polarity of the surfactant and the large chain increases the stability of the reverse micelles. The main disadvantages of these surfactants are their high cost and toxicity. In that sense, the design of mixed fluorosurfactant/hydrocarbon surfactant (78) systems can give impressive gains in the area of reducing foaming to improve dynamic surface tension. They also reduce and enhance fluorine efficiency, while being cost effective (16) but the main problem they faced is that they hydrolizes over time.

The performance of non-fluorous and non-siloxane surfactants are still under investigation, they showed to be able to absorb a significant amounts of H_2O at accessible conditions, and have low price, and low toxicity. These are the series Dynol and Ls surfactants (60, 61, 62).

The work is still fruitful in the supercritical area, the past and prospective work has been reviewed by Goetheer et al. (30). There are reviews in applications in

polymerization, synthesis and mechanism (53), in green chemical synthesis and processing (4), environmental implications (87), industrial applications, possible trends of supercritical technology, and economic issues (73). In conclusion, today's and future investigation is focused in answering the question, whether the use of $scCO_2$ can create new products, eliminate waste, save energy and/or enhance safety to the point where the cost of the products are reduced and a more sustainable process is created.

References

1. Abbott, A. P.; Corr, S.; Durling, N. E.; Hope, E. G. Hydrogen Bond Interactions in Liquid Supercritical Hydrofluorocarbons. *J. Phys. Chem. B* **2003**, 107, 10628-10633.

2. Ayala, G. A.; Kamat, S.; Beckman, E. J.; Rusell, A. J. Solubilization and Activity of Proteins in Compressible-Fluid Based Microemulsions. *Biotech. Bioeng*. **1992**, 39, 806.

3. Bartscherer, K. A.; Minier, M.; Renon, H. Microemulsions in Compressible Fluids--A Review. *Fluid Phase Equilib.* **1995**, 107, 93-150.

4. Beckman, E. J. Supercritical and Near-Critical CO_2 in Green Chemical Synthesis and Processing. *J. Supercrit. Fluids* **2004**, 28, 121-191.

5. Blitz, J. P.; Yonker, C. R.; Smith, R. D. Infrared Spectroscopic Studies of Supercritical Fluid Solutions. *J. Phys. Chem*. **1989**, 93, 6661-6665.

6. Bristow, S.; Shekunov, B. Y.; York, P. Solubility Analysis of Drug Compounds in Supercritical Carbon Dioxide Using Static and Dynamic Extraction Systems. *Ind. Eng. Chem. Res*. **2001**, 40 (7), 1732-1739.

7. Bulgarevich, D. S.; Sako, T.; Sugeta, T.; Otake, K.; Takebayashi, Y.; Kamizawa, C.; Horikawa, Y.; Kato, M. The Role of General and Hydrogen-Bonding Interactions in the Solvation Processes of Organic Compounds by Supercritical CO_2/n-Alcohol Mixtures. *Ind. Eng. Chem. Res*. **2002**, 41 (9), 2074-2081.

8. Cason, J. P.; Khambaswadkar, K.; Roberts, C. B. Supercritical Fluid and Compressed Solvent Effects on Metallic Nanoparticle Synthesis in Reverse Micelles. *Ind. Eng. Chem. Res*. **2000**, 39 (12), 4749-4755.

9. Cason, J. P.; Roberts, C. B. Metallic Copper Nanoparticle Synthesis in AOT Reverse Micelles in Compressed Propane and Supercritical Ethane Solutions. *J. Phys. Chem. B* **2000**, 104 (6), 1217-1221.

10. Clarke, M. J.; Harrison, K. L.; Johnston, K. P.; Howdle, S. M. Water in Supercritical Carbon Dioxide Microemulsions: Spectroscopic Investigation of a New Environment for Aqueous Inorganic Chemistry. *J. Am. Chem. Soc.* **1997**, 119 (27), 6399-6406.

11. Consani, K. A.; Smith, R. D. Observations on the Solubility of Surfactants and Related Molecules in Carbon Dioxide at 50°C. *J. Supercrit. Fluids* **1990,** 3 (2), 51-65.

12. da Rocha, S. R. P.; Harrison, K. L.; Johnston, K. P. Effect of Surfactants on the Interfacial Tension and Emulsion Formation Between Water and Carbon Dioxide. *Langmuir* **1999**, 15, 419-428.

13. da Rocha, S. R. P.; Johnston, K. P. Interfacial Thermodynamics of Surfactants at the CO_2-Water Interface. *Langmuir* **2000**, 16, 3690-3695.

14. Dardin, A.; DeSimone, J. M.; Samulski, E. T. Fluorocarbons Dissolved in Supercritical Carbon Dioxide. NMR Evidence for Specific Solute-Solvent Interactions. *J. Phys. Chem. B* **1998**, 102, 1775-1780.

15. Dickson, J. L.; Psathas, P. A.; Salinas, B.; Ortiz-Estrada, C.; Luna-Barcena, G.; Hwang, H. S.; Lim, K. T.; Johnston, K. P. Formation and Growth of Water-in-CO_2 Miniemulsions. *Langmuir* **2003**, 19 (12), 4895-4904.

16. DuPont ™ Zonyl ® FSN Fluorosurfactant; http://www.dupont.com/zonyl/catalog.html

17. Eastoe, J.; Bayazit, Z.; Martel, S.; Steytler, D. C.; Heenan, R. K. Droplet Structure in a Water-in-CO_2 Microemulsion. *Langmuir* **1996**, 12, 1423-1424.

18. Eastoe, J.; Cazelles, B. M. H.; Steytler, D. C.; Holmes, J. D.; Pitt, A. R.; Wear, T. J.; Heenan, R. K. Water-in-CO_2 Microemulsions Studies by Small-Angle Neutron Scattering. *Langmuir* **1997**, 13 (26), 6980-6984.

19. Eastoe, J.; Dupont , A.; Steytler, D. C. Fluorinated surfactants in supercritical CO_2. *Current Opinion in Coll. Interface Sci.* **2003**, 8, 267–273.

20. Eastoe, J.; Paul, A.; Downer, A.; Steytler, D. C.; Rumsey, E. Effects of Fluorocarbon Surfactant Chain Structure on Stability of Water-in-Carbon Dioxide Microemulsions. Links between Aqueous Surface Tension and Microemulsion Stability. *Langmuir* **2002**, 18, 3014-3017.

21. Eastoe, J.; Paul, A.; Nave, S.; Steytler, D. C.; Robinson, B. H.; Rumsey, E.; Thorpe, M.; Heenan, R. K. Micellization of Hydrocarbon Surfactants in Supercritical Carbon Dioxide. *J. Am. Chem. Soc.* **2001**, 123, 988-989.

22. Fink, D.; Hancu, D.; Valentine, R.; Beckman, E. J. Toward the Development of "CO_2-philic" Hydrocarbons. 1. Use of Side-Chain Functionalization to Lower the Miscibility Pressure of Polydimethylsiloxanes in CO_2. *J. Phys. Chem. B* **1999**, 103, 6441-6444.

23. Fulton, J. L.; Johnston, K. P. Reverse Micelles and Microemulsions Phases in Supercritical Fluids. *J. Phys. Chem*. **1988**, 92(10), 2903-2907.

24. Fulton, J. L.; Pfund, D. M.; McClain, J. B.; Romack, T. J.; Combes, J. R.; Maury, E. E.; Samulski, E. T.; DeSimone, J. M.; Capel, M. Aggregation of Amphiphilic Molecules in Supercritical Carbon Dioxide: A Small Angle X-ray Scattering Study. *Langmuir* **1995**, 11 (11), 4241-4249.

25. Fulton, J. L.; Yee, G. G.; Smith, R. D. Hydrogen Bonding of Methyl Alcohol-*d* in Supercritical Carbon Dioxide and Supercritical Ethane Solution. *J. Am. Chem. Soc*. **1991**, 113, 8327-8334.

26. Gale, R. W.; Fulton, J. L.; Smith, R. D. *J. Am. Chem. Soc*. **1987**, 109, 920-921.

27. García, J. E. "*The Solubility of Acetaminophen, Ibuprofen, and Naproxen in Supercritical Carbon Dioxide*." MS Thesis, University of Puerto Rico, **1998**.

28. Ghenciu, E. G.; Beckman, E. J. Affinity Extraction into Carbon Dioxide. 1. Extraction of Avidin Using a Biotin-Functional Fluoroether Surfactant. *Ind. Eng. Chem. Res*. **1997**, 36 (12), 5366-5370.

29. Ghenciu, E. G.; Russell, A. J.; Beckman. E. J.; Steele, L.; Becker, N. T. Solubilization of Subtilisin in CO_2 Using Fluoroether-Functional Amphiphiles. *Biotech. Bioeng*. **1998**, 58 (6), 572-580.

30. Goetheer, E. L. V.; Vorstman, M. A. G.; Keurentjes, J. T. F. Opportunities for Process Intensification Using Reverse Micelles in Liquid and Supercritical Carbon Dioxide. *Chem. Eng. Sci.* **1999**, 54, 1589-1596.

31. Gupta, R. B.; Combes, J. R.; Johnston, K. P. Solvent Effect on Hydrogen Bonding in Supercritical Fluids. *J. Phys. Chem*. **1993**, 97, 707-715.

32. Harrison, K. L.; Johnston, K. P.; Sanchez, I. C. Effect of Surfactants on the Interfacial Tension Between Supercritical Carbon Dioxide and Polyethylene Glycol. *Langmuir* **1996**, 12 (11), 2637-2644.

33. Heitz, M. P.; Carlier, C.; deGrazia, J.; Harrison, K. L.; Johnston, K. P.; Randolph, T. W.; Bright, F. V. Water Core within Perfluoropolyether-Based Microemulsions Formed in Supercritical Carbon Dioxide. *J. Phys. Chem. B* **1997**, 101, 6707-6714.

34. Hoefling, T. A.; Beitle, R. R.; Enick, R. M.; Beckman, E. J. Design and Synthesis of Highly CO_2-Soluble Surfactants and Chelating Agents. *Fluid Phase Equilib.* **1993**, 83, 203-212.

35. Hoefling, T. A.; Enick, R. M.; Beckman, E. J. Microemulsions in Near-Critical and Supercritical CO_2. *J. Phys. Chem.* **1991**, 95 (19), 7127-7129.

36. Hoefling, T. A.; Newman, D. A.; Enick, R. M.; Beckman, E. J. Effect of Structure on the Cloud-Point Curves of Silicone-Based Amphiphiles in Supercritical Carbon Dioxide. *J. Supercrit. Fluids* **1993**, 6 (3), 165-171.

37. Hoefling, T. A.; Stofesky, D.; Reid, M.; Enick, R. M.; Beckman, E. J. The Incorporation of a Fluorinated Ether Functionality into a Polymer or Surfactant to Enhance CO_2-Solubility. *J. Supercrit. Fluids* **1992**, 5 (4), 237-241.

38. Holmes, J. D.; Steytler, D. C.; Rees, G. D.; Robinson, B. H. Bioconversions in a Water-in-CO_2 Microemulsion. *Langmuir* **1998**, 14, 6371-6376.

39. Holmes, J. D.; Ziegler, K. J.; Audriani, M.; Lee, C. T.; Bhargava, P. A.; Steytler, D. C.; Johnston, K. P. Buffering the Aqueous Phase pH in Water-in CO_2 Microemulsions. *J. Phys. Chem. B* **1999**, 103 (27), 5703-5711.

40. Ikushima, Y. Supercritical Fluids: An Interesting Medium for Chemical and Biochemical Processes. *Adv. Coll. Interface Sci.* **1997**, 71-72, 259-280.

41. Ikushima, Y.; Saito, N.; Arai, M. Supercritical Carbon Dioxide as Reaction Medium: Examination of its Solvent Effects in the Near-Critical Region. *J. Phys. Chem.* **1992**, 96 (5), 2293-2297.

42. Jacobson, G. B.; Lee, Jr. C. T.; Johnston, K. P. Organic Synthesis in Water/Carbon Dioxide Microemulsions. *J. Org. Chem.* **1999**, 64, 1201-1206.

43. Jacobson, G. B.; Lee, Jr., C. T.; da Rocha, S. R. P.; Johnston, K. P. Organic Synthesis in Water/Carbon Dioxide Emulsions. *J. Org. Chem.* **1999**, 64, 1207-1210.

44. Jacobson, G. B.; Lee, T. Jr.; Johnston, K. P.; Tumas, W. Enhanced Catalyst Reactivity and Separations Using Water/Carbon Dioxide Emulsions. *J. Am. Chem. Soc.* **1999**, 121 (50), 11902-11903.

45. Jara-Morante, E. "*The Solubility of Imipramine HCl in Supercritical Carbon Dioxide.*" MS Thesis, University of Puerto Rico, **1999**.

46. Ji, M.; Chen, X.; Wai, C. M.; Fulton, J. L. Synthesizing and Dispersing Nanoparticles in Water-in-Supercritical Carbon Dioxide Microemulsions. *J. Am. Chem. Soc.* **1999**, 121, 2631-2632.

47. Johnston, K. P.; Harrison, K. L.; Clarke, M. J.; Howdle, S. M.; Heitz, M. P.; Bright, F. V.; Carlier, C.; Randolph, T. W. Water-in-Carbon Dioxide Microemulsions: An Environment for Hydrophiles Including Proteins. *Science* **1996**, 271, 624-626.

48. Kamlet, M. J.; Abboud, J-L. M.; Abraham, M. H.; Taft, R. W. Linear Solvation Energy Relationships. 23. A Comprehensive Collection of the Solvatochromic Parameters, π^*, α, and β, and Some Methods for Simplifying the Generalized Solvatochromic Equation. *J. Org. Chem.* **1983**, 48, 2877-2887.

49. Kane, M. A.; Baker, G. A.; Pandey, S.; Bright, F. V. Performance of Cholesterol Oxidase Sequestered within Reverse Micelles Formed in Supercritical Carbon Dioxide. *Langmuir* **2000**, 16, 4901-4905.

50. Kazarian, S. G.; Gupta, R. B.; Clarke, M. J.; Johnston, K. P.; Poliakoff, M. How Is Hydrogen-Bonding Influenced by Solvent Density?. The Spectroscopic Study and Modeling of the Interaction between a Proton Donor and Acceptor from the Gas Phase to Supercritical Fluid States. *J. Am. Chem. Soc.* **1993**, 115 (24), 11099-11109.

51. Kazarian, S. G.; Vincent, M. F.; Bright, F. V.; Liotta, C. L.; Eckert, C. A. Specific Intermolecular Interaction of Carbon Dioxide with Polymers. *J. Am. Chem. Soc.* **1996**, 118, 1729-1736.

52. Keiper, J. S.; Simham, R.; DeSimone, J. M. New Phosphate Fluorosurfactans for Carbon Dioxide. *J. Am. Chem. Soc.* **2002**, 124 (9), 1834-1835.

53. Kendall, J. L.; Canelas, D. A.; Young, J. L.; DeSimone, J. M. Polymerizations in Supercritical Carbon Dioxide; *Chem. Rev.* **1999**, 99 (2), 543-563.

54. Kim, S.; Johnston, K. P. Molecular Interactions in Dilute Supercritical Fluid Solutions. *Ind. Eng. Chem. Res*. **1987**, 26 (6), 1206-1213.

55. Lalanne, P.; Tassaing, T.; Danten, Y.; Cansell, F.; Tucker, S. C.; and Besnard, M. CO_2-Ethanol Interaction Studied by Vibrational Spectroscopy in Supercritical CO_2. *J. Phys. Chem. A* **2004**, 108 (14), 2617-2624.

56. Laurence, C.; Nicolet, P.; Dalati, T.; Abboud, J-L. M.; Notario, R. The Empirical Treatment of Solvent-Solute Interactions: 15 Years of π*. *J. Phys. Chem.* **1994**, 98, 5807-5816.

57. Lee Jr., C. T.; Bhargava, P.; Johnston, K. P. Percolation in Concentrated Water-in-Carbon Dioxide Microemulsions. *J. Phys. Chem. B* **2000**, 104, 4448-4456.

58. Lee Jr., C. T.; Psathas, P. A.; Johnston, K. P.; deGrazia J.; Randolph, T. W. Water-in-Carbon Dioxide Emulsions: Formation and Stability. *Langmuir* **1999**, 15 (20), 6781-6791.

59. Li, H.; Zhang, X.; Han, B.; Liu, J.; He, J.; Liu, Z. Effect of Phase Behavior and Pressure on the Constant-Volume Heat Capacity and Intermolecular Interaction of CO_2 ± Ethanol and CO_2 ± n-Pentane Mixtures in the Critical Region. *Chem. A. Eur. J.* **2002**, 8 (2), 451-456.

60. Liu, J.; Han, B.; Li, G.; Zhang, X.; He, J.; and Liu, Z. Investigation of Nonionic Surfactant Dynol-64 Based Reverse Microemulsions Formed in Supercritical Carbon Dioxide. *Langmuir* **2001**, 17, 8040-8043.

61. Liu, J.; Han, B.; Wang, Z.; Zhang, J.; Li, G.; Yang, G. Solubility of Ls-36 and Ls-45 Surfactants in Supercritical CO_2 and Loading Water in the CO_2/Water/Surfactant Systems. *Langmuir* **2002**, 18 (8), 3086-3089.

62. Liu, J.; Han, B.; Zhang, J.; Li, G.; Zhang, X.; Wang, J.; Dong, B. Formation of Water-in-CO_2 Microemulsions with Non-fluorous Surfactant Ls-54 and Solubilization of Biomacromolecules. *Chem. A. Eur. J.* **2002**, 8 (6), 1356-1360.

63. Liu, Z.; Can Erkey, C. Water in Carbon Dioxide Microemulsions with Fluorinated Analogues of AOT. *Langmuir* **2001**, 17, 274-277.

64. Loeker, F.; Marr, P. C.; Howdle, S. M. FT-IR Analysis of Water in Supercritical Carbon Dioxide Microemulsions Using Monofunctional Perfluoropolyether Surfactants. *Colloids and Surfaces A: Physicochem. Eng. Aspects* **2003**, 214, 143-150.

65. Mawson, S.; Yates, M. Z.; O'Neill, M. L.; Johnston, K. P. Stabilized Polymer Microparticles by Precipitation with a Compressed Fluid Antisolvent. 2. Poly(propylene oxide)-and Poly(butylene oxide)-Based Copolymers. *Langmuir* **1997**, 13, 1519-1528.

66. McFann, G. J.; Johnston, K. P.; Howdle, S. M. Solubilization in Nonionic Reverse Micelles in Carbon Dioxide. *AIChE J.* **1994**, 40 (3), 543-555.

67. Meredith, J. C.; Johnston, K. P.; Seminario, J. M.; Kazarian, S. G.; Eckert, C. A. Quantitative Equilibrium Constants between CO_2 and Lewis Bases from FT-IR Spectroscopy. *J. Phys. Chem.* **1996**, 100, 10837-10848.

68. Mertdogan, C. A.; Byun, H. S.; McHugh, M. A.; Tuminello, W. H. Solubility of Poly(tetrafluoroethylene-co-19 mol % hexafluoropropylene) in Supercritical CO_2 and Halogenated Supercritical Solvents. *Macromolecules* **1996**, 29, 6548-6555.

69. Meziani, M. J.; Sun, Y. Spectrophotometry Study of Aqueous Salt Solution in Carbon Dioxide Microemulsions. *Langmuir* **2002**, 18, 3787-3791.

70. Niemeyer, E. D.; Bright, F. The pH within PFPE Reverse Micelles Formed in Supercritical CO_2. *J. Phys. Chem. B* **1998**, 102, 1474-1478.

71. O'Neill, M. L.; Cao, Q.; Fang, M.; Johnston, K. P.; Wilkinson, S. P.; Smith, C. D.; Kerschner, J. L.; Jureller, S. H. Solubility of Homopolymers and Copolymers in Carbon Dioxide. *Ind. Eng. Chem. Res.* **1998**, 37, 3067-3079.

72. O'Shea, K. E.; Kirmse, K. M.; Fox, M. A.; Johnston, K. P. Polar and Hydrogen-Bonding Interactions in Supercritical Fluids. Effects on the Tautomeric Equilibrium of 4-(Phenylazo)-1-naphthol. *J. Phys. Chem.* **1991**, 95 (20), 7863-7867.

73. Perrut, M. Supercritical Fluid Applications: Industrial Developments and Economic Issues. *Ind. Eng. Chem. Res.* **2000**, 39, 4531-4535.

74. Poliakoff, M.; Howdle, S. M.; Kazarian, S. G. Vibrational Spectroscopy in Supercritical Fluids: From Analysis and Hydrogen Bonding to Polymers and Synthesis. *Angew. Chem. Int. Ed. Engl.* **1995**, 1275-1295.

75. Porschmann, J.; Blasberg, L.; Mackenzie, K.; Harting, P. Application of Surfactants to the Supercritical Fluid Extraction of Nitroaromatic Compounds from Sediments. *J. Chromatography A* **1998**, 816, 221-232.

76. Pulido-Ayazo, J. C. "*The Solubility of Anti-Cancer and Anti-AIDS Drugs in Supercritical Fluids.*" MS Thesis, University of Puerto Rico, **2003**.

77. Rosen, M. J. *Surfactants and Interfacial Phenomena*, New York-Wiley, **1978.**

78. Sagisaka, M.; Yoda, S.; Takebayashi, Y.; Otake, K., et.al. Preparation of W/scCO$_2$ Microemulsions Using Fluorinated Surfactants. *Langmuir* **2003**, 19, 220-225.

79. Sarbu, T.; Styranec, T. J.; Beckman, E. J. Design and Synthesis of Low Cost, Sustainable CO_2-philes. *Ind. Eng. Chem. Res.* **2000**, 39(12), 4678-4683.

80. Senapati, S.; Keiper, J. S.; DeSimone, J. M.; Wignall, G. D.; Melnichenko, Y. B.; Frielinghaus, H.; Berkowitz, M. L. Structure of Phosphate Fluorosurfactant Based Reverse Micelles in Supercritical Carbon Dioxide. *Langmuir* **2002**, 18, 7371-7376.

81. Shim, Jae-Jim; Yates, M. Z.; and Johnston, K. P. Latexes Formed by Rapid Expansion of Polymer/CO_2 Suspensions into Water. 1. Hydrophilic Surfactant in Supercritical CO_2. *Ind. Eng. Chem. Res.* **2001**, 40 (2), 536-543.

82. Sigman, M. E.; Lindley, S. M.; Leffler, J. E. Supercritical Carbon Dioxide: Behavior of π^* and β Solvatochromic Indicators in Media of Different Densities. *J. Am. Chem. Soc.* **1985**, 107 (6), 1471-1472.

83. Singley, E. J.; Liu, W.; Beckman, E. J. Phase Behavior and Emulsion Formation of Novel Fluoroether Amphiphiles in Carbon Dioxide. *Fluid Phase Equilib.* **1997,** 128, 199-219.

84. Smith, R. D.; Fulton, J. L.; Blitz, J. P.; Tingey, J. M. Reverse Micelles and Microemulsions in Near-Critical and Supercritical Fluids. *J. Phys. Chem.* **1990**, 94, 781-787.

85. Suleiman, D.; Jara-Morante, E. Removal of Ethylene Glycol from HES with Supercritical Fluid Carbon Dioxide. Technical Report, **2003**.

86. Webb, P. B.; Marr, P. C.; Parsons, A. J.; Gidda, H. S.; Howdle, S. M. Dissolving Biomolecules and Modifying Biomedical Implants with Supercritical Carbon Dioxide. *Pure Appl. Chem.* **2000**, 72 (7), 1347-1355.

87. Wells, S. L.; DeSimone, J. CO_2 Technology Platform: An Important Tool for Environmental Problem Solving. *Angew. Chem. Int. Ed.* **2001**, 40 (3), 518-527.

88. Westwood, S. A. In *Supercritical Fluid Extraction and its Use in Chromatographic Sample Preparation*. 1st edition, **1993.**

89. Winsor, P. A. *Trans. Faraday Soc*. **1948**, 44, 376-398.

90. Yano, J.; Füredi-Milhofer, H.; Wachtel, E.; Garti, N. Crystallization of Organic Compounds in Reversed Micelles. II. Crystallization of Glycine and l-Phenylalanine in Water-Isooctane-AOT Microemulsions. *Langmuir* **2000**, 16(26), 10005-10014.

91. Yazdi, A. V.; Lepilleur, C.; Singley, E. J.; Liu, W.; Adamsky, F. A.; Enick, R. M.; Beckman, E. J. Highly Carbon Dioxide Soluble Surfactants, Dispersants and Chelating Agents. *Fluid Phase Equilib.* **1996**, 117, 297-303.

92. Yee, G. G.; Fulton, J. L.; Smith, R. D. Aggregation of Polyethylene Glycol Dodecyl Ethers in Supercritical Carbon Dioxide and Ethane. *Langmuir* **1992**, 8 (2), 377-384.

93. Yee, G. G.; Fulton, J. L.; Smith, R. D. Fourier Transform Infrared Spectroscopy of Molecular Interactions of Heptafluoro-1-butanol or 1-Butanol in Supercritical Carbon Dioxide and Supercritical Ethane. *J. Phys. Chem*. **1992**, 96 (15), 6172-6181.

94. Yonker, C. R.; Frye, S. L.; Kalkwarf, D. R.; Smith, R. D. Characterization of Supercritical Fluid Solvents Using Solvatochromic Shifts. *J. Phys. Chem*. **1986**, 90, 3022-3026.

95. Yonker, C. R.; Smith, R. D. Solvatochromic Behavior of Binary Supercritical Fluids: The Carbon Dioxide/2-Propanol System. *J. Phys. Chem*. **1988**, 92, 2374-2378.

96. Yonker, C. R.; Smith, R. D. Solvatochromism: A Dielectric Continuum Model Applied to Supercritical Fluids. *J. Phys. Chem*. **1988**, 92, 235-238.

97. Zhang, X.; Gao, L.; Liu, Z.; He, J.; Zhang, J.; Han, B. Effect of Size and Polarity of Solutes on Partial Molar Volumes and Intermolecular Interaction in Supercritical Fluids. *J. Supercrit. Fluids* **2002**, 23, 233–241.

98. Zielinski, R. G.; Kline, S. R.; Kaler, E. W.; Rosov, N. A Small-Angle Neutron Scattering Study of Water in Carbon Dioxide Microemulsions. *Langmuir* **1997**, 13, 3934-3937.

CHAPTER 2

Techniques, Materials and Experimental Set-up

An electronic radiation is a transverse energy wave that is composed of an oscillated electric field component and an oscillating magnetic field component. These components are orthogonal to each other, and orthogonal to the direction of propagation of the wave, as well. A wave is characterized by a wavelength (λ), which is the physical length of one complete oscillation, and the frequency (v), which is the number of oscillations per second. The electromagnetic radiation is classified according its λ, and v; the molecular effects on the matter are different depending on the electromagnetic wave used. The nomenclature used for the electromagnetic spectrum is presented in Figure 2-1.

Wavelength λ [nm]		Energy [kcal/mol]	Molecular Effects
High frequency shorter λ $\quad$ 10^{-9}	Gamma rays	10^6	
10^{-7}	X rays	10^4	Ionization
	Vacuum UV	10^2	
10^{-5}	Near UV		Electronic transitions
10^{-4}	Visible	10	
10^{-3}	Infrared (IR)	1	Molecular vibration
10^{-1}	Microwave	10^{-2}	Rotational motion
10^2	Radio	10^{-4}	
Lower frequency Longer λ $\quad$ 10^4		10^{-6}	Nuclear spin transition
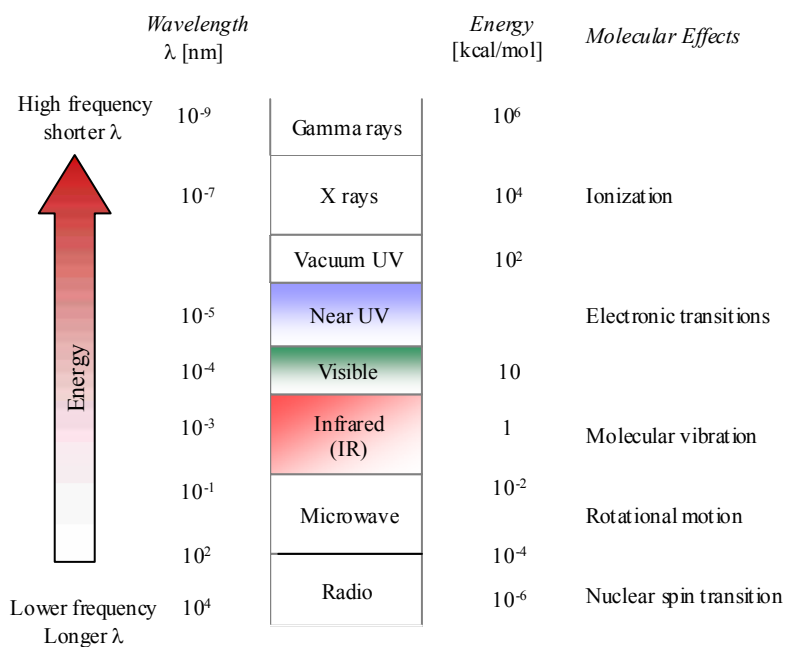
Figure 2-1: Electromagnetic spectrum (19).

According to the quantum theory (1), the frequency is proportional to its energy so that

$$E = h \times v \times c$$

where:

    h: Planck's constant (6.62391×10^{-27} erg-sec)

    v: frequency (cm^{-1})

    c: 2.997930×10^{10} cm/sec

This investigation employed primarily spectroscopic (UV-Vis and IR) techniques. The local chemical microenvironment (e.g., dipolarity/polarizability) can only be studied using molecular probes with UV-Vis spectroscopy that enable the detection of electronic transitions. Molecular interactions are studied using FT-IR spectroscopy.

2.1 The Ultraviolet-Visible Spectroscopy

Ultraviolet-Visible spectroscopy (UV=200–400 nm, Visible=400–800 nm) corresponds to electronic excitations between the energy levels that correspond to the molecular orbital of the systems. In particular, transitions involving π orbitals and lone pairs (n= non-bonding) are important, and therefore UV-Vis spectroscopy is of most use for identifying conjugated systems which tend to have stronger absorptions. Ultraviolet (UV) spectroscopy uses electron transitions to determine bonding patterns.

The lowest energy transition that can occur is between the highest occupied molecular orbital (HOMO) and the lowest unoccupied molecular orbital (LUMO) in the ground state. The absorption of the electromagnetic radiation excites an electron from the HOMO to the LUMO and creates an excited state. The more highly conjugated the system, the smaller the HOMO-LUMO gap (ΔE), and therefore the lower the frequency and longer the wavelength, λ. The unit of the molecule that is responsible for the absorption is called the chromophore, of which the most common are C=C ($\pi \to \pi^*$) and C=O ($n \to \pi^*$) systems.

There are several types of electronic transitions: $\sigma \to \sigma^*$ (alkanes), $\sigma \to \pi^*$ (carbonyl compounds), $\pi \to \pi^*$ (alkenes, carbonyl compounds, alkynes, and azo compounds), $n \to \sigma^*$ (oxygen, nitrogen, sulfur, and halogen compounds), $n \to n^*$ (carbonyl compounds) (18).

σ→σ* Transitions

An electron in a bonding σ orbital is excited to the corresponding anti-bonding orbital. The energy required is large. For example, methane (which has only C-H bonds, and can only undergo $\sigma{\rightarrow}\sigma^*$ transitions) shows an absorbance maximum at 125 nm. Absorption maxima due to $\sigma{\rightarrow}\sigma^*$ transitions are not seen in typical UV-Vis. spectra (200–700 nm).

n→σ Transitions*

Saturated compounds containing atoms with lone pairs (non-bonding electrons) are capable of $n{\rightarrow}\sigma^*$ transitions. These transitions usually need less energy than $\sigma{\rightarrow}\sigma^*$ transitions and therefore occurs at a short wavelength. They can be initiated by light whose wavelength is in the range 150–250 nm. A disadvantage in study compounds having this type of chromospheres is that the relatively weak bands tend to be obscured by other more active absorbing groups. This is particularly evident in the case of ≡C–O–, ≡C–Halogenated–, and ≡C–N< functional groups. The number of organic functional groups with $n{\rightarrow}\sigma^*$ peaks in the UV region is small. Those comprise alcohols, ethers, sulphides, amines, alkyl halides, ozonides and peroxides.

n→π and π→π* Transitions*

Most absorption spectroscopy of organic compounds is based on transitions of n or π electrons to the π^* excited state. This is because the absorption peaks for these transitions fall in an experimentally convenient region of the UV-Vis range spectrum (200–700 nm).

The solvent in which the absorbing species is dissolved also has an effect on the spectrum of the species. Peaks resulting from $n{\rightarrow}\pi^*$ transitions are shifted to shorter wavelengths (blue shift) with increasing solvent polarity. This arises from increased solvation of the lone pair, which lowers the energy of the n orbital. Often (but not always), the reverse (i.e., red shift) is seen for $\pi{\rightarrow}\pi^*$ transitions. This is caused by attractive polarization forces between the solvent and the solute, which lower the energy

levels of both the excited and unexcited states. This effect is greater for the excited state, and so the energy difference between the excited and unexcited states is slightly reduced resulting in a small red shift. This effect also influences $n \rightarrow \pi^*$ transitions, but it is overshadowed by the blue shift resulting from solvation of lone pairs.

The basic optical configuration for UV-Vis is presented in Figure 2-2. The double monochromator instrument is generally used for applications in which a high degree of photometric accuracy and repeatability is required.
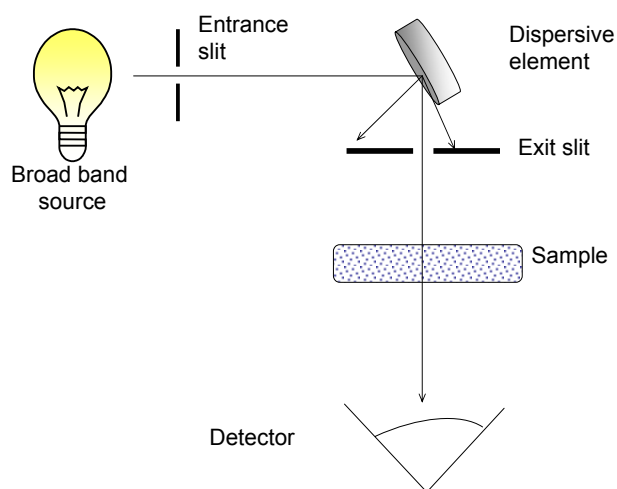
Figure 2-2: Ultraviolet-Visible basic configuration (20).

Most instrumentation used to measure the region from 190–2500 nm utilizes a combination of quartz Tungsten-halogen lamp for the visible and near-infrared regions (350–2500 nm), and a DC deuterium lamp for the ultraviolet region (190–350 nm).

2.2 The Infrared Spectroscopy

Infrared (IR) spectroscopy measures the bond vibration frequencies in a molecule and it is used to determine the functional groups.

The infrared light comprises several regions, which are described in Table 2-1.

Table 2-1: Infrared region (17)

	Wavelength [nm]	Wavenumber [cm^{-1}]
Limit on red light	800	12500
Near infrared	800–2500	12500–4000
Mid infrared	2500–25000	4000–400
Far infrared	25000–10000	400–10

The energy of radiation of the infrared region is of the same order of magnitude as rotation and vibration energies of molecules; consequently, strong interactions between infrared radiation and matter can be expected. When a beam of infrared radiation of certain frequency hits a molecule, two situations can exist. If the vibration of the molecule differs in frequency from that of the incident radiation, no interaction takes place. However, if the molecule vibrates with the same frequency from that of the incident, it can absorb a certain amount of energy and rise to a higher energy level (excited state). This transition is quantized and results in an increase of the amplitude of the vibration. The absorbed energy is the difference between the energies of the two levels, and plotting this energy against the frequency or the wavenumber one obtains the absorption spectrum of the substance.

Classical electrodynamics and modern quantum theory show that the interaction of radiation and matter, resulting either in absorption or emission of energy, is possible only when a dipole moment variation is involved. Consequently, only vibrations or rotations of the molecule resulting in a change in the dipole moment are infrared active. All other are infrared inactive and can be observed by Raman spectroscopy. Molecular spectra enable the direct derivation of discrete energy levels of a molecule. From these levels one can obtain detailed information about the motions of electrons and nuclei in the molecule. The study of electronic motions provides the theoretical background for the understanding of chemical valence. From the vibrational frequencies one can calculate with great accuracy the forces between the atoms in a molecule and the heat of

dissociations of molecules. From the rotational frequencies one can calculate the intermolecular distances and obtain accurate information about molecular geometry. Together with other new methods (e.g., microwave spectroscopy, UV, NMR, MS, etc) infrared spectroscopy is a powerful tool in organic and physical-organic chemistry.

A basic IR spectrophotometer has the elements described in Figure 2-3.
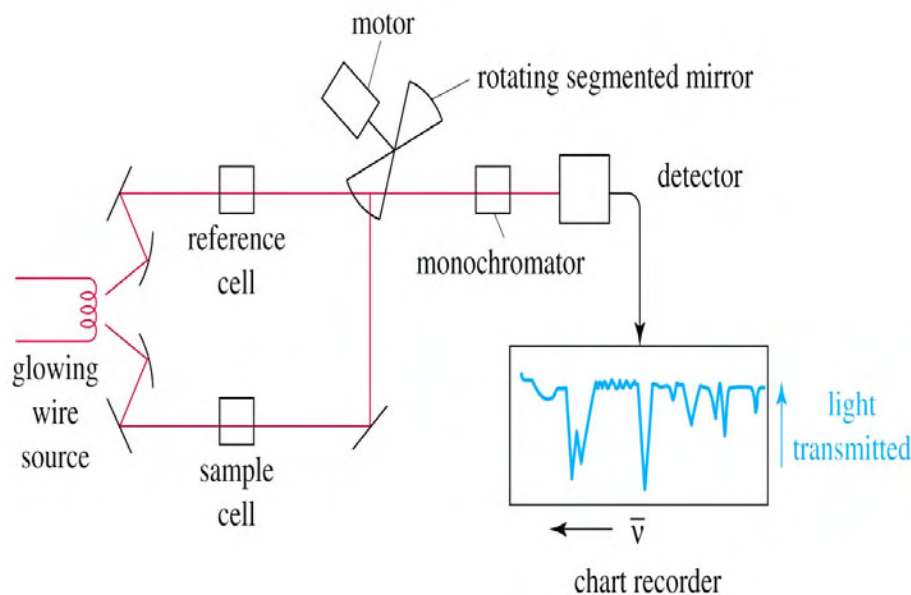
Figure 2-3: Basic configuration of IR spectrophotometer (19).

All IR spectrometers have a source of infrared radiation which is usually some solid material heated to incandescence by an electric current. The Nernst Glower is a source composed mainly of oxides of rare earths such as zirconium, yttrium and the Globar is a silicon carbide rod. Other materials have been used as well. All these sources are fairly efficient emitters of infrared radiation and approach the energy distribution of a black body. Most IR sources are operated at a temperature where the energy maximum is near the short wavelength limit of the spectrum.

The infrared detector is a device that measures the infrared energy of the source which has passed through the spectrometer. In one way or another, these devices change

radiation energy into electrical energy which can be processed to generate a spectrum. There are two basic types: thermal detectors and selective detectors.

In a dispersive instrument, the device that analyzes the radiation to evaluate the intensity for each wavelength resolution is namely a monochromator, and in a Fourier Transform instruments it is done by interferometers.

In a Fourier Transform Infrared (FT-IR), a Michelson interferometer consists of two plane mirrors, one fixed and one moveable, and a beam splitter. The radiation from the source is made parallel and strikes the beam splitter at 45°, transmitting half of the radiation and reflecting the other half. The biggest advantage that the FT spectrometers have over dispersive spectrometers is the large signal-to-noise ratio. In a dispersive instrument the intensity of each resolution element of wavelength is measured one by one in sequence and only a small spectral range falls on the detector at any one time. In a FT-IR instrument the detector measures the intensities of all the resolution elements simultaneously. This advantage is most useful when spectral energy available is low, or when large scale expansion is needed to record very weak bands, in addition the spectra can be recorded in less time (4).

FT-IR is a powerful analytical technique for bulk characterization that can give us specific information from organic materials (surface composition and vibrational structure).

The common materials used for the windows for UV-Vis and IR spectroscopy are summarized in Table 2-2, also with their respective spectroscopic properties.

Table 2-2: Windows spectroscopic properties (20)

Material	Wavelength [nm]	Wavenumber [cm^{-1}]	Refractive Index	Technique
Al_2O_3 (Sapphire)	200–6500	50000–1538	1.76	UV-Vis
ZnS (Zinc Sulfide)	570–14700	17000–680	2.26	IR
BaF_2 (Barium fluoride)	200–11500	50000–870	1.46	IR

The design of the high pressure cell needed for a particular IR experiment clearly

depends on the nature of the experiment, the temperature, the maximum operating pressure, the optical pathlength, the particular range of the IR, which will restrict the choice of windows, and finally whether the content of the cell needed to be stirred. The main challenge to apply this technique with SCF's is the high pressures that the cell should be able to resist. As far as we know there are a few cells which are commercially available, which a rating pressure less than 300 bar. In general the weakest part of the IR cell are the transparent windows, also the sealing of these windows to the cell body is usually a difficult engineering task. Because it is known that SCF's can cause swelling in some polymers, thus it is important to select carefully and adequately the materials of what the seals are made of. An interesting summary of the characteristics of the high-pressure IR cell designed and principal considerations to take account is presented by Poliakoff et al. (12).

2.3 Experimental Set-up

The UV-Vis experiments were performed in the experimental set up described in Figure 2-4.
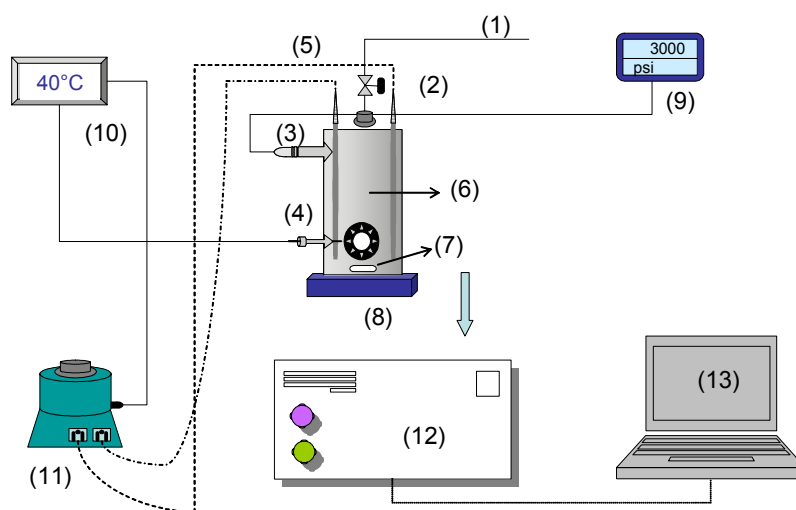
Figure 2-4: UV-Vis experimental set-up.

The UV-Vis spectroscopy set up consists of the following elements:

(1) CO_2 admission tubing connected to a syringe pump (Isco Inc. Model 260D)

(2) High Pressure valve and cap

(3) Transducer connection

(4) Thermocouple

(5) Heating elements

(6) Stainless steel cell

(7) Magnetic stirrer

(8) Hot plate

(9) Transducer

(10) Temperature display

(11) Power supply for heating elements

(12) UV-Vis spectrophotometer

(13) Acquisition data computer

The same configuration is kept for the FT-IR experiments the only difference is the cell that is used for the spectroscopic measurements, which is described in Figure 2-5.
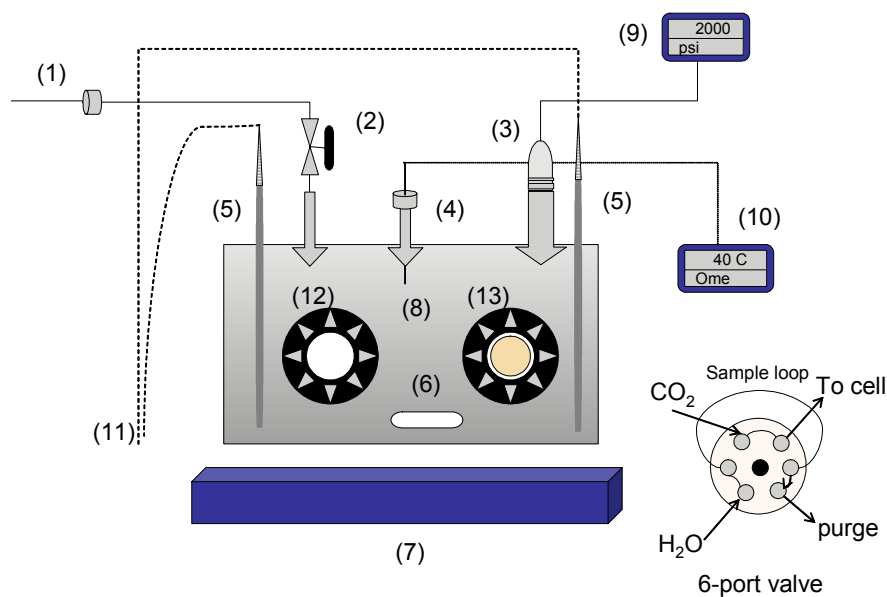
Figure 2-5: IR-UV-Vis high pressure cell.

This configuration comprises the next elements:

(1) CO_2 admission tubing from syringe pump

(2) High pressure valve

(3) Transducer connection

(4) Thermocouple

(5) Heating elements

(6) Magnetic stirrer bar

(7) Hot plate

(8) Stainless steel cell

(9) Pressure display

(10) Temperature display

(11) Connection to power supply for heating elements

(12) Sapphire windows for UV-Vis spectrophotometer

(13) BaF_2 windows for IR spectrophotometer

When H_2O addition experiments were carried out, a 6-port valve (Valco Instruments

Co. Inc.) with a 50 μL, and 250 μL sample loop was connected after the high pressure valve.

The experimental set up for the extraction of Ethylene Glycol from Hydroxyl ethyl starch (HES) can be seen in Figure 2-6

The set up's components are:

(1) CO_2 from tank

(2) Cosolvent from deposit

(3) Te of mixing

(4) Cosolvent syringe pump

(5) CO_2 syringe pump

(6) Dual pump controller

(7) Extraction cell

    (7.a) Glass wool fiber

    (7.b) Solute

(8) Extraction camera

(9) Bifurcation Tee

(10) Thermo Nicolet FT-IR

(11) Acquisition data computer

(12) Expansion nozzle
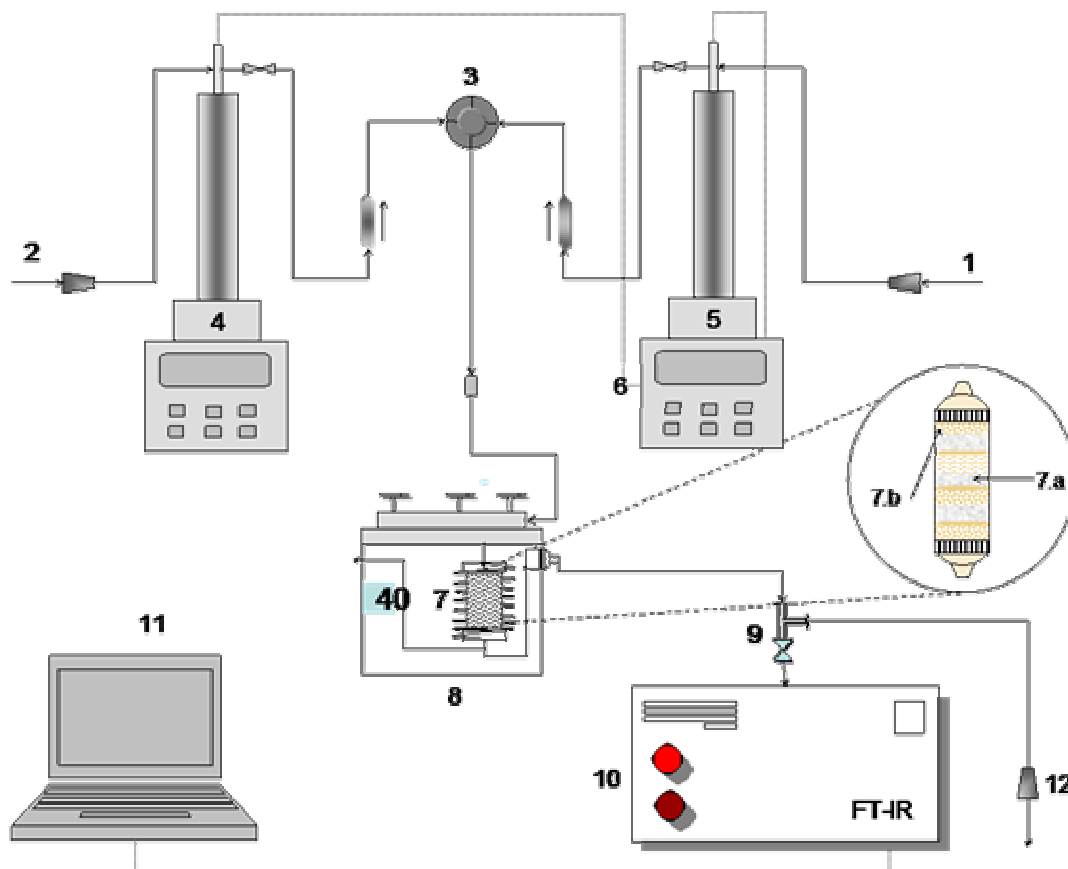
Figure 2-6: Ethylene Glycol extraction experimental set-up.

The specifications of the syringe pump and the camera of extraction are depicted elsewhere (9), the FT-IR is connected on line to the high pressure IR cell and a capillary restrictor is used for the decompression.

2.4 Experimental Procedures

2.4.1. UV-Vis Spectroscopy

The UV-Vis studies were performed in a spectrophotometer (Hewlett-Packard 8450, Agilent Technologies Inc., CA, 1nm resolution and less than ±0.2 nm wavelength accuracy) using a stainless steel high-pressure homemade cell of 8.5 cm^3 volume with

2.33 cm pathlength. The sapphire windows were sealed with thinner Teflon O-rings. Temperature was measured with a thermocouple (Omega Inc., CT) connected to a heater and control set up. The cell was pressurized using a syringe pump (Isco Inc.) and a pressure transducer (up to 3300 psig range) was used to measure the pressure in the cell.

For all the experiments, the concentration in the cell was 1.13% PL92 (with respect to scCO$_2$ at 72 bar), 40 μL water and 0.1 mg of indicator. In a typical experiment, the indicator in solution of methanol was loaded into the cell; then the methanol was evaporated in vacuum. After evaporated the methanol, the cell was heated up to the set temperature, once the temperature was equilibrated, H$_2$O and surfactant were loaded and the cell was properly closed. The air was extracted with a vacuum pump and the cell filled with scCO$_2$; mixing was achieved with a magnetic stirrer. Measurements were taken during stirring, because the spectrum showed unstable once it was stopped. At least three measurements were done for each condition, at different time intervals.

For experiments with the other surfactants, the high-pressure sample cell used for these studies was made of titanium and the sapphire windows sealed with gold metal O-rings. The cell was 13 cm^3 volume and 2.54 cm path length. For each surfactant: PL31, P17R2, Gele, and Zonyl the concentration was 0.42% (with respect to scCO$_2$ at 83 bar), 0.25% (91 bar), and 1.2% (75 bar) respectively at 308.15 K respectively. The indicator dissolved in methanol was loaded into the cell. The methanol was evaporated before the run after applying a vacuum to the system. The quantity of indicator remaining in the cell was 0.1 mg, and the quantity of H$_2$O was 48 μL.

2.4.2. FT-IR Spectroscopy

We used an 82.5 cm^3 stainless steel high-pressure cell, with two types of windows BaF$_2$ for IR, and sapphire for UV-Vis. Every window was sealed to the cell with thin aluminum o-rings and Teflon seals. The pathlength measured of the UV-windows is 5 cm. The FT-IR used was a Vector 22 (Bruker) spectrophotometer. 64 scans were taken with a resolution of 2 cm^{-1}. The OPUS spectrophotometer software was used for data

handling. The experimental set-up is shown in Figure 2-4 and the cell is presented in Figure 2-5. In an experimental procedure, first the cell was heated up to 40°C, then the surfactant, H_2O, and solute were loaded to the cell, and closed properly. Once the air was extracted from the cell with a vacuum pump, CO_2 was added, until high pressure was achieved. The cell was stirred at all the times while it was pressurized. It was also stirred for approximately 1 hour before the IR spectrums were taken assuring in this way that the thermodynamic equilibrium (temperature, pressure, and concentration) was achieved. Using the same cell, the UV spectrums were taken to detect the drug in the UV-Vis spectrometer. For the H_2O addition experiments, a 6-port switching valve was connected to the cell with a sample loop of 50 μL, and 250 μL.

2.4.3. Supercritical Fluid Extraction

We used a supercritical extractor adequate for this kind of processes. The polymer (HES) was supplied by BBRAUN PR and the analysis of the final product was done in B BRAUN Crissier Switzerland.

The experimental set up is showed in Figure 2-6. The extraction with $scCO_2$ pure was described elsewhere (9), for all the experiments dynamic extractions was performed. The extraction time, depending on the flow used ranges from 2 to 5 hours. For the cosolvent-$scCO_2$ extraction, two syringe pumps were used one was loaded with cosolvent and the other with CO_2. These pumps are adequately controlled with a single controller unit which regulates the flow of both fluids (CO_2 and cosolvent) into the extraction chamber. Previously to the extraction the cell was prepared loading with 2.55±0.14 g of HES supported in glass wool fiber, simulating a distillation column. This distribution was determined to be adequate to avoid channeling and minimizing the mass transfer limitations. Then, the cell was put on the extraction chamber which was already heated to the extraction temperature. Same considerations stated for any $scCO_2$ extraction were taken to assure thermodynamic equilibrium (9). For the decompression we used a capillary restrictor but previous to the restrictor a bifurcation Tee was connected. A nearby valve allowed to the extraction fluid to flow into the FT-IR cell and therefore be

able to take the spectrum every time it was required.

When a surfactant was used static extractions were performed, approximately 30 min were enough to fill up the extraction camera and allows contact between the load of the cell (HES and surfactant) and the $scCO_2$. The mixture HES-surfactant was prepared previously mixed with magnetic stirring. The same extraction procedure described above was followed.

2.5 Materials

In the following sections the materials used for our investigation are described. As previously stated, three commercial types of surfactants were used in this investigation. Each type of surfactant is described in detail ahead. The compounds employed for our investigation are a range of commercially known surfactants (e.g., pluronics, Zonyl, Glycolic acid), and pharmacological drugs of clinical and commercial interest.

2.5.1. Surfactants

2.5.1.1 Pluronics

The triblock copolymers poly(ethylene oxide)-block(propylene oxide)-block-poly(ethylene oxide) (PEO-PPO-PEO) are a commercially known class of surfactants, introduced by BASF in the early 1950s under the trade name of Pluronics. Their unique structure allows a novel approach in the design and application in the surface active agents. This has been given considerable attention owing to their applications in industry (i. e., detergents, stabilizers, emulsifiers, cosmetic, drug solubilization, protection of microorganisms from damage in bio-processing, and controlled release) and to their amphiphilic behavior in solutions. These properties lead to a self assembled structure in various environments. These triblocks copolymers and poly(ethylene glycol) alkyl ether nonionic surfactants posses the same hydrophilic moiety (PEO). The general characteristics of theses type of surfactants are given in Table 2-3.

Table 2-3: General characteristics of pluronic surfactants (5, 11)

Pluronic L31	
Chemical structure	
Formula	$(EO)_1(PO)_{16}(EO)_1$
Molecular weight	1056
	HLB: PEO/PPO = 100/950 Transparent viscous 1w% soluble in H_2O at 37°C
Pluronic L92	
Formula	$(EO)_8(PO)_{52}(EO)_8$
Molecular weight	3750
Characteristics	HBL: PEO/PPO = 748/2990 Transparent viscous 1w% soluble in H_2O at 26°C
Pluronic 17R2	
Chemical structure	
Formula	$(PO)_{15}(EO)_{10}(PO)_{15}$
Molecular weight	2125
Characteristics	HBL: PEO/PPO = 425/1700 Transparent viscous 1w% soluble in H_2O at 35°C

The most characteristic property of PEO-PPO-PEO block copolymer is the inverse temperature dependence of micellization (8). Depending upon the order of the hydrophilic and hydrophobic moieties, different types of pluronic are formed; these are the pluronic L and pluronic R surfactants. This configuration allows incremental alteration of both hydrophobic and hydrophilic moieties. In addition, heteric or alternating EO/PO structures can be introduced internally or at the end of the molecule.

Finally, total molecular weight can be varied. Their size and shape depends on: pressure, temperature, concentrations, additives, and block copolymer compositions. These nonionic surfactants may form micelles in non-polar solvents, and water addition plays a very important role in micellization. The micellization of these co-block polymers is very similar to the behavior of conventional surfactants, which follow a closed association mechanism with equilibrium between unimers and micelles.

Their main differences due to its structural differences are summarized in Table 2-4.

Table 2-4: Differences between pluronic surfactants type L and R (2)

Pluronic®	Pluronic R®
Better emulsifiers	Exhibit lower foaming
Better dispersants	Are better defoamers
Cover a broader range of molecular weight	Exhibit reduced gelling tendencies
Terminated by primary OH groups (higher reactivity and acidity)	Terminated by secondary OH groups (lower reactivity and acidity)

The solubility and phase behavior of these surfactants was studied in $scCO_2$ (11). For pluronic R series, the P17R2 is the most soluble in $scCO_2$ and results indicate that its solubility depend on the PEO block and the total copolymer molecular weight. The same trend solubility is followed by L type surfactants, and this order also depends on the increase in PPO block. It was seen that the location of the block copolymers influences the solubility in $scCO_2$, the terminal hydroxyl groups in the PPO outer blocks form weaker hydrogen bond than the hydroxyl groups in the PEO blocks. The solubility of PPO oligomers is significantly greater than PEO oligomers due to the steric and chemical effects of the added methyl substitute to the PEO backbone.

2.5.1.2 Gele

The principal characteristics of this surfactant are summarized in Table 2-5.

Table 2-5: General characteristics of Gele surfactant (14)

Glycolic acid Ethoxylate Lauryl Ether CAS 27306-90-7	
Chemical structure	
Formula	$C_{14}H_{26}O_2(EO)_{2-5}$ (x=11–13, y≈2-5)
Molecular weight	≈ 360
	Stabilizer for emulsions and non sensitive to hard water n^{20}/D: 1.45 (lit) Fp: >230°F Density: 1 g/mL

2.5.1.3 Zonyl

The trade name Zonyl refers to a group of fluorinated alkanes with ethylene oxide head-groups, which constitute the hydrophilic portion of the surfactant, and a linear fluorinated hydrocarbon that constitute the hydrophobic part.

The general characteristics can be seen in Table 2-6.

Table 2-6: General characteristics of Zonyl surfactant (6)

	Zonyl FSO-100 fluorosurfactant CAS 101027-76-3
Chemical structure	$F-(CF_2-CF_2)_3-(CH_2-CH_2O)_{10}-(CH_2-CH_2O)-H$
Formula	$C_6H(EO)_{11}F_{13}$
Molecular weight	≈ 950
Characteristics	Nonionic surfactant. Turbid liquid n^{20}/D: 1.382 (lit) Fp: 72°F Density: 1.06 g/mL

Zonyl surfactants are of high performance wetting and leveling additives for paints, adhesive inks and other coatings. To effectively wet the substrate, the surface tension of the formulation must be lower than the surface energy of the substrate. This effect is

capable of creating low surface tension at low concentrations. It dramatically reduces surface tension in liquids, below levels possible using hydrocarbon or silicone surfactants alone. They are more effective in aqueous or solvent based systems, high and low pH system and powder and radiation cured coatings.

The properties of perfluorinated compounds are distinctly different from those of their analogous hydrocarbons due to the size and highly electronegative nature of the fluorine atom. The polarizability of CF_4 is 1.5 times larger than that of CH_4 because CF_4 has much higher electron density and somewhat longer bond lengths than CH_4. This higher polarizability is balanced by a large and very repulsive hard sphere potential. The large hard sphere effectively prevents induced dipoles from interacting at short distances where these forces are higher. For the higher perfluoroalkanes, the fluorocarbon chain is known to be much more rigid than an alkane chain. The physical properties of perfluorinatedalkanes for carbon number above 5 differ only slightly from those of their hydrocarbons.

Semifluorinated compounds formed by the replacement of one or more CH_2 or CH_3 groups with CF_2 or CH_3 groups can vary greatly from their hydrogenated analogous, specially in their contribution to the overall dipole moment of each unit of the molecular backbone. For n-perfluoroalkanes the replacement of all hydrogens by fluorines do not create a dipole in the molecule, and little change in the properties of the compound is observed. Placement of CF_2 or CF_3 group next to a CH_2 results in a strong electron withdrawing effect of the fluorinated group on the hydrogenated group creating a local dipole (e.g., the local dipole of CF_2CH_2 position makes possible a site for a weak intramolecular hydrogen bonded with the terminal OH group).

Specific solute-solvent molecular interactions between CO_2 and fluorinated compounds will cause red shifts of the vibrational bands. Based upon the regular solution theory, the underlying basis of the higher solubility of the perfluorinated compound is probably the high repulsive nature of the fluorine atoms that inhibits solute-solute induced dipole interactions (21). In general there are three mechanisms that enhance the

solubility of a fluorinated compound in a low dielectric constant fluid such as CO_2. Primarily the substitution of fluorinated methyl or ethyl groups can alter the chemical/physical properties of the new compound. Second, the repulsive properties of the fluorine atoms impart steric constrains which reduce the solute-solute and the aggregate-aggregate attractive interactions. Finally, the creation of new local dipole within the molecule around the CF_2- to CH_2 transition may provide a route for CO_2 quadrupole /solute dipole interactions leading to enhance the solubility.

Mixed fluorosurfactant/hydrocarbon surfactant systems can give impressive gains in the area of reducing foaming to improve dynamic surface tension. They also reduce and enhance fluorine efficiency, while being cost effective. Compared to their hydrogenated counterparts, fluorinated chains are more hydrophobic, which endows CF group stronger associative potential. As the associative ability is concerned, a CF_2 is equal to 1.7 CH_2 (22, 7). It was seen that switching the terminal group $H-CF_2-$ to CF_3-causes almost identical changes in critical micellar concentration

2.5.2. Pharmacological Drugs

The solutes used in this research are well known pharmacological drugs of commercial interest. The principal characteristics of acetaminophen and imipramine HCl are summarized in Table 2-7, and Table 2-8 respectively.

Table 2-7: General characteristics of acetaminophen (16)
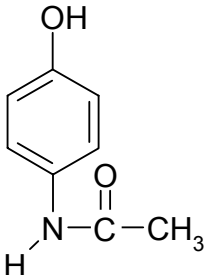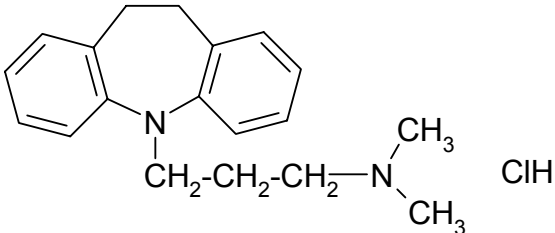
Acetaminophen CAS 103-90-2		
Chemical structure	Chemical name	N-Acetyl-4-aminophenol
	Trade name	Paracetamol
	Formula	$C_8H_9NO_2$
	Molecular weight	151.2
	Characteristics	Analgesic. Soluble: water slightly soluble. Ethanol, 50 mg/mL. DMSO, 5 M.

Table 2-8: General characteristics of imipramine HCl (16)

Imipramine HCl CAS 113-52-0	
Chemical structure	
Chemical name	10,11-Dihydro-N,N-dimethyl-5H-dibenz(b,f)azepine-5-propanamine hydrochloride
Trade name	Tofranil
Formula	$C_{19}H_{24}N_2 \bullet HCl$
Molecular weight	316.9
Characteristics	Tricyclic antidepressant. Color: white. Solubility: - Water 50 mg/mL.

The field of volume substitution (e.g. hemorrhagic shock) or hemodilution (e.g. arterial occlusive disease, Fontaine II B, III) is today inconceivable without the use of colloidal plasma substitutes. For both these indications, of the exogeneous plasma substitutes (starch, gelatins, dextran), Hydroxy Ethyl Starch (HES) has found the greatest acceptance in recent years. HES play an important role in many areas of medicine where they are mainly used as plasma volume expanders, and can be used also in dialysis. The lower disturbance of coagulation and the clearly reduced incidence of serious anaphylactoid reactions compared with dextran are responsible for the good acceptance of HES in the field of volume replacement and hemodilution. In addition, it has been possible to show that HES has a sufficient to good volume efficacy and a differentiated therapy being possible by using the various known HES preparations differing in molecular weight and substitution degree.

The methods to obtain HES (e.g., chemically, bio-chemically) yield a product having

a broad molecular weight distribution with a considerable proportions of low molecular compounds (e.g., glucose, maltose or oligosaccharides) and by-products (e.g., NaCl) or the enzyme used in the process. The starches with a high content of amylopectin, the highly branched component of starch (e.g., potatoes, wax maize starch or waxy rice starch) are preferable for obtain a desirable product. The important consideration to have an adequate product is to obtain a compound with a mean molecular weight of 60,000-600 000; thus, can be completely broken down within a physiologically reasonable time.

In this respect, only hydroxyethyl starches substituted predominantly in 6-position with a C_2/C_6 ratio of anhydroglucose units is 8-20 or being highly substituted were used for pharmaceutical purposes. These hydroxyethyl starches are made by reaction of wax maize starch with ethylene oxide. This process also employs 2-chloroethanol as hydroxyethylation agent. The hydroxyethylation is carried out under alkaline conditions at room temperature, the pH value held at a value of about 12 and the temperature held at a value of about 20°C (15).

2.5.3. Carbon Dioxide (CO_2)

The use of CO_2 as a solvent and raw material has been investigated continuously in academia and/or industry. CO_2 is promoted as a green solvent and its use in this role has spread throughout the chemical and research communities. Besides its environmental advantages CO_2 has chemical properties that provide its solvent qualities. Table 2-9, summarizes the principal properties of CO_2, which is the most common fluid used in supercritical technology.

Table 2-9: General characteristics of carbon dioxide (10)

Carbon dioxide CAS 124-38-9		
Chemical structure	Formula	CO_2
	Molecular weight	44.01
O=C=O	Characteristics	Indoor gas, slightly soluble in H_2O.
Physical properties (13)		
Critical temperature (K)		304.15
Critical pressure (bar)		73.8
Critical density (g/cm^3)		0.468
Polarizability (α cm^3)		27.6×10^{-25}
Permanent Dipole moment (μ D)		0.0
Quadrupole moment (Q erg$^{1/2}$-cm$^{5/2}$)		-4.3×10^{-26}
Dielectric constant		1.1–1.5

CO_2 has a low critical temperature, hence it makes possible to obtain liquid-like densities and by implication a liquid-like solvent characteristics at near room temperature. Due to its structural symmetry, CO_2 does not have a dipole moment, the relatively large electronegative oxygen atoms bestow to the molecule an especially large quadrupole moment. This quadrupole moment operates over a much shorter distance than dipolar interactions, and it is the responsible for its high critical pressure (compared with analogous alkanes like ethane that has a similar molecular weight and critical temperature, fluoroalkane, and hydroalkane). Initially, the solvent power calculated by $\delta=1.25[Pc^{1/2}]$ (Hildebran parameter) was over-predicted, but CO_2 has chemical properties that makes a versatile and useful material when is used strategically.

The non-polar nature of CO_2, is reflected in the value of its polarizability, which is similar to methane, a very non-polar SCF. The quadrupolar nature of scCO_2 works against it, to dissolves solutes with non-polar repeated segments; since, quadrupole interactions dominate the interchange energy as the temperature is lowered. scCO_2 is expected to be a weak solvent for solutes with a large dipole moment, where the interchange energy is expected to be dominated by solute-solute interactions rather than solute-CO_2 interactions. Consequently, it is necessary for hydrocarbons solutes and

copolymers to have some polarity to be dissolved by $scCO_2$.

CO_2 can not be oxidized, because it is produced by complete oxidation of organic compounds, thus it is one of the very few organic solvents that could be considered for the direct reaction of H_2 and O_2 to form H_2O_2.

CO_2 is an aprotic solvent therefore it can be used in process where labile protons could interfere with it. Due to CO_2 is also immune to free radical and does not support chain transfer is useful in polymerization reactions.

CO_2 is miscible in gases at all proportions above 304 K. Liquid and $scCO_2$ can absorbs much higher quantities of H_2 and O_2 than typical organic solvents or H_2O. Due to its high diffusivities, we can eliminate the mass transfer limitations of gas into the liquid phase. It is important to mention that the total miscibility is only with gases that exhibit critical temperature $\leq$ 304 K (e.g., H_2, O_2, CO).

The addition of CO_2 to a mixture of fluorinated solvents and low molecular weight organic materials can create an homogeneous single phase, at moderate pressures, while the decompression returns to a two phase system.

CO_2 exhibit low viscosity (1/10 of H_2O), thus the Reynolds number are high. Therefore, CO_2 has higher fluidity than conventional solvents. This low viscosity accompanied with its liquid-like density permit CO_2 an excellent heat transfer capacity.

The lower surface tension of CO_2 than conventional organic solvents, permit the CO_2 be able to penetrate easily in complex geometries better than simple liquids, and also solutes would be expected to diffuse faster within catalyst pores.

CO_2 is benign solvent and cross-contamination of the other phase, especially in liquid-liquid extraction, does not exist.

CO_2 can be used as diluent in reactions, especially in H_2-O_2 mixture, where the CO_2 expands the non explosive regime in the gas phase. As an example, Dupont's scientists discovered that the addition of CO_2 to tetrafluoro ethylene (TFE) enhances the stability of the monomer and inhibit the runaway decomposition, hence the explosion of the monomer. The CO_2-TFE mixture constitutes an atypical azeotrope mixture that persists,

unlike other azeotropes, over a wide range of concentration. This reason, that obviously enhances the safety production, spurs Dupont to construct a polymerization plant employing CO_2 as solvent for the production of fluoropolymers.

Against the advantages mentioned above, CO_2 has also disadvantages, but depending on the process where it is employed they can be somehow helpful. CO_2 has a lower dielectric constant, which means a low solvent power, thus it is not a good solvent for many polar molecules. The thermodynamic interaction between CO_2 and methylene groups is not favorable, thus, ethane is better solvent for hydrocarbons.

CO_2 is a Lewis acid and will react with strong bases (e.g., amines, phosphines, and alkylanions) forming carbamates, they can alter the solubility characteristic of the solutes. While alkyl-funcional primary and secondary amines react readily with CO_2, tertiary amines are not reactive. However, the presence of electron withdrawing groups in close proximity to the nitrogen atom (as in aniline) prevents formation of carbamates. CO_2 reacts also with metal alkoxides, metal alkyl and metalhydrides, also reacts reversibly with some enzymes and leads to a low activity, but this can be hinder by the formation of carbamates.

Anionic polymerizations can not be conducted in CO_2, because CO_2 reacts with carbanions to form relatively unreactive carboxylates. In Ziegler-type reactions polymerizations CO_2 poisons the catalyst, terminating the reaction. In the presence of H_2O, CO_2 forms H_2CO_3 with a pH 2.88, this can be detrimental for biomolecules and thus enzymatic reactions. In the other hand, this can be useful in the extraction of contaminants from steel waste into H_2O. Therefore, depending on the circumstance this can be an advantage or disadvantage, because the low pH of H_2O in contact with CO_2 enhances the back extraction of caffeine in decaffeination process (3).

References

1. Avram, M.; Mateescu, G.H. Infrared Spectroscopy. Applications in Organic Chemistry. Wiley-Interscience. **1972**.

2. BASF Corporation; http://www.basf.com/businesses/chemicals/performance/database

3. Beckman, E. J. Supercritical and Near-critical CO_2 in Green Chemical Synthesis and Processing. *J. Supercrit. Fluids* **2004**, 28, 121-191.

4. Colthup, N. B.; Daly, L. H.; Wiberley, S. E. Introduction to Infrared and Raman Spectroscopy, Academic Press Inc. **1964**.

5. da Rocha, S. R. P.; Harrison, K. L.; Johnston, K. P. Effect of Surfactants on the Interfacial Tension and Emulsion Formation Between Water and Carbon Dioxide. *Langmuir* **1999**, 15, 419-428.

6. DuPont ™ Zonyl ® FSN Fluorosurfactant; http://www.dupont.com/zonyl/catalog.html

7. Eastoe, J.; Paul, A.; Rankin, A.; Wat, R. Fluorinated Nonionic Surfactants Bearing Either CF3- or H-CF2- Terminal Groups: Adsorption at the Surface of Aqueous Solutions. *Langmuir* **2001**, 17 (25), 7873-7878.

8. Guo, C.; Wang, J.; Liu, H.; Chen, J. Hydration of Conformation of Temperature-Dependent Micellization of PEO-PPO-PEO Block Copolymers in Aqueous Solutions by FT-Raman. *Langmuir* **1999**, 15 (8), 2703-2708.

9. Jara-Morante, E. *"The Solubility of Imipramine HCl in Supercritical Carbon Dioxide,"* MS Thesis, University of Puerto Rico, **1999.**

10. NIST Webbook; http://www.nist.gov/

11. O'Neill, M. L.; Cao, Q.; Fang, M.; Johnston, K. P.; Wilkinson, S. P.; Smith, C. D.; Kerschner, J. L.; Jureller, S. H. Solubility of Homopolymers and Copolymers in Carbon Dioxide. *Ind. Eng. Chem. Res.* **1998,** 37, 3067-3079.

12. Poliakoff, M.; Howdle, S. M.; Kazarian, S. G. Vibrational Spectroscopy in Supercritical Fluids: From Analysis and Hydrogen Bonding to Polymers and Synthesis. *Angew. Chem. Int. Ed. Engl.* **1995**, 1275-1295.

13. Prausnitz, J. M.; Lichtenthaler, R. N.; Gomez de Azevedo, E. G. Molecular Thermodynamics of Fluid-Phase Equilibria. Second edition, Prentice-Hall Inc. **1986**.

14. Sigma-Aldrich; http://www.sigma-aldrich.com

15. Sommermeyer, K. Procedure for Preparation of Hydroxyethyl Starch with Hydrolytically Adjusted Molecular Weight. Ger. Offen. DE 10140594 A1 6 Mar **2003**. Patent CA.

16. Stecher, P. G.; The Merck Index. An Encyclopedia of Chemicals and Drugs. Rahway, N. J. Merck **1968**. 8[Th] Ed. Paul G. Stecher, editor.

17. Tanner, P. A.; http://www.personal.cityu.edu.hk/~bhtan.

18. Unknown. http://www.chem.vt.edu/chem-ed/courses/spec/intro/em-rad.html

19. Wade, Jr. L. G. *Organic Chemistry*, 5th Edition. Prentice Hall **2003**.

20. Workman, J. Jr. UV-Vis-NIR Spectroscopy in Applied Spectroscopy: A Compact Reference for Practitioners. Academic Press., **1998**, 31.

21. Yee, G. G.; Fulton, J. L.; Smith, R. D. Fourier Transform Infrared Spectroscopy of Molecular Interactions of Heptafluoro-1-butanol or 1-Butanol in Supercritical Carbon Dioxide and Supercritical Ethane. *J. Phys. Chem*. **1992**, 96 (15), 6172-6181.

22. Zhuang, D. Q.; Cao, Y.; Zhang, H. D.; Yang, Y. L.; Zhang, Y. X. Interaction of Fluorocarbon and Hydrocarbon Hydrophobically co-modified PAA with a Nonionic Surfactant: Rheological Properties of Polymer Solutions in the Absence of Salt. *Polymer* **2002**, 43, 2075-2084.

CHAPTER 3

Ultraviolet-Visible Spectroscopy

Solvatochromism is defined as the phenomenon that UV-Vis absorption spectra of some molecules are highly sensitive to the surrounding medium, and the position of maximum is believed to indicate certain solvent properties, such as polarity or hydrogen-bonding. The effect of a given solvent on the course of a chemical or physical change is usually rationalized in terms of the solvent's polarity. The Hydrogen bonding causes the solvatochromic shift through the large bulk dielectric constant, among solvent molecules and through the specific solute-solvent hydrogen bonding interactions.

Kamlet-Taft solvent parameters (α, β, $\pi*$, and others) are one of the important approaches in achieving insight into solvent strength for pure SCFs and mixtures (16). The $\pi*$ scale is an index of solvent dipolarity/polarizability, which measures the ability of a solvent to stabilize a charge or a dipole, by virtue of its dielectric effects. The α scale of solvent hydrogen bond-donor acidities (HBD), describes the ability of a solvent to donate a proton in a solvent to solute hydrogen bonding. The β scale of hydrogen bond-acceptor (HBA), provides a measure of the solvent's ability to accept a proton (donate an electron pair), in a solvent to solute hydrogen bond. This scale has also been used to evaluate hydrogen bonding acceptor strength of solid HBA bases dissolved in non-HBA solvents.

The $\pi*$, α and β parameters are related through a schematic equation in the form of the linear solvation energy relationship (LSER) (12) such as the following:

$$XYZ \;=\; XYZ_0 \;+\; s\pi* \;+\; a\alpha \;+ b\beta \qquad\qquad (3\text{-}1)$$

where:

XYZ: solvent property.

XYZ_0: solvent property in a reference solvent.

a, b, s: susceptibility constants from linear regressions.

The same relationship is obtained for shift absorption maxima of a variety of

indicators solutes in a range of solvents, such that:

$$\nu_{max} = \nu_0 + s\pi^* + a\alpha + b\beta \qquad (3\text{-}2)$$

where:

ν_{max} : wavenumber of the absorbance maxima in the test solvent

ν_0: wavenumber of the absorbance maxima in the reference solvent usually cyclohexane.

3.1 Indicator

The π^* scale for solvents was based on the treatment of the solvatochromic shifts undergone by selected electronic absorption bands of a variety of "molecular probes". These probes were aromatic molecules, mostly of the A-C_6H_4-D type (Figure 3-1), where A and D stands for electron- acceptor (such as NO_2) and electron-donor (such as $N(CH_3)_2$) respectively.
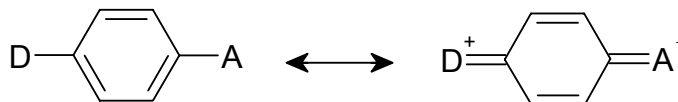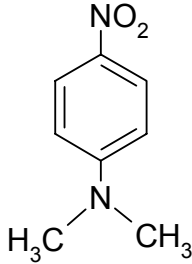

Figure 3-1: Solvatochromic shift of molecular probes.

The indicator used for our work was N,N-dimethyl-p-nitroaniline. Its general characteristics can be seen in Table 3-1. It is a derivative of 4-nitroaniline, and has been known to show a large solvatochromic shift, because of its large dipole moment and significantly different energy between the ground and excited states. N,N-dimethyl-p-nitroaniline is quite sensitive to non-specific medium effects and it is not appreciably affected by band shape problems. The Figure 3-2 shows the ground and excited state of the indicator. Studies reflect that the stabilization of the excited state is through hydrogen bonding association with the solvent, as a complex structure.

Table 3-1: Characteristics of N,N-dimethyl-4-nitroaniline

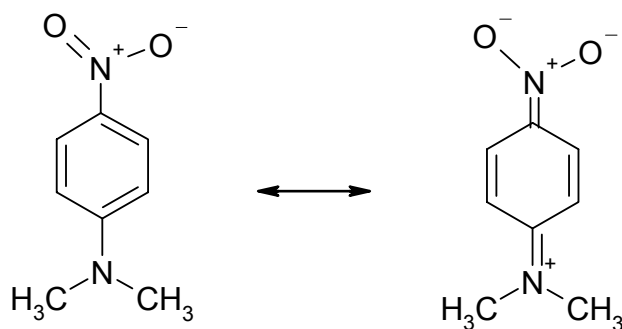| Chemical structure		
	Chemical name	N, N-dimethyl-4-nitroaniline
	Formula	$C_8H_{10}N_2O_2$
	CAS	100-23-2
	Molecular weight	166.18
	Characteristics	Yellow powder λ_{max}: 550, 450 nm

Figure 3-2: Ground and excited state of the indicator.

When placed in a medium with HB capabilities (e.g., H_2O), the kind of specific interactions that can form are depicted in the Figure 3-3. Many authors (19) have pointed out that the type A hydrogen bond with the amino nitrogen does not cause the spectral shift; therefore, in our case when H_2O will be added to the $scCO_2$, there is only one type of hydrogen bond to be considered; the one placed in one of the nitro oxygen. The capacity of the indicator to form type B-hydrogen bond is suppressed due to the presence of the CH_3^- group, interaction that is possible in nitroaniline.
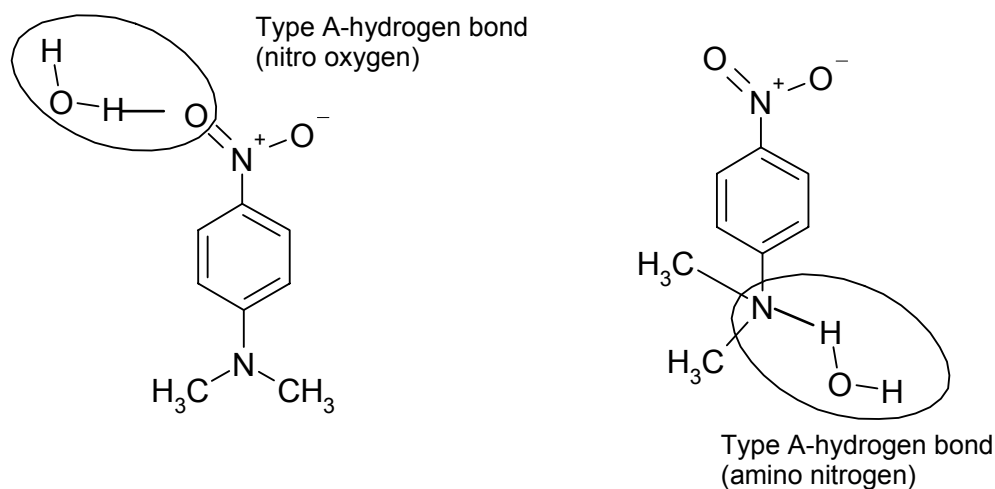
Figure 3-3: Specific interactions of the indicator.

The UV-Vis spectrum of our indicator dissolved in diethyl ether $((C_2H_5)_2O)$, acetonitrile (CH_3CN), and water (H_2O) can be seen in Figure 3-4b. The solvatochromic shift ($\nu_{max}=10^7/\lambda_{max}$) correlated with the parameter π^* (Figure 3-4a) shows the behavior of our indicator in different microenvironments (14). The frequency at maximum absorbance shifts to lower energies (red-shifts) as the polarizability/dipolarity of the solvents increases, due in part by specific hydrogen bonding interactions, (notice the large shift when the indicator is dissolved in water).
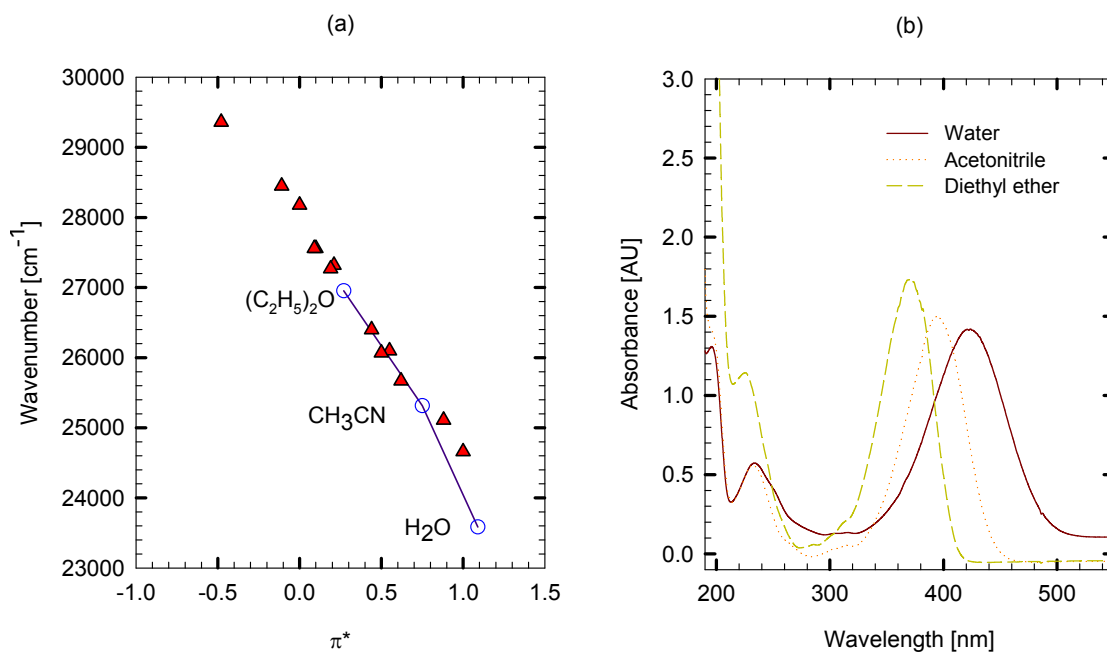
Figure 3-4: Behavior of the indicator in different solvents.

For this indicator, the value of the susceptibility constants (equation 3-1) was obtained by measuring its absorption spectra in 16 solvents of different polarity and solvent type (1). Those results were correlated in the form of the linear solvation energy relationship (3-3) and the following equation was obtained:

$$\nu_{max} = 27956 - 562\alpha - 3326\pi^* \qquad r^2=0.95 \qquad (3\text{-}3)$$

The shifts measured for the three solvents correlate extremely well with this equation with only a 0.30% of error.

According to the Kamlet-Taft scale of solvent dipolarity/polarizability, applicable to solvent-solute system where no specific interactions occur (e.g., hydrogen bonding or charge-transfer effects), π^* is defines as:

$$\pi^* = \frac{(\nu_{max} - \nu_0)}{s} \qquad (3\text{-}4)$$

Whenever specific solvent-solute interactions (such as hydrogen bonding) are excluded, medium effects on the frequencies of the maxima of the solvatochromic bands

of any two indicators are linearly related to a high degree of precision, the π^* value can be obtained by equation 3-5, this equation holds for all non-hydrogen bond donor solvents and up to the gas phase.

$$\pi^* = \frac{(\nu_{max} - \nu_{c-C_6H_{12}})}{(\nu_{DMSO} - \nu_{c-C_6H_{12}})} \qquad (3\text{-}5)$$

where:

$$\nu_{c-C_6H_{12}} = 28.18 \times 10^3 \text{ cm}^{-1}$$

$$\nu_{DMSO} = 24.66 \times 10^3 \text{ cm}^{-1} \ (14)$$

These solvents are used as reference by taking $\pi^*(c\text{-}C_6H_{12}) = 0$ and $\pi^*(DMSO) = 1$ by definition.

3.2 Indicator-scCO$_2$

The interest in supercritical solvents in many processes (e.g., extraction, chromatography, and chemical reactions) has stimulated interest in the relationship between density and the solvent properties of these fluids. Yonker et al. (28), have adopted the Kamlet-Taft π^* polarity scale and applied it to a wide range of SCF's at various temperatures and pressures. These studies have shown that solvent-solute interactions cause an increase in the local solvent density surrounding the solute. This phenomenon has also been confirmed using dynamics simulations and integral calculation (25).

Most studies have been carried out with less polar solvents such as CO_2 and NO_2, where the contribution of hydrogen bonding to solvent polarity is small and both behave similarly. The quantification of the hydrogen bond acceptor property (β parameter) of scCO$_2$ measured by Sigman et al. (24), was found to be small and invariant with pressure.

Figure 3-5a shows the absorbance of indicator in scCO$_2$ and Figure 3-5b the solvatochromic shift of the spectrum, both in terms of pressure at three temperatures; the UV spectrums are shown in the Appendix A.
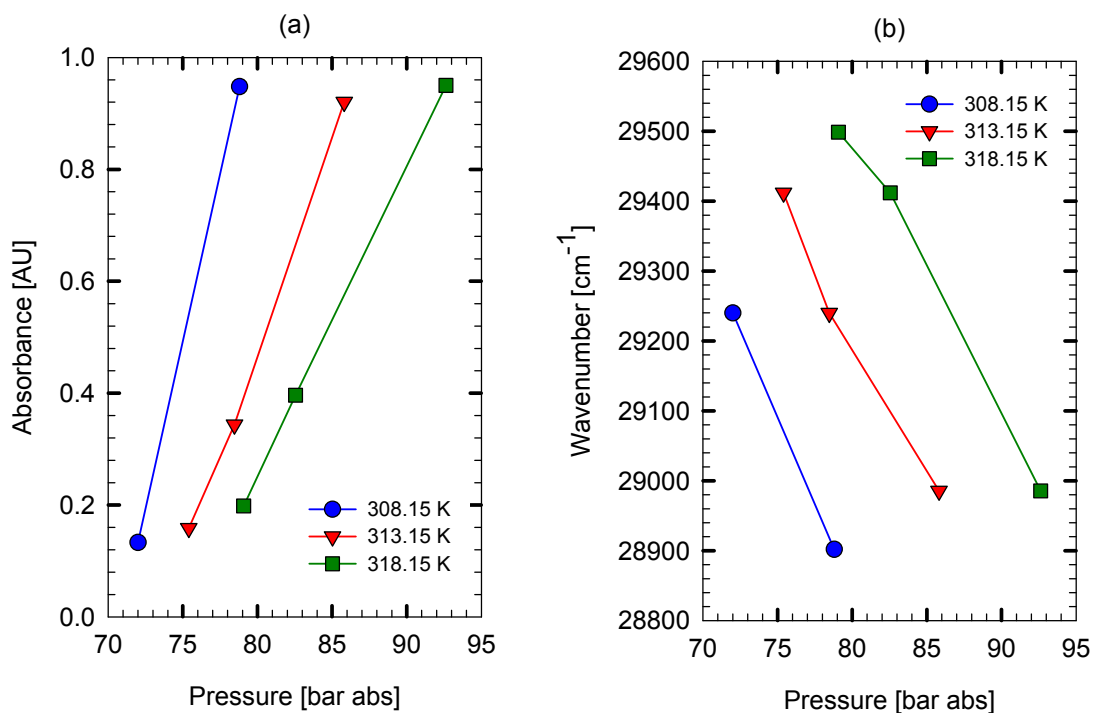
Figure 3-5: Absorbance and wavenumber as function of pressure (Indicator-scCO$_2$).
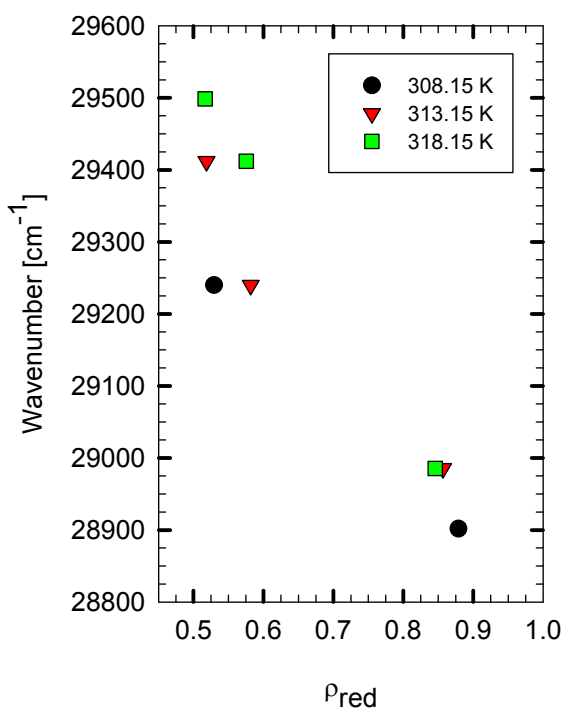

Figure 3-6: Wavenumber vs. reduced density.

The red shift indicates a $\pi \rightarrow \pi^*$ transition absorbance band of C=C that is stabilized by dipole-induced-dipole forces as the dipolarity/polarizability of the solvents increases; this trend is apparent for aprotic liquid solvents at ambient temperature. Although the isotherms differ by 5°C only, there are clear differences among them. The solute stabilizes at higher energy at 318.15 K than 308.15 K; however the optical density is higher at low temperature, maybe because the

dielectric constant for $scCO_2$ decreases with increasing temperature. The variation of the wavenumber with reduced density for $scCO_2$ is depicted in the Figure 3-6. At low ρ_r (<0.8), we can see a linear dependency but above it the tendency seems to change. There is no fix point where this change occurs, this depends on the kind of system formed (e.g., attractive, or non- attractive solutions). The more attractive the system, the lower the ρ_r where this change occurs. As many authors have pointed out, this trend is a result of the quadrupole moment of CO_2, and a proper behavior for solvents having higher order multipoles (e.g., CO_2).

The π^* values can be obtained from the equation 3-5 and its behavior with pressure can be seen in the Figure 3-7. The π^* varies linearly and proportional with pressure, but π^* decreases as temperature increases.

Figure 3-7: Dipolarity/polarizability vs.pressure.

According the equation 3-4, for non-hydrogen bonding solvents there is a linear variation between the π^* and $(\nu_{max}-\nu_0)$ where the slope represent the susceptibility value. If we correlate linearly our data we obtain a value equal to -3333.33. This value is close to that reported by Abbot et al. (1) (-3326).

The models for dipole solvation can be microscopic or macroscopic. The macroscopic model is related to the continuum model dipole solvation similar to that proposed by Onsager (27). This model recognizes no specific solvent molecule or localization of solvent structure and assumes no differences in solvent orientation close to
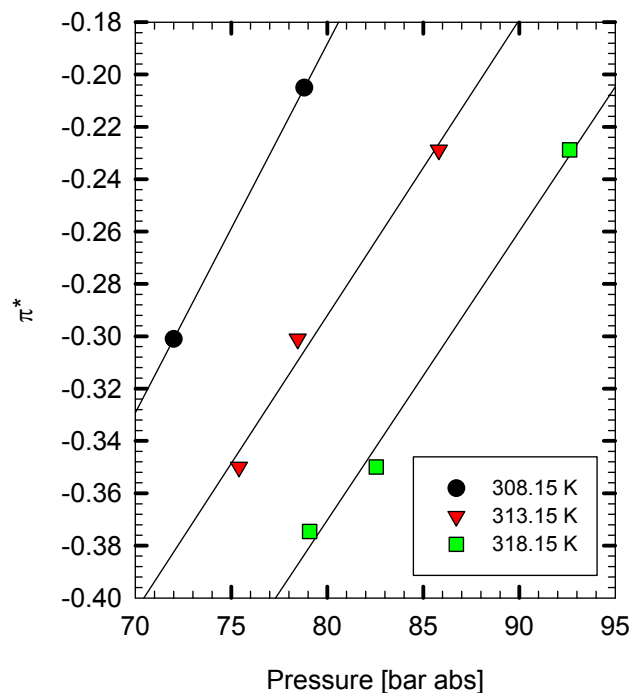
or far removed from the solute molecule. The effect of the physical contributions (e.g., dispersion, induction and dipole-dipole forces) may be calculated with the McRae-Bayliss expression (2):

$$\Delta v = dispersion\ terms +\ B\left(\frac{n^2-1}{2n^2+1}\right) + C\left(\frac{\varepsilon-1}{\varepsilon+2} - \frac{n^2-1}{n^2+2}\right) \qquad (3\text{-}6)$$

where:

    ε: dielectric constant

    n: refractive index

    Δv: differences between the v_{max} in a given solvent minus the value in the gas phase.

Assuming that the dispersion terms are neglected, the B term describes interactions between the solute dipole and induced dipole in the solvent, and the C term describes dipole-dipole forces. For non polar, polarizable solvents $\varepsilon=n^2$, the second term becomes zero, and the first term can be expressed by what is called the Onsager reaction field function which is given by equation 3-7 (28).

$$L(n^2) = \frac{n^2-1}{2n^2+1} \qquad (3\text{-}7)$$

  where:

    n = refractive index.

The refractive index for $scCO_2$ as a function of pressure and temperature can be determined from the specific Lorentz-Lorentz refraction equation 3-8 (3) as a function of molar volume.

$$\frac{n^2-1}{n^2+2}\left(\frac{1}{V}\right) =\ 6.600 + \frac{1.25}{V} - \frac{264}{V^2} \qquad (3\text{-}8)$$

where:

    V= molar volume in cm^3/g-mol

As stated by many authors (27, 28), there are three important points in this kind of graph. The first point is that there are two linear regions for π^* as a function of $L(n^2)$. The second important point is that the region where the slope changes is dependent on the
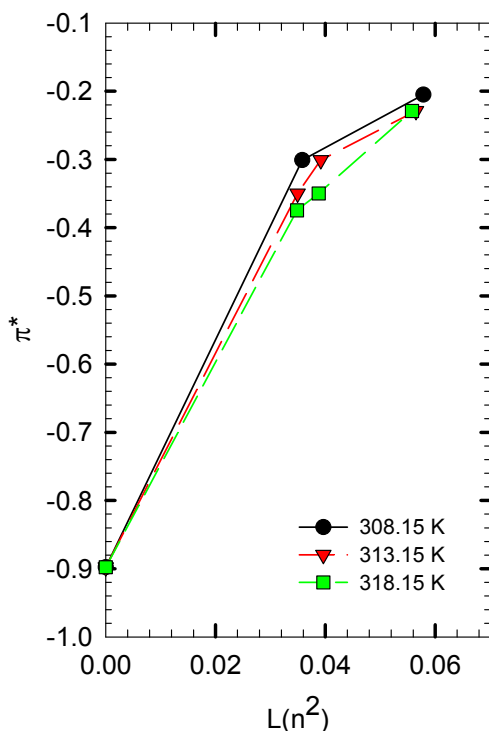
Figure 3-8: Onsager reaction field.

fluid, and the third is that the intercept $(L(n^2) \to 0)$ gives us the values for π^*_{gas}.

Using equation 3-5, and data reported by Laurence et al. (14), we can obtain π^*_{gas}; giving a value of the (-0.8977). In Figure 3-8 we just observed the low density region. The value reported by Essfar et al. (27) is -1.06 and the sudden qualitative changes in the dependence of π^* with Onsager reaction field for 2-nitroanisole has been reported to occur at a density of 0.29 g/cm^3 (pressure of 88.6 atm) (28). For our data this can be observed between the range of density 0.24-0.27 g/cm^3 (pressure 77-80 atm), obviously we can not precise the pressure 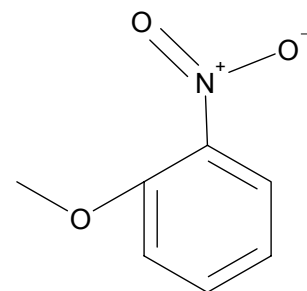due to the little quantity of data that we could measure[5]. This break observed might be expected to occur at a density where the solvent molecules saturate the cybotactic region (region of solvent molecules whose solvation structure is determine by the presence of the solute molecule), and the transition between gas-like and liquid-like behavior occurs.

The results would indicate that the interaction between our indicator with scCO$_2$ is more attractive than with 2-nitroanisole. Relating with their chemical structure (Figure 3-9), we can suggest that the presence of O in 2-nitroanisole does not promote clustering of CO$_2$ molecules around it. That is possible with our indicator through interaction with the amine groups, even though it could be weak. The slope of the

Figure 3-9: 2-nitroanisole.

---

[5] The seals of the window of the UV-high pressure cell, presented continuous leaking upon cooling.

curve at the high density region reflects the polarity of the medium. The polarity is mainly due to the large quadrupole moment of $scCO_2$ or the "local" dipole of the CO_2 molecule (27). The polarity calculated with our data ranges from -0.38 to -0.21, different values were reported for CO_2, showing great discrepancies at the low density region.

Sigman et al. (24), measured the π^* for various indicators in $scCO_2$; the data obtained has a similar behavior of N,N-diethyl-4-nitroaniline. As can be seen in Figure 3-9, they are negative and decrease smoothly towards the value for vacuum as the density of $scCO_2$ decreases.
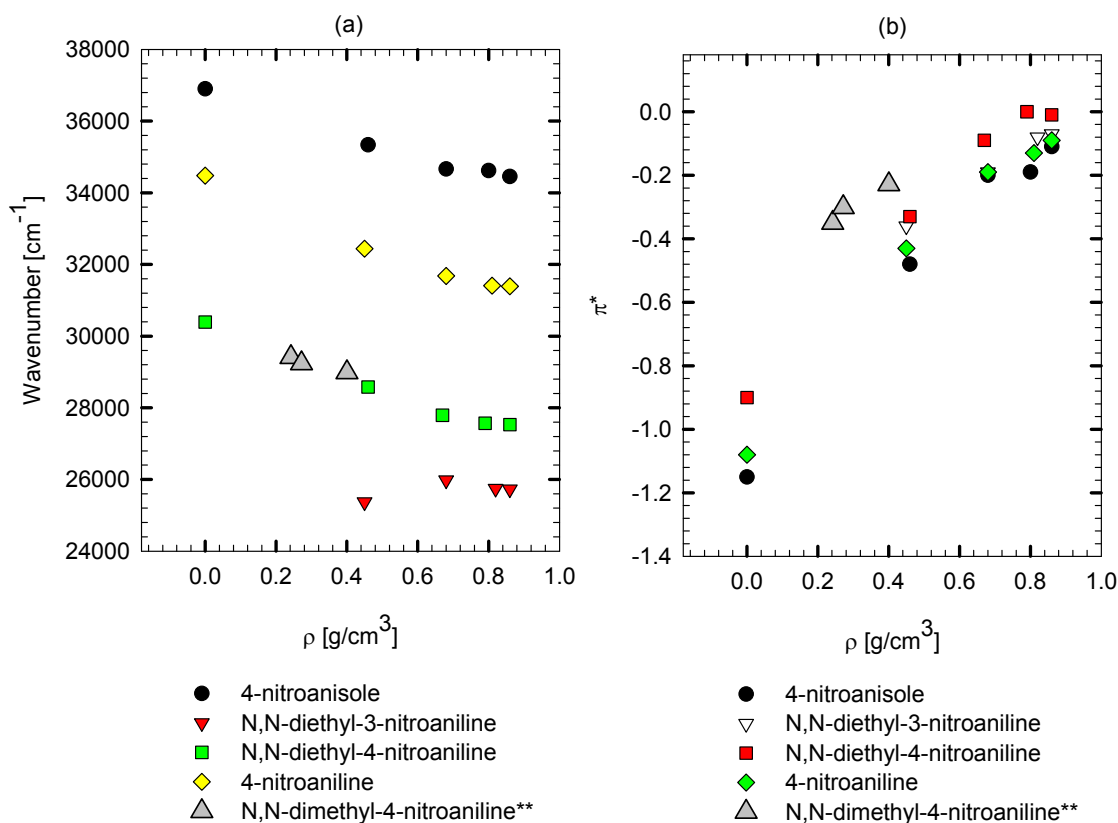

Figure 3-10: Various indicators in $scCO_2$ (** This investigation).

In SCF the density can be varied over a wide range, then the type and number of interactions, between the solute and the solvent that occur due to changes in the intermolecular distance (local density), will be density dependent. Hence, it is clear the

importance to sample a wide range of solute-solvent interactions until saturation in the cybotactic region of the solute molecule. According to a method suggested by Kim et al. (13), the ν_{max} for pure indicator vapor reported in 14, was correlated linearly with the data of isotherm 318.15 K (Figure 3-11). This line corresponds to the hypothetical density dependence of the indicator in a homogeneous surrounding (e.g., liquid), and the intersection of the horizontal line with the experimental and hypothetical density dependence of ν_{max} gives the actual bulk and the corresponding expected local density. In Figure 3-11a, we can see this hypothetical local density, and in the next Figure 3-11b, the variation of the ratio local density/bulk density with respect to the reduced density. It seems that the local density decreases with pressure, but what this behavior means is that the number of $scCO_2$ molecules surrounding the indicator is decreasing, and the saturation of the solvation shell is achieved at low pressure through the dipole-induced dipole interactions.
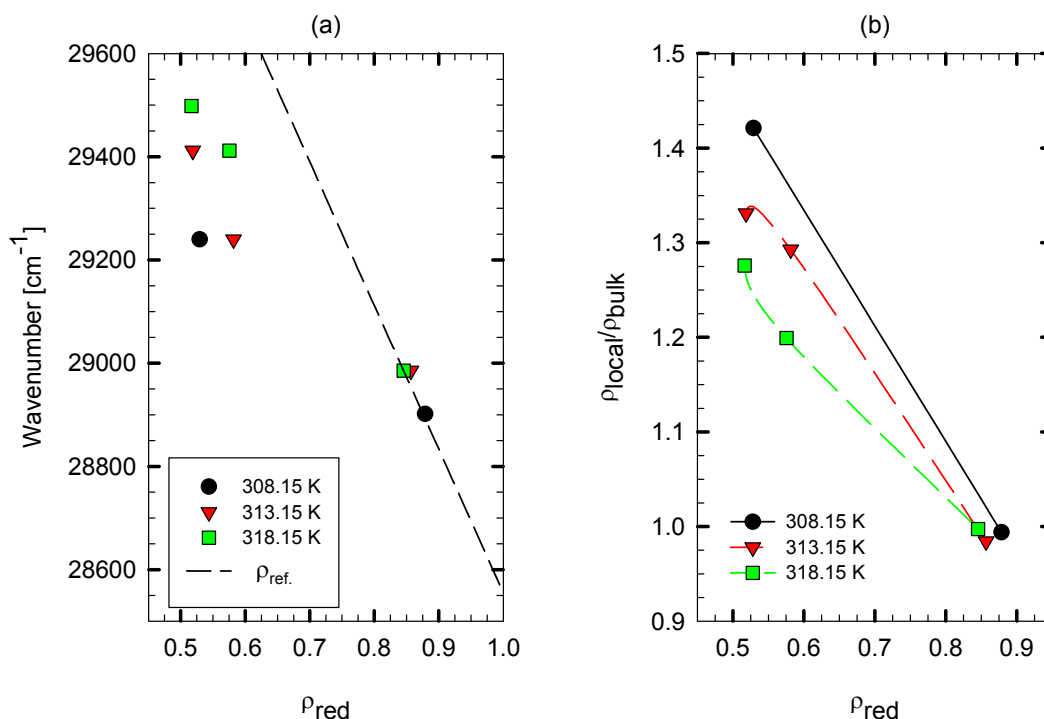

Figure 3-11: (a) Local density based on 318 K. (b) Variation of the local density with reduced density.

3.3 Indicator-H_2O-scCO_2

The specific solute-binary fluid interactions in the local environment of the solute molecules have direct relevance to supercritical fluid extraction (SFE), chromatographic selectivity, and molecular diffusion (26). The enrichment of the cosolvent by both specific and non-specific solute-solvent interactions should provide a basis for understanding solvent modifier effects in SCFs, as well as the phenomena of cluster formation in pure and binary SCF solutions.

The ground state of a dilute solute probe solvated by pure scCO_2 has equilibrium energy of solvation that is largely determined by dipole-induced dipole interactions with the solvent molecules. This assumes that there are not specific intermolecular interactions such as HB or charge-transfer complex formation. With the introduction of a polar substance, both the dipole-dipole and specific intermolecular interactions become possible.

For binary fluid mixtures containing a polar cosolvent the solvatochromic behavior of the solute can be described by the equation 3-9.

$$V_{max} = V_0 + s\pi^* + a\alpha \quad (3\text{-}9)$$

If we include the net effect in the $\pi^{*\prime}$ value the equation 3-9 can be reduced to (26):

$$V_{max} = V_0 + s\pi^{*\prime} \quad (3\text{-}10)$$

Here $\pi^{*\prime}$ contains the HB contribution coupled with the solvent polarity/polarizability. This equation can be used to determine the $\pi^{*\prime}$ value of a binary supercritical fluid containing a cosolvent capable of HB with the solute. From literature data (01) there are values for the indicator, also we found the s and v_0 values for our indicator are -3333.33 and 28180 cm^{-1} respectively, so we can obtain our $\pi^{*\prime}$ values.

$$\pi^{*\prime} = \frac{28180 - V_{max}}{3333.33} \quad (3\text{-}11)$$
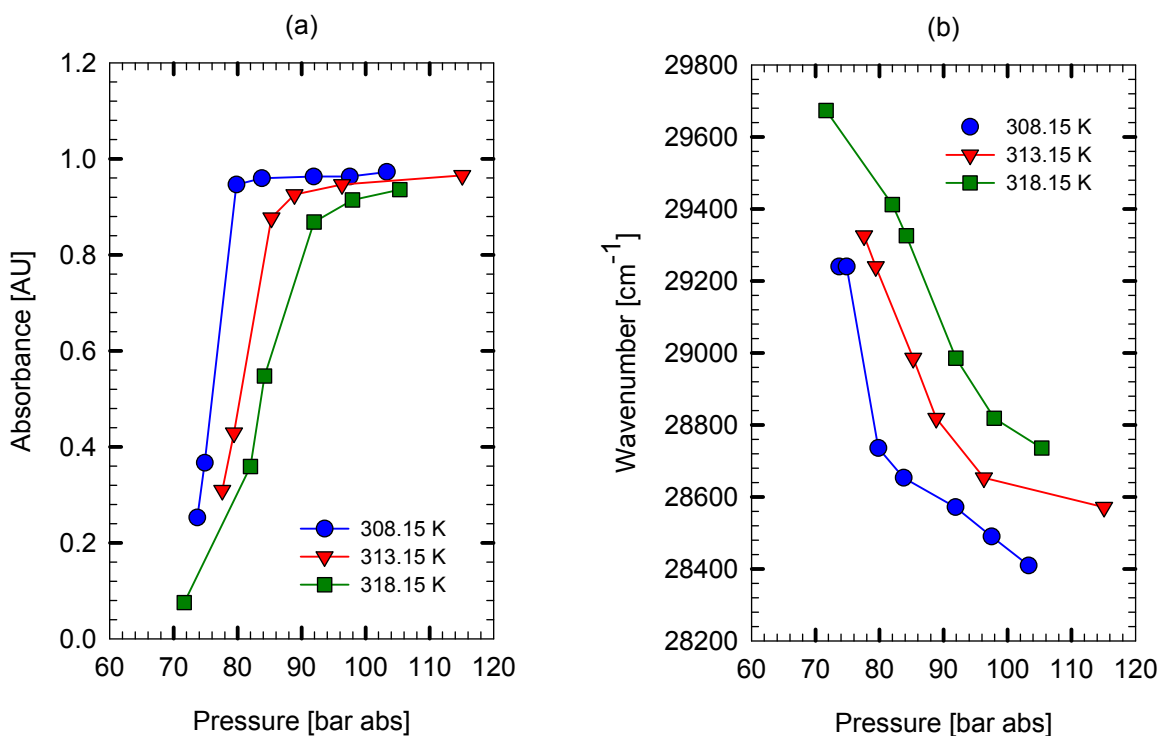
(a)

(b)

Figure 3-12: (a) Absorbance, and (b) Wavenumber vs. pressure (Indicator-H_2O-scCO_2 system).

Three isotherms were measured for the system Indicator-H_2O-scCO_2. The results in terms of maximum absorbance and wavenumber dependence with pressure can be seen in the Figure 3-12a and Figure 3-12b, respectively. As the previous system, the red shift of the spectrum is reported, and a changing microenvironment as well, although the optical density is not changing at $P > 85$ bar.

The solvatochromic information will directly reflect the local composition of the solvent molecules and will be related to the number of cosolvent and solvent molecules contained in the cybotactic region. However, the grouping of the specific and non-specific intermolecular interactions, will not allow us to determine the extent of HB interactions in the local composition about the solute.

Figure 3-13 shows the $\pi^{*\prime}$ values as function of pressure; there is clearly not a linear relationship, but the values increases as pressure increases. The range of variation of $\pi^{*\prime}$ goes from -0.45 to -0.14, compared with the previous system Indicator-scCO$_2$ (Figure 3-7). The addition of H$_2$O does not increase the polarity appreciably. However, the local density in the cybotactic region increases with pressure. As it was previously defined $\pi^{*\prime}$ (equation 3-11), it contains two contributions, hydrogen bonding interactions
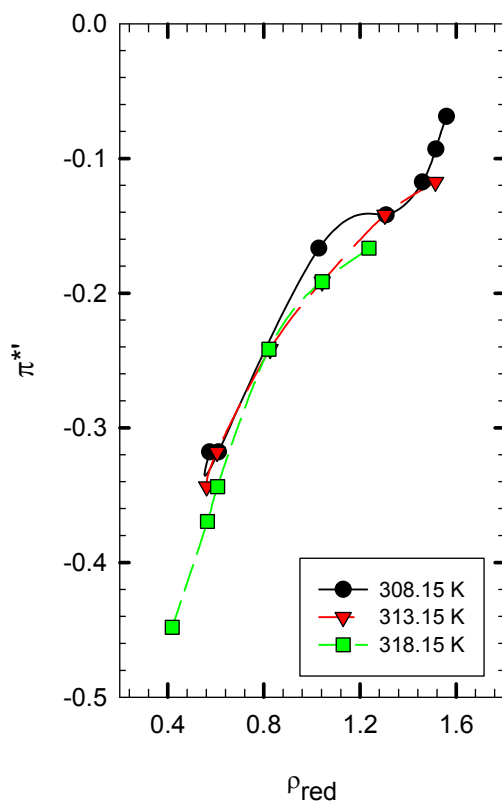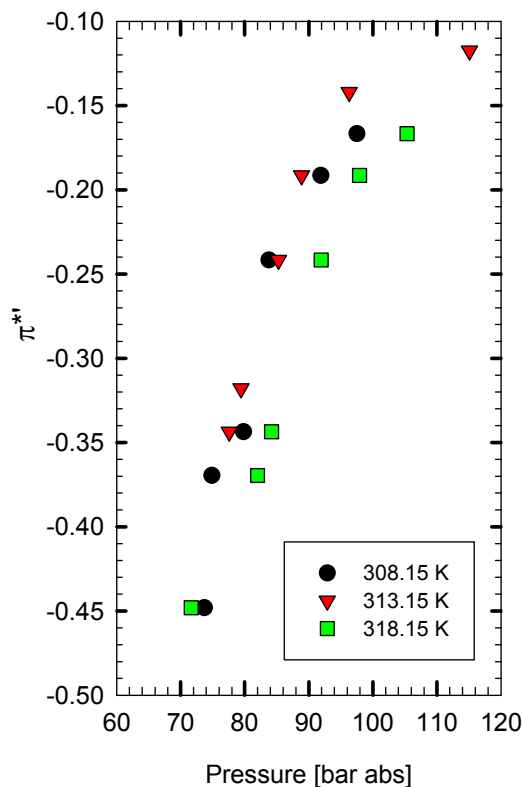

Figure 3-13: Polarizability vs. pressure.

and non-specific density dependent, which may or may not depend on density.

There are a fixed number of interaction sites between the indicator, H$_2$O, and CO$_2$, involving the nitro group and the benzene ring, that once those sites are saturated, the lifetime of these associations determine the solvatochromic shift seen for the binary fluid as well as the local densities of scCO$_2$ and the cosolvent molecules. In Figure 3-14 we observed that the polarizability decreases as the

Figure 3-14: Polarizability vs. reduced density.

temperature increases, especially at high reduced density. The behavior of the curve could indicate the existence of interactions that do not depend on density, these could be HB generated by the presence of H_2O that are sensitive to temperature.
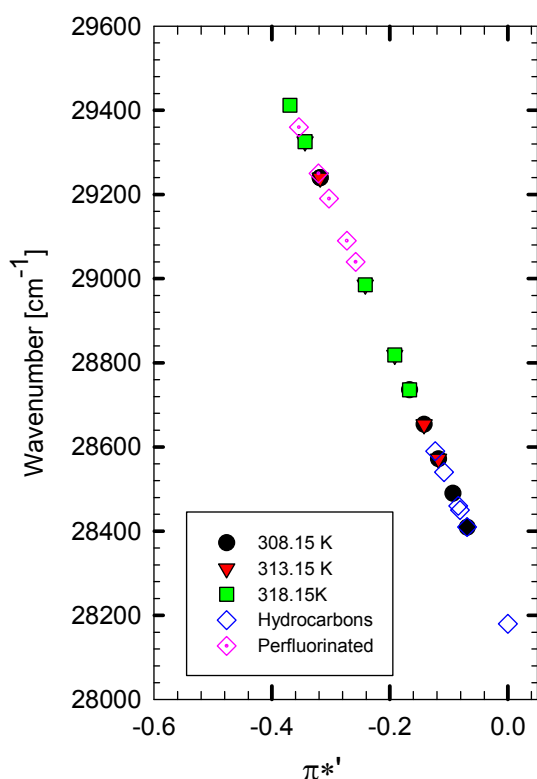

Figure 3-15: Solvatochromic shifts in various solvents.

It is possible to compare the polarity for our system with other solvents, according to the solvatochromic shift (14), as can be observed in Figure 3-15. The system has a changing polarity similar to the perfluorinated solvents at low pressure and similar to non-aromatic hydrocarbons at high pressure.

According to Yonker et al. (26), and Bulgarevich et al. (5), one can determine the difference in solvatochromic shift ($\Delta\pi^*$) between the calculated for the bulk composition (π^*_{calc}) and the experimentally measured value $\pi^{*\prime}$ for the binary supercritical fluid, by the next equation:

$$\Delta\pi^* = \pi^{*\prime} - (X_{12}\pi_1^* + X_{32}\pi_3^*) \quad (3\text{-}12)$$

where:

X$_{12}$= composition of cosolvent

X$_{32}$= composition of the dense gas

π_1^*= polarity pure cosolvent

π_3^*= polarity pure SCF

Different relationships between the bulk binary fluid composition and the local composition of the cosolvent arise from the equation. If ($\Delta\pi^*= 0$), the bulk and local composition of the cosolvent are the same; if ($\Delta\pi^*>0$), the local composition of cosolvent

is greater than the bulk composition; and if ($\Delta\pi^* < 0$), the local composition is depleted in cosolvent compared to the bulk.

The same procedure described previously is used to obtain the local density behavior of the system Indicator-H_2O-scCO_2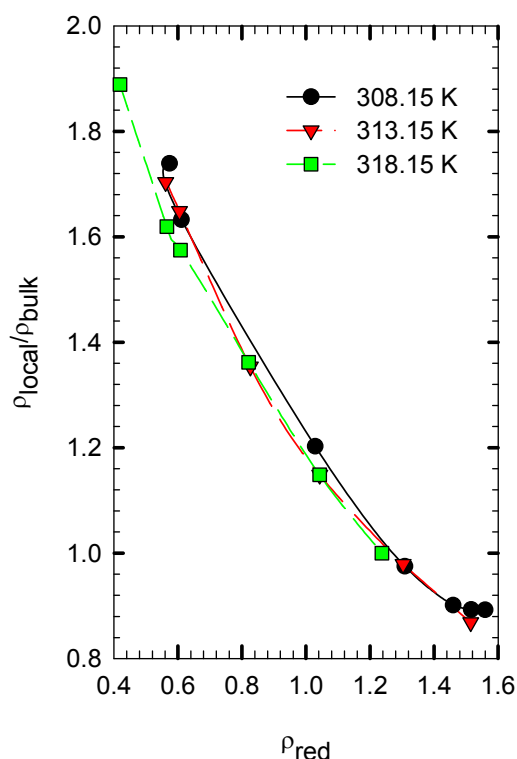 and in Figure 3-16 we can see the variation of the ratio of local to bulk density. The curve continually decreases with increase of pressure, this suggesting that the maximum clustering occurs at low densities, where the solvation shell is beginning to form. Note that even though polarity is increasing, it does not necessarily mean a high aggregation of molecules (e.g., H_2O or CO_2).

According to equation 3-3 the indicator is susceptible to hydrogen bond donor solvents. The formation of hydrogen bonds between the indicator and H_2O is prevailing, with the displacement of CO_2 molecules out of the solvation shell as pressure increases; as these specific forces can be saturated by the formation of stoichiometric complexes between both molecules. The location of the maximum local density is the result of two competing effects, the solvent inhomogeneity and solute-solvent interactions. If the dominant effect for cluster formation is due to the inhomogeneity near the critical point, the cluster should be limited to the close vicinity of critical point. On the other hand, if the solute-solvent attraction is predominant, the cluster formation is maximized at lower densities than the critical point.

Figure 3-16: Local density variation (Ind-H_2O-scCO_2).

3.4 Surfactants-Indicator-H_2O-scCO_2

Once the indicator and H_2O in scCO_2 were evaluated, the effect of the surfactant was

incorporated next. PL92 pluronic surfactant was used and the experiments were performed in the sep-up described in Figure 2-4, using the stainless steel cell (8.5 cm^3).

3.4.1. PL92-Indicator-H$_2$O-scCO$_2$

The results for the PL92 surfactant-indicator-H$_2$O-scCO$_2$ can be seen in Figure 3-17.
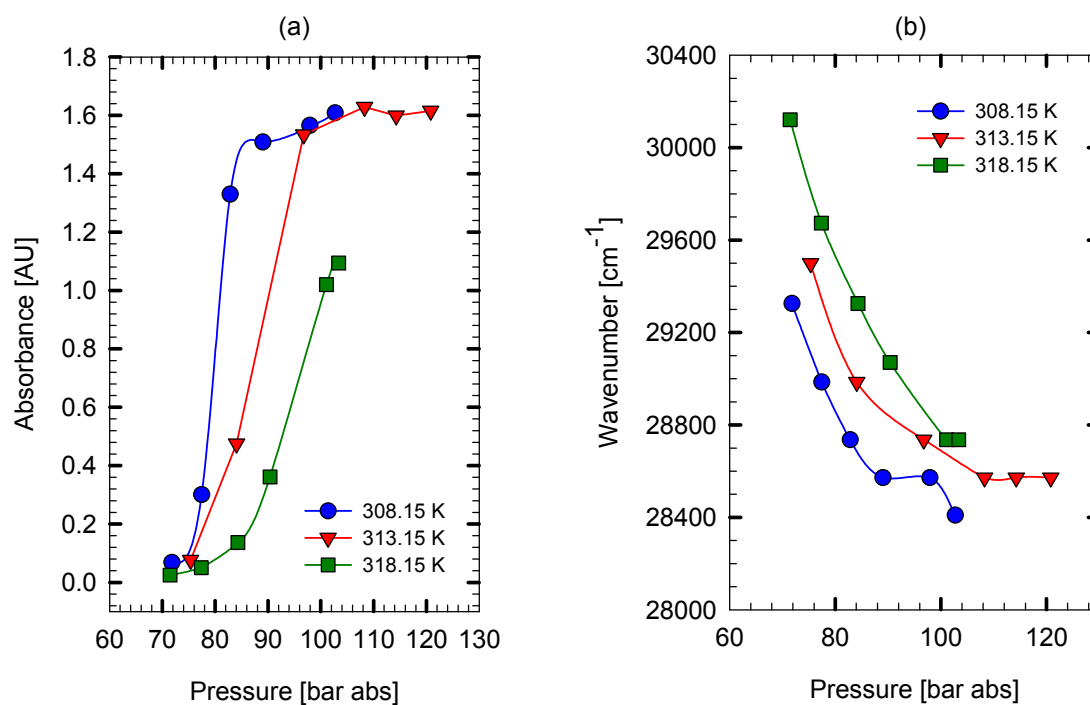
Figure 3-17: (a) Absorbance, and (b) Wavenumber vs. pressure (PL92-Indicator-H$_2$O-scCO$_2$).

Figure 3-19: λ_{max} vs. pressure.

Comparing with the previous systems evaluated we observed differences in the absorbance (Figure 3-17a) measured. Especially in presence of the surfactant, the indicator seems to be more solubilized, but the system reaches saturation even if the pressure is increased. The solvatochromic shift shown in the Figure 3-17b, describes a descending concave curve with respect to pressure.

It can be seen that there are no differences in the microenvironments formed by the three systems studied. It is important to note that any microstructure formed in the scCO$_2$ fluid phase, is a changing microenvironment affected by pressure. The effect of pressure on λ_{max} can be seen in Figure 3-19. For 308.15 K and 318.15 K isotherms a change in λ_{max} is observed with increase of pressure. At 313.15 K λ_{max} increases with pressure until 108 bar, where there is no further increase. This pressure dependence was attributed to the existence of a two-phase region, a transparent fluid phase and a viscous

Figure 3-18: π^* vs. reduced density.

phase of melted surfactant (22). Above this pressure, the system changes to a single reverse micellar phase, where no influence of pressure on the spectra was noticed. However, we can not determine the effect of the surfactant in the system. It is important to point out that we could not reach its cloud point pressure (362 bar (7)), so it could be possible that a two phase system is taking place.

As before, we calculated the polarity of our system with equation 3-11, the results can be seen in Figure 3-18. Compared with the system without surfactant, there is not a great increase in polarity. The change in direction of the curve is more evident for all isotherms, and the temperature range studied does not have an effect in the polarity.

Again, we calculated the local density augmentation in the surrounding of the indicator, following the same method and we observed that the local density decreased with increase of pressure or density (Figure 3-20). The maximum aggregation was obtained at low pressures. As the pressure was raised, the CO_2 molecules are being replaced by H_2O, thus the $\pi^{*\prime}$ values increase. However, the surfactant does not seem capable to trap enough H_2O to achieve a water like-polarity microenvironment.
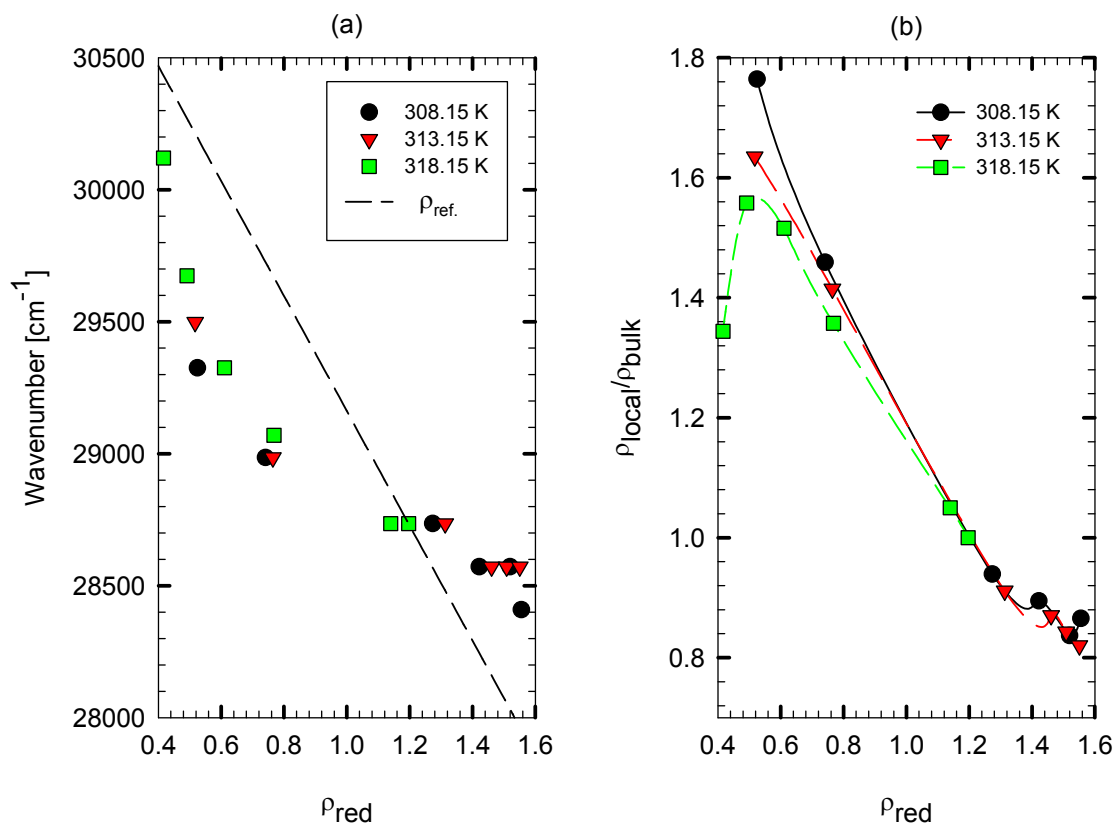
Figure 3-20: (a) Local density based on 318 K. (b) Variation of the local density with reduced density.

Another way to characterize the microenvironment of the microstructure formed in the supercritical phase is through the use of the dielectric constant in the form of the parameter $(\varepsilon-1)/(2\varepsilon+1)$. This is a parameter that expresses the sum of the polarization effects due to the permanent and the induced dipole moments of solvent molecules. The dielectric constant for $scCO_2$ is obtained from the next equation 3-13 (17).

$$\left(\frac{1}{\rho}\right) \times \left(\frac{\varepsilon-1}{\varepsilon+2}\right) = 7.676 \times 10^{-3} \quad (3\text{-}13)$$
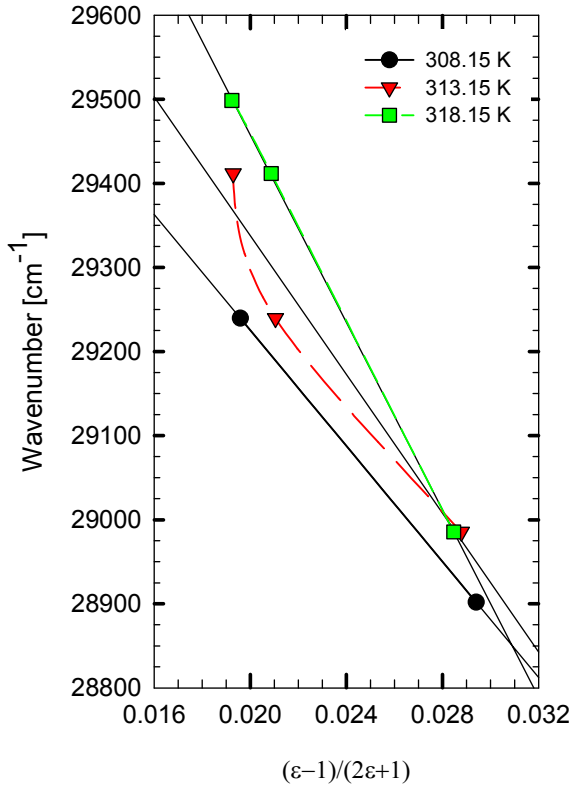
where:

ρ = density in [gmol/L]

Figure 3-21: Wavenumber vs. $(\varepsilon-1)/(2\varepsilon+1)$ (Ind-scCO$_2$).

If we graph wavenumber vs. $(\varepsilon-1)/(2\varepsilon+1)$ (Figure 3-21), the shift appreciably deviates downward from a linear line. Such deviation has been noticed for scCO$_2$ solvent and CF$_3$H (19) and attributed to the local density enhancement. That is, the effective dielectric constant around a solute molecule becomes much larger than the bulk dielectric constant at a specific density because of the gathering of solvent molecules due to the solute-solvent attractive interaction.

For the system Indicator-H$_2$O-scCO$_2$, the dielectric constant of the medium is affected by the presence of H$_2$O, so we need to calculate the dielectric constant of the mixture. For pure H$_2$O, the dielectric constant is given by the equation (2):

$$\frac{(2\varepsilon+1)\,(\varepsilon-1)}{9\varepsilon} = \frac{N_A\rho}{3}\left(\frac{\alpha}{\varepsilon_0} + \frac{g\mu^2}{3\varepsilon_0\kappa T}\right) \qquad (3\text{-}14)$$

where:

ε_0 : permittivity of vacuum (8.854×10^{-12} C^2/J-m)

α : molecular polarizability (1.636×10^{-40} C^2/J-m^2)

μ : molecular dipole moment (6.138×10^{-30} C-m)

κ : Boltzman constant (1.380×10^{-23} J/K)

N_A: Avogadro number (6.023×10^{23} mol^{-1})

g : Kirkwood factor.

The Kirkwood factor is calculated from the equation in term of series of constants:

$$g = 1 + \sum_{h=1}^{11} N_h \left(\frac{\rho}{\rho_c} \right)^{i_h} \left(\frac{T_c}{T} \right)^{j_h} + N_{12} \left(\frac{\rho}{\rho_c} \right) \left(\frac{T}{228\kappa} - 1 \right)^{-1.2} \quad (3\text{-}15)$$

where:

i_h, j_h, N_h : Constants given in (21).

Values for H_2O density were obtained at every thermodynamic condition. Differences can be seen between the indicator-scCO$_2$ (Figure 3-21) system and the one with the presence of H_2O (Figure 3-23), even though only the low region density was evaluated with the former. The $(\varepsilon\text{-}1)/(2\varepsilon+1)$ ratio increased with respect to temperature, but it decreased with pressure. The range of variation is from 0.058 to 0.12 approximately equal for the system with PL92 (Figure 3-22).
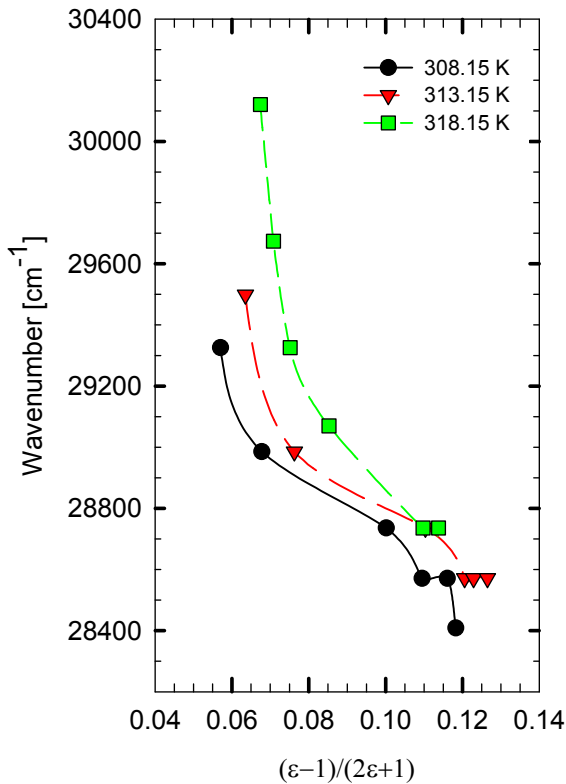

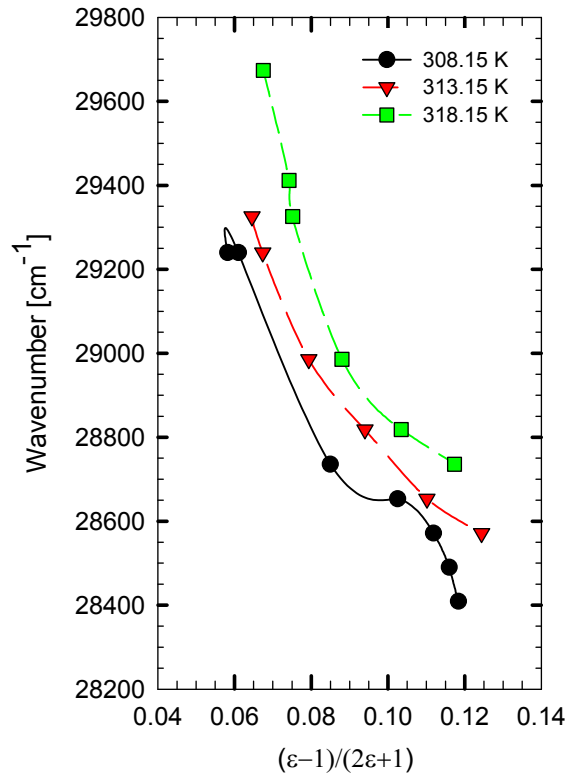Figure 3-22: Wavenumber vs. $(\varepsilon\text{-}1)/(2\varepsilon+1)$ (PL92-Indicator-H_2O-scCO$_2$).

Figure 3-23: Wavenumber vs. $(\varepsilon\text{-}1)/(2\varepsilon+1)$ (Indicator-H_2O-scCO$_2$).

3.4.2. Surfactants-Indicator-H$_2$O-scCO$_2$

The other surfactants were evaluated in the same way. The procedure was described in section 2.4.2.

The results can be observed in Figure 3-24 and Figure 3-25. Unfortunately little can be deduced from the few data that has been measured. It is important to point out that the systems were very unstable[6] and it was not possible to obtain an adequate spectrum, as can be observed in the spectrum shown in Appendix D, Appendix E, Appendix F, and Appendix G. However, we can see different behaviors of the PL31 and P17R2 from the Zonyl and Gele surfactants. PL31 has only two hydroxyl terminal groups; hence the capacity to form hydrogen bond with H$_2$O is limited. Although, P17R2 possesses 10 ethylene oxide (EO) and can trap more H$_2$O, the absorbance does not increase beyond that of PL31. There must be a steric hindrance for its limit to solvate H$_2$O molecules, and consequently to solubilize the indicator, through the oxygen molecules distributed along the backbone of the surfactant.

For PL31, as pressure increased, the indicator was more soluble; this trend was favored by temperature. At 323.15 K, the absorbance seems to reach a plateau, suggesting that the cloud point of the system is very close. However, as pressure increases, the solubility of the PPO increases, then it would be possible that the tail-tail attraction strengthens producing the aggregation of the CO$_2$-philic tails and therefore the microenvironment collapse. For all the temperatures studied, the π^* values increases with pressure. Studies have demonstrated the aggregation of polyether by intramolecular hydrogen bonding through the terminal H with the nearest O of the EO group; therefore, limiting the existence of active sites for interacts with H$_2$O. This would explain the little capacity of P17R2 to trap H$_2$O. PPO has weaker segment-segment interactions; thus, weaker self association. The conformation in the co-block surfactant P17R2 would prevent the aggregation of the PPO groups; and therefore, present more stability.

---

[6] Unstability defines the incapability of the system to achieve steady state producing the deformation of the UV-spectra.

For P17R2, the point where a sudden change in the trend of the curve indicates the cloud point. This is accompanied by an increase in the π^* and perhaps structural changes in the microenvironment formed, which create a more favorable environment for the indicator and H_2O molecules. This does not produce an increase in the absorbance, especially at 308.15 and 313.15 K that slightly increases with pressure. At 323.15 K, above the cloud point pressure, the absorbance is decreasing. It seems that the pressure is breaking up the nonionic surfactant aggregation, which would be expected to reduce solubilization; this also produces the decrease in the π^* values. The same phenomenon is observed for P17R2 at 308.15 K and pressures above 200 bar.

Conversely to the spectrum at 323.15 K, at the lower temperature studied, the increase in density appears to change the subtle balance of forces at the surfactant interface and induce structural changes in the aggregates, such as spacing between head groups and the distribution of H_2O, but these changes do not create a more favorable environment for the indicator.

Gele was unstable (Appendix F), which only allowed measurements at low pressures. However, the decreasing trend in wavenumber suggests a changing environment. It could be possible that the cloud point was not achieved. The high aggregation capacity of the surfactant is because of the self aggregation tendency of the carboxylic acid terminal group that forms dimers easily.

Zonyl present the higher absorbance of all the surfactants studied. It was only possible to measure the spectrum at 323.15 K (Appendix G). The trend described is almost constant as well as the polarity. The plateau described in Figure 3-24 corresponds to wavenumber and pressure, and would be indicative of a micellar phase. Much of the unstability of the system could be due to the low length of the fluorinated tails, compared with the long EO head (11 EO groups). There is also the possibility to form intramolecular hydrogen bond in the polyether and the terminal H.
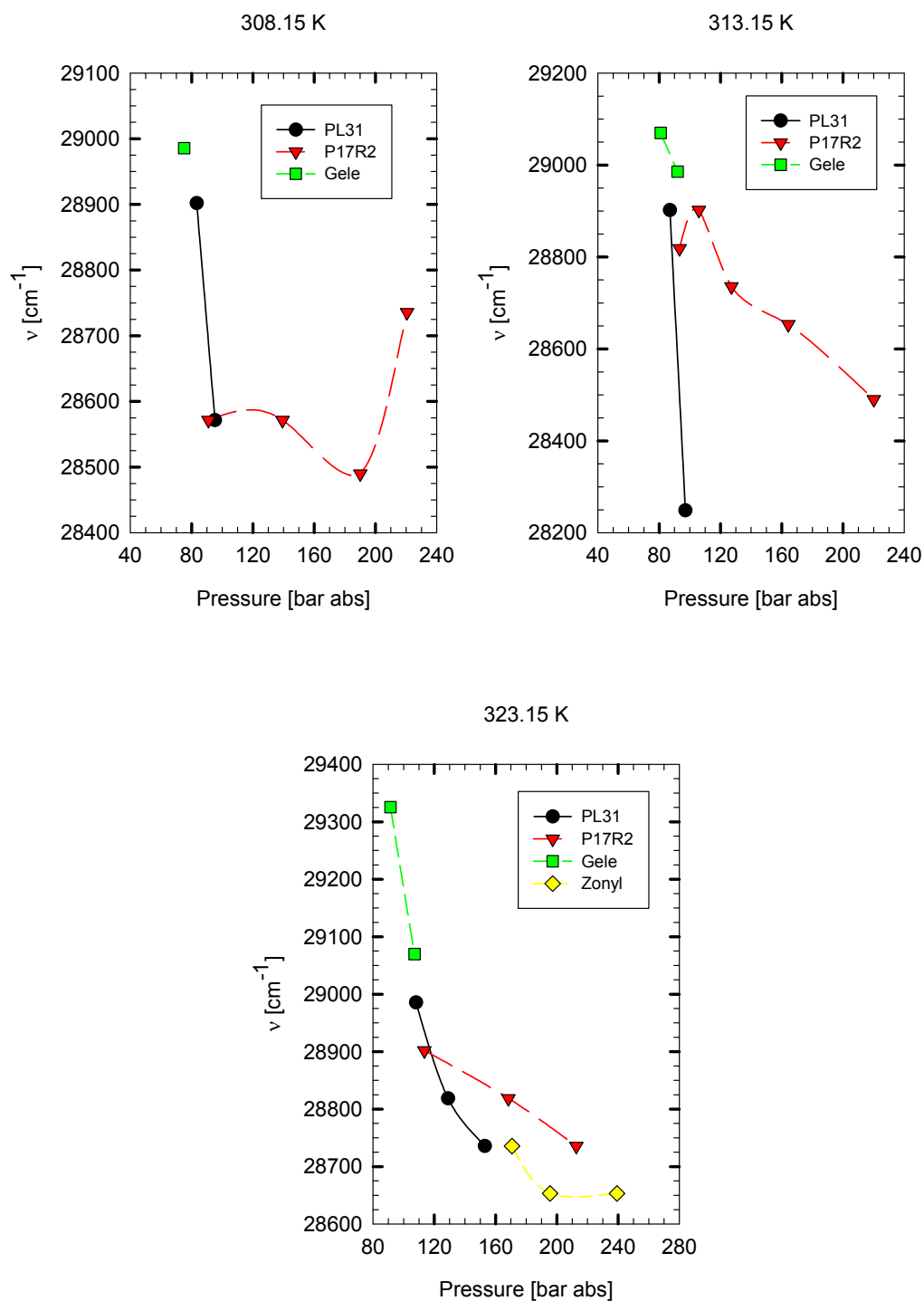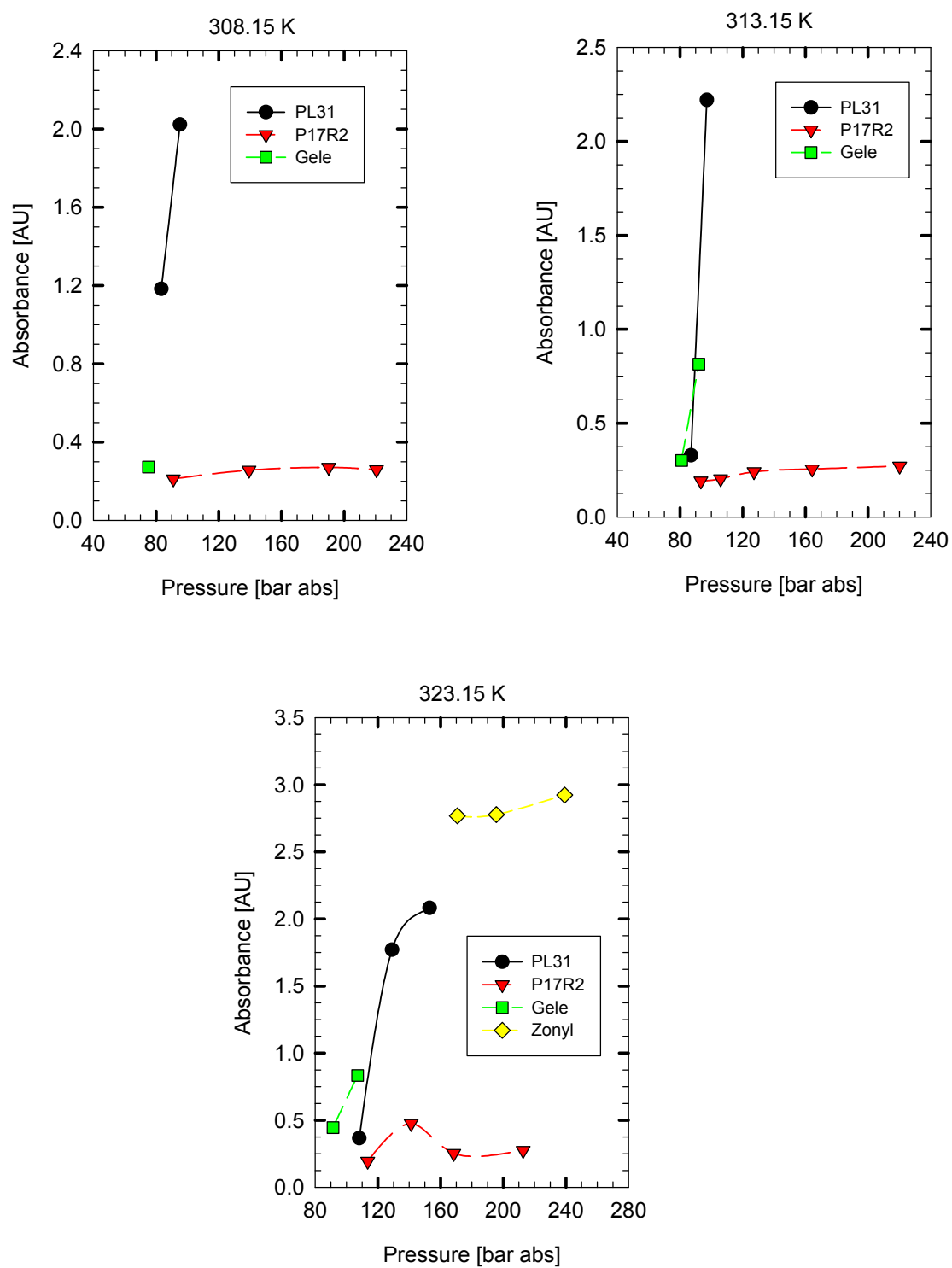
Figure 3-24: Solvatochromic shift with pressure (Surfactants-Indicator-H_2O-scCO$_2$).

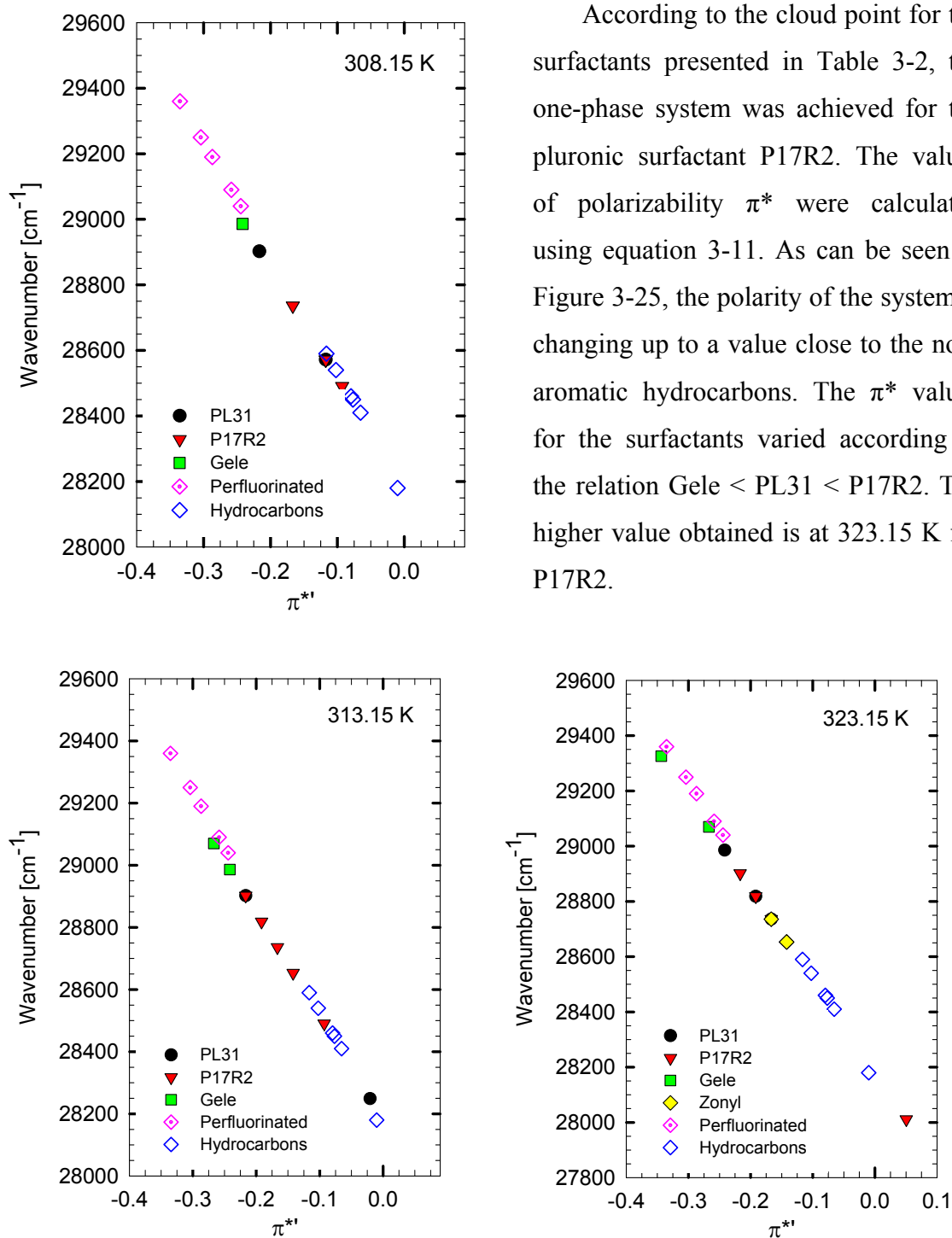Figure 3-25: Absorbance vs. pressure (Surfactants-Indicator-H_2O-scCO$_2$).

According to the cloud point for the surfactants presented in Table 3-2, the one-phase system was achieved for the pluronic surfactant P17R2. The values of polarizability π^* were calculated using equation 3-11. As can be seen in Figure 3-25, the polarity of the system is changing up to a value close to the non-aromatic hydrocarbons. The π^* values for the surfactants varied according to the relation Gele < PL31 < P17R2. The higher value obtained is at 323.15 K for P17R2.

Figure 3-26: Comparison of variation solvatochromic shift vs. polarizability with other solvents.

Table 3-2: Cloud point and solubility of the surfactants

Name	MW	Pressure [bar]	Temperature [°C]	Solubility [%]
PL92	3750	362	40	0.146[7]
PL31	1056	165	40	0.278[18]
P17R2	2125	156	40	0.202[18]
Zonyl	950	136	25	0.400[6]

3.5 Drug-surfactant-H_2O-scCO$_2$ system

We evaluated the solvato-chromic shift of acetaminophen with different solvents; ethanol (C_2H_5OH), diethyl ether ((C_2H_5)$_2$O), acetonitrile (CH_3CN) and water (H_2O). From Figure 3-27, we conclude that the solute is quite sensitive to its surrounding micro-environment. Acetaminophen shifts to opposite direction (blue-shifts) compared to our indicator. It corresponds to $\eta \rightarrow \pi^*$ transition in
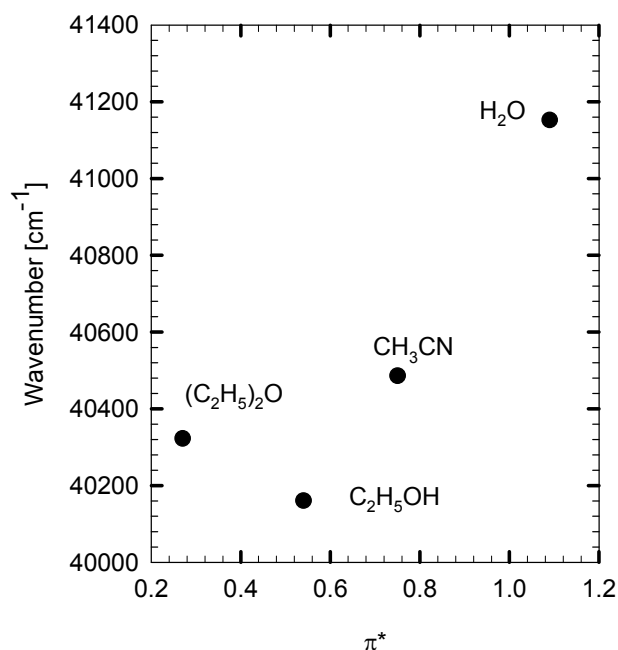

Figure 3-27: Acetaminophen in various solvents.

the absorbance band of C=O induced by HBD solvents. That stabilizes the solute ground state through the donation of a hydrogen bond, generally the blue shift is larger than the red shift. Imipramine HCl, does not shift in a changing microenvironment, as was probed when solubilized in H_2O and methanol (CH_3OH, λ_{max} at 251 nm), it was not possible to dissolve in less polar solvents. The shift in the maximum absorbance was evaluated at 313.15 K, these are depicted in the Figure 3-28 and Figure 3-29.
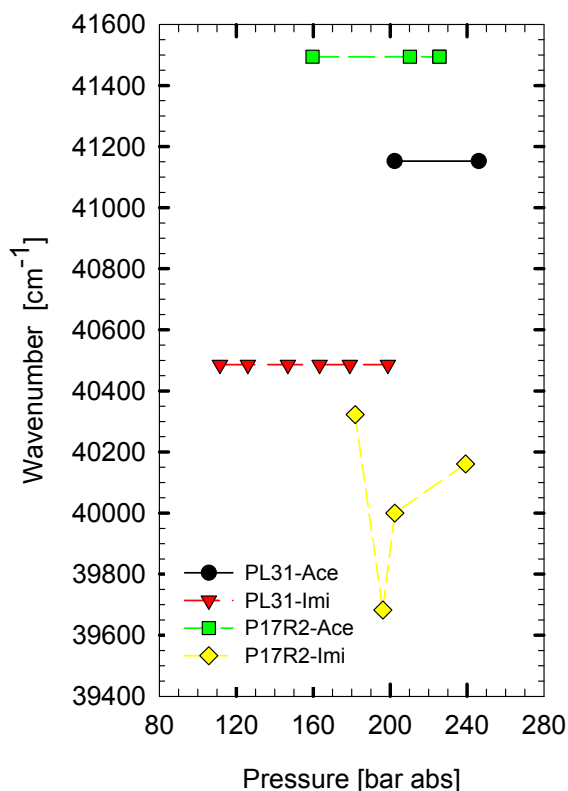
Figure 3-28: Solvatochromic shift at 313.15 K.

If we make a rough correlation with the three ν_{max} measured for acetaminophen, when dissolved in the more polar solvents, we obtain the next correlation, from where $\pi^{*\prime}$ values were calculared:

$$\nu_{max} = 39157 + 1818\pi^{*\prime} \quad (3\text{-}16)$$

The values for ν_{max} resemble that of H_2O energy, and the value for $\pi^{*\prime}$ calculated is about 1.09 and 1.28 for PL31 and P17R2 respectively. These results suggest that the drug is surrounded by H_2O molecules, more than $scCO_2$; however, we can not assure that the reverse micelle microstructure was formed, even though the cloud point of PL31 and P17R2 was achieved. The results also show that increasing pressure of $scCO_2$ does not change the microenvironment formed in the one phase micellar solutions.

The increasing absorbance for an unchanging polarity microenvironment suggests that more solute is being solubilized in the fluid phase due to a density increase. This increase in
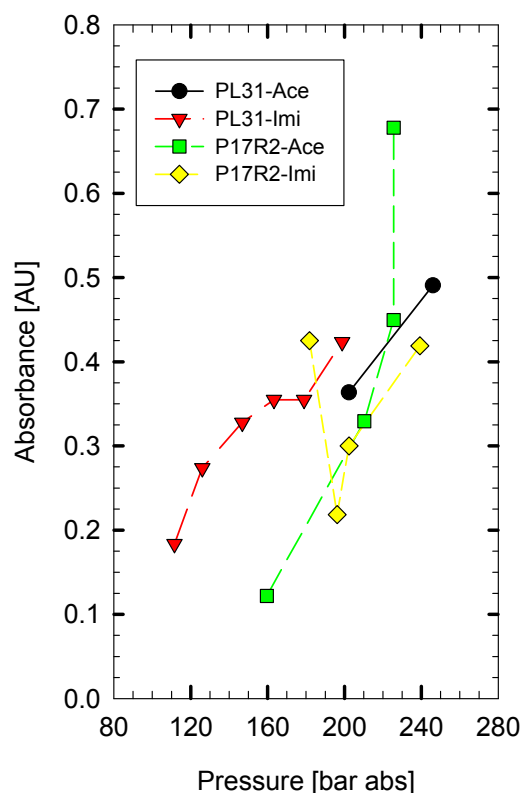

Figure 3-29: Absorbance at 313.15 K.

density also dissolves more H_2O in the supercritical phase and provokes conformational changes in the surfactant interface. This is especially the case when acetaminophen is used. The question remaining is whether the quantity of water saturating the fluid phase is enough to dissolve the imipramine salt, considering that 0.32% is in the form of H_2CO_3. The increase in absorbance with pressure would indicate that the saturation of the intermolecular interactions was not achieved and the microstructure was growing (e.g., increasing H_2O molecules and increasing the surfactant solubilization), but the balance was so unstable that it collapsed (e.g., aggregation of the surfactant or interaction between hydrophobic chains versus size of the solute).

3.6 Solvation Shell and Second Virial Coefficient: A Theoretical Approach

In order to estimate the solvation number of solvent molecules around the solute for pure $scCO_2$, we followed the method suggested by Kajimoto et al. (11). In that sense, we use the Ewald et al. (8), equation proposed for the solubility of solids at medium-density gas

$$\ln\left(\frac{x_2}{x_2^0}\right) = (V_2^S - 2B_{12})\frac{1}{V} + \left(V_2^S B_{11} - \frac{3}{2}C_{112}\right)\frac{1}{V^2} + \left(V_2^S C_{111} - \frac{4}{3}D_{1112}\right)\frac{1}{V^3} + \ldots (3\text{-}17)$$

where:

x_2, x_2^0 : mole fraction of the solute 2 with and without gas molecules 1.

V_2^S : molar volume of the solid solute.

V : molar volume of the gas.

$B_{12}, B_{11}, C_{111}, C_{112}, D_{1112}\ldots$: virial coefficient

We can truncate the equation and arrange in the next form:

$$\ln\left(\frac{c}{c_0}\right) = (V_S - 2B_{12})\frac{1}{V} \qquad (3\text{-}18)$$

The term $ln(c/c_0)$, can be represented approximately by $ln(D) + cte$, where D is the optical density at the low density region. At first step we plot $ln(D)$ vs. density of the solvent ($scCO_2$) [mol/cm^3], and correlate linearly, we obtained the next equation:

$$\ln(c) = \left(V_S - 2B_{12}\right)\rho + \ln(c_0) \qquad (3\text{-}19)$$

From the slope of the equation we can obtain the value for the second virial coefficient, at each temperature. The molar volume of the solute is calculated with the method of Marrero–Pardillo (20).

B_{12}, denotes the second mutual virial coefficient reflecting the interaction between the solid vapor and the solvent gas that is function of temperature. The second virial coefficient is related to the intermolecular potential by the expression:

$$B_{12} = \frac{4\pi N_A}{2} \int_0^\infty \left(1 - \exp\left(\frac{-V(r)}{\kappa T}\right)\right) \times r^2 dr$$

$$V(r) = \begin{cases} +\infty, & r \geq r_1, \\ \dfrac{-C_6}{r^6}, & r \geq r_1 \end{cases} \qquad (3\text{-}20)$$

where:

N_A: Avogadro's number

κ: Boltzmann constant

r: radius of the core potential

C_6: parameter that need to be evaluated.

With the value of the B_{12} known, we can used the equation 3-20 for obtain the value of the C_6 parameter. The form of the function *V(r)*, correspond to the Sutherland potential, it was used by Kajimoto et al. (11); however, any potential could be used.

To calculate the particular density of SCF at which just one solvent molecule is in the solvation shell of solute we used the equation

$$1 = 4\pi\rho_1 \int_r^R \exp\left(\frac{-V(r)}{\kappa T}\right) \times r^2 dr \qquad (3\text{-}21)$$

The results obtained and compared with others are summarized in the Table 3-3.

Table 3-3: Second virial coefficient (318.15 K)

Parameter	Indicator-scCO$_2$	4-nitroaniline-scCO$_2$ (5)	DMABN-CF$_3$H (11)
T/T$_c$	1.046	1.046	1.080
V$_s$ [cm^3/mol]	472.9	100	100
-B$_{12}$ [cm^3/mol]	316	296	1400
r$_{sol}$ [Å]	5.72	3.5	4
Rshell [Å]	15	7.9	6
C$_6$ [Å^6/cm]	1.3×10^9	1.3×10^6	4.1×10^6
ρ_1 [g/cm^3]	0.0104	0.0660	0.0250

This means that at a 0.0104 g/cm^3 one molecule of solvent is surrounding the solute. The π^* values determined by 4-nitroaniline in the range of pressures of our work varies from -0.37 to -0.20 (5), similar to our values ranging from -0.37 to -0.23, the higher value of the second virial coefficient B$_{12}$ than in 4-nitroanile-scCO$_2$ indicates that the interaction of N,N-dimethyl-p-nitroaniline-scCO$_2$ is stronger than 4-nitroaniline-scCO$_2$, at 318.15 K.

For the other temperatures are shown in Table 3-4.

Table 3-4: Second virial coefficient at 308 and 313.15 K

Parameter	Temperature [K]	
	308.15	313.15
T/T$_c$	1.013	1.029
V$_s$ [cm^3/mol]	472.9	472.9
-B$_{12}$ [cm^3/mol]	28.03	340
r$_{sol}$ [Å]	5.72	5.72
Rshell [Å]	15	15
C$_6$ [Å^6/cm]	7.5×10^8	1.3×10^9
ρ_1 [g/cm^3]	0.0102	0.0105

For 308.15 K as well as 313.15 K there is not enhanced in the local density. The strength of the interaction between the indicator and scCO$_2$ increases with decrease of temperature. However, the value of B$_{12}$ greatly decreases, perhaps due to pressures being near to the critical conditions.

References

1. Abbott, A. P.; Corr, S.; Durling, N. E.; Hope, E. G. Hydrogen Bond Interactions in Liquid Supercritical Hydrofluorocarbons. *J. Phys. Chem. B* **2003**, 107, 10628-10633.

2. Bennett, G. E.; Johnston, K. P. UV-Visible Absorbance Spectroscopy of Organic Probes in Supercritical Water. *J. Phys. Chem.* **1994,** 98 (2), 441-447.

3. Besserer, G. J.; Robinson, D. B. Refractive Indices of Ethane, Carbon Dioxide and Isobutane. *J. Chem. Eng. Data* **1973**, 18 (2), 137-140.

4. Bulgarevich, D. S.; Sako, T.; Sugeta, T.; Otake, K.; Takebayashi, Y.; Kamizawa, C.; Uesugi, M.; Kato, M. Microscopic Solvent Structure of Subcritical and Supercritical Methanol from Ultraviolet/Visible Absorption and Fluorescence Spectroscopies. *J. Chem. Phys.* **1999**, 111 (9), 4239-4250.

5. Bulgarevich, D. S.; Sako, T., Sugeta, T.; Otake, K.; Sato, M.; Uesugi, M.; Kato, M. Microscopic Solvent Structure of Supercritical Carbon Dioxide and its Mixtures with Methanol in the Cybotactic Region of the Solute Molecule. *J. Chem. Phys.* **1998,** 108 (10), 3915-3921.

6. da Rocha, S. R. P.; Psathas, P. A.; Klein, E.; Johnston, K. P. Concentrated CO_2-in-Water Emulsions with Nonionic Polymeric Surfactants. *J. Coll. Interface Sci.* **2001**, 239 (1), 241-253.

7. da Rocha, S. R. P.; Harrison, K. L.; Johnston, K. P. Effect of Surfactants on the Interfacial Tension and Emulsion Formation Between Water and Carbon Dioxide. *Langmuir* **1999,** 15, 419-428.

8. Ewald, A. H.; Jespon, W. B.; Rowlinson, J. S. *Discuss. Faraday Soc.* **1953**, 19, 238-242.

9. Hyatt, J. A. Liquid and Supercritical Carbon Dioxide as Organic Solvent. *J. Org. Chem.* **1984**, 49, 5097-5101.

10. Ikushima, Y.; Saito, N.; Arai, M. Supercritical Carbon Dioxide as Reaction Medium: Examination of its Solvent Effects in the Near-Critical Region. *J. Phys. Chem.* **1992**, 96 (5), 2293-2297.

11. Kajimoto, O.; Futakami, M.; Kobayashi, T.; Yamasaki, K. Charge-Transfer State Formation in Supercritical Fluid: N, N-dimethylamino benzonitrile in CF_3H. *J. Phys. Chem.* **1988**, 92 (5), 1347-1352.

12. Kamlet, M. J.; Abboud, J-L. M.; Abraham, M. H.; Taft, R. W. Linear Solvation Energy Relationships. 23. A Comprehensive Collection of the Solvatochromic Parameters, π^*, α, and β, and Some Methods for Simplifying the Generalized Solvatochromic Equation. *J. Org. Chem.* **1983**, 48, 2877-2887.

13. Kim, S.; Johnston, K. P. Molecular Interactions in Dilute Supercritical Fluid Solutions. *Ind. Eng. Chem. Res.* **1987**, 26 (6), 1206-1213.

14. Laurence, C.; Nicolet, P.; Dalati, T.; Abboud, J-L.; M.; Notario, R. The Empirical Treatment of Solvent-Solute Interactions: 15 Years of π^*. *J. Phys. Chem.* **1994**, 98, 5807-5816.

15. Liu, D.; Zhang, J.; Han, B.; Fan, J.; Mu, T.; Liu, Z.; Wu, W.; Chen, J. Effect of Compressed CO_2 on the Properties of AOT Reverse Micelles Studied by Spectroscopy and Phase Behavior. *J. Chem. Phys.* **2003**, 119 (9), 4873-4878.

16. Lu, J.; Boughner, E. C.; Liotta, C. L.; Eckert, C. A. Nearcritical and Supercritical Ethanol as a Benign Solvent: Polarity and Hydrogen Bonding. *Fluid Phase Equilib.* **2002**, 198, 37-49.

17. Michels, A.; Michels, C. *Philos. Trans. R. Soc. London*. **1933**.

18. O'Neill, M. L.; Cao, Q.; Fang, M.; Johnston, K. P.; Wilkinson, S. P.; Smith, C. D.; Kerschner, J. L.; Jureller, S. H. Solubility of Homopolymers and Copolymers in Carbon Dioxide. *Ind. Eng. Chem. Res.* **1998**, 37, 3067-3079.

19. Oka, H.; Kajimoto, O. UV Absorption Solvatochromic Shift of 4-Nitroaniline in Supercritical Water. *Phys. Chem. Chem. Phys.* **2003**, 5, 2535-2540.

20. Prausnitz, J. M.; Lichtenthaler, R. N.; Gomez de Azevedo, E. G. Molecular Thermodynamics of Fluid-Phase Equilibria. Second edition, Prentice-Hall Inc. **1986**.

21. Release on the Static Dielectric Constant at Ordinary Water Substance from Temperatures from 238K to 873K and Pressures up to 1000 MPa. The International Association for the Properties of Water and Steam, Erlangen, Germany, **1997**.

22. Shervani, Z.; Ikushima, Y. Micropolarities of Sodium Bis(2-Ethylhexyl) Sulfosuccinate Reverse Micelles Prepared in Supercritical Ethane and Near Critical Propane. *Colloid Polym. Sci*. **1999**, 277, 595-600.

23. Shervani, Z.; Ikushima, Y. The Investigation of Water/AOT/Supercritical Ethane Reverse Micelles by UV-Vis Spectroscopy. *J. Supercrit. Fluids* **1998**, 13, 375-379.

24. Sigman, M. E.; Lindley, S. M.; Leffler, J. E. Supercritical Carbon Dioxide: Behavior of * and Solvatochromic Indicators in Media of Different Densities. *J. Am. Chem. Soc*. **1985**, 107 (6), 1471-1472.

25. Tucker, S. C. Solvent Density Inhomogeneities in Supercritical Fluids. *Chem. Rev*. **1999**, 99 (2), 391-418.

26. Yonker, C. R.; Smith, R. D. Solvatochromic Behavior of Binary Supercritical Fluids: The Carbon Dioxide/2-Propanol System. *J. Phys. Chem*. **1988**, 92, 2374-2378.

27. Yonker, C. R.; Smith, R. D. Solvatochromism: A Dielectric Continuum Model Applied to Supercritical Fluids. *J. Phys. Chem*. **1988**, 92, 235-238.

28. Yonker, C. R.; Frye, S. L.; Kalkwarf, D. R.; Smith, R. D. Characterization of Supercritical Fluid Solvents Using Solvatochromic Shifts. *J. Phys. Chem*. **1986**, 90, 3022-3026.

CHAPTER 4

Fourier Transform Infrared Spectroscopy

Solvent effects on IR spectra can be significant and informative. Bellamy et al. (9), studied solvent-induced frequency shifts on the N–H stretching in pyrrole. In the same form Josien and Reisse et al. (9), studied the solvent effects in aldehydes, ketones (C=O), and halocyclohexanes (C–X). Further studies in $scCO_2$ (9), probed that CO_2 could be in the ether-ethyl acetate hydrogen bond basicity range. The Lewis acidity and basicity of CO_2 has also been measured with IR spectroscopy, based on its interactions with pyrrole and ketones (18), as well as with carboxylic acids (2, 19).

Many studies about reverse micelles using FT-IR spectroscopy have been reported. In the absence of CO_2, the broad band of hydroxyl stretching $v(O–H)$ centered at 3600 cm^{-1} is usually used for those investigations. This absorption band can be utilized to study the properties of H_2O in the reverse micelles; even though it is overlapped with the intense absorption of CO_2 in the region of 3840-3470 cm^{-1}. The changes of carbonyl stretching vibration $v(C=O)$ (situated around 1730 cm^{-1}) with pressure, also provide information on reverse micelles (14), and will be further explored in this study.

4.1 Supercritical Carbon Dioxide ($scCO_2$): IR Spectrum

The activity of rotation and vibration bands in the infrared (IR) is determined by the simultaneous change in dipole moment. The CO_2 molecule has four possible vibrational modes, which are shown in the Figure 4-1. Figure 4-2 shows two very strong bands at 667.3 and 2349.3 cm^{-1}, assigned to the fundamentals asymmetric bending (v_2) and asymmetric stretching (v_3) respectively. It has a fundamental symmetric stretching vibration (v_1) that is inactive in IR. However, this single strong vibration can be detected by Raman spectroscopy at 1337 cm^{-1} only. The deformation vibration (v_{2a}) (out of plane), and (v_{2b}) (in plane), involves the alteration of the O=C=O angle, these two vibration modes have the same frequency, thus are called doubly degenerate.
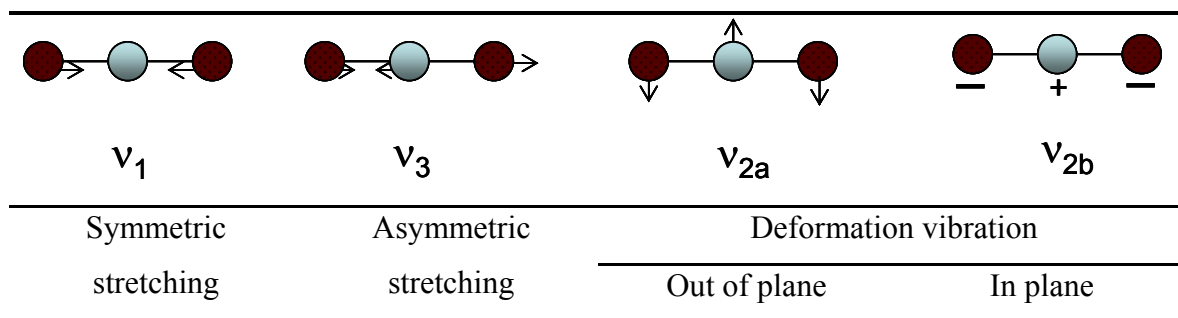
Figure 4-1: Vibrational modes of CO_2.

Surprisingly, two strong bands (1 in Figure 4-2) are observed at 1384.6 cm^{-1} and 1281.5 cm^{-1}. The mean value 1333.1 cm^{-1} is very close to that normally expected for the first overtone of the fundamental v_2 ($2\times667.3=1334.6$ cm^{-1}, 1). Since the energy level for the fundamental v_1 is very close to that of the overtone $2v_2$, a Fermi resonance takes place. This results in the shift of the first level towards a higher energy, and of the second level towards a lower energy accompanied by a substantial increase in intensity of the respective bands. The intensity of the bands is also intensified because of the increase of intermolecular interactions originated by the supercritical state. $scCO_2$ IR spectrum also presents two overtone/combination bands in the region 3400-3900 cm^{-1} from (v_1+v_3) and ($2v_2+v_3$) (2 in Figure 4-2), and at higher frequencies three peaks assigned to ($2v_1+v_3$) and ($v_1+2v_2+v_3$) (3 in Figure 4-2). At the Near-IR appear little band for the symmetric stretch overtone $3v_3$.
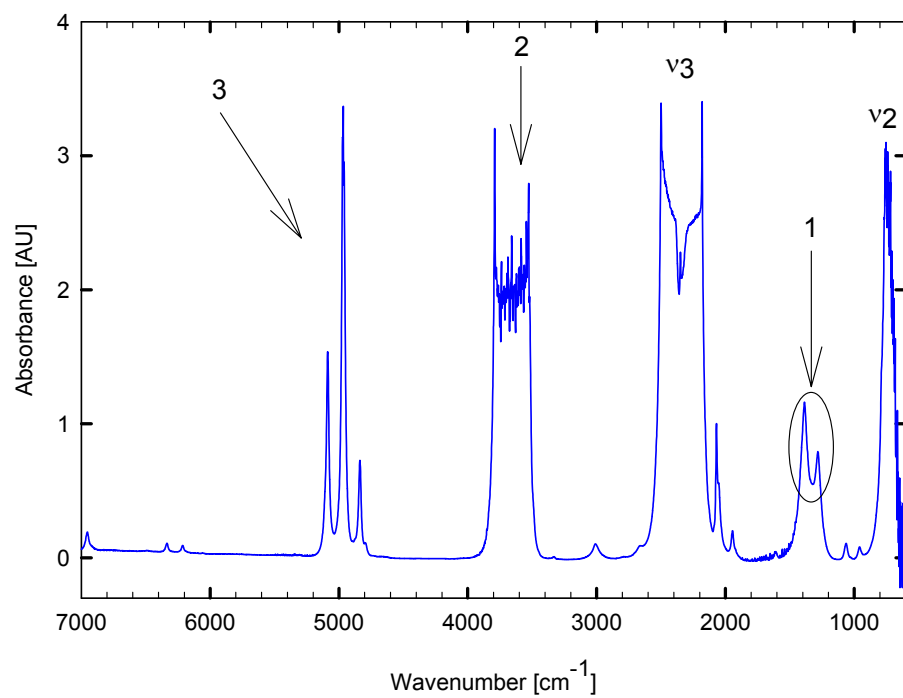
Figure 4-2: IR spectrum of CO_2 (205 bar, 40°C).
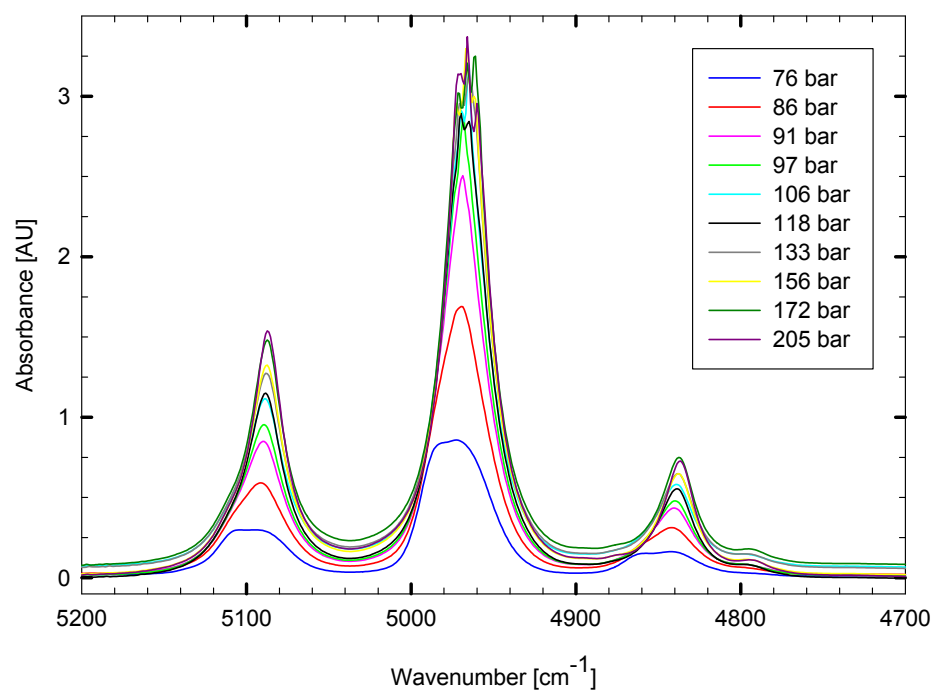
Figure 4-3: Effect of pressure in CO_2 IR spectrum (region 5200-4700 cm^{-1}).

The FTIR spectroscopy has been largely limited to the observation of changes in two bands, resulting from Fermi resonance as pressure of $scCO_2$ is changing. The high frequency peaks have been used to characterize the supercritical fluids. Especially the overtone $(3v_3)$, that is clearly observed in near-IR (4). If we examine Figure 4-3, we can observe the changes in the shape and the shift to lower frequencies of the maximum absorbance when pressure is increasing. This is caused by the enhancement of intermolecular interactions occurring in the bulk $scCO_2$. The loss in rotational freedom of $scCO_2$ as density increases may be related to the changes in molecular interactions between the CO_2 molecules, because of their closeness provoked by the high-pressure. If we plot this shift versus fluid density we can observe the decreasing trend until reaches a constant plateau at higher interaction liquid-like densities (Figure 4-4). This phenomenon has also been observed by other investigators (4).
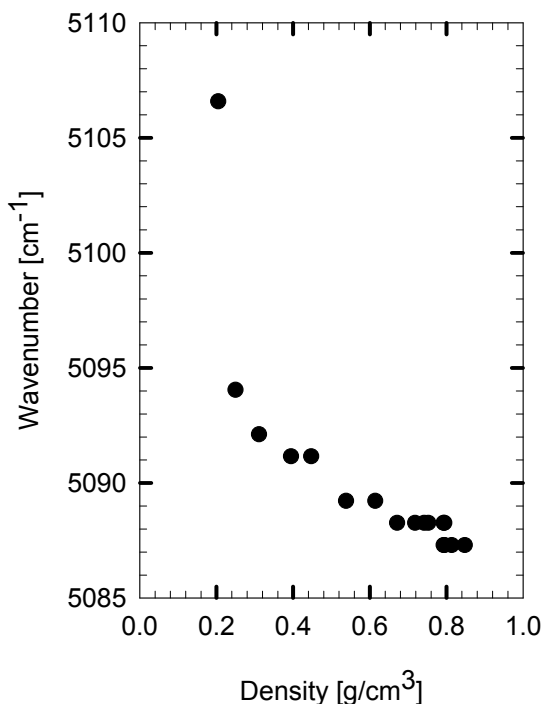
Figure 4-4: Shift in frequency maximum.

4.2 H₂O-scCO₂ IR Spectrum

The H_2O molecule is an ubiquitous molecule which is far from being inert. Even though its simplicity and familiar chemical structure, it alone possesses an important property which has interesting consequences: hydrogen bonding (HB). It has two acceptor sites for HB and two donor sites, which gives it exceptional possibilities to establish a great number of HB's with neighboring molecules. The HB capability makes of H_2O a highly versatile molecule. When embedded in a macromolecule it can rapidly

change the HB configurations established with the hydrophilic groups of the macromolecule or other H_2O molecules. This versatile behavior makes of H_2O, at the same time not so easy to study.

One approach that can potentially overcome these difficulties is using IR spectroscopy. It is a powerful technique to observe and study HB, which appears in a particular number around H_2O molecules. Rather than completing a study about H_2O alone the research looked at its effects to other molecules. The regions 1000-1400 and 1700-2500 cm^{-1} have been used to study the effects of H_2O over amide of peptide groups, of proteins when they bind to H_2O, mainly due to C=O stretch and C–N–H bending vibrations (16). The HB's are directional and give the ice a tetragonal structure ordering around the O atom, and in the liquid phase only 5% of the hydrogen bonded structure is lost. This implies that broken HB's are not at the origin of the fluidity of H_2O and that the majority of HB in H_2O should be probably bent HB's. This is the reason of its anomalous behavior, compared with others liquids. H_2O has a few vibrational bands, but because of the extremely high concentration of HB's, these bands have a large coefficient of absorption that appears opaque to IR. The spectrum of H_2O (at 27°C and 1 bar) is conformed of two bands at $v>1000$ cm^{-1}. The first one has a well-pronounce sharp peak at 1640 cm^{-1}, corresponding to the bending mode (v_2) of the isolated H_2O molecule that is centered at 1595 cm^{-1} (15). It has a wide compound at around 2150 cm^{-1}, which has been attributed to vibrational bands and culminate around 500 cm^{-1} with an image component at about 1150 cm^{-1} that is hard to detect because it is overlapped by much more intense bands. The second type of bands corresponds to stretching (O–H) and are the broad bands extending from 2800 to 4000 cm^{-1}, with a maximum in 3300 cm^{-1}. This band is comprised of the symmetrical (v_1) and anti-symmetrical (v_3) that broaden considerably, due to the effect of HB and Fermi resonance between v_1 and $2v_2$ that complicates the structure, as well. The modes of vibration of a simple H_2O molecule are seen in the Figure 4-5.
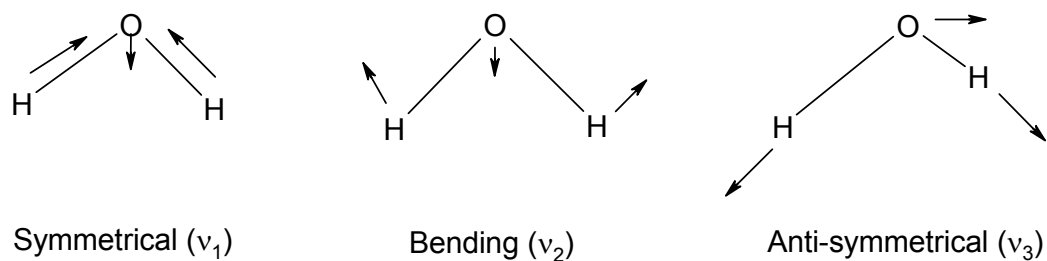
Figure 4-5: Vibrational modes of molecular H_2O.

Their counterparts at the vapor phase are the symmetrical (v_1) and anti-symmetrical (v_3) stretching bands at 3657 and 3756 cm^{-1}. They posses characteristic bands for HB systems, such as: they are intense, broad, and posses their own structure. The intensities of these bands are very sensitive to environment and to the state of H_2O association via HB. Indeed, when H_2O interacts with the environment (e.g., H_2O dissolved in a solvent or absorbed into a polymer) with the two protons of H_2O participating in HB, these bands shift to lower wavenumber.
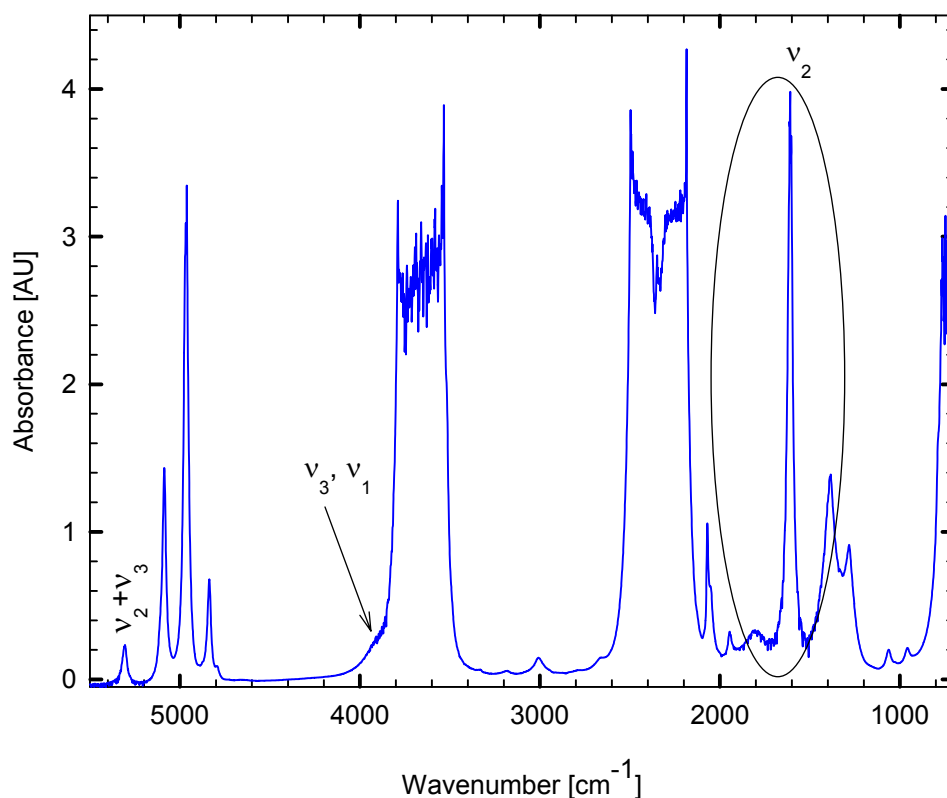
Figure 4-6: IR spectrum of H_2O-$scCO_2$ (215 bar, 40°C).

The spectrum of 1w% of H_2O dissolved in $scCO_2$ at 215 bar and 40°C was measured, which is seen in Figure 4-6. The presence of H_2O is verified by a peak at 1611 cm^{-1}, corresponding to the bending O–H vibration of hydrogen bonded H_2O, with a shoulder at slightly higher frequency from the overtone of 500 cm^{-1} band. The ν_3 and ν_1 stretching band are overlapped with the $scCO_2$. Only the shoulder at 3700 cm^{-1} can be seen and another peak appears at approximately 5100 cm^{-1} ($\nu_3 + \nu_2$), as a result of the combinations bands of the lower frequency bands.
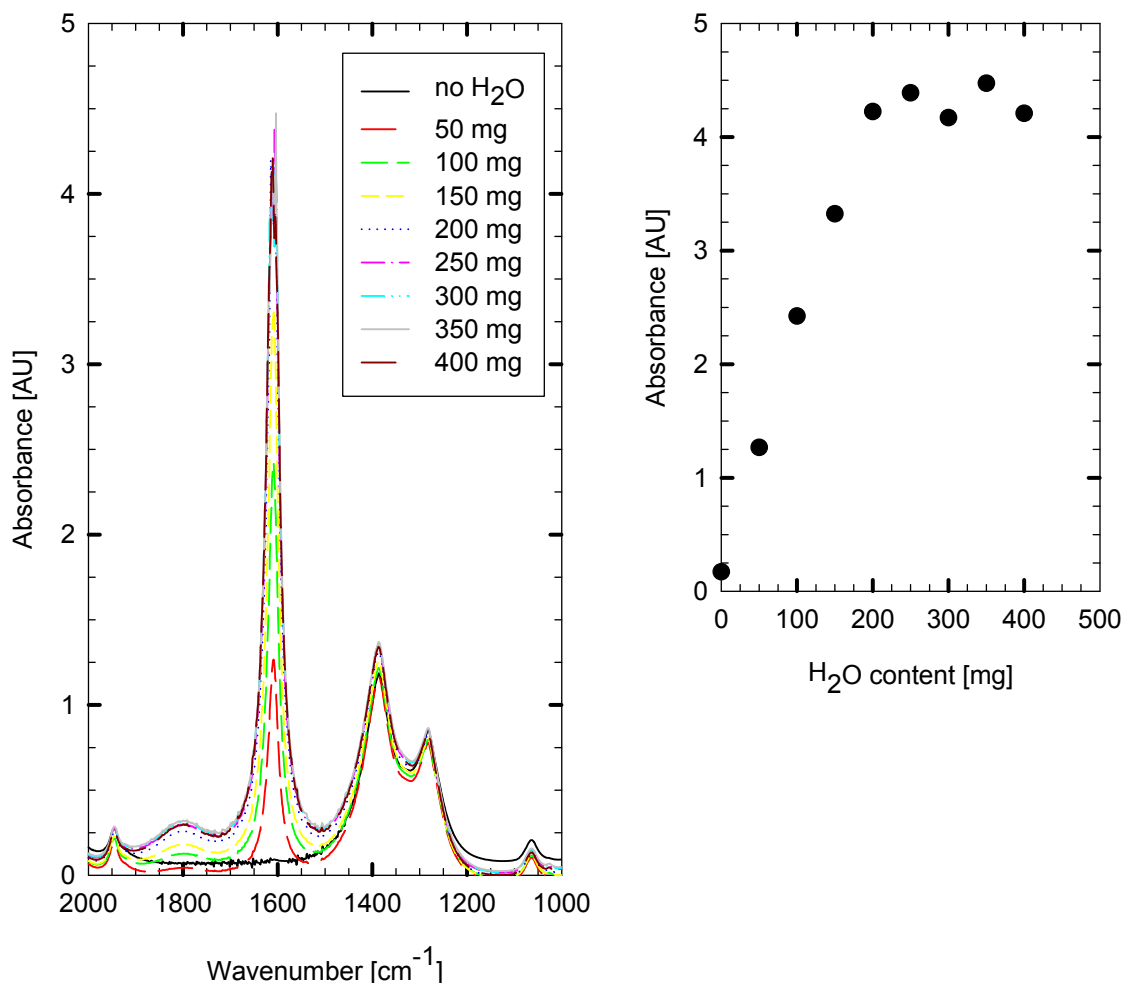
Figure 4-7: Effect of H$_2$O addition in scCO$_2$ (215 bar, 40°C).

To identify the H$_2$O peaks in the spectrum and their effect in the H$_2$O-scCO$_2$ system, a H$_2$O-addition experiment was conducted, at constant temperature. Approximately 50 mg of H$_2$O was added every time. The results can be seen in Figure 4-7 left, and the variation of absorbance with the amount of H$_2$O (Figure 4-7, right). One can observe that the bending vibration can be used to determine the H$_2$O solubilized in scCO$_2$ phase. The point of saturation (range 150–200 mg) coincides approximately, with H$_2$O solubility calculated with thermodynamics (13). The high frequency peak (5100 cm^{-1}) does not vary

appreciably as H_2O is added to the system.

4.3 Surfactant-scCO$_2$ System

The principal characteristics of the surfactants used in our work are described in Tables 2-3, 2-5 and 2-6. Here we present the IR spectrum of the surfactants in the supercritical phase, and describe the principal characteristics that identify them.

4.3.1 PL31 and P17R2 in scCO$_2$: IR Spectrum

The PL31 and P17R2 pluronic surfactant IR spectrums are similar, due to their similar composition. The characteristic infrared spectral features are seen in Figure 4-8 .
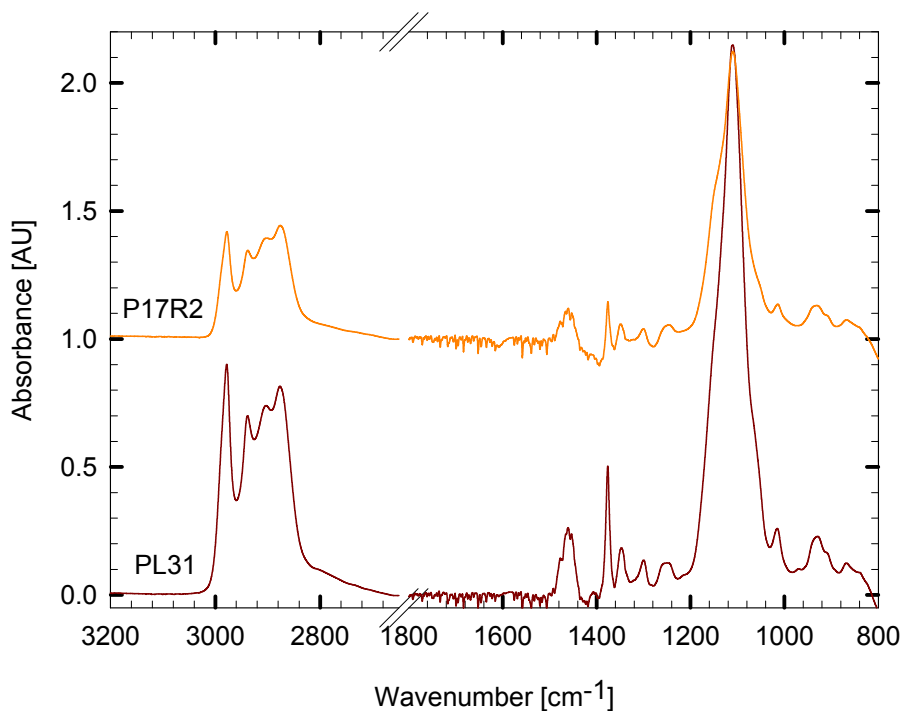
Figure 4-8: IR spectrum of pluronic surfactants in scCO$_2$ (40°C).

The important bands appearing in the region 2800-3000 cm^{-1} correspond to the C–H stretching vibration. Those vibrations come from the methyl or methylene groups, and

Figure 4-9 summarizes the vibration mode of these groups. In the case of the methylene group, it presents vibrations similar to H_2O molecule (Figure 4-5). A good resolution is able to detect at least, four absorption bands arising from symmetrical stretching for methyl (vCH_3) and asymmetrical stretching methylene (vCH_2) groups.

| Asymmetric stretch | Asymmetric deformation |

| Symmetric stretch | Symmetric deformation |

| Rock | Torsion |
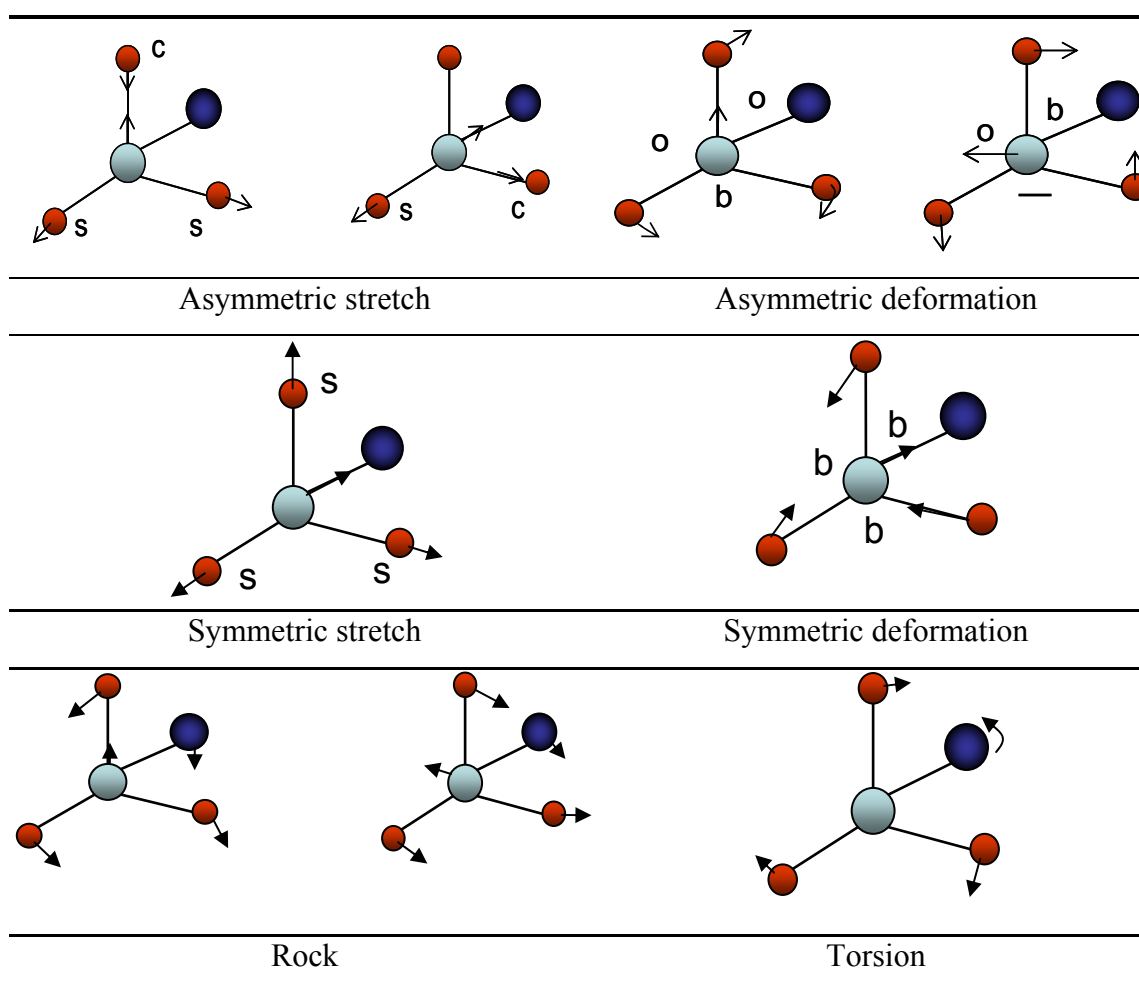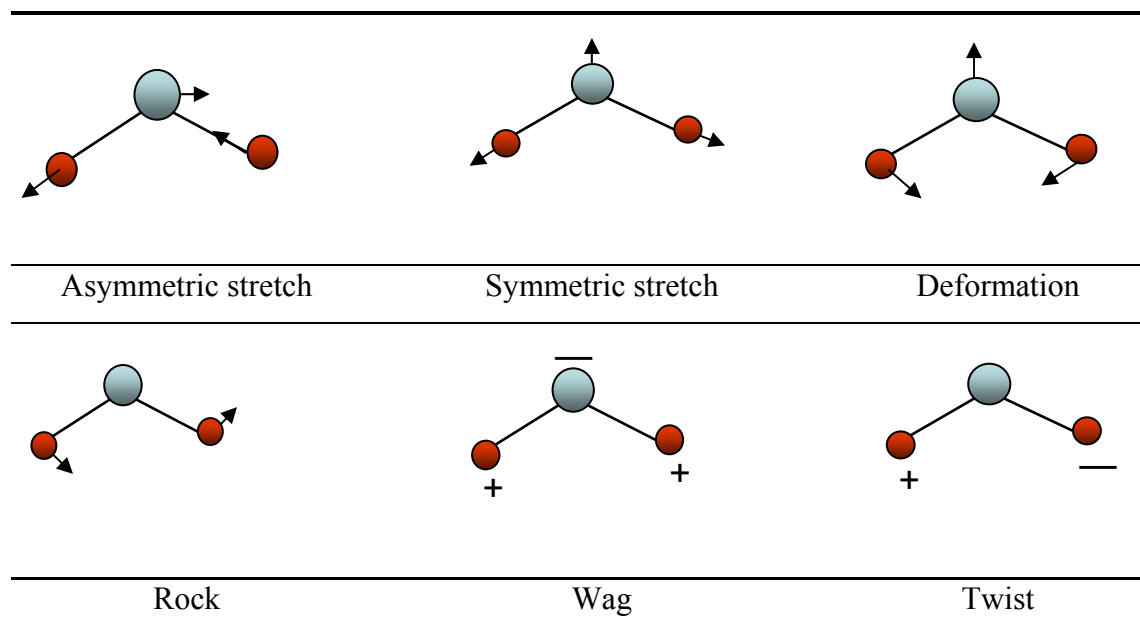
Figure 4-9: Characteristic vibrational modes of methyl and methylene groups (5).
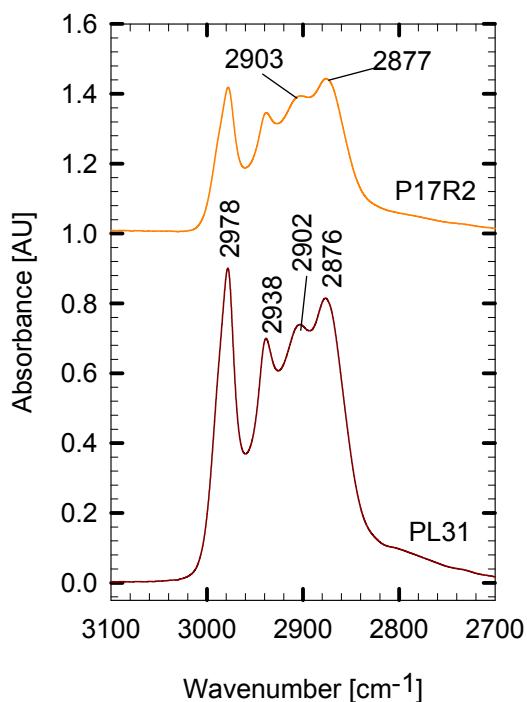
Figure 4-10: Aliphatic stretching mode.

The frequency of the νCH_3 sym vibration is 2872 cm^{-1} and for νCH_3 asym vibration is 2962 cm^{-1} (1). The νCH_2 sym of the methylene group gives rise to an absorption band at 2853 cm^{-1} and for the νCH_2 asym arises at 2926 cm^{-1}. The intensity of the asymmetrical vibrations of νCH_3 and νCH_2 are stronger than the symmetrical vibrations. This is helpful to determine the molecular structure of the compounds. In Figure 4-10 we assign the peak at 2978 and 2902 cm^{-1} to the νCH_3 asym, and νCH vibration respectively. These shifts are due to the temperature and the disordered state of

the surfactant in the fluid phase. The peaks at 2938 and 2876 cm^{-1} correspond to the νCH_2 asym and νCH_3 sym respectively. Because the νCH_2 and νCH_3 sym are more sensitive to the conformational changes, these have often been used for detect phase transition and conformational changes in low molecular weight surfactants. This can be seen through the decrease in the wavenumber and bandwidth, change that may corresponds to the unimer-to-micelle transition (8).

The region 1500-1200 cm^{-1}, corresponds to the bending modes of δCH_2 and δCH_3. The symmetrical δCH_3 gives rise to the absorption at 1365-1380 cm^{-1}. Studies have shown that this vibration mode is independent of the crystalline state, and depends on the number of carbon atoms in the molecule. The existence of these bands indicates a branched structure of CH_3. In Figure 4-11 we can observe a peak at 1376 cm^{-1} for both surfactants indicative of the δCH_3 sym vibration. It has been observed for polyethylene at 1375 cm^{-1} (1). The δCH_3 sym and νCH_3 asym enables the determination of the degree of branching of the substance. According to the structure and formula, PL31 has CH_3 groups as many as P17R2, hence the difference

Figure 4-11: Aliphatic bending mode.

in intensity of the peak is because PL31 is more soluble than P17R2. The band near 1347 cm^{-1} (1350 cm^{-1}) (8), corresponds to the out of phase δCH_2 wagging mode in a gauche conformation. The band 1299 cm^{-1} (1300 cm^{-1}) (8) is assigned to out of phase δCH_2

motions of gauche conformers[7].

The band due to C–O stretching mode for aliphatic ethers has been observed in the region 1200-1000 cm^{-1}. In this region we observe a peak around 1109 cm^{-1} for both surfactants (Figure 4-10). This region also corresponds to the C–C vibrations, but the dipole moment variations of the polar C–O bond are much larger than in C–C bonds, therefore the νC–O bands are stronger than νC–C. The only difference between them is seen in the bandwidth which is broader for P17R2 than for PL31 and gives the appearance of a shoulder in the left side of the peak.

The δCH$_3$ asym vibration of the methyl group gives rise to a band around 1460 cm^{-1} (7). It is more evident in alkanes of low molecular weight, but in longer chains it is overlapped by the scissoring vibration of the methylene groups (δCH$_2$). The region of 1480-1460 cm^{-1} (Figure 4-12) corresponds to this vibration. It is known that this band is very sensitive to the intermolecular interaction, and is often used as a key band to check the state of packing of the methylene chain. The shift to lower frequency (1453 cm^{-1}) indicates a weak molecular interaction. Therefore, the relative intensity of these frequencies can give us an intermolecular interaction parameter for the interaction of block copolymer chains.

Figure 4-12: Methyl asymmetric vibration.

[7] Conformation where the functional groups attached to two adjacent carbons are 60° apart.

4.3.2 Zonyl in scCO₂: IR Spectrum

The perfluorinated surfactant Zonyl when solubilized in $scCO_2$ at 194 bar and 40°C shows an IR spectrum. Differences can be seen in the region of 2000-2500 cm^{-1}. Both sides of the broaden band increases, while with pluronics only the right side. If we subtract the effect of $scCO_2$, we can analyze the important features of the Zonyl surfactant in Figure 4-13.
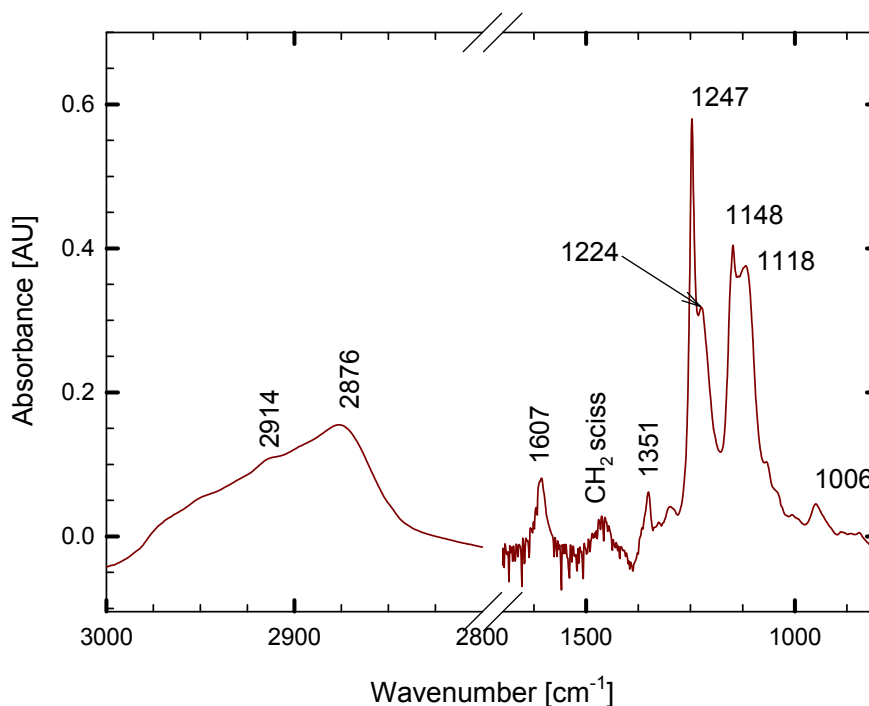
Figure 4-13: Zonyl IR spectrum at 194 bar and 40°C.

As previously described, we assign the νCH_2 sym at 2876 cm^{-1} and a little shoulder at 2914 cm^{-1}. This is verified with the bands in the region around 1450-1480 cm^{-1} assigned to the δCH_2 scissoring vibration. A peak at 1607 cm^{-1} corresponds to the O–H accompanied with the saturation band from H_2O, which should be from impurities. The out of phase δCH_2 wag appears at 1351 cm^{-1}. The CF_3 group absorbs strongly at 1350-1120 cm^{-1}, and the CF_2 at 1280-1120 cm^{-1}, so it is not easy to differentiate (5). At 1247

cm^{-1} corresponds to CH$_{2w}$ (CH$_2$ wagging) intensified by the presence of the fluorine groups. The frequency of the peak at 1118 cm^{-1} can be assigned to the asymmetric stretching mode of the C–O–C.

The stretching vibration of halogen compounds (e.g., vC–Cl, vC–Br, and vC–I) lies in the range of 500-800 cm^{-1}. The C-F bond is an exception because its vibrations occur at 1000-1400 cm^{-1}.

4.3.3 Gele in scCO$_2$: IR Spectrum

The IR spectrum of Gele in scCO$_2$ at 178 bar and 40°C is shown in Figure 4-14.
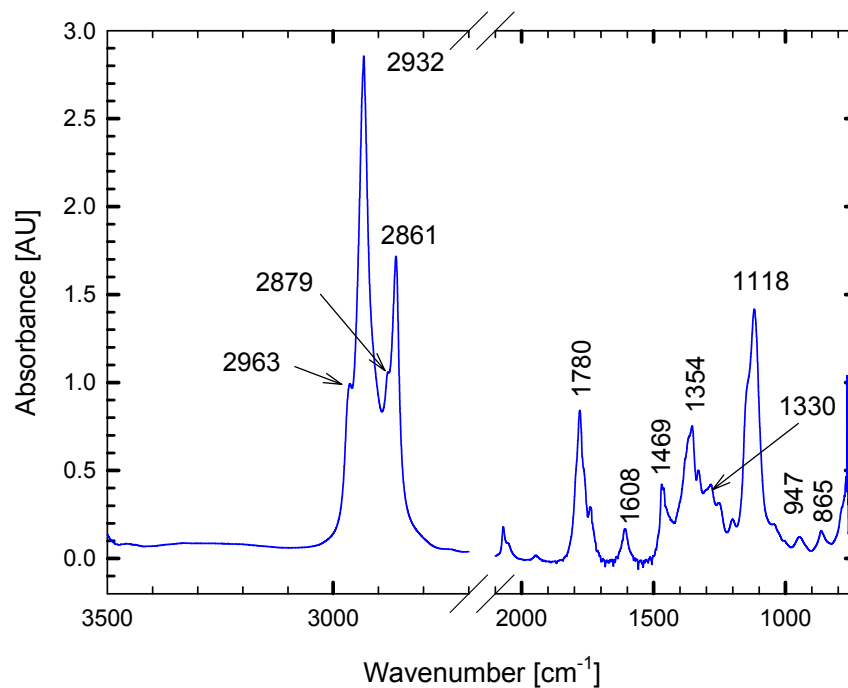
Figure 4-14: Gele IR spectrum (178 bar and 40°C).
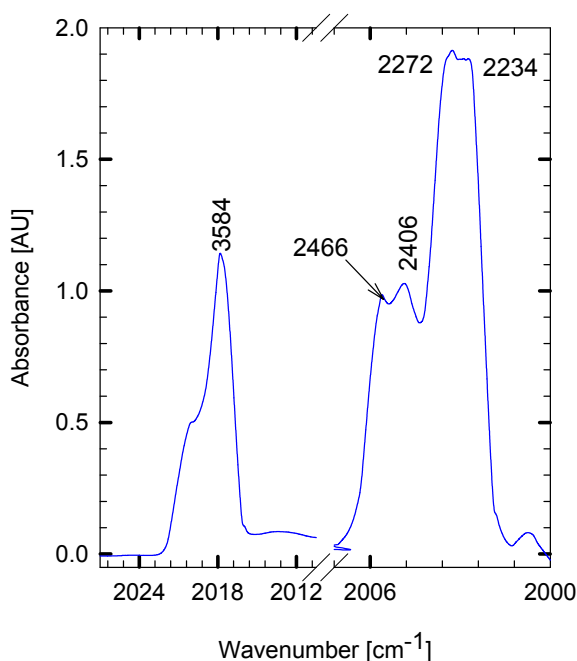
Figure 4-15: Overtone and 2000-2400 cm^{-1} region.

Besides the characteristic peaks of the aliphatic compounds, which are similar to the others surfactants. This carboxylic surfactant presents the characteristic peak at 1780 cm^{-1}, and a shoulder at 1740 cm^{-1}. These are attributed to the stretching vibration of the monomer and dimer, respectively. The C=O stretching vibration bands of the acetic acid monomer and dimer in scCO$_2$ were detected at 1772 cm^{-1} and 1722 cm^{-1}, those of palmitic acid monomer and dimer appear at 1762 and 1716 cm^{-1} (11). The higher intensity at 1780 cm^{-1} indicates that the surfactant monomeric form is preferred than the dimer form, which is more stable in scCO$_2$ than in organic solvents. This is because of the interaction between CO$_2$ and carboxylic acids through the quadrupole-OH group or via Lewis acid-base type interaction (2). The quadrupole-OH interaction is stronger than that between non-polar or weakly polar organic solvents and carboxylic acids. The formation of monomers is favored by an increase of pressure, and the dimerization is increased with the increase of carbon number of carboxylic acids. The influence of the CH$_2$ chain length of acids on dimerization in scCO$_2$ is similar in the organic solvents. However, have little effect on the specific interactions of CO$_2$ with the acid functional group, suggesting no difference in steric hindrance.

In the region where the broaden scCO$_2$ peaks appear (2000-2500 and 3100-4000 cm^{-1}), the subtracted spectrum where smoothed and the band found can be seen in Figure 4-15. The peak at 3584 cm^{-1} is an overtone of the vibration at 1780 cm^{-1}.

The comparison among the spectrums of the surfactants solubilized in scCO$_2$, can be

seen in Figure 4-16.
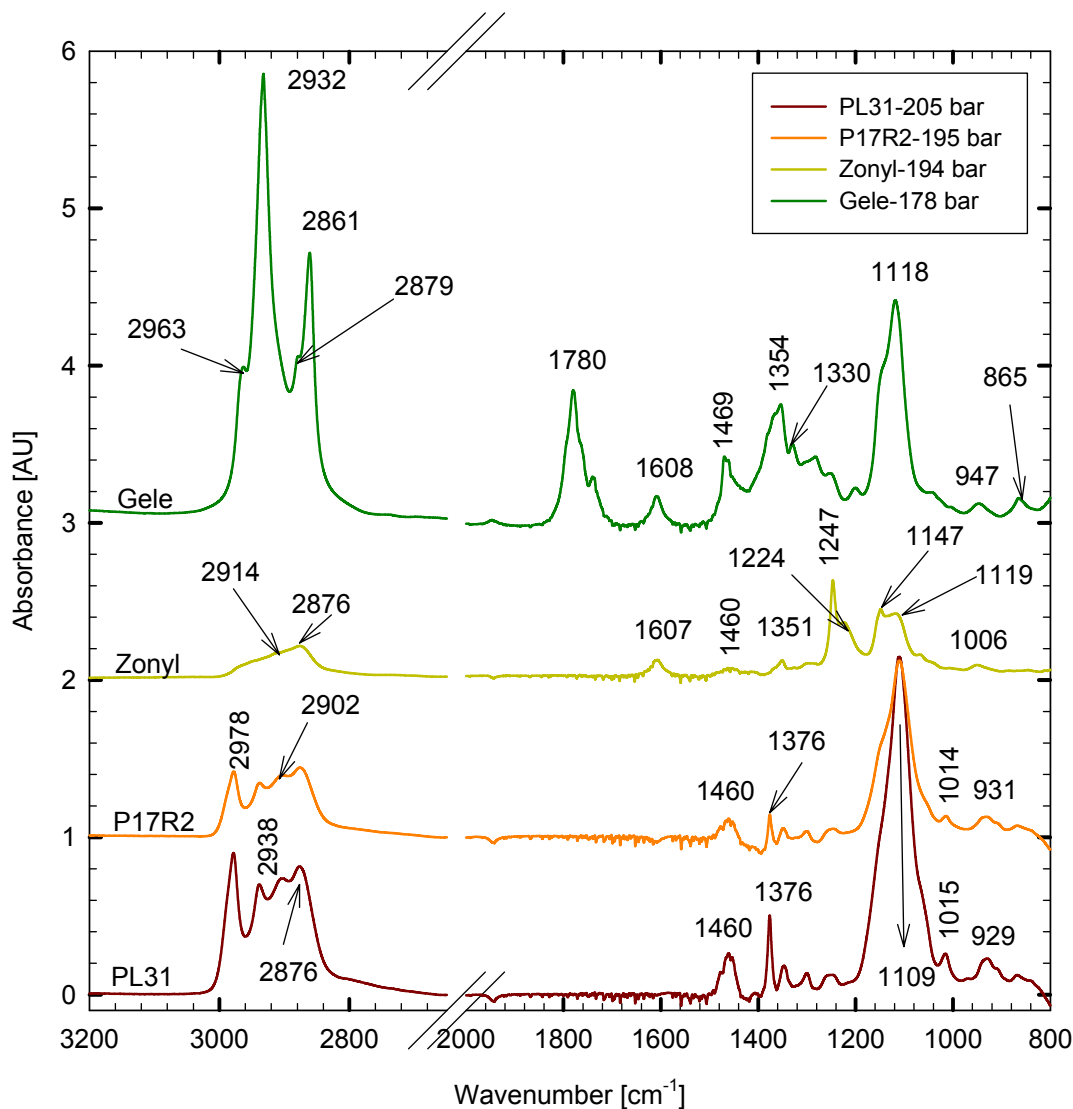
Figure 4-16: Comparison of IR spectrums of the surfactants used in this investigation.

In the region corresponding to stretching vibration (3000-2800 cm^{-1}) we can see differences among the surfactants. The asymmetric stretching vibration νCH_3 is a stronger peak at 2978 cm^{-1}, and characterize the pluronic surfactants, while in Gele this vibration mode appears as a shoulder only, and shifted to lower frequencies (2963 cm^{-1}). The strong intensity in pluronic surfactants IR spectrum is because of the greater number

of CH_3 in pluronic surfactant (16 for PL31, and 30 for P17R2), while Gele has only one terminal CH_3. Differences between PL31 and P17R2 could come from the different conformational structure of them. The interactions of Gele with $scCO_2$ is stronger, this could be because a terminal group attached to a long aliphatic chain that is quite CO_2-philic. The asymmetric stretching vibration $\nu(CH_2)$ appears at quite similar frequencies for pluronics and Gele, 2938 cm^{-1} and 2932 cm^{-1} respectively. The strong peak at 2861 cm^{-1} in Gele spectrum corresponds to the symmetric stretching vibration $\nu(CH_2)$. In pluronics and Zonyl appears a peak at 2876 cm^{-1} corresponding to symmetric stretching (CH_3) while in Gele appears at 2879 cm^{-1} as a shoulder. There is a $\Delta\nu=15$ cm^{-1} between the asymmetric stretching CH_3 of pluronic surfactants and Gele. This would indicate a different interaction force between the surfactants and the $scCO_2$.

In the finger print region we can observe the vibration at 1780 cm^{-1} this characterize the carbonyl compounds. The deformation of CH_2 is a strong peak at 1460 cm^{-1} in pluronic, just visible in Zonyl and slightly shifted to 1469 cm^{-1} in Gele. However, it is considerer that this vibration mode is influenced by structural elements and the intensity increases with the number of CH_2 groups. It agrees with pluronics that have 80 to 36 CH_2 groups, but not for Gele and Zonyl (with 17 and 22 CH_2 groups respectively). It is also important to mention that this is not a unique vibration mode because generally it overlaps with the asymmetric deformation mode of CH_3. As we can see the symmetric bending of $\delta(CH_3)$ can help us to differentiate the pluronics from Gele and Zonyl. Meanwhile in the region around 1354 cm^{-1}, Gele presents a broad band corresponding to the out of phase deformation CH_{2w}. To characterize Zonyl we find a peak at 1247 cm^{-1} assigned to C–F (alkyl). Another interesting characteristic is the vibration corresponding to C–O, in both pluronic surfactants this strong vibration appears at 1109 cm^{-1}, while in Gele it is shifted to higher frequency 1118 cm^{-1}; this would suggest the differences in the interactions with $scCO_2$. In Zonyl C–O vibration mode at 1119 cm^{-1} is overlapped with the C–F vibration mode. These are the main features that can help us to differentiate among the surfactants used in this investigation.

4.4 Drug-Surfactant-H_2O-scCO_2: Microemulsion Formation?

All the experiments were done at 40°C using the set-up presented in section 2.3 and following the experimental procedure explain in section 2.4.

4.4.1 Acetaminophen

The formation of microemulsions was analyzed through the shift of the characteristic peaks of the spectrum and to probe the different states of solubilized H_2O molecules the deconvolution method was used. For acetaminophen (Ace)-surfactant systems the peaks were centered at 3245 ± 30, 3474 ± 35, 3588 ± 42, 3737 ± 29 (for H_2O), and 3877 ± 18 (for solute). The full widths at half height of were 144 ± 3, 70 ± 10, 55 ± 7, 47 ± 6, and 66 ± 12 respectively. The physical meaning of these regions will be explained in the next sections.

4.4.1.1 PL31

First, PL31 surfactant (160 mg) was dissolved in scCO_2. Then, aqueous solution of Ace in H_2O was added to the system, the composition can be seen in Table 4-1.

Table 4-1: Conditions of PL31-Ace-H_2O-scCO_2

Condition	*Pressure [bar]*	*Composition [w%]*				W_0^8
		PL31	Ace*	H_2O	scCO_2	
Without H_2O-Ace	178.40	0.240	0.000	0.000	99.76	0.00
1220 mg H_2O-0.050 mg	169.41	0.239	0.007	1.788	97.97	439
1285 mg H_2O-0.255 mg	168.59	0.239	0.037	1.884	97.88	462
1350 mg H_2O-0.460 mg	169.27	0.239	0.067	1.975	97.79	485

* Acetaminophen (Ace) is multiply by 100

---

[8] W_0=[H_2O]/[surfactant] molar ratio.
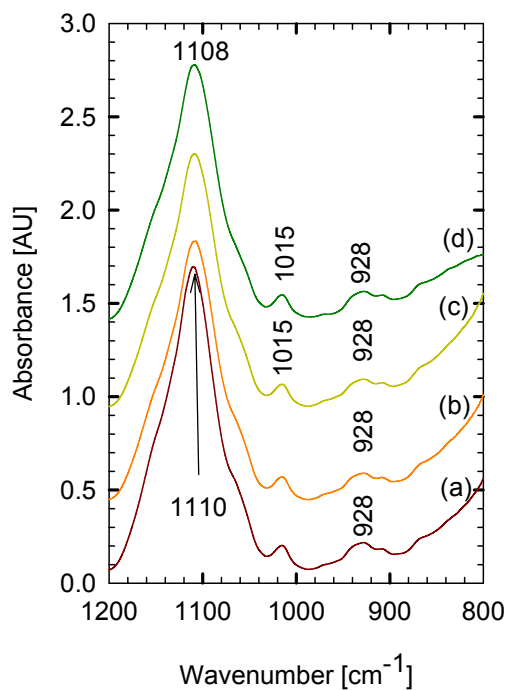
Figure 4-17: C-O peak variation.
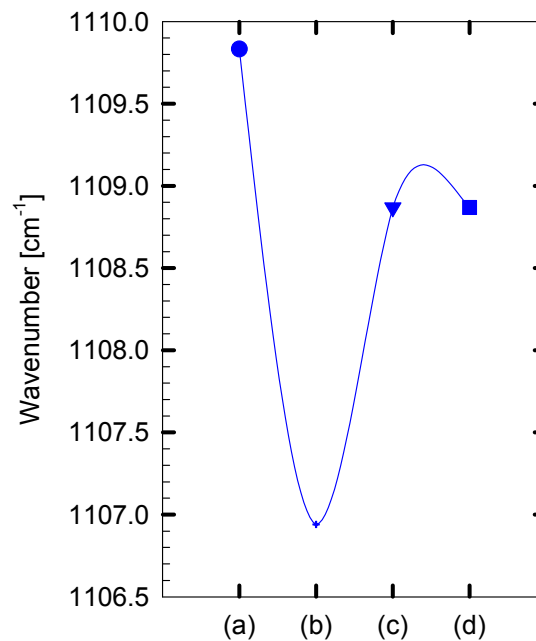
Figure 4-18: C-O shift (PL31-Ace).
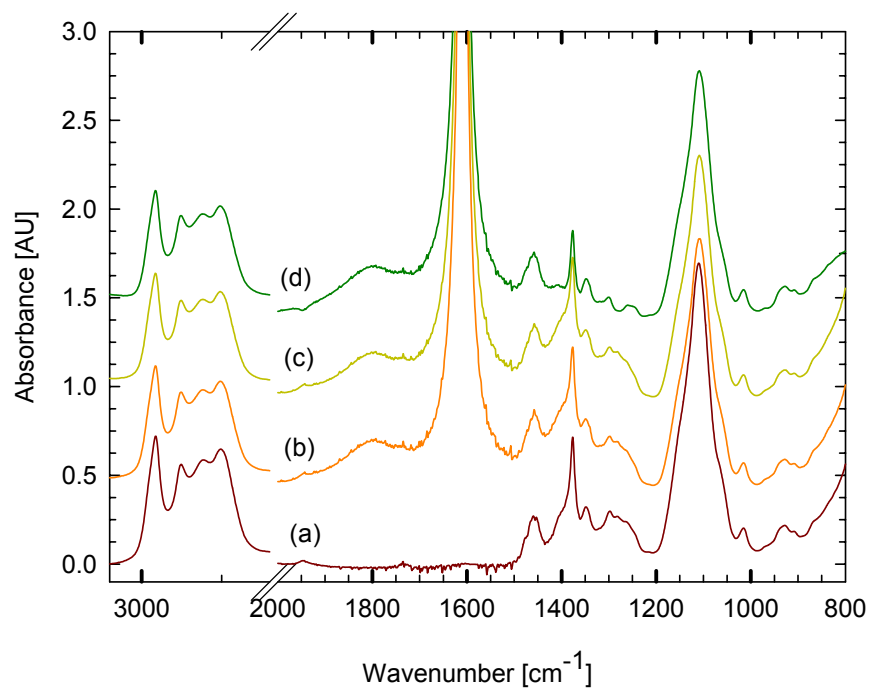
Figure 4-19: (a) without H_2O, (b) 1220 mg H_2O, (c) 1285 mg H_2O, and (d) 1350 mg H_2O.

The complete spectrum of every experimental condition can be observed in Figure 4-19. At 1609 cm^{-1} appears the peak corresponding to $\delta(OH)$ vibration mode. It has been suggested that shifts in this position may be used to distinguish bound and bulk H_2O in micellar systems. In this study the data reveals a little broadening, even though this broadening does not provides conclusive spectroscopic evidence for reverse micelle formation, it suggests that surfactant rich environments are presents for H_2O in addition to bulk CO_2 (17).

There is some appreciable change in the region of 1200–800 cm^{-1} caused by water addition, as can be seen in Figure 4-18. The shift of the peak of C–O is shown in Figure 4-17. The slight decrease of frequency would be indicative of a more interacting structure. The increase of H_2O produces an abrupt shift, as well as the well known C–O stretching band shifting to lower frequency when H_2O molecules bind to EO groups. The sudden increase indicates that the bond is not strong. Finally, it gets to a transition point where the EO-H_2O bond becomes strong. Coincidently, the peak initially at 1298 cm^{-1} shifts to a more evident peak at 1301 cm^{-1}. This would indicate a preferable tendency to form gauche conformers around the C–C. This was explained by the dielectric effect of the aqueous media, and HB between the polyethylene oxide chain and H_2O (2).

These changes can be observed in Figure 4-20. Also in this region there is
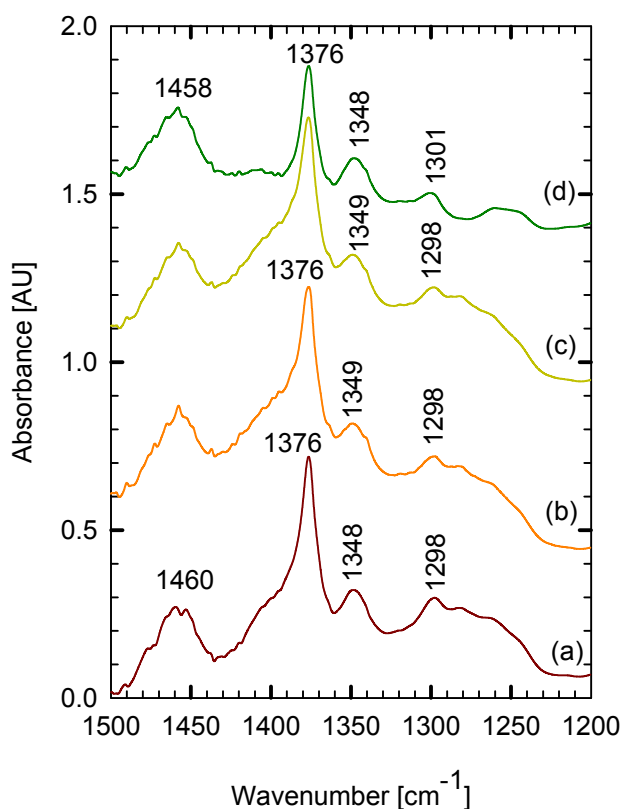
Figure 4-20: (a) No H_2O and Ace, (b) 1220 mg H_2O, (c) 1285 mg H_2O, and (d) 1350 mg H_2O.

an apparent decrease in intensity of the peak at 1349 cm^{-1}, provoked by the widening of the bandwidth. This would indicate the change of the C–C gauche conformation, as well as the decrease of the rotational freedom, due to the enriched hydrogen bonding surrounding.

In Figure 4-20 there is a slight change in the spectrum. When there is not H_2O we can see two peaks at 1460 and 1453 cm^{-1}. When H_2O is added the left shift to 1458 cm^{-1} is more evident. The region of 4200-3050 cm^{-1}, after subtraction and smooth of the spectrum we observe many microenvironments (Figure 4-21). The absorption band at the highest wavenumber (around 3737 cm^{-1}) behaves as monomeric-like isolated H_2O analogous to gas-phase spectrum of H_2O. The band around 3588 cm^{-1} has been assigned to the non-hydrogen bonded H_2O molecules which have penetrated into the surfactant layer. The region around 3474 cm^{-1} is assigned to the hydrogen bonded dimers bound at the interface. The absorption band at the lowest wavenumber (3245 cm^{-1}) is ascribed to the OH stretch in the hydrogen bond chain, which is presented as free H_2O in the core of the micelle (7). At a highest wavenumber, we observe a peak around 3850 cm^{-1}, this peak may correspond to the solute (acetaminophen) from the amine vibration, which undergoes to a blue shift because of the HB polar surroundings.
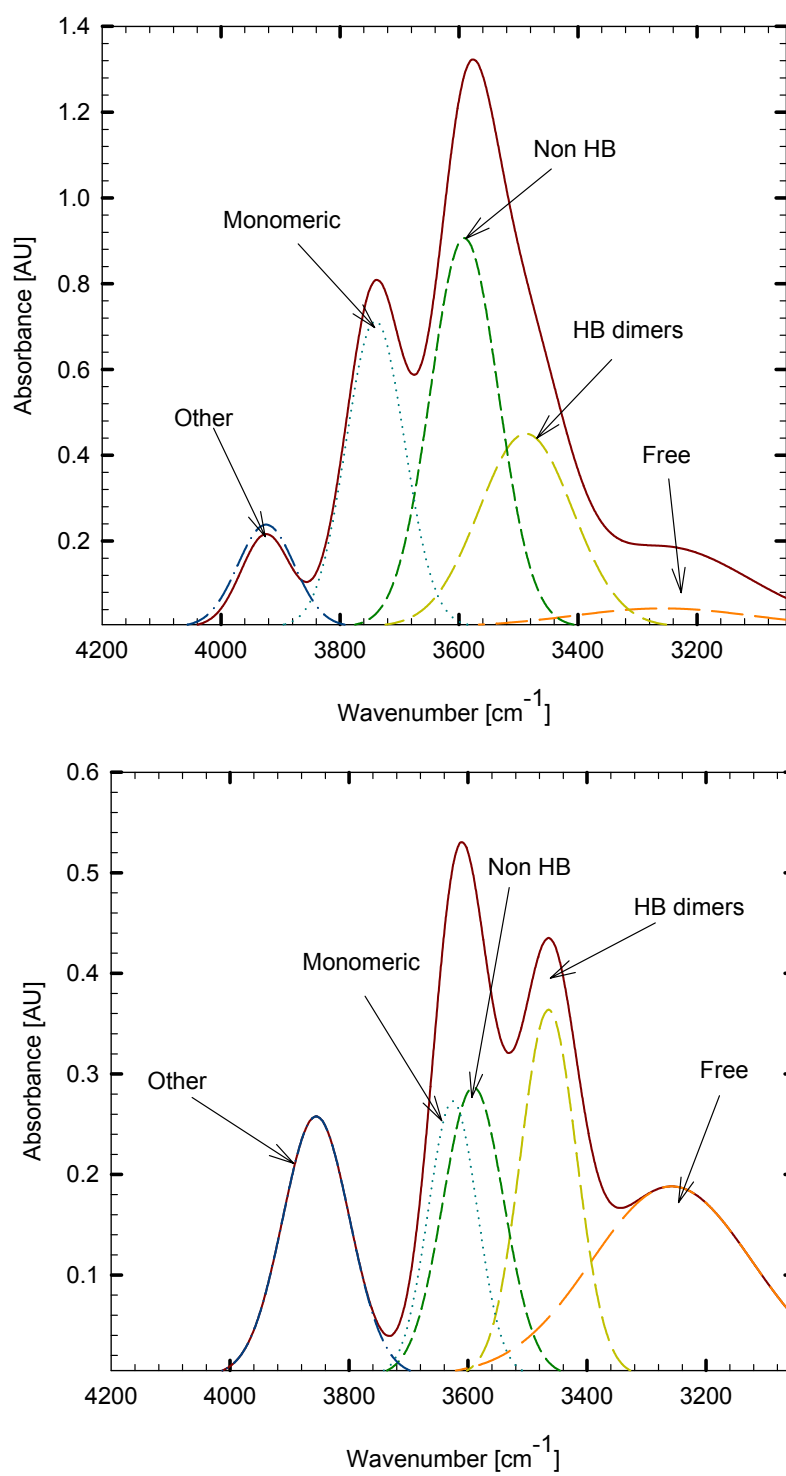
Figure 4-21: Region ν(OH) vibration (up) 1220 mg H₂O, (down) 1350 mg H₂O.

From the Gaussian-curve fitted the area ratio of each type of H_2O was obtained. Assuming that the frequency dependence in the absorptivity of each OH stretching species was negligible, we calculate the number of each type of H_2O molecule from the Beer's law (10). The variation of these types of H_2O with respect to effective H_2O ratio is observed in Figure 4-22.

Since the other types of H_2O (e.g., NHB, HB, and monomeric H_2O) decrease, we can say that the free-H_2O enhancement is produced by the diffusion from the other H_2O types and from H_2O added to the system as well. The peak at 3878 cm^{-1} increase as W_0 increases, indicating that the solute concentration is augmented, which suggests an increase of solubilization in the core of the reverse micelle.

It is also interesting to explore the lower effective H_2O ratio. In other experiment, the quantity of surfactant was higher (171.4 mg), and less quantity of H_2O was added. All the curves show an increasing trend (Figure 4-23). Besides, from the fitted curves, we can say that at high pressures the quantity of H_2O needed to form reverse micelles is 500 mg approximately.
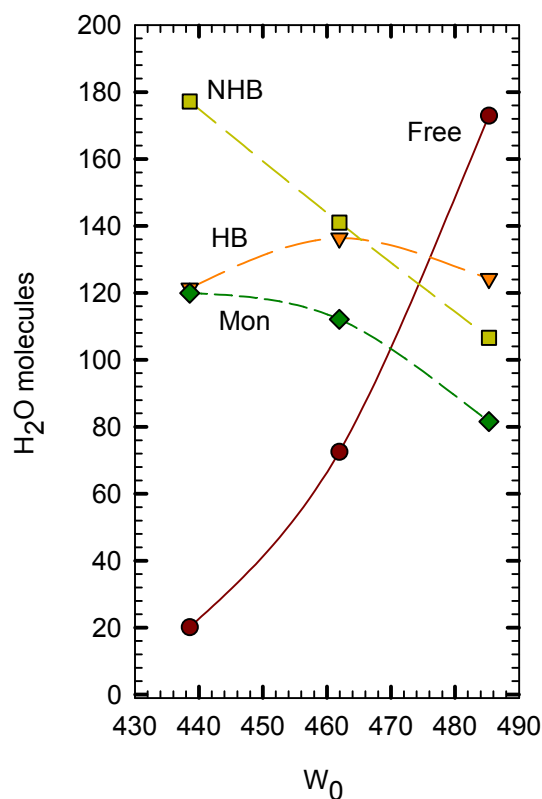
Figure 4-22: Distribution of types of H_2O.
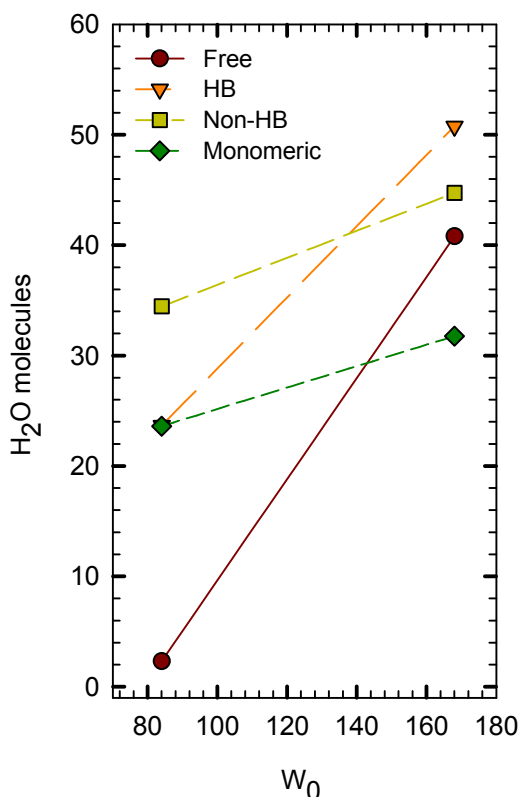
Figure 4-23: Distribution of types of H_2O.

The solute was detected via UV-Vis (Figure 4-24), Ace shows a maximum absorbance at 242 nm. The intensity of Ace decreases as H_2O and Ace is added to the system. It is possible that Ace is solubilized in the microstructure formed in the fluid phase, and it is not proportional to H_2O. We can suppose that if the reverse micelles or microemulsions are formed, the size of the inner core of the emulsion is limiting the quantity of Ace solubilized.
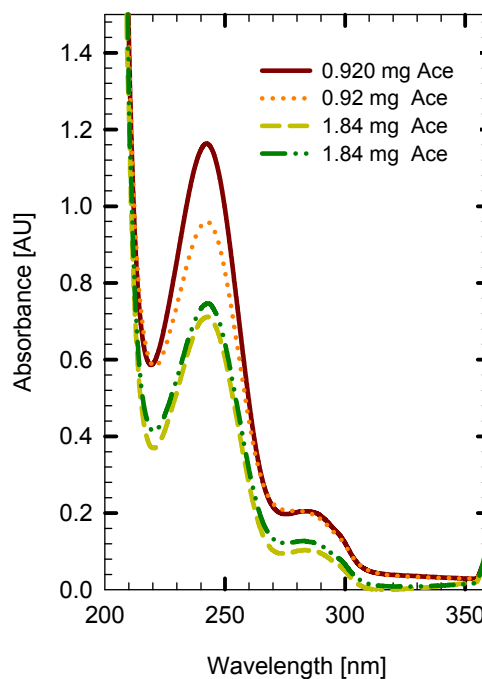
After the last addition water pools can be seen through the windows, turning the system cloudy. PL31 is not capable to prevent core attraction, because at elevated pressures it is more solubilized in scCO$_2$ and the closeness of the polar heads provoke coagulation. The presence of Ace should compromise the phase behavior of the system.

Figure 4-24: UV spectrum.

4.4.1.2 P17R2

Initially, P17R2 (147.7 mg), Ace (0.149 mg), and H_2O (716 mg) were mixed with $scCO_2$. The effect of H_2O addition in the system was evaluated with P17R2 and Ace composition kept constant (Table 4-2). The pressure increases because $scCO_2$ was used to feed the H_2O into the cell.

Table 4-2: Composition of effect of H_2O addition (P17R2-Ace)

Condition	Pressure [bar abs]	Composition [w%]				W_0
		P17R2	Ace*	H_2O	$scCO_2$	
716 mg-170 bar	169.958	0.218	0.022	1.056	98.725	572
1448 mg-189 bar	189.496	0.210	0.021	2.060	97.730	1157
2193 mg-186 bar	186.092	0.209	0.021	3.100	96.691	1753
2938 mg-192 bar	192.219	0.203	0.021	4.033	95.764	2348

* Ace is multiply by 100

The water to surfactant molar ratio varies from 572 to 2348. The IR spectrums are shown in Figure 4-25. It is important to mention that the last spectrum (d) was taken 24 hours after the last addition, and the system remained stable. The main differences can be seen in the region corresponding to the δCH_3 and δCH_2 vibration, with the appearance of saturation bands produced by H_2O presence.
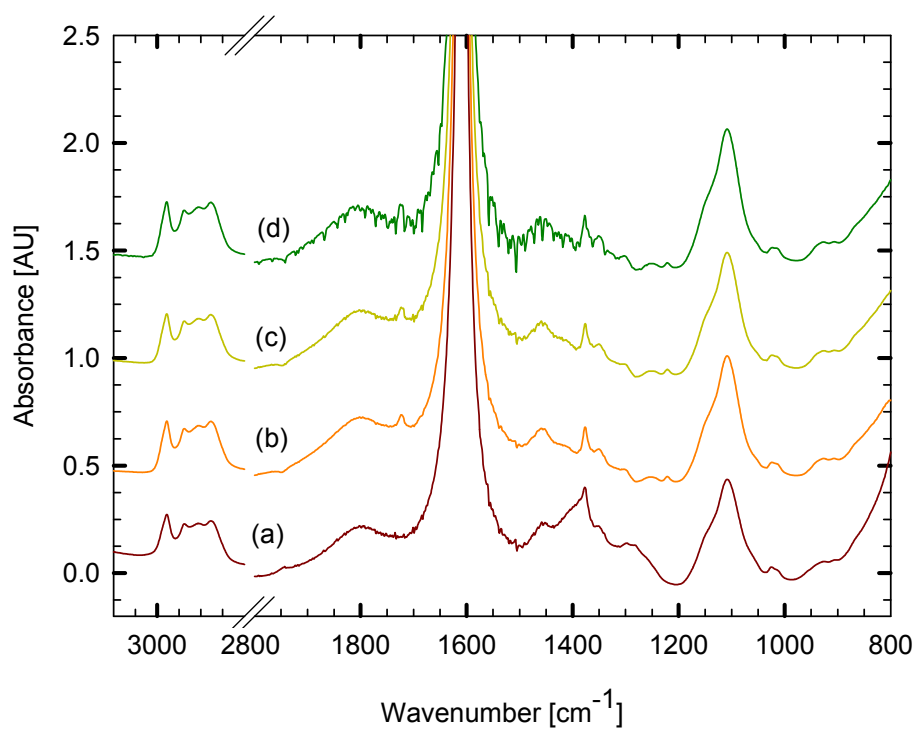
Figure 4-25: (a) 1%, (b) 2%, (c) 3%, and (d) 4% of H_2O.
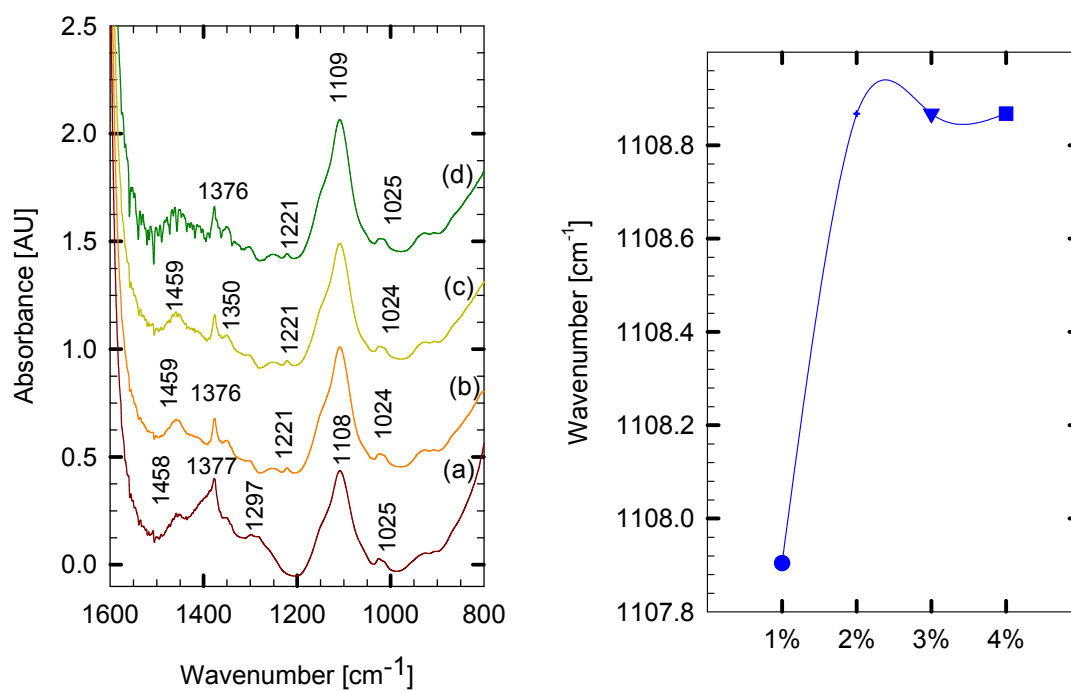
Figure 4-26: (right) 1600-800 cm^{-1} region, (left) C–O shift.

The broad of the bandwidth and decrease in intensity indicates a more disordered structure. The peak that in pure P17R2 appears at 1014 cm^{-1} (Figure 4-11), here is shifted to 1024 cm^{-1} (Figure 4-26). Conversely, this is not observed with PL31, and it could be indicative of a different form of interaction upon hydration, due to their conformational differences (type L and R). When approximately 5% of H_2O is added to the system, the spectrum shows several peaks at the region 1500-1400 cm^{-1}. Upon H_2O addition, the intensity of the peak at 1297 cm^{-1} decreases. Conversely to the PL31-Ace system the C–O shift initially increases as H_2O is added, and after 2% of H_2O the interaction between EO and H_2O becomes stronger that is deduced because not further C–O shift is observed.

In the region of 4200-3050 cm^{-1}, after subtraction and smooth of the spectrum, it shows variation, specifically when 2% of H_2O is in the system. Again, the appearance of other peaks corresponding to v(HO---n) as it is shown in Figure 4-27.
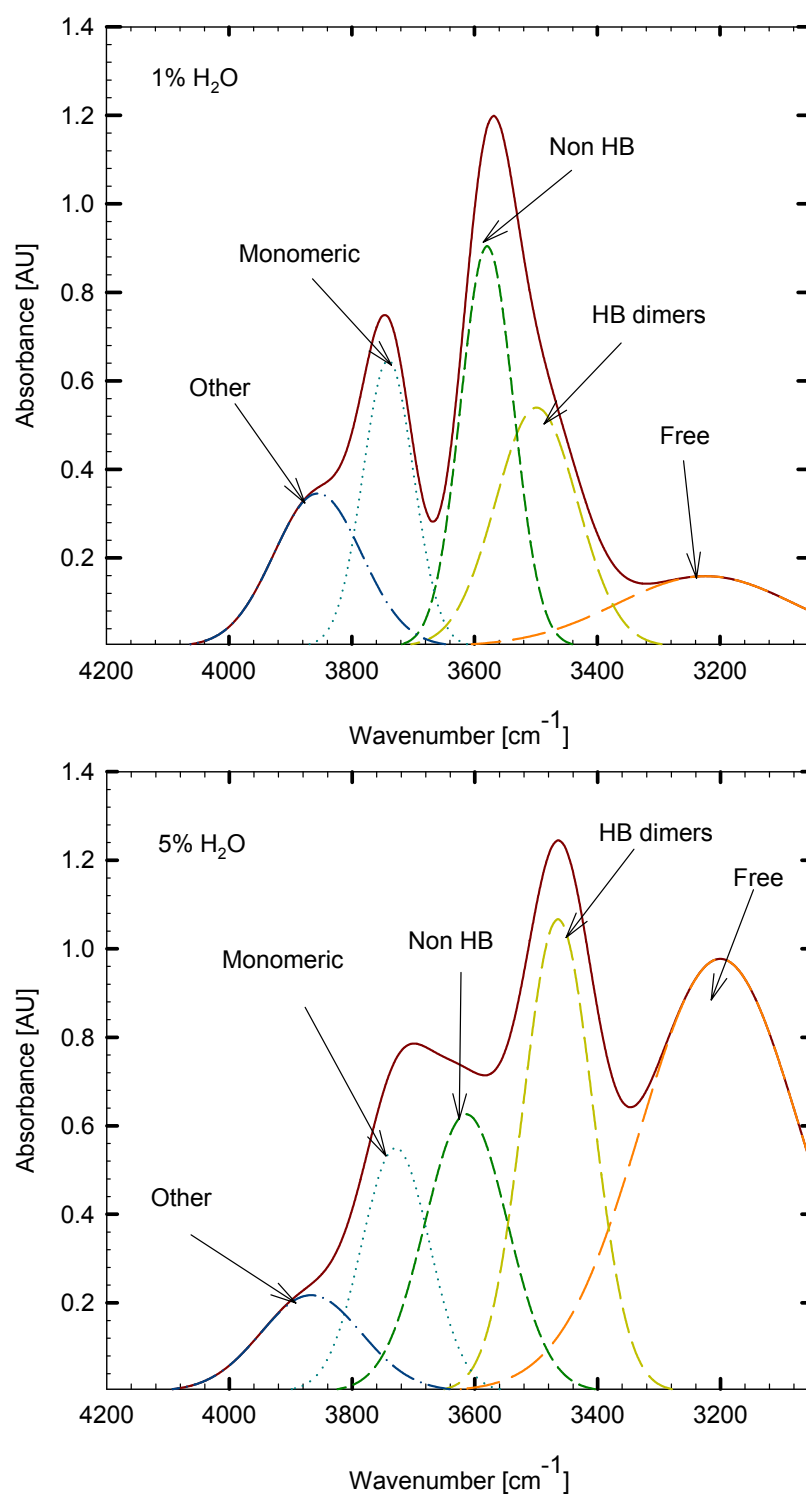
Figure 4-27: Region ν(OH) vibration (up) 1%, (bottom) 5% of H_2O (P17R2-Ace).
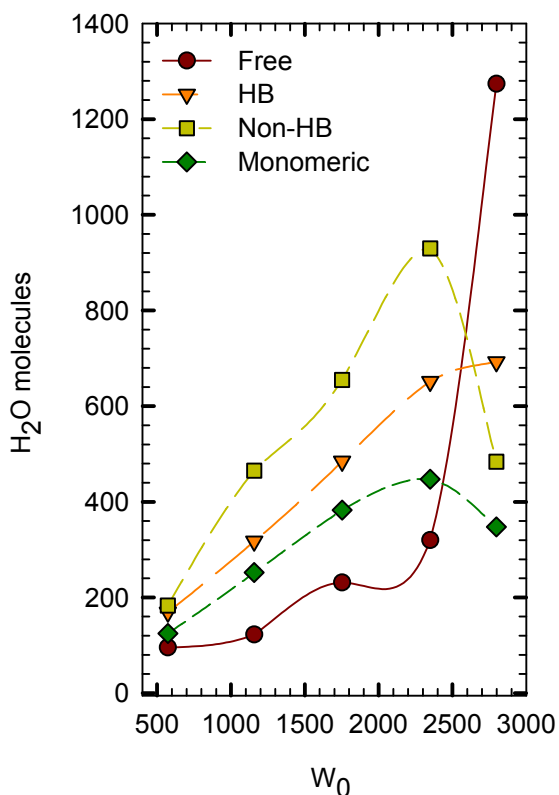
Figure 4-28: H_2O distribution (high W_0 region).

The distribution of the types of H_2O obtained from the curve fitting is shown in Figure 4-28. As we observe all the types of H_2O increases as H_2O is added to the system until 4% is reached. Further the 4% of H_2O $W_0 = 2348$, the free H_2O steeply increases but the system became unstable and a two phase system is observed. The lower W_0 region can be observed in Figure 4-29. All the curves continually ascend as H_2O is added to the system.

Compared with the PL31-Ace system, P17R2-Ace could not aggregate free H_2O in the core of the micelle at low values of W_0 as can be seen in Figure 4-30. PL31-Ace needed only 0.70% of H_2O to aggregate free H_2O. However, because PL31 surfactant has a higher solubility in $scCO_2$ than P17R2, the system is more unstable. P17R2 can stabilize more the microestructure formed in the supercritical phase, because of the concentration gradients created by the EO groups.

Figure 4-29: Distribution of H_2O (low W_0 region).
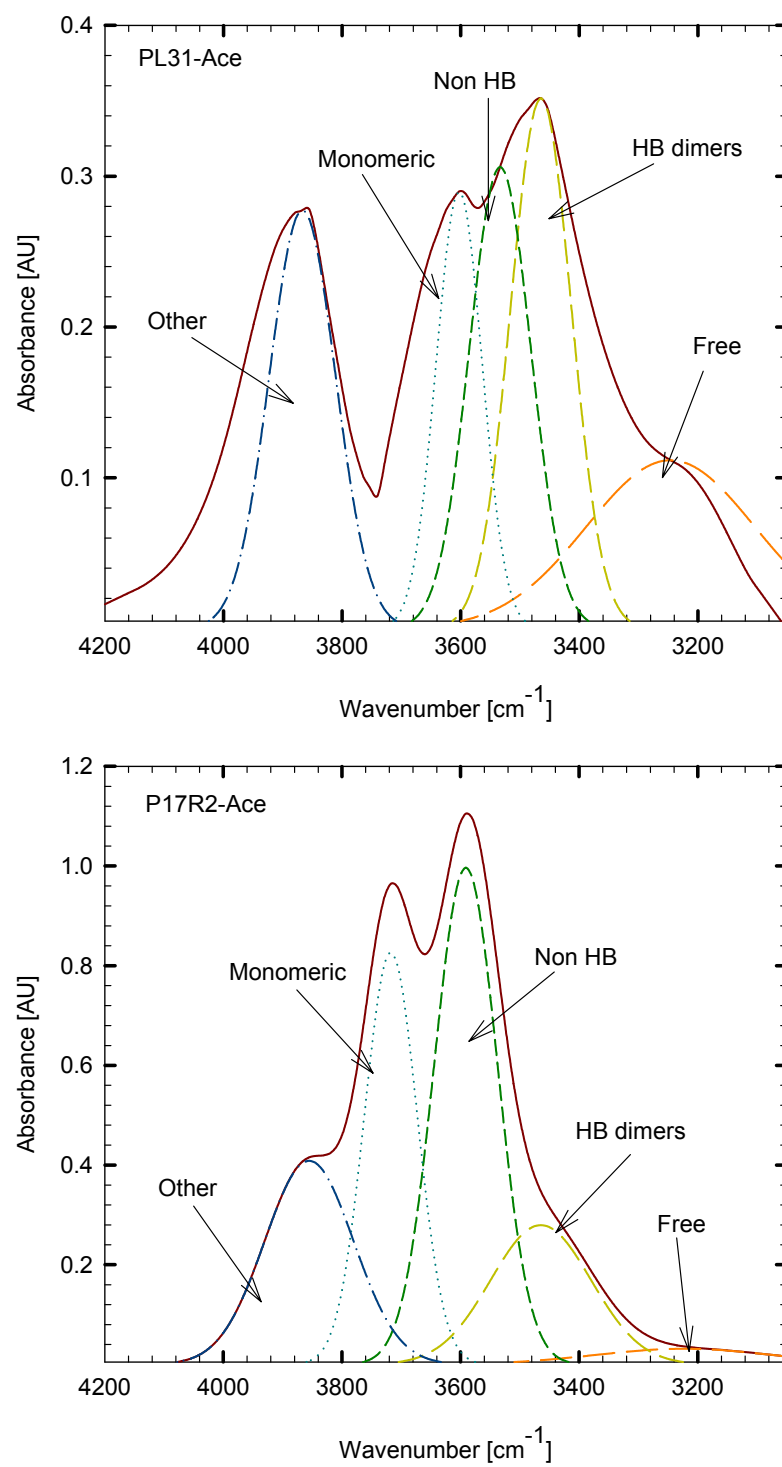
Figure 4-30: Comparison of PL31-Ace and P17R2-Ace 0.7% H_2O (region OH).
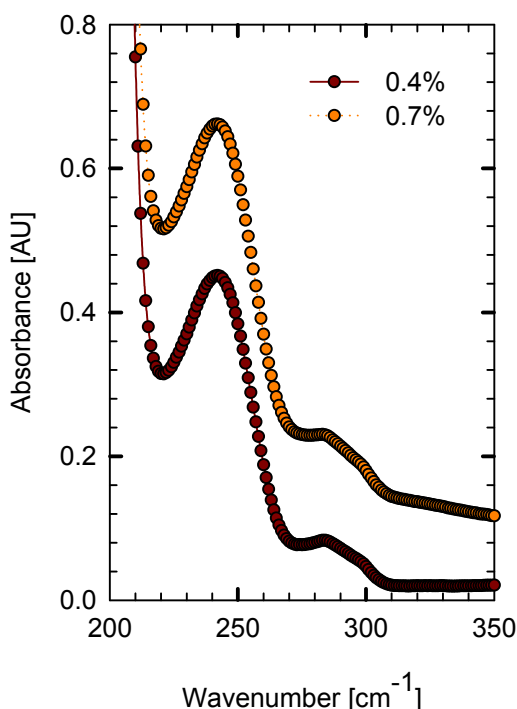
Figure 4-31: UV spectrum (P17R2-Ace).

The presence of acetaminophen was detected by UV, as can be seen in Figure 4-31. The maximum absorbance is registered at 242 nm for both spectrums. The intensity of both spectrums is closely the same. If we assume that any microstructure was formed because of the small amount of H_2O in the system, here we can consider the cosolvency effect of H_2O, as was suggested by other authors (11).

In all the cases, the absorption band at the highest wavenumber is due to H_2O molecules that are trapped between surfactants. These water molecules should behave as monomer-like isolated H_2O, analogous to the gas-phase spectrum of H_2O. The band around 3588 cm^{-1} has been assigned to the non-hydrogen bonded H_2O molecules, which have penetrated into the surfactant layer. The band around 3474 cm^{-1} is assigned to hydrogen-bonded dimers bound at the interface. And the absorption at the lowest wavenumber is ascribed to the OH stretch in the hydrogen bonded polymeric chains. This type of H_2O is present as free H_2O in the core of micelle. (7, 10)

4.4.1.3 Zonyl

The system Zonyl-Ace has a composition shown in Table 4-3 with a H_2O to surfactant molar ratio of 290.28.

Table 4-3: Composition of Zonyl-Acetaminophen-H_2O-scCO$_2$

Component	Mass [mg]	Weight composition [%]
Zonyl	66.00	0.093
Acetaminophen	2.84	0.004
H_2O	363.00	0.512
scCO$_2$	70450.00	99.391
Total		100

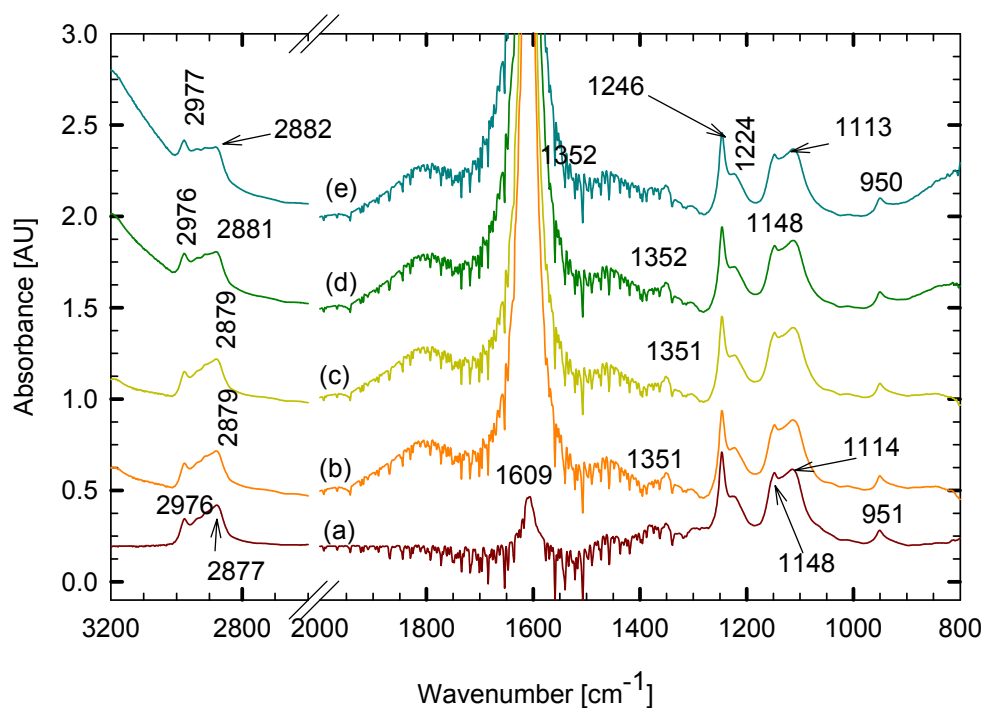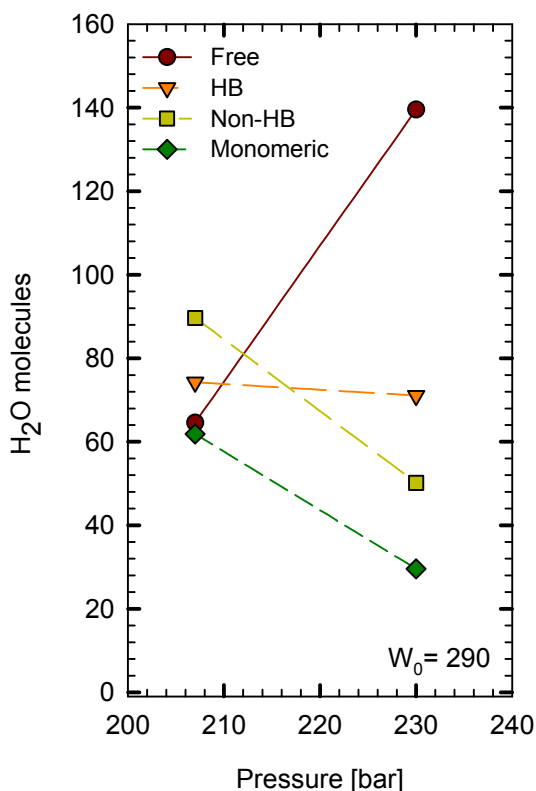The IR and UV spectrum is shown in the next Figure 4-32:

Figure 4-32: (a) without H_2O, (b) 0.52%-207 bar (c) 208 bar-after 3 h, (d) 229 bar, and (e) 229 bar without stirring.

The equilibrium in concentration was achieved at less than 3 hours of mixing, thus the system seem to be kinetically stable at 208 bar.

Figure 4-33: Distribution of H_2O.

In the region corresponding to $\nu(OH)$, the different microenvironments mentioned previously are already formed (Figure 4-35). Increasing the pressure promotes the microemulsion formation. As can be seen in Figure 4-33 with 051% H_2O, increasing the pressure provokes the redistribution of H_2O enhancing the free H_2O in the core micelle, either, monomeric and non hydrogen bonded H_2O decreases while HB H_2O which is placed at the interface stays unchanged. When the pressure was increased, and the stirring was stopped, the system became cloudy and foam appeared.

This could indicate that the system is unstable and phase separation occurred. The absorbance of acetaminophen is shown in Figure 4-34. Ace is detected and when H_2O is added the absorbance of the Ace diminishes, even though some microstructure is formed. This could be originated by the unstability of the system; thus, when foams are generated the Ace begins to precipitate.

Figure 4-34: Acetaminophen UV spectrum.
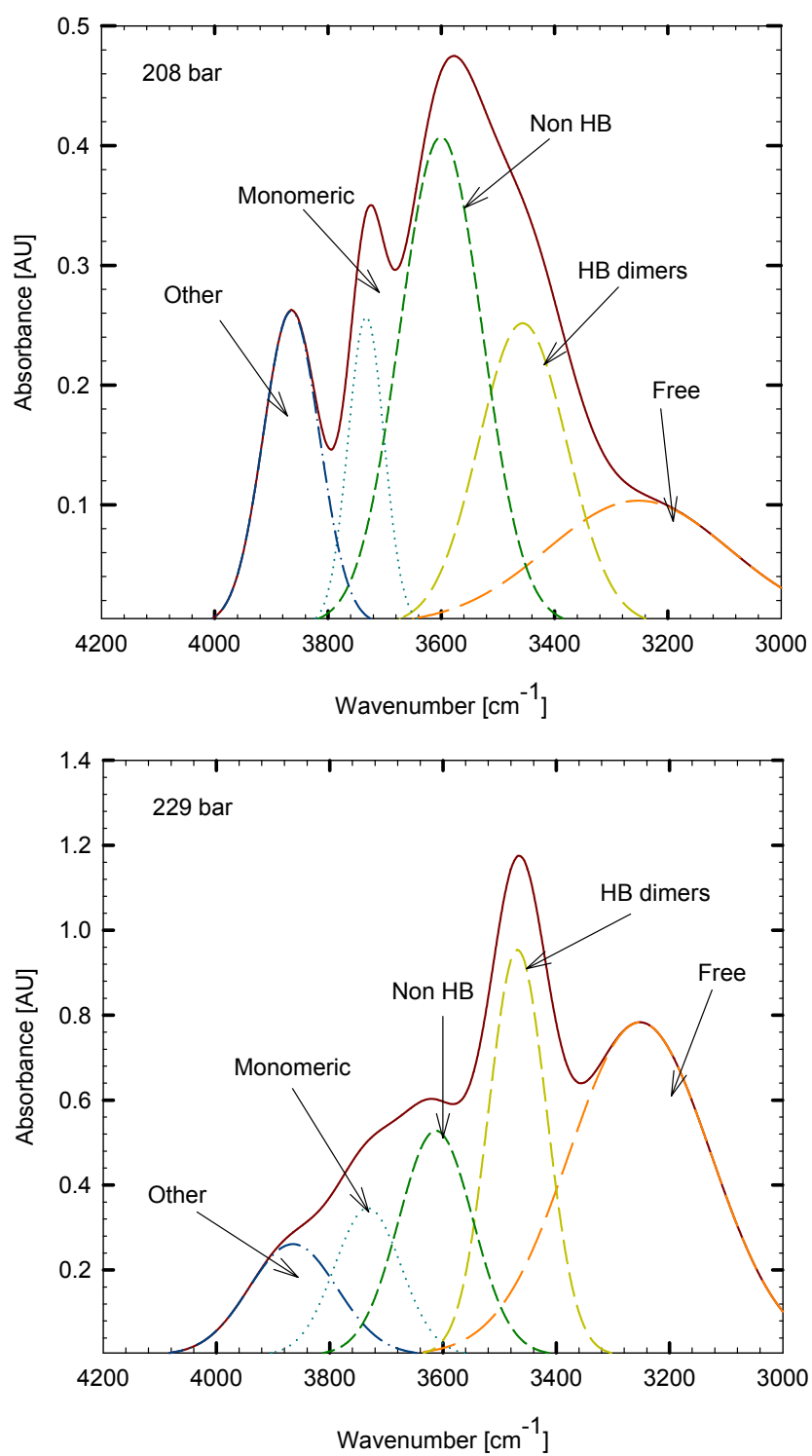
Figure 4-35: Distribution of H$_2$O types 0.57% H$_2$O (Zonyl-Ace).

The effect of H_2O addition was also studied. Zonyl (66 mg) was mixed with $scCO_2$. Then Ace (0.92 mg) was added to the cell, in aqueous solution (250 mg). The conditions are summarized in Table 4-4.

Table 4-4: Composition of Zonyl-Acetaminophen-H_2O-$scCO_2$

Condition	Pressure [bar abs]	Composition [w%]				W_0
		Zonyl	Ace	H_2O	$scCO_2$	
without H_2O	193.580	0.096	0.000	0.000	99.904	0.00
250 mg -208 bar	208.488	0.094	0.001	0.355	99.550	200
363 mg-208 bar	208.488	0.093	0.004	0.514	99.388	290

As it is observed in Figure 4-36, all the types of H_2O increases as H_2O is added to the system. It is interesting to see that H_2O in the core of the micelles decreases after
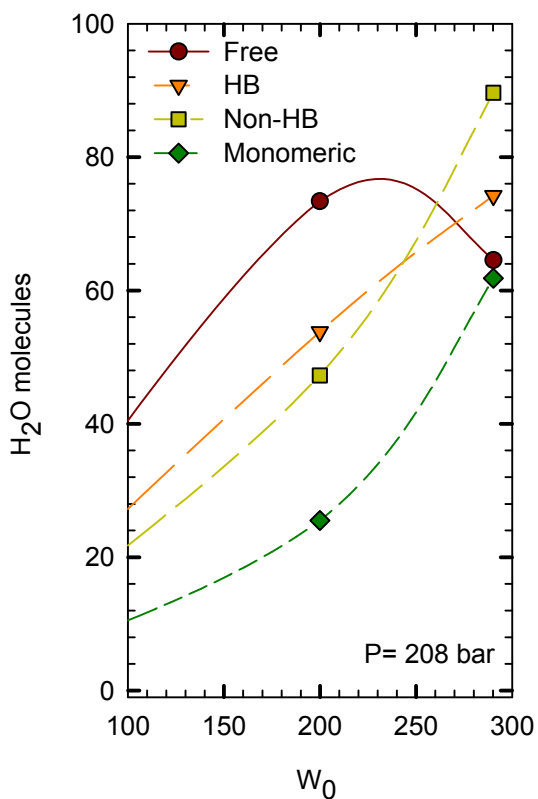
Figure 4-36: Distribution of H_2O.
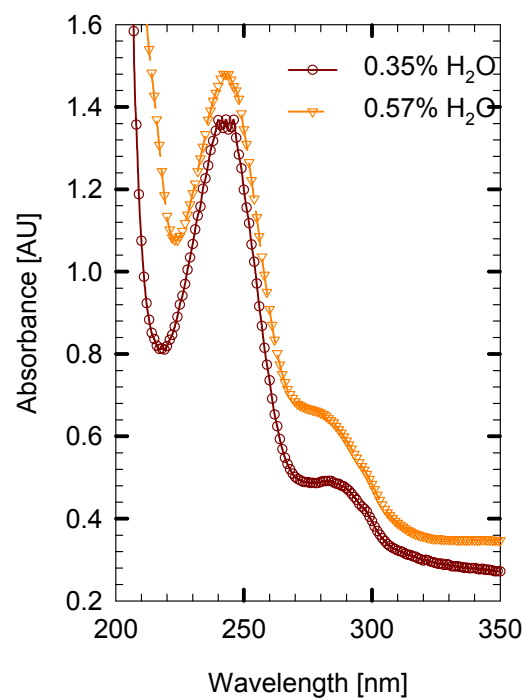
Figure 4-37: Acetaminophen UV spectrum.

250 mg of H_2O. In both cases, Ace was detected in UV, as can be observe in Figure 4-37. Again the system becomes unstable, producing foaming, and phase separation. This effect can be seen in the deformation of the UV maximum absorbance.

The addition of H_2O makes the system unstable and it was observed by visual inspection through the window cell. Zonyl is not able to prevent aggregation due to its solubility in $scCO_2$, and does not created the gradient concentration to stabilize the microstructure.

4.4.1.4 Gele

Gele (171.4 mg), Ace (54.9 mg), and $scCO_2$ were mixed. Then, H_2O were added to the cell. The experimental conditions are summarized in Table 4-5.

Table 4-5: Composition Gele-Acetaminophen-H_2O-$scCO_2$ (effect of H_2O)

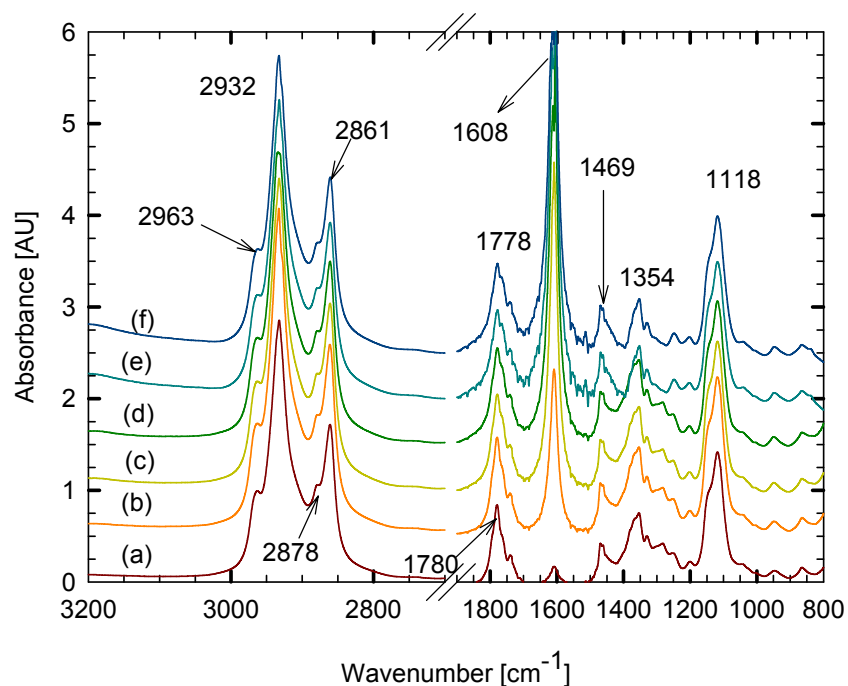| Condition	Pressure [bar abs]	Composition [w%]				W_0
		Gele	Ace	H_2O	$scCO_2$	
without H_2O-178 bar	177.923	0.252	0.081	0.000	99.667	0.00
50 mg-193 bar	193.172	0.247	0.079	0.072	99.601	5.83
100 mg-208 bar	207.603	0.243	0.078	0.142	99.537	11.87
150 mg-220 bar	219.924	0.240	0.077	0.210	99.473	17.50
200 mg-217 bar	217.065	0.241	0.077	0.281	99.401	23.34
250 mg-221 bar	220.946	0.240	0.077	0.350	99.334	29.17

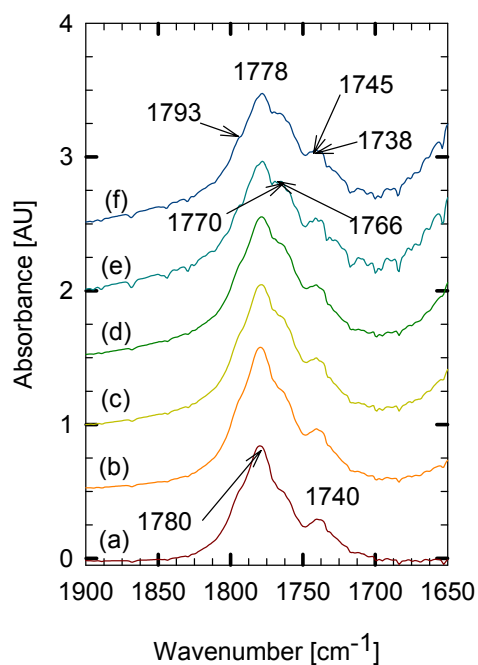Figure 4-38: (a) without H_2O, (b) 0.07%, (c) 0.14%, (d) 0.21%, (e) 0.28%, and (f) 0.35%.

Figure 4-39: Carboxylic region C-O.

The IR spectrums are shown in Figure 4-38. The characteristic region corresponding to the C=O vibration is seen in Figure 4-39. As H_2O is added, the deformation of the peak is evident. The appearance of others peaks around it, suggest the formation of entities with different degree of solvation; open dimers that usually appear at lower frequencies. At those conditions (pressure and temperature), the surfactant is solubilized by $scCO_2$. As was stated by many authors (12) the enhanced solubility of compounds containing carbonyl groups in $scCO_2$ can be attributed to the free

electrons on the carbonyl oxygen interacting with the slightly acidic carbon of CO_2 in a Lewis acid-Lewis base type interaction. This can be seen in the deformation vibration of CO_2, which is not possible to see with our windows. However, the interaction of the acidic proton with CO_2 acting as a Lewis base is also accepted as the responsible of the solvent-solute interactions in CO_2, but this interaction is weaker than the other. Other change occurs at the region around 1364 cm^{-1} (Figure 4-40), where as H_2O is added the peak shifts to 1354 cm^{-1} and a peak at 1330 is more evident. Also it is observed the deformation of the region around 1469 cm^{-1} that corresponds to the CH_{2sc} bending vibration and this suggests the increase of the rotational freedom.
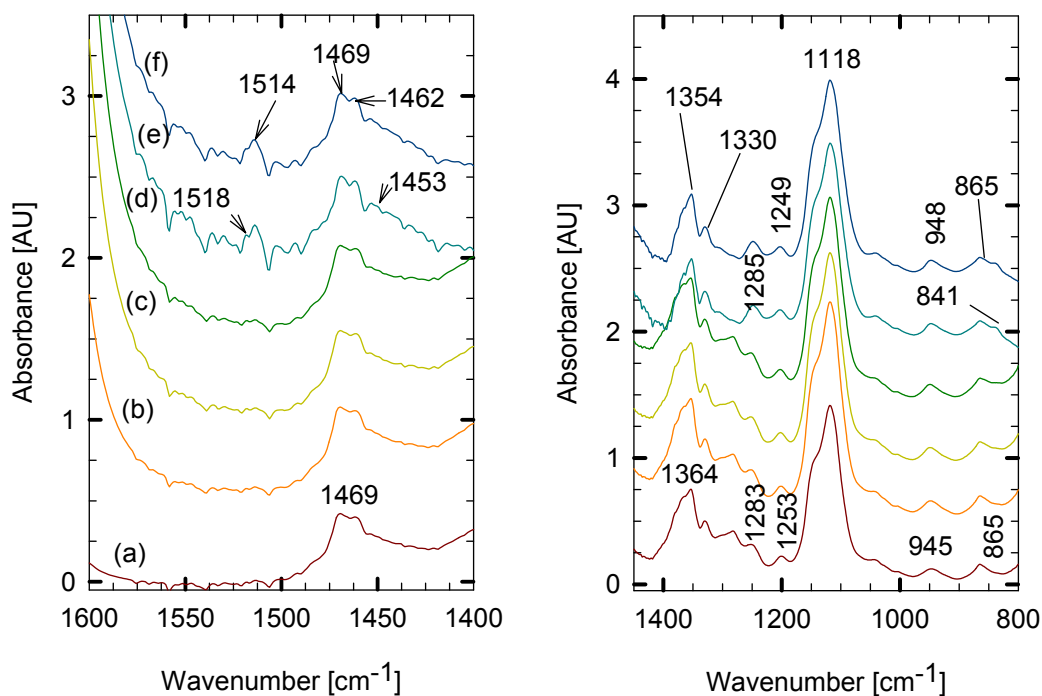
Figure 4-40: Region 1600-800 cm^{-1}.

The region 4200-3050 cm^{-1} is seen in Figure 4-41, as in the other experiments the shape dependence of the spectrum with the addition of H_2O is shown.
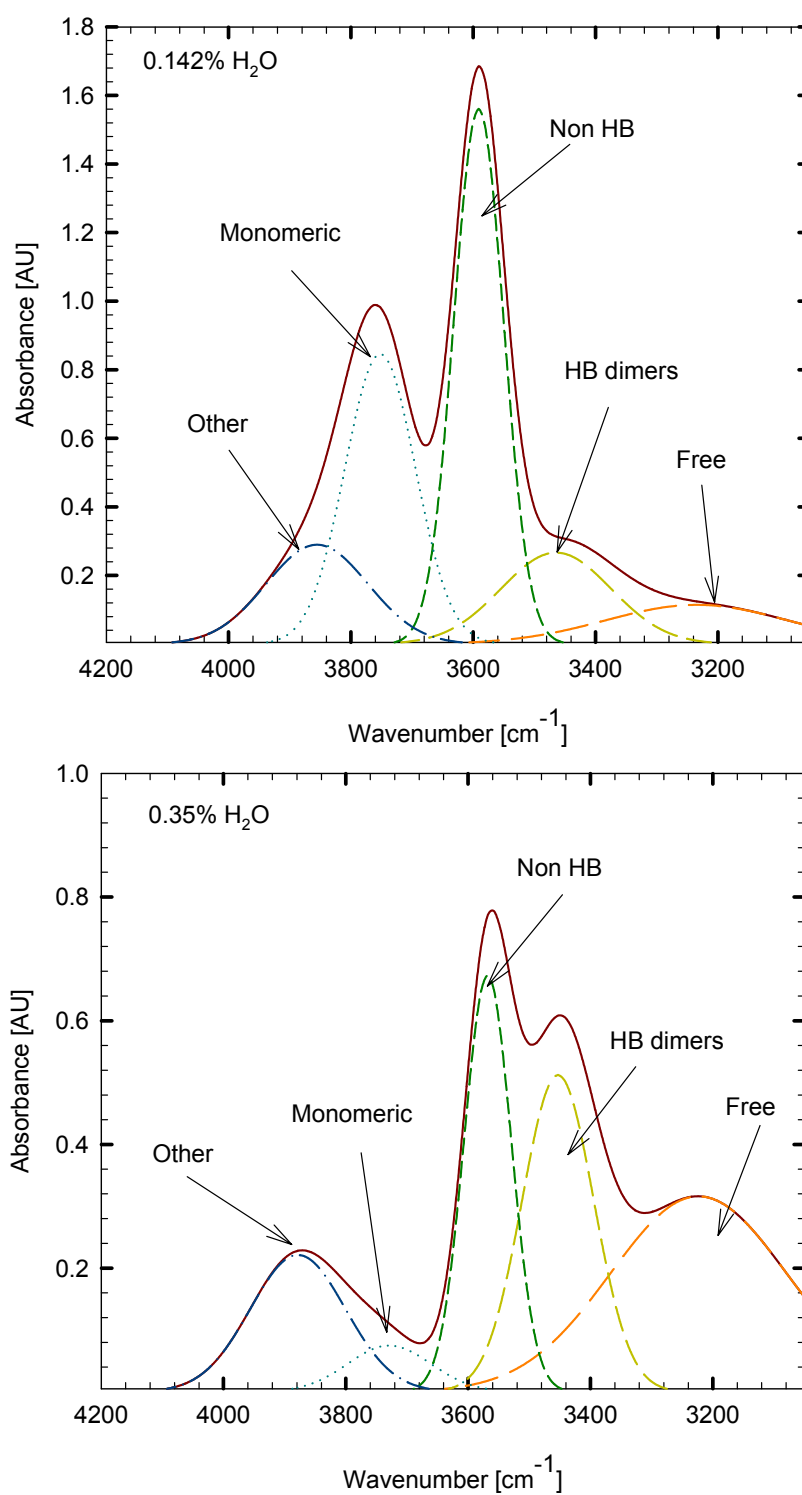
Figure 4-41: Distribution of H_2O (region OH).
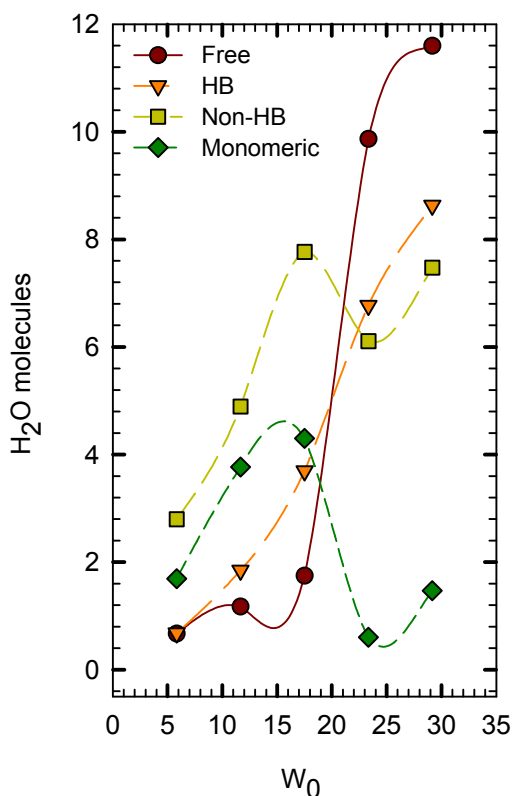
Figure 4-42: Types of H_2O behavior.

Figure 4-42, shows the trends described by the types of H_2O generated with Gele. All the curves increase as W_0 is added. At near 17.50 the free H_2O increases steeply and only monomeric H_2O shows an inflection point at that W_0. In the UV spectrum (Figure 4-43) we can observe the different spectrums, this suggest the existence of a maximum corresponding to the solute (Acetaminophen). However, it is not possible to assure that, because of the deformation of the spectrum and the system does not reach to steady state. Then phase separation occurs.

4.4.2 Imipramine HCl

For imipramine HCl (Imi)-surfactant systems the peaks were centered at 3210 ± 9, 3481 ± 23, 3585 ± 38, 3725 ± 20 (for H_2O), and 3816 ± 19 (for solute). The full widths at half height of were 146 ± 3, 71 ± 9, 55 ± 8, 52 ± 8, and 69 ± 5 respectively.

4.4.2.1 PL31

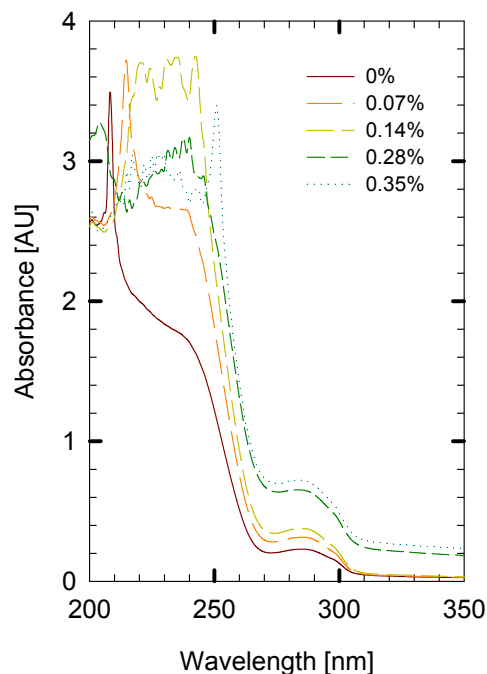The effect of pressure was studied. The

Figure 4-43: Acetaminophen UV spectrum

composition (Table 4-6) was kept constant and the water/surfactant molar ratio was 386.22 approximately.

Table 4-6: PL31-Imipramine HCl-H_2O-scCO_2 (effect of pressure)

Component	Mass [mg]	Weight composition [%]
PL31	33.79	0.048
Imipramine HCl	0.60	0.001
H_2O	363.00	0.510
scCO_2	70728.00	99.441
Total		100

The IR spectrum is shown in Figure 4-44. The increase of pressure increases the solubility of the surfactant, this can be seen through the increase of the peak at 1460 cm^{-1}, and around of 1109 cm^{-1} (C–O). There is also a linear dependence of the CH_2/CH_3 ratio with pressure, and a decrease of the wavenumber at C–O too. The characteristic CH_3 umbrella deformation[9] (1376 cm^{-1}) stays along the increase of pressure. In the region corresponding to the δCH_2 vibration mode, we can observe that the appearance of a peak at 1346 cm^{-1} would indicate the increase of rotation freedom of the out of plane CH_{2w} vibration mode in the gauche conformation. The peak detected at 1015 cm^{-1} in non aqueous PL31 is shifted to 1025 cm^{-1} that decreases proportionally to the increase of the C–O peak.

---

[9] The symmetric CH_3 deformation has been described as an umbrella vibration where all three hydrogens move toward each other together.
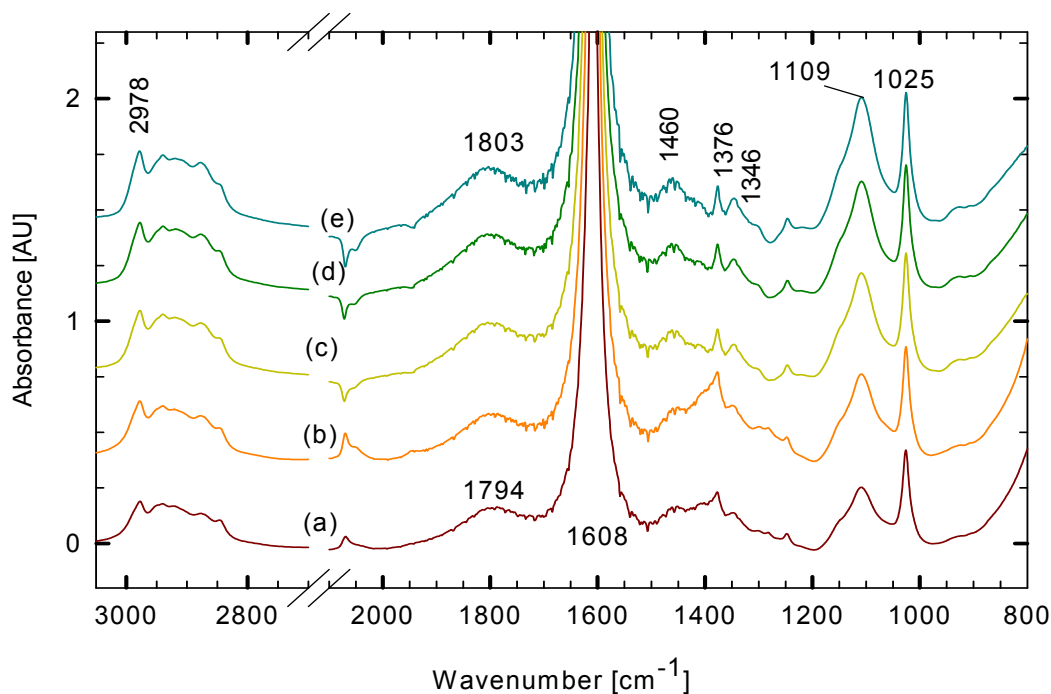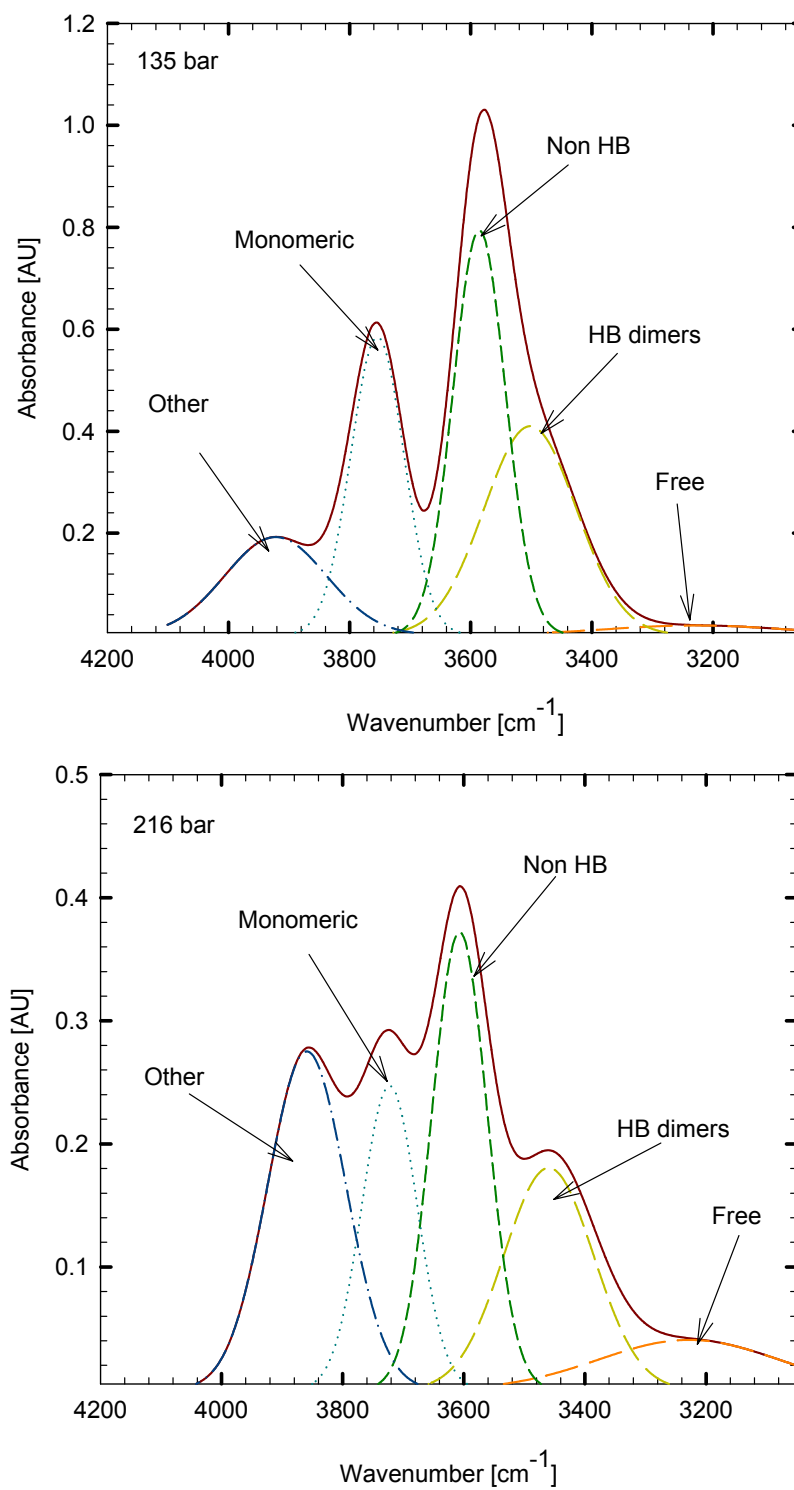
Figure 4-44: (a) 110 bar, (b) 135 bar, (c) 163 bar, (d) 185 bar, and (e) 216 bar.

The region corresponding to OH stretching vibration after smoothing is seen in Figure 4-45. The partitioning of the broaden OH region different microenvironments occurs approximately around 163 bar.
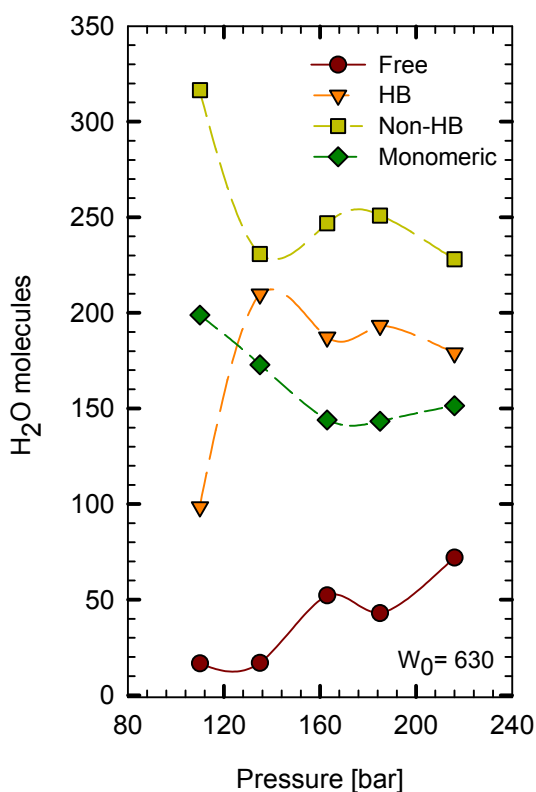
Figure 4-45: Distribution of H_2O (region OH).

Figure 4-46: H_2O-types distribution vs. pressure.

Figure 4-47 shows the pressure dependence of the types of H_2O, as pressure increases the curves decreases until 163 bar approximately. Above this pressure the HB and non-HB type H_2O were almost constant indicating that the types of H_2O molecules did not change with pressure.

The effect of H_2O addition is evaluated in the next experiment. PL31 (174.54 mg) was mixed with $scCO_2$. Then, H_2O was loaded. The conditions are summarized in Table 4-7.

Table 4-7: PL31-Imipramine HCl-H_2O-$scCO_2$ (effect of H_2O addition)

| Condition	Pressure [bar abs]	Composition [w%]				W_0
		PL31	Imi*	H_2O	$scCO_2$	
without H_2O-201 bar (a)	200.592	0.250	0.000	0.000	99.750	0.00
0.071%-205 bar (b)	204.744	0.249	0.026	0.071	99.680	16.81
0.142%-205 bar (c)	205.221	0.249	0.052	0.142	99.608	33.61
0.211%-215 bar (d)	215.432	0.246	0.078	0.211	99.542	50.42
0.279%-226 bar (e)	225.643	0.243	0.103	0.279	99.477	67.22
0.625%-226 bar (f)	225.643	0.243	0.230	0.625	99.130	151.25
0.989%-204 bar (g)	204.472	0.247	0.364	0.989	98.760	235.29

* It was multiply by 100.
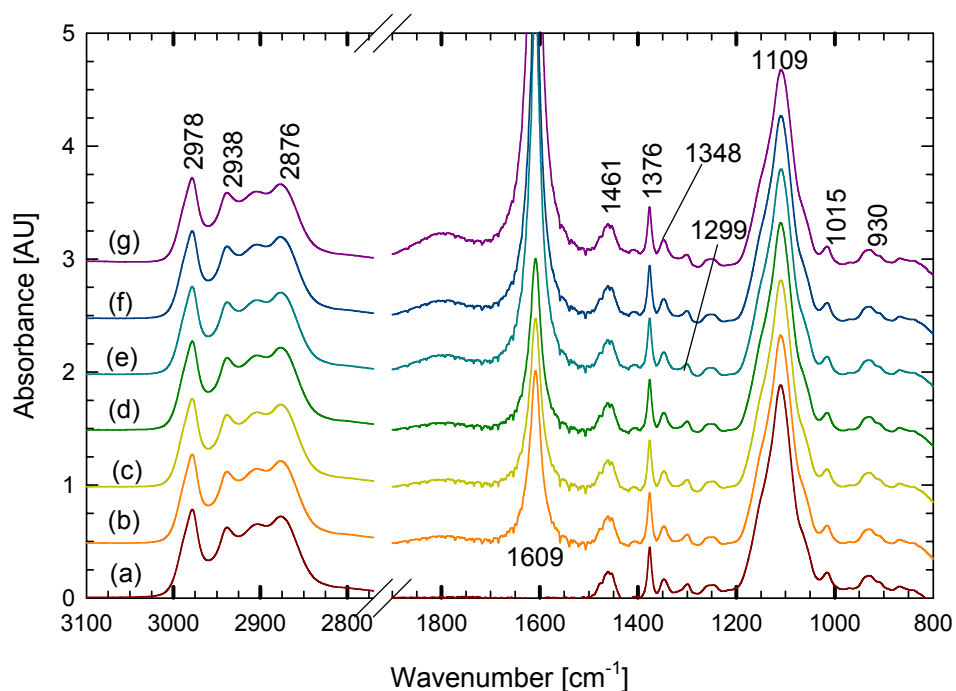
Figure 4-48: PL31-Imipramine HCl-H_2O-scCO_2 (effect of H_2O addition).

The IR spectrum is observed in Figure 4-48. There is not appreciable change in the IR spectrum of the system. The region corresponding a ν(OH) stretching vibration from H_2O can be seen in Figure 4-49. The four characteristics peaks were found with a low intensity, this could mean that the capacity of the PL31 to trap H_2O is little, and this could be an effect of the solute used with this system.
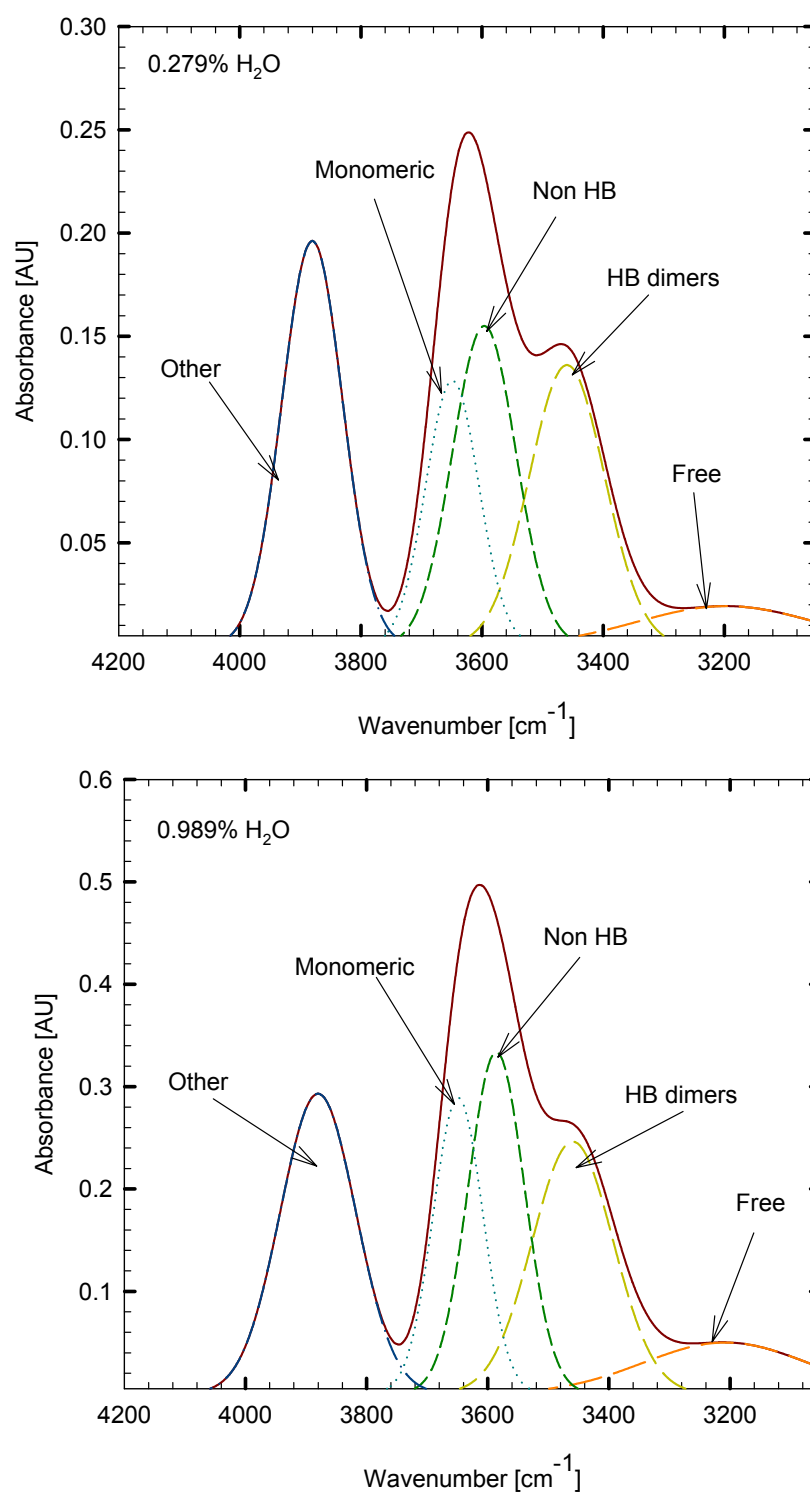
Figure 4-49: Distribution of H$_2$O (region OH).

The variation of each type of H_2O is presented in Figure 4-50. The trend described by the curves is ascending with an inflexion point at $W_0 = 33.61$. After this value the ascending slope decreases, specifically the free H_2O takes lower values than the other types of H_2O.

The presence of imipramine HCl was detected as water was added to the system (Figure 4-51). The intensity of the peak increases as H_2O concentration increases. The maximum intensity for all the measurements is detected at 251 nm. In the
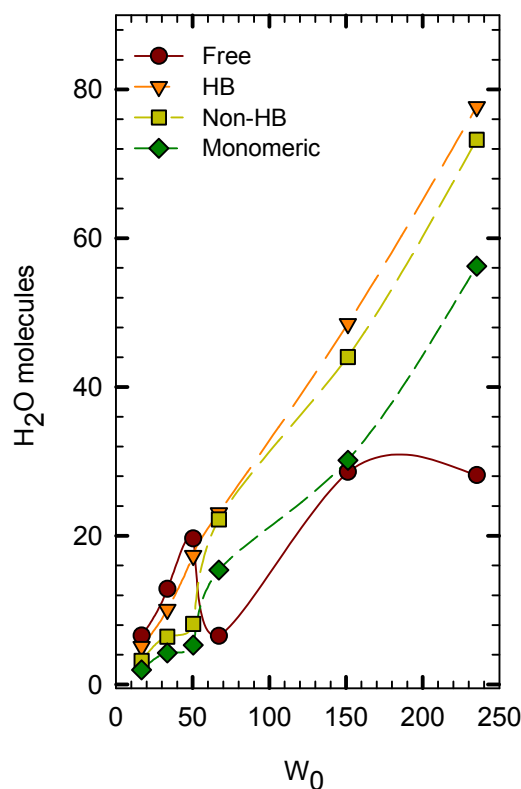
Figure 4-50: Variation of H_2O types.
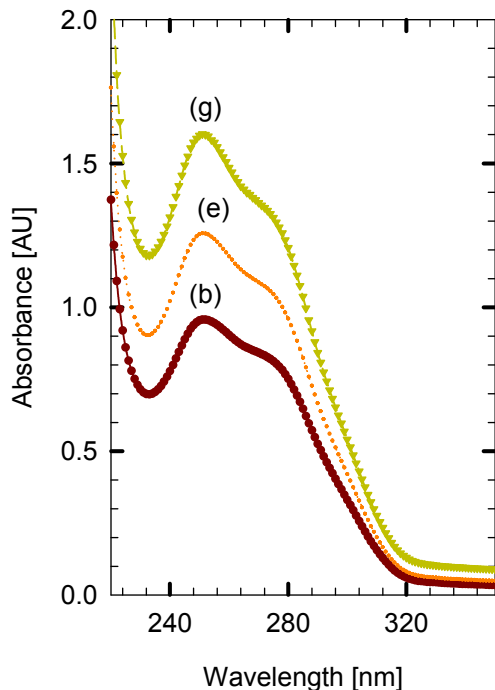
two last experiments, enhancement of H_2O increases the solubilization of imipramine, but we can not precise that it was solubilized in the core of the microemulsion because it could also be solubilized by the H_2O in the fluid phase.

4.4.2.2 P17R2

The pressure was varied at constant mass compounds. As pressure increased, the water to surfactant molar ratio was 1193.71.

Figure 4-51: UV spectrum.

The composition of the system can be seen in Table 4-8.

Table 4-8: P17R2-Imipramine HCl-H_2O-scCO_2 composition

Component	Mass [mg]	Weight composition [%]
P17R2	35.90	0.064
Imipramine HCl	0.599	0.001
H_2O	363.00	0.648
scCO_2	55647.00	99.287
Total		100

The IR spectrum is shown in Figure 4-52.
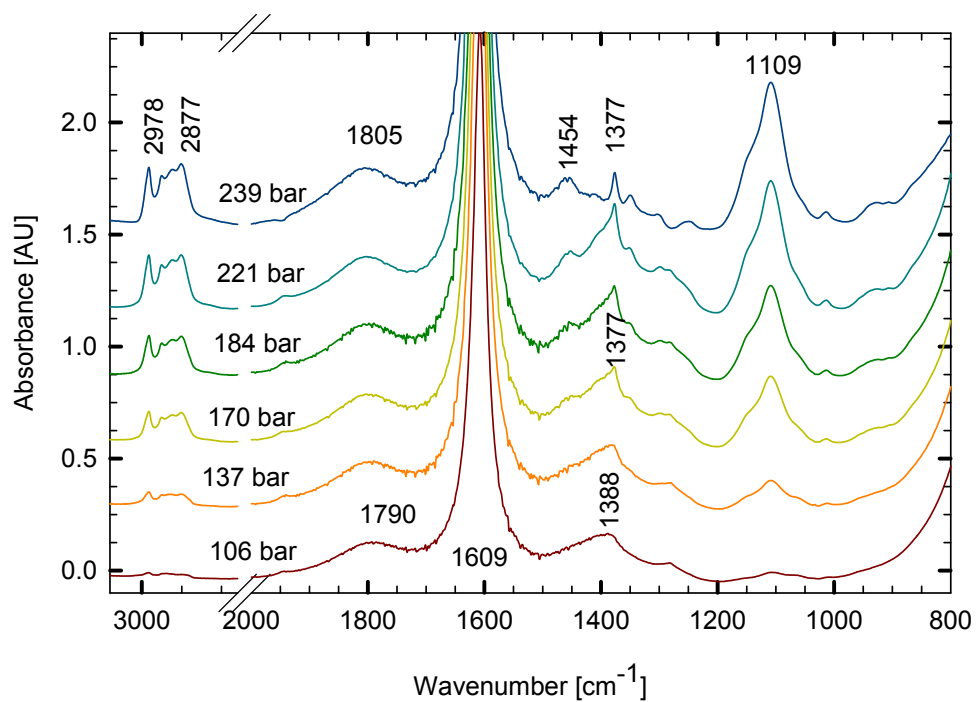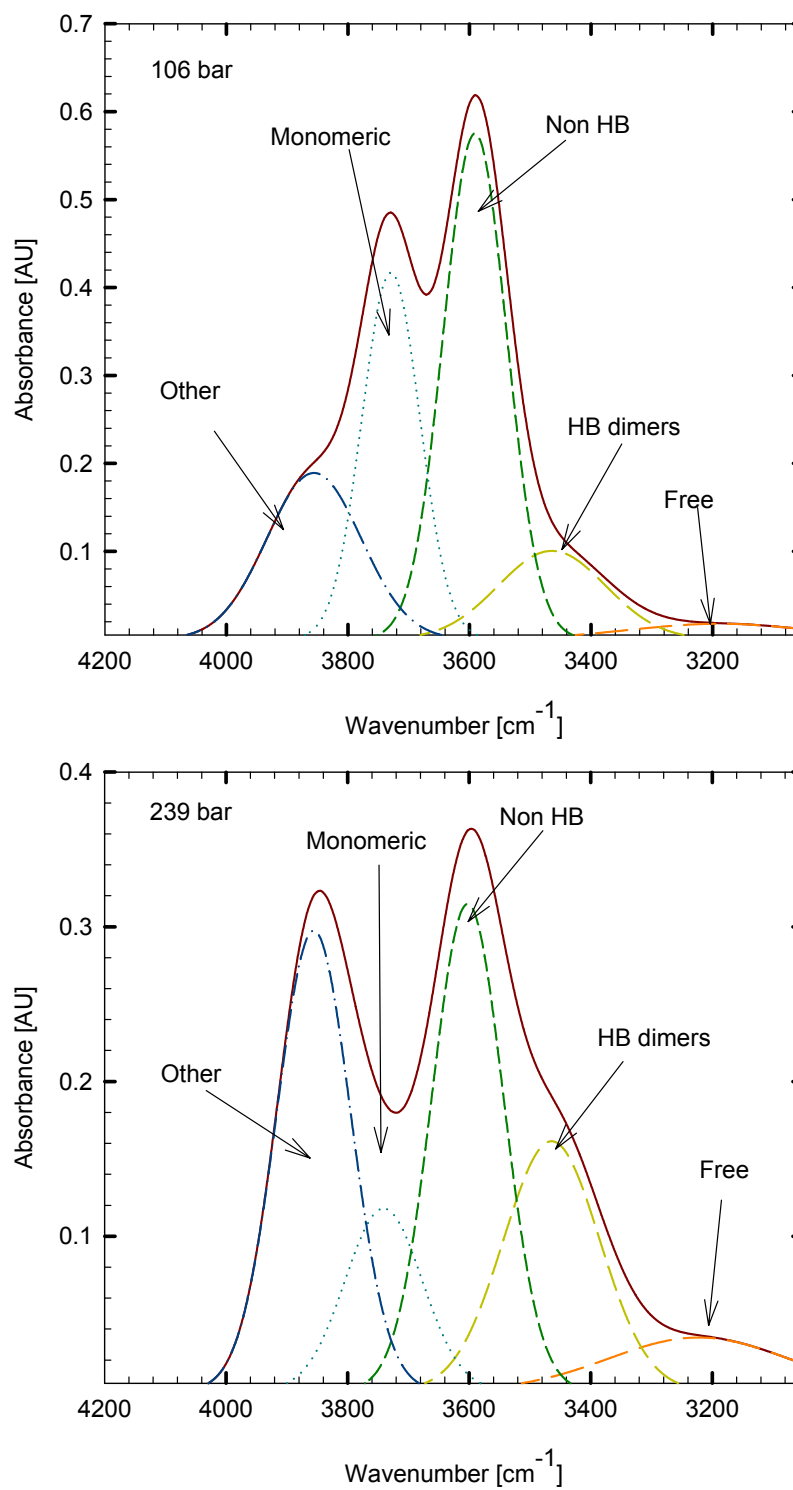

Figure 4-52: IR spectrum of P17R2-imipramine HCl-H_2O-scCO_2.

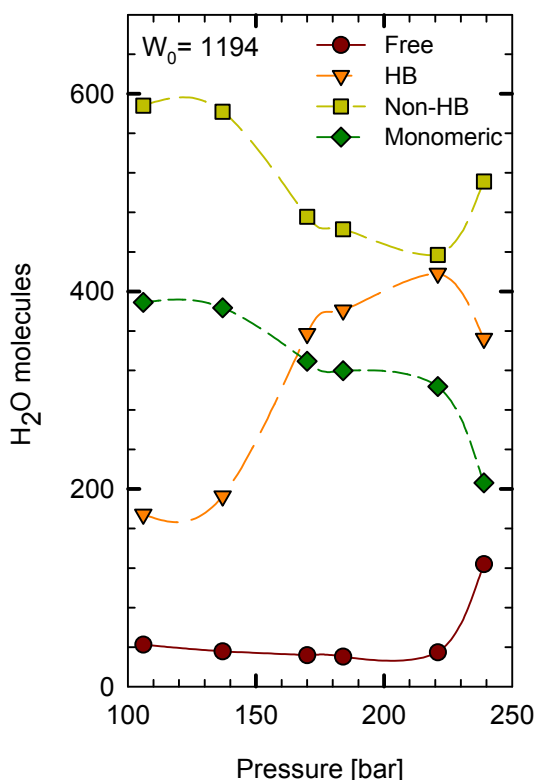Figure 4-53: Distribution of H_2O types (region (O—H).

Figure 4-54: Pressure dependence of H_2O types.

The surfactant was solubilized at pressure around 137-170 bar (Figure 4-52). There is any appreciable shift in the characteristics peak that could denote micellization. Just, a broaden in the near region of $\delta(OH)$, as pressure increases would suggest a effect of surfactant. In the region corresponding to the stretching vibration $\nu(OH)$ (Figure 4-53), as pressure increases, a peak at 1454 cm^{-1} is more evident, and the initial peak at 1388 cm^{-1} is shifted to 1377 cm^{-1}. There is evidence of H_2O trap in the microenvironment formed.

Figure 4-54 shows the pressure dependence of the types of H_2O formed in the system. HB H_2O shows an inflexion point at approximately 137 bar that ascends until 170 bar, after this pressure the curve present a plateau. Non-HB and monomeric H_2O also present an inflexion point at this pressure. The free H_2O has lower values than the other types, this could indicates the low capacity of the system to trap H_2O which did not enhance with pressure.

This experiment was done to precise the effect of H_2O. P17R2 (174.54 mg), and $scCO_2$ were mixed. Imipramine HCl was loaded to the cell in aqueous solution. The conditions are summarized in Table 4-9. The measurements at (c) and (e) conditions were done without stirring and although the pressure began to increase the system shown to be stable.

Table 4-9: Composition P17R2-imipramine HCl-H_2O-scCO$_2$ (effect of H_2O addition)

Condition	Pressure [bar abs]	Composition [w%]				W_0
		P17R2	Imi*	H_2O	scCO$_2$	
without H_2O-206 bar	206.3	0.249	0.000	0.000	99.751	0.00
0.042%-219 bar (b)	218.8	0.245	0.016	0.042	99.403	20.29
0.345%-221 bar (c)	221.5	0.244	0.129	0.350	99.405	169.10
0.699%-218 bar (d)	217.8	0.244	0.257	0.699	99.054	338.19
0.694%-226 bar (e)	225.6	0.242	0.255	0.694	99.061	338.19

* It was multiply by 100

The IR spectrum shows no appreciable change, it only broaden in the region corresponding to CH_{2sc} vibration (Figure 4-55). In Figure 4-56 we can see the region corresponding to stretching $\nu(OH)$ vibration. After adding 250 mg of H_2O different microenvironments of HB are observed.
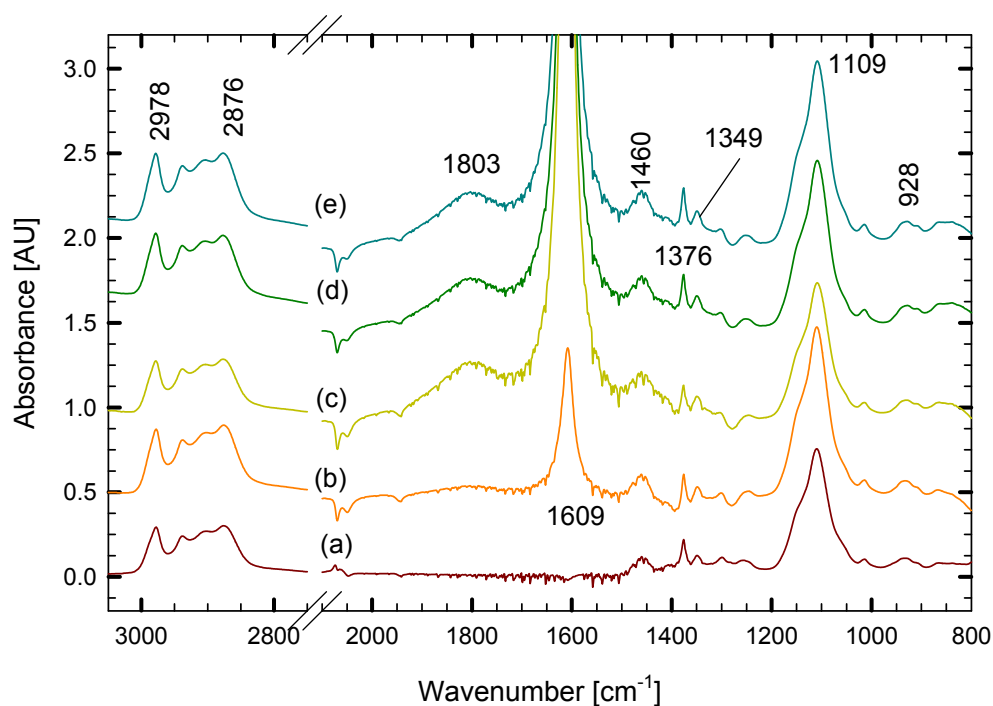
Figure 4-55: (a) 0% H_2O, (b) 0.04%, (c) 0.35%, (d) 0.70%, and (e) 0.7%-226 bar.
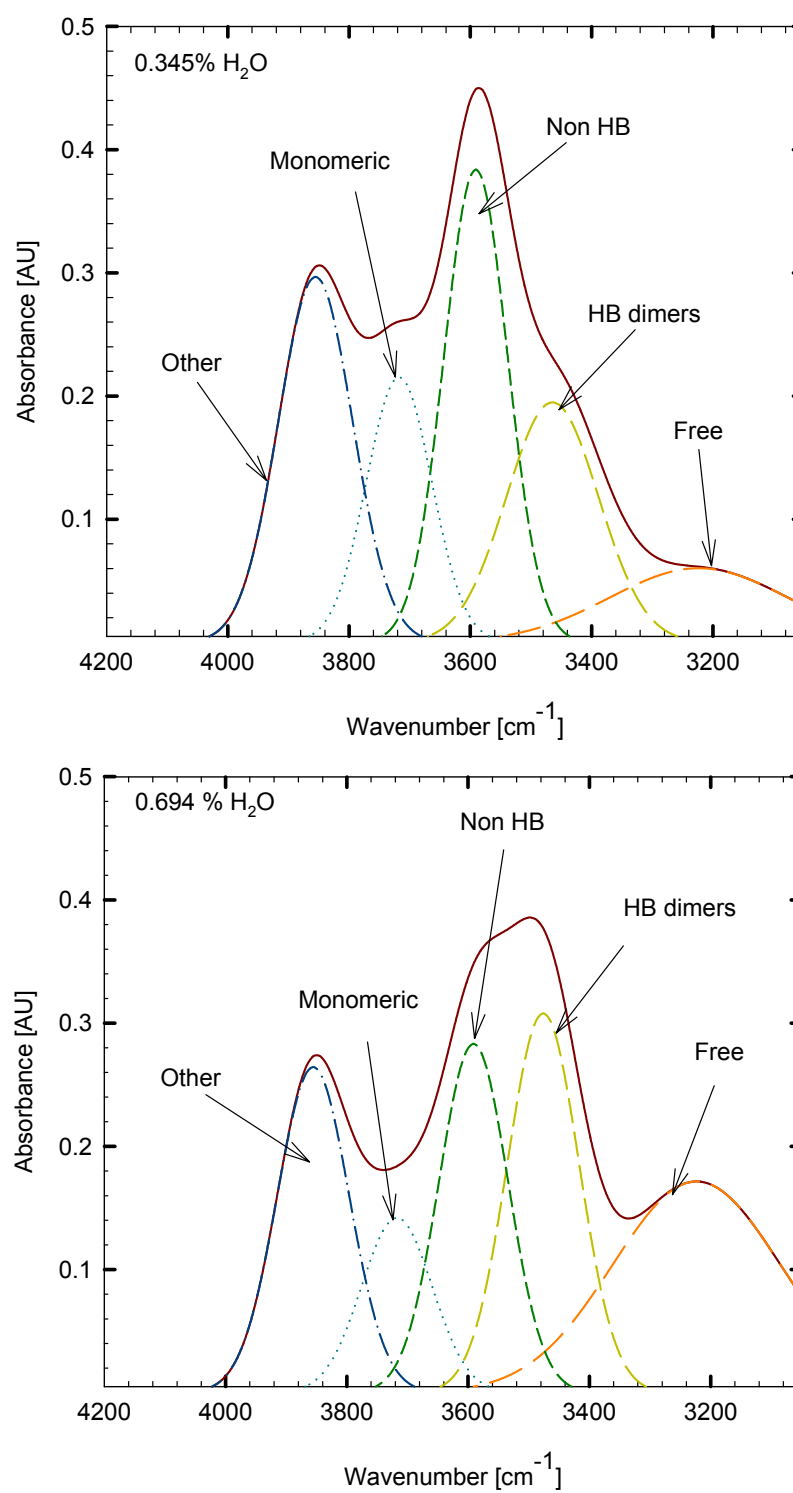
Figure 4-56: Distribution of H$_2$O types (region (OH—n)).

In Figure 4-57, the curves increase as H_2O is added to the system. At $W_0=$ 169.10 the free H_2O steeply increases, compared with the other types of H_2O. This denotes the H_2O added mainly goes to improve the core of the reverse micelle. Imipramine HCl is detected, the maximum absorbance is verified at 251 nm (Figure 4-58). There is no difference in the intensity of the spectrum, even though H_2O was added. However, after the last addition
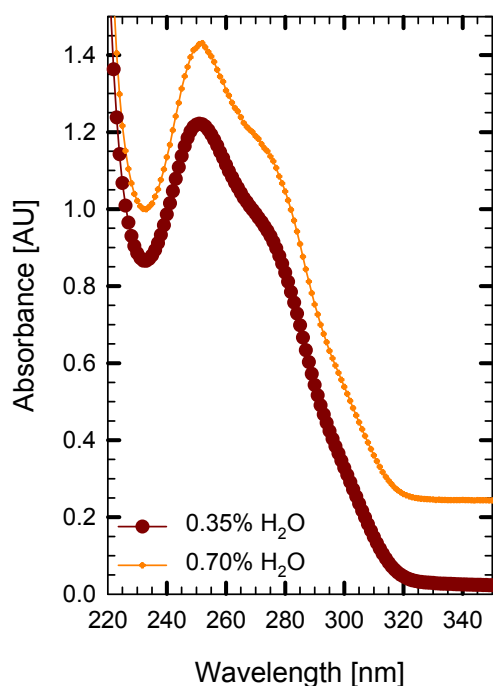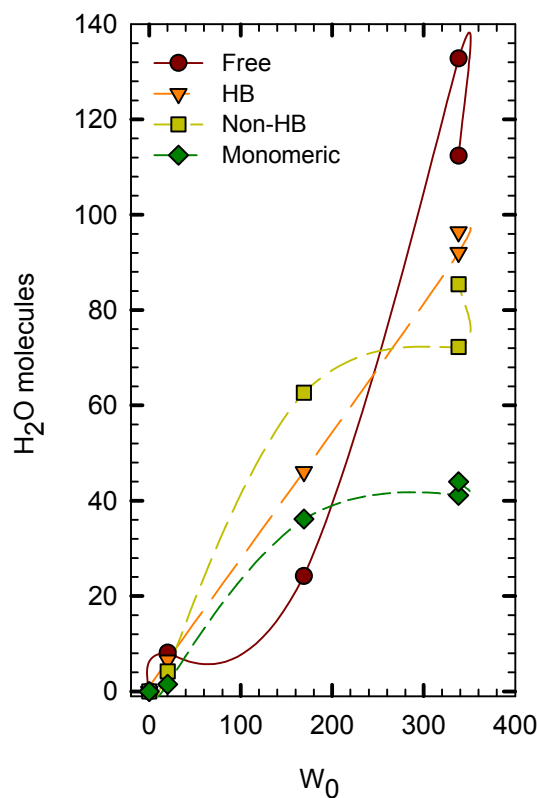

Figure 4-57: Variation of types of H_2O.

the system turned cloudy. Compared with P17R2-Ace, imipramine HCl is not promoting micellization. Imipramine HCl has compromised the phase behavior and interaction of the compounds.

4.4.2.3 Zonyl

The effect of H_2O was evaluated until a high water/surfactant molar ratio, up to 400. Zonyl (66 mg) was mixed with $scCO_2$. Aqueous solution of Imipramine HCl was

Figure 4-58: Imipramine HCl UV spectrum.

loaded to the cell. This experiment was at the conditions depicted in Table 4-10.

Table 4-10: Zonyl-imipramine HCl-H_2O-scCO_2 (effect of H_2O addition)

Condition	Pressure [bar abs]	Composition [w%]				W_0
		Zonyl	Imi*	H_2O	scCO_2	
without H_2O-192 bar (a)	191.674	0.096	0.000	0.000	99.904	0.000
3e-4%-217 bar (b)	217.270	0.093	0.000	0.000	99.900	0.17
0.354%-210 bar (c)	209.850	0.094	0.130	0.354	99.551	199.92
0.708%-207 bar (d)	207.331	0.093	0.260	0.708	99.196	399.83
0.697%-224 bar (e)	223.805	0.092	0.256	0.697	99.209	399.83

* values are multiply by 100

The IR spectrum can be seen in Figure 4-59.
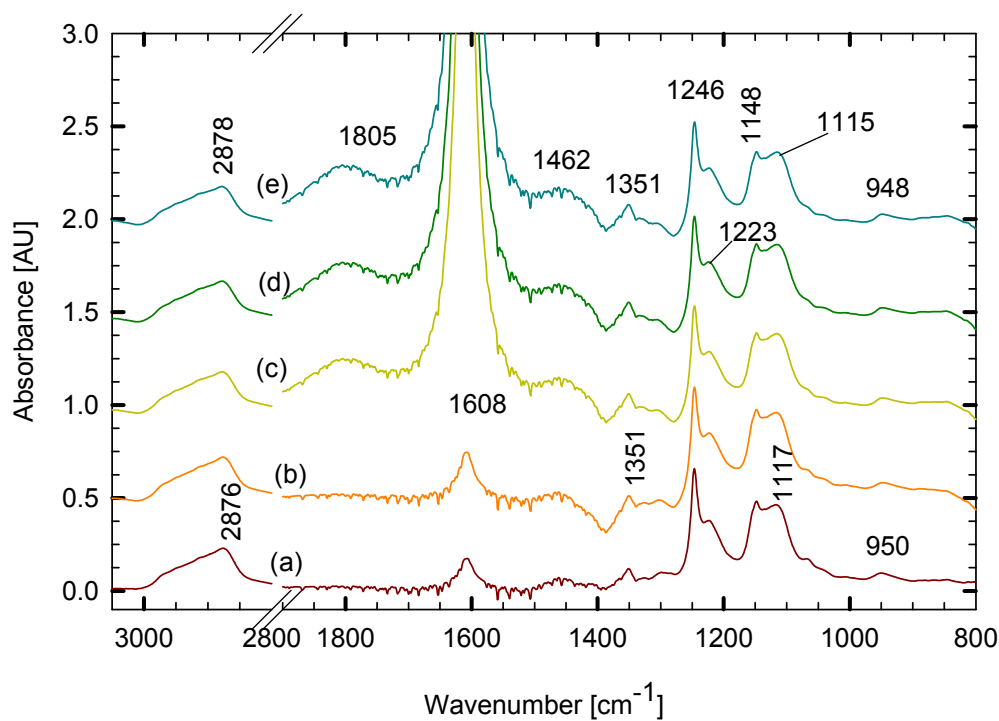
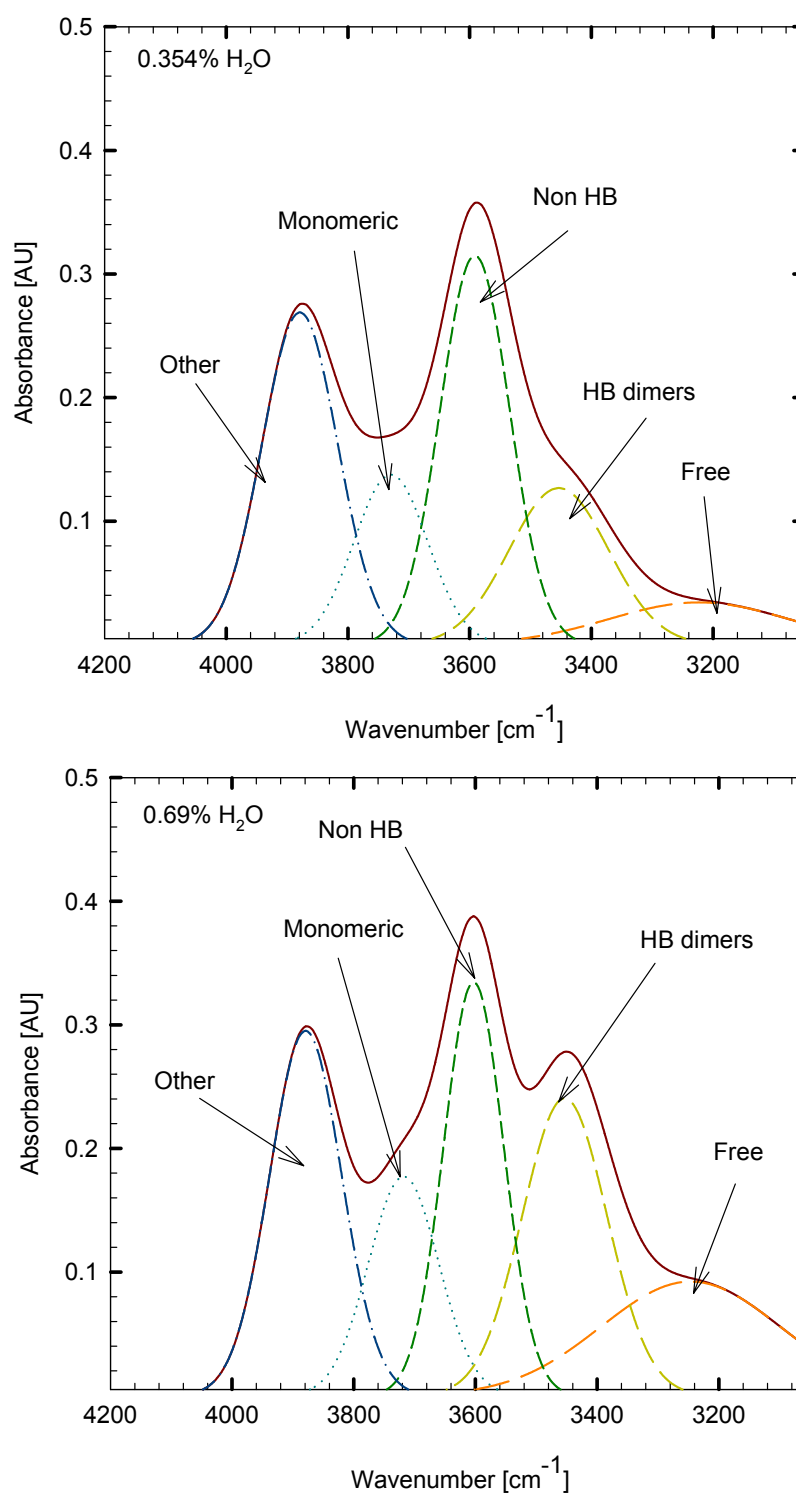Figure 4-59: (a) without H_2O, (b) 3.4e-4%, (c) 0.35%, (d) 0.70%, and (e) 0.70%-224 bar.
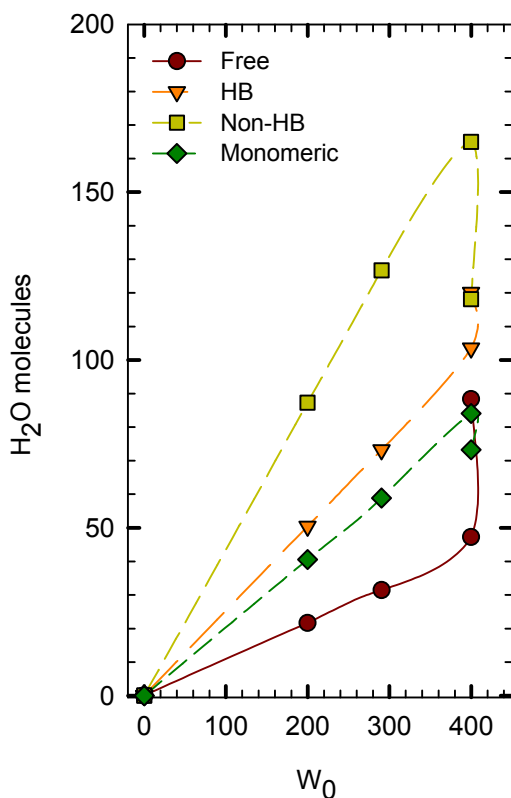
Figure 4-60: Distribution of H$_2$O types (region (OH—n)).

The little quantity of H_2O loaded in the second probe (spectrum b) was enough to cause a change in the region corresponding to 1464 cm^{-1}, widening and increasing the intensity significantly. But it is not enough to be verified to in the $\nu(OH)$ vibration. Next, 250 mg of H_2O was added and this quantity of H_2O provoked little change in the region at 1464 and 1351 cm^{-1}. However, these changes were more evident in the high frequency region, as can be seen in Figure 4-59.

Even through the conditions are quite

Figure 4-61: Variation of H_2O types.

similar to the previous experiment, the spectrums looked different in the region 3300-4000 cm^{-1} (Figure 4-60).

One factor for changing in this set of experiments is that imipramine HCl is increasing too. As a salt, the solute ionized in the aqueous solutions. It is already known that the presence of salts, can improve or hindrance the formation of microemulsions (6). In this case, imipramine HCl is hindering the formation of the $\nu(OH)$ corresponding to lower frequencies
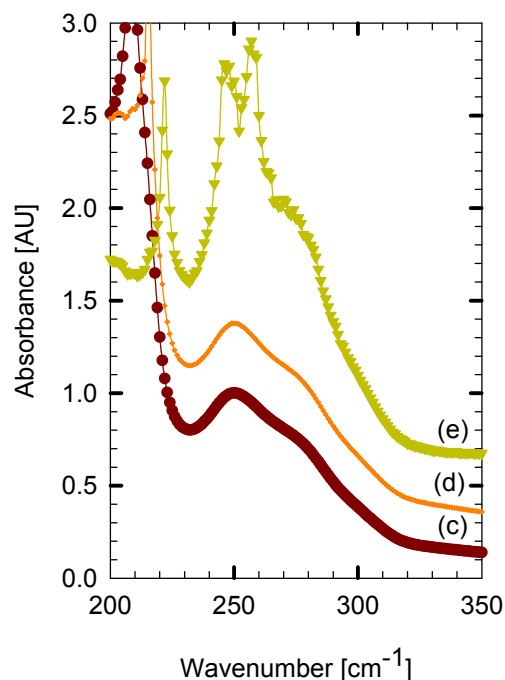
Figure 4-62: Imipramine HCl UV spectrum.

by a loss in hydrogen bonding capability. If we compare with the experiment when Ace is used, the capacity of Zonyl to trap H_2O is higher. The UV spectrum of imipramine HCl is shown in Figure 4-62. The maximum absorbance is detected at 250 nm. After, 500 mg of H_2O and stirring is stopped (spectrum e) the system becomes unstable and cloudy.

4.4.2.4 Gele

The effect of pressure was evaluated. The composition is shown in Table 4-11. The water to surfactant molar ratio was 194.85.

Table 4-11: Gele-imipramine HCl-H_2O-scCO_2

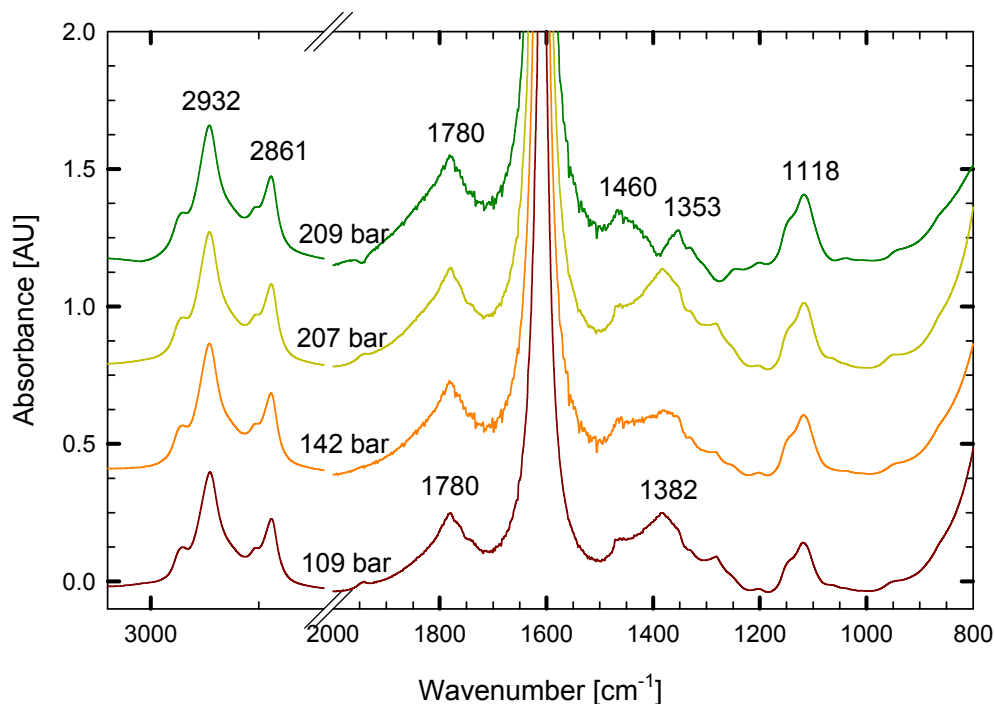| Component	Mass [mg]	Weight composition [%]
Gele	37.26	0.065
Imipramine HCl	0.60	0.001
H_2O	363.00	0.636
scCO_2	56686.00	99.298
Total		100

Figure 4-63: Gele-imipramine HCl-H_2O-scCO_2 (effect of pressure).

Figure 4-63 shows the diverse changes provoke by the increase in pressure. The carbonyl group $v(C=O)$ appear at 1780 cm^{-1}, because of its wavenumber frequency it corresponds to its monomeric form. It is possible that the surfactant concentration is dilute to avoid self-aggregation, thus the peak at 1740 cm^{-1} denoting dimerization is not detected. Neither, the C=O group interacting with the acidic proton of H_2O to generate open dimerization is detected at the conditions of the system. Presence of H_2O does not promote dimerization. This region stays almost unchanged upon an increase in pressure. Obvious changes are produced in the region 1500-1200 cm^{-1}, where initial peak at 1382 cm^{-1} is shifted to 1353 cm^{-1} due to the widen of the near region, and an increase of intensity of the peak at 1460 cm^{-1}, which initially was a shoulder at the frequency of 1470 cm^{-1}. In the lower frequency the peak corresponding to C–O vibration mode varies from 1119 cm^{-1} to 1117 cm^{-1} as pressure is enhanced. As was previously stated this peak is sensitive to HB, thus it is possible that it is interacting with H_2O.
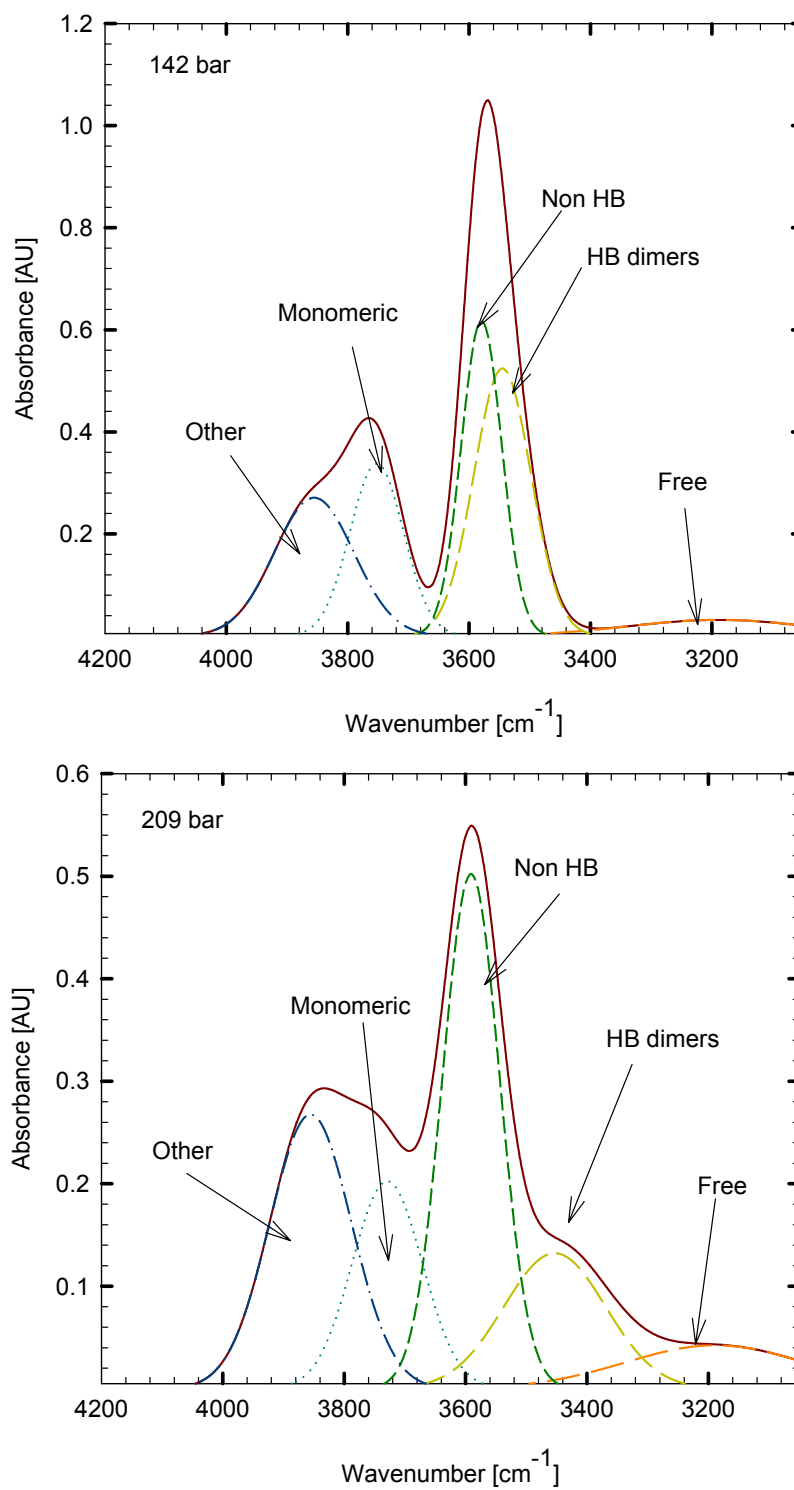
Figure 4-64: Distribution of H$_2$O types (region (OH—n).
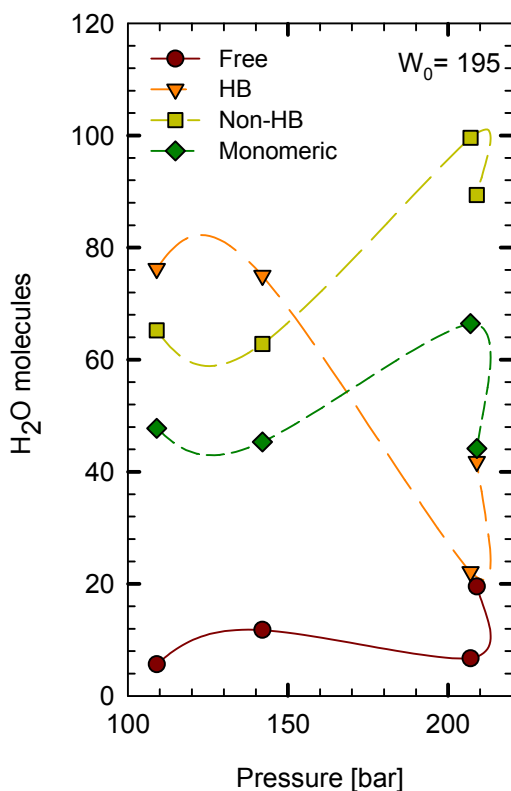
Figure 4-65: Pressure dependence of H_2O.

In the high frequency region, as can be observed in Figure 4-64, only at high pressure (209 bar) the presence of the characteristic HB peaks are detected. In Figure 4-65, the pressure dependence of H_2O is shown in all the ranges of pressures, the free H_2O does not present a great variation. HB H_2O is the only that varies significantly.

In the UV spectrum (Figure 4-66) we can detect imipramine HCl with a maximum absorption at the wavelength of 249 nm. After the higher pressure the system becomes unstable, through the windows we can see presence of water drops.

The effect of water in the system was evaluated in the next set of experiments. Gele (171.4 mg) was mixed with imipramine HCl (55.8 mg), and scCO$_2$. H_2O was added up to 350 mg. The composition of each experimental condition is detailed in Table 4-12. The IR spectrum is presented in Figure 4-67.
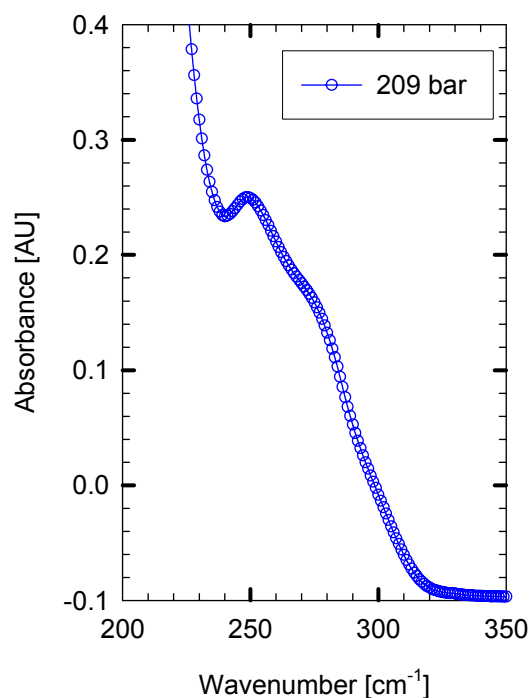

Figure 4-66: UV spectrum.

Table 4-12: Gele-imipramine HCl-H_2O-scCO$_2$ (effect of H_2O addition)

| Condition	Pressure [bar abs]	Composition [w%]				W_0
		Gele	Imi	H_2O	scCO$_2$	
without H_2O-203 bar	203.042	0.245	0.080	0.000	99.675	0.00
0.071%-205 bar	205.084	0.244	0.079	0.071	99.605	5.83
0.142%-211 bar	210.871	0.243	0.079	0.142	99.537	11.67
0.212%-212 bar	211.824	0.242	0.079	0.212	99.467	17.50
0.282%-212 bar	211.824	0.242	0.079	0.282	99.397	23.34
0.352%-214 bar	214.138	0.241	0.079	0.352	99.328	29.17
0.421%-217 bar	217.133	0.240	0.078	0.421	99.261	35.01
0.492%-213 bar	213.253	0.241	0.078	0.492	99.188	40.84
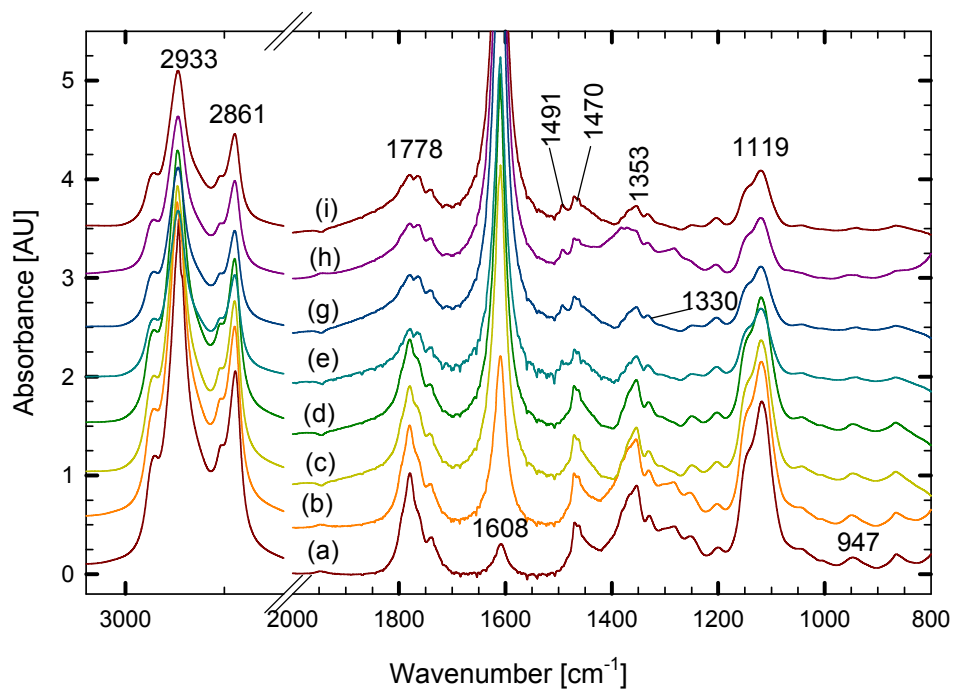
Figure 4-67: (a) 0%, (b) 0.07%, (c) 0.14%, (d) 0.21%, (e) 0.28%, (f) 0.35%, (g) 0.42%, (h) 0.49%, and (i) more time.

The increased quantity of Gele produce the formation of dimers as can be seen

through the appearance of the peak at 1740 cm^{-1}. Through the appearance of others peak around this region we can deduce that the formation of open dimers is promote upon H_2O addition. There is a change in the lower frequency region evidently there is interaction among the surfactant, H_2O, and the fluid phase.

The presence of H_2O also promotes the appearance of the different micro-environments in the ν(OH--n) region (Figure 4-69). According to the intensity of the peaks, we can deduce that the surfactant does not have a high capacity to trap H_2O. Although, the presence of the solute was detected it is not possible to assure the state of hydration of the solute. In Figure 4-68 we observe the variation of the types of H_2O it seems that the H_2O goes mainly as a non-HB H_2O which penetrates into the surfactant layer. It is followed by HB that augmented as W_0 increases. Either, free H_2O and monomeric H_2O do not show a clear trend. Since, the deformation of the UV spectrum

Figure 4-68: Variation of H_2O types.

is also observed when Ace is used as solute this effect is induced by the surfactant (Figure 4-70).
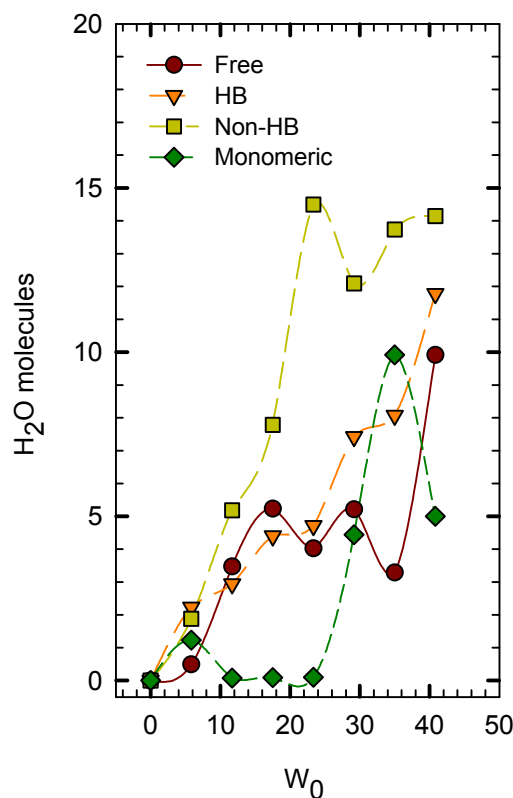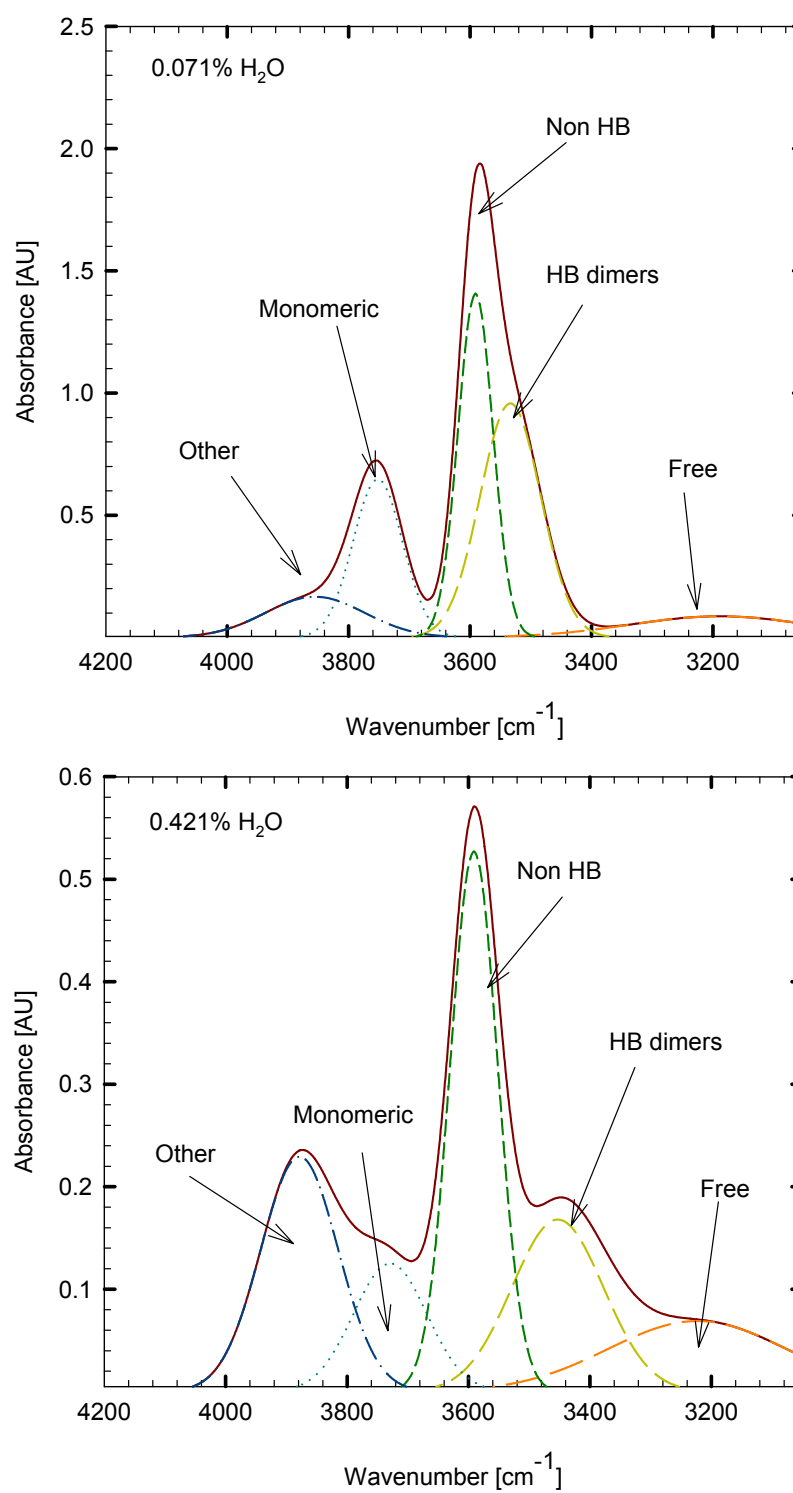
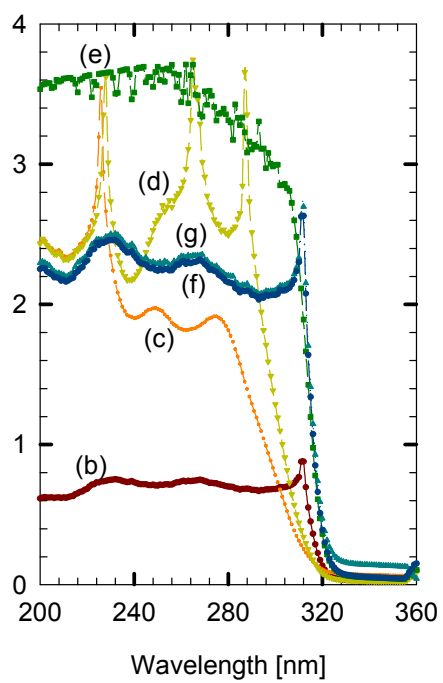Figure 4-69: Distribution of H$_2$O types (region (OH—n).

Figure 4-70: UV spectrum.

References

1. Avram, M.; Mateescu, G.H. Infrared Spectroscopy. Applications in Organic Chemistry. Wiley-Interscience. **1972**.

2. Begum, R.; Yonemitsu, T.; Matsuura, H. Conformational Behaviour of Cyclic and Open-Chain Poly(Oxyethylene) Compounds in Water Studied by Infrared Spectroscopy. *J. Mol. Struct*. **1998**, 447, 111-117.

3. Bell, P. W.; Thote, A. J.; Park, Y.; Gupta, R. B.; Roberts, C. B. Strong Lewis Acid-Lewis Base Interactions Between Supercritical Carbon Dioxide and Carboxylic Acids: Effects on Self-association. *Ind. Eng. Chem. Res*. **2003**, 42 (25), 6280-6289.

4. Blitz, J. P.; Yonker, C. R.; Smith, R. D. Infrared Spectroscopic Studies of Supercritical Fluid Solutions. *J. Phys. Chem*. **1989**, 93, 6661-6665.

5. Colthup, N. B.; Daly, L. H.; Wiberley, S. E. Aliphatic groups, in Introduction to Infrared and Raman Spectroscopy. Academic Press INC., 1964, 191.

6. da Rocha, S. R. P.; Psathas, P. A.; Klein, E.; Johnston, K. P. Concentrated CO_2-in-Water Emulsions with Nonionic Polymeric Surfactants *J. Colloid Interface Sci*. **2001** 239(1) 241-253.

7. Guo, C.; Liu, H. Z.; Chen, J. Y. A Fourier Transform Infrared Study on Water-Induced Reverse Micelle Formation of Block Copoly(Oxyethylene-Oxypropylene-Oxyethylene) in Organic Solvent. *Colloids and Surfaces A: Phys. Eng. Aspects*. **2000**, 175, 193-202.

8. Guo, C.; Liu, H. Z.; Chen, J. Y. A Fourier Transform Infrared Study of the Phase Transition in Aqueous Solutions of Ethylene oxide-propylene oxide Triblock Copolymer. *Colloid Polym. Sci*. **1999**, 277, 376-381.

9. Hyatt, J. A. Liquid and Supercritical Carbon Dioxide as Organic Solvent. *J. Org. Chem.* **1984**, 49, 5097-5101.

10. Ikushima, Y. Supercritical Fluids: An Interesting Medium for Chemical and Biochemical Processes. *Advances in Colloid and Interface Science*. **1997**, 71-72, 259-280.

11. Iwai, Y.; Uno, M.; Nagano, H.; Arai, Y. Measurement of Solubilities of Palmitic Acid in Supercritical Carbon Dioxide and Entrainer Effect of Water by FTIR Spectroscopy. *J. Supercrit. Fluids*. **2004**, 28, 193-200.

12. Kazarian, S. G.; Vincent, M. F.; Bright, F. V.; Liotta, C. L.; Eckert, C. A. Specific Intermolecular Interaction of Carbon Dioxide with Polymers. *J. Am. Chem. Soc*. **1996**, 118, 1729-1736.

13. King, M. B.; Mubarak, A.; Kim, J. D.; Bott, T. R. The Mutual Solubilities of Water with Supercritical and Liquid Carbon Dioxide. *J. Supercritical Fluids*, **1992**, 5 (4), 296-302.

14. Liu, D.; Zhang, J.; Han, B.; Fan, J.; Mu, T.; Liu, Z.; Wu, W.; Chen, J. Effect of Compressed CO_2 on the Properties of AOT Reverse Micelles Studied by Spectroscopy and Phase Behavior. *J. Chem. Phys*. **2003**, 119 (9), 4873-4878.

15. Marechal, Y. Infrared spectra of water. I. Effect of Temperature and H/D Isotopic Dilution. *J. Chem. Phys*. **1991**, 95 (8), 5565-5573.

16. Marechal, Y. Observing the Water Molecule in Macromolecules and Aqueous Media Using Infrared Spectrometry. *J. Mol. Struct*. **2003**, 648, 27-47.

17. McFann, G. J.; Johnston, K. P.; Howdle, S. M. Solubilization in Nonionic Reverse Micelles in Carbon

Dioxide. *AIChE J*. **1994**, 40 (3), 543-555.

18. O'Shea, K. E.; Kirmse, K. M.; Fox, M. A.; Johnston, K. P. Polar and Hydrogen-Bonding Interactions in Supercritical Fluids. Effects on the Tautomeric Equilibrium of 4-(Phenylazo)-1-naphthol. *J. Phys. Chem*. **1991**, 95(20), 7863-7867.

19. Yamamoto, M.; Iwai, Y.; Nakajima, T.; Arai, Y. Fourier Transform Infrared Study on Hydrogen Bonding Species of Carboxylic Acids in Supercritical Carbon Dioxide with Ethanol. *J. Phys. Chem.* **1999**, 103 (18), 3525-3529.

CHAPTER 5

Extraction of Ethylene Glycol from Hydroxy Ethyl Starch: A Practical Study of Supercritical Fluid Processing

5.1 Introduction

Hydroxy Ethyl Starch (HES) is a plasma volume expander (PVE) used for the compensation of surgical blood loss. It is produced in the Sabana Grande, manufacturing facility of B BRAUN Puerto Rico in a batch reactor from the reaction of cornstarch with ethylene oxide in the presence of a base (Figure 5-1).
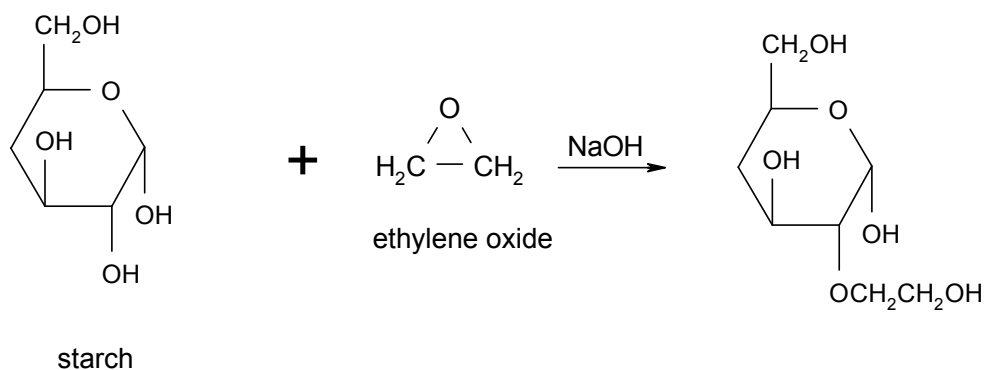

Figure 5-1: HES based reaction.

After the reaction, the polymer follows a series of purification steps. This includes acetone and water washings, acetone stripping, filtration, drying, etc. Although the goal of producing a "pure" HES product is achieved (1-10 mg/kg), several challenges remain in the separation processes. Some of them include:

i)   Time required to purify one batch due to the separation challenges ($\approx$ 30 or more hours of processing)

ii) Unacceptable residual amounts of undesired substances (*e.g.,* ethylene glycol)

As an alternative to the numerous separation processes for the polymer purification, the use of a supercritical fluid provides the tools for the precipitation and separation of

159

the polymer directly from the reaction mixture in a single step. In addition to the increased efficiency, one also replaces the use of Volatile Organic Compounds (VOCs, *e.g.,* acetone) and the reduction of the processing time. This research has focused on a solvent replacement to separate one of the components in CO_2 and to purify HES. This approach is even more appealing, considering that higher temperatures or lower pressures are not viable options for the stability of the polymer.

The major impurities in HES are ethylene glycol (EG) and ethylene chlorohydrin (ECH). EG is used for the dehydration of gas streams containing the acid gases (e.g., H_2S and CO_2). The properties and characteristics of EG are summarized in Table 5-1.

Table 5-1: Characterisitcs of ethylene glycol (13)

Ethylene Glycol CAS 107-21-1	
Formula	$C_2H_6O_2$
Chemical structure	
Molecular weight	62.07
Boiling point [°C]	196-198
Solubility	Miscible with H_2O (it absorbs twice its weight of H_2O). Soluble with lower aliphatic alcohols, glycerol, acetic acid, acetone and similar ketones, aldehydes, pyridine, and similar coal tar bases. It is slightly soluble in ether but practically insoluble in benzene and its homologues, chlorinated hydrocarbons, petroleum ethers, and oils
Characteristics	Clear, odorless, slightly viscous, sweet-tasting liquid, and has low vapor pressure.

The ingestion of EG can cause central nervous system depression, its metabolites can cause severe acidosis and damage to the brain, hearts and kidney. It has hazardous properties when it is found in high concentrations, thus its separation is of crucial importance. Union Carbide measured the solubility of CO_2 in EG at 25°C and 12 bar, and Hayduk et al., reported its solubility at 25°C and 1 atm. Vapor-phase equilibria of EG in CO_2 at elevated pressures has been measured by Jou et al.; other references for vapor-

phase concentration of EG in CO_2 at various pressures and temperatures can be found in reference (6). Even thought, the partitioning of poly(ethylene glycols) in SCF's was studied (4), little is known about the solubility of EG in $scCO_2$. One interesting feature of these results is that the partitioning of those polymers is favored by increase in pressure and low molecular weight of the poly(ethylene glycol).

The IR spectrum (Figure 5-2) of EG in $scCO_2$ shows two $\nu(OH)$ bands at 3644 cm^{-1} and 3612 cm^{-1}. The first corresponds to the $\nu(O-H)$ stretching vibration of the free hydroxyl group and the second the stretching vibration of the hydroxyl involved in the OH•••O hydrogen bonding (intramolecular). In general in glycols, $\Delta\nu$ between these frequencies varies within a large limit depending on the relative positions of the OH groups.
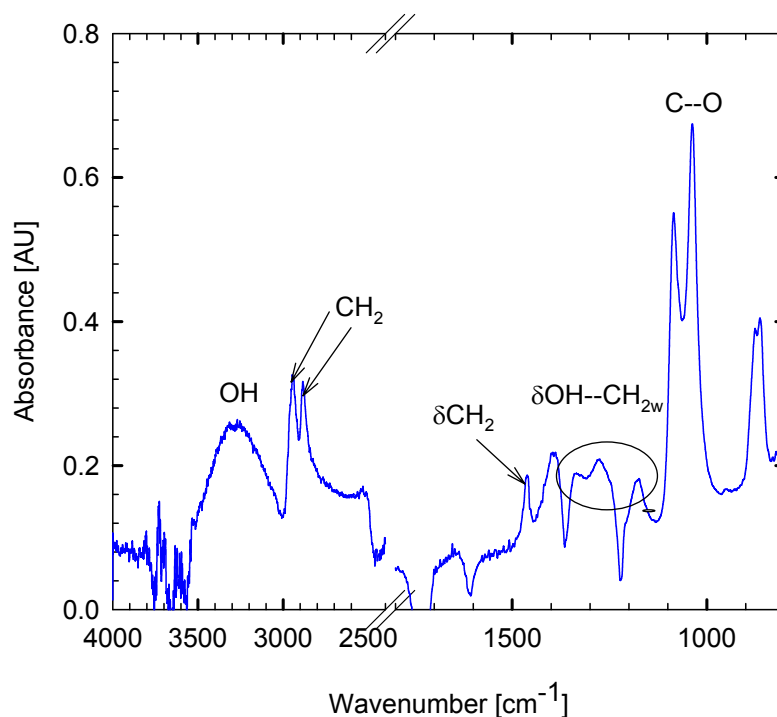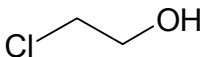

Figure 5-2: IR spectrum of ethylene glycol.

At high concentration of diols a peak arising from the intermolecular HB of (OH) appears at 3264 cm^{-1}. This absorption shows all the characteristics observed in

monohydroxylic alcohols (broad and strong bands). (OH) in EG can acts as HB proton donor and acceptor as it was determined by its solvatochromic values α=0.90, β=0.52. Besides, it has a polarizability close to H_2O (π^*= 0.92). The peaks at 2946 and 2885 cm^{-1} correspond to $\nu(CH_2)$ vibration mode, and the $\delta(CH_2)$ at 1461 cm^{-1}. Broaden bands attributed to the $\delta(OH\text{---}CH_{2w})$ (peaks at 1395, 1276 cm^{-1}) and a peak at 1174 cm^{-1}. The carbonyl group at 1037 and 1085 cm^{-1}, it is not a pure C–O vibration stretching but interacts strongly with attached C–C bond stretching, in primary alcohols this involves the asymmetric C–C–O stretching vibration. In the bonded state the primary alcohols have diffuse association bands near $\delta(OH\text{---}CH_{2w})$ which disappear upon dissolution.

Ethylene chlorohydrin (ECH) is other impurity found in HES polymer. It is used as a solvent for waxes, celluloses resins, and as a cleaning agent. It is also has hazardous properties. It is produced by the oxidation of EG with chlorides generated in the reaction. In Table 5-2 are listed some physical properties of this compound.

Table 5-2: Characteristics of ethylene chlorohydrin (13)

Ethylene chlorohydrin CAS 107-07-3	
Formula	C_2H_5ClO
Chemical structure	
Molecular weight	80.51
Boiling point [°C]	129
Solubility	Miscible in water, DMSO, ethanol and acetone
Characteristics	Clear poisonous liquid, faint ethereal odor. It is sensitive to moisture and heat.

Reports of the solubility of this compound in $scCO_2$ were not found, at least in the literature reviewed. The IR spectrum of ECH (Figure 5-3) presents representative peaks at 830–560 cm^{-1} region corresponding to C–Cl and strong CH_{2w} band at 1300–1240 cm^{-1} coming from the CH_2–Cl group. C–O at 1100 cm^{-1} and the characteristic $\nu(CH_2)$.
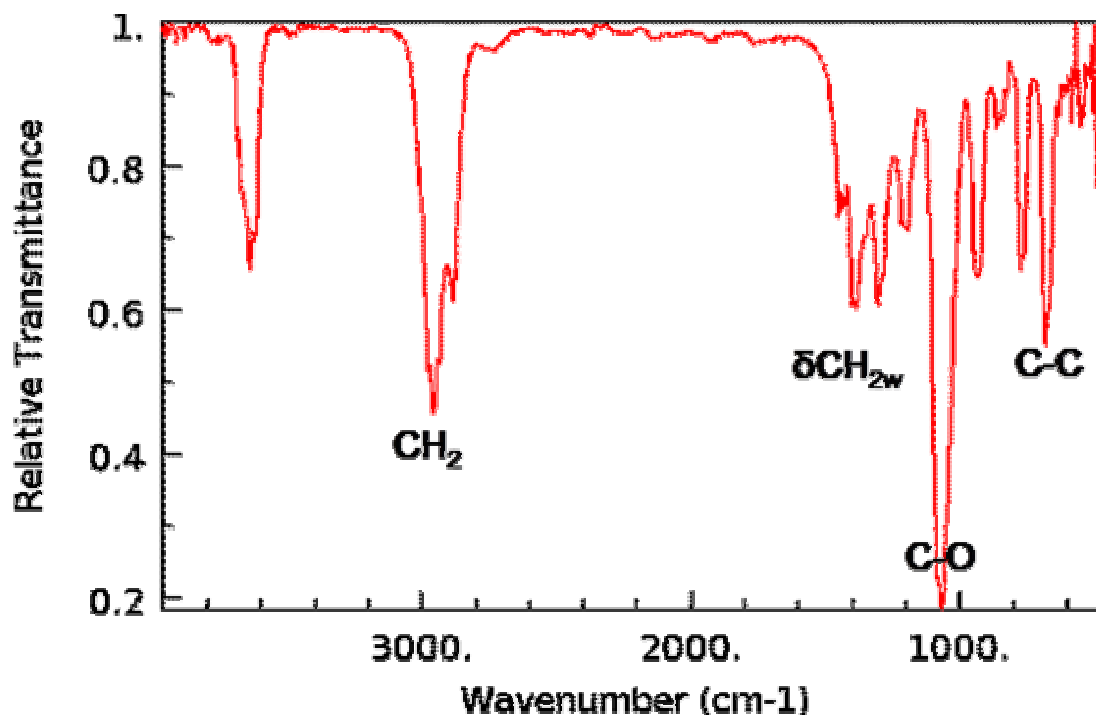
Figure 5-3: IR spectrum of ethylene chlorohydrin (13).

Many strategies to reduce the contents of EG and ECH in the HES polymer were used. These are: $scCO_2$ pure, $scCO_2$ with cosolvents, $scCO_2$ with surfactants. The equipments used are described in chapter 2 section 2.4, and the procedure described in (15). The composition analysis was done by BBRAUN Crissier Switzerland and an in-line FT-IR was used to monitor the molecular interactions from solutes and solvents.

5.2 Removal of EG and ECH with Pure $scCO_2$

Pure $scCO_2$ was used first to remove EG and ECH from HES. The CO_2 used in the extraction has impurities that were detected with the FT-IR, those were the peak at 2970 cm^{-1} corresponding to CH vibration region from the volatile hydrocarbons, 1723 cm^{-1} to carboxyl compounds from carboxylic acid, and 891 cm^{-1}. The water contents can be seen at 1610 cm^{-1} corresponding to δ(OH) vibration, and the vapor phase saturation bands

along the spectrum. The spectrum can be seen in the Appendix H.

Two lots of HES with different characteristics provided by BBRAUN PR were used. The Table 5-3 shows their initial concentrations.

Table 5-3: Characteristics of HES used in the investigation (lot 1 and lot 2)

	HES lot 1	HES lot 2
Batch number	0060278528	9700048362
Molecular weight	259 883	201 100
Ethylene Glycol [ppm w/w]	42 236	788.5
2-Chloroethanol [ppm w/w]	27.9	13.30*

* Detection Limit

After performing extraction in a wide range of pressures (100–300 bar) and temperatures (40–60°C), the conditions of maximum solubility were found. These are at 200 bar and 50°C. The extractions were performed using 241.65 ± 13.58 [mL] of scCO$_2$, a flow of 1.34 ± 0.34 [mL/min] during an average time of 3 hours. The final results can be seen in Table 5-4

Table 5-4: Final concentration of EG and ECH after extraction with scCO$_2$

	HES lot 1	HES lot 2
Batch number	0060278528	9700048362
Molecular weight	264 600	199 400
Ethylene Glycol [ppm w/w]	21 902 (48%*)	31.61 (96%)
2-Chloroethanol [ppm w/w]	12.70 (54%)	13.30**

(*) Percentage of extraction, (**) Detection limit

The IR spectrums at different time of extraction were recorded and can be seen in Figure 5-4. The principal characteristics are seen in the region from 2200-800 cm^{-1}. This region shows small peaks and specifically the δ(OH) vibration mode, with strong saturation bands denoting the presence of H$_2$O. At the beginning of the extraction this vibration mode appears at 1651 cm^{-1}, shifting to 1609 cm^{-1}. Some authors denote that the shift of the vibration is provoked by the δ(OH) hydrogen bonded (10). The peak initially

at 1246 cm^{-1} is shifting to 1285 cm^{-1} along extraction corresponding to $\delta(OH\text{---}CH_{2w})$. The peak at 1173 and 1037 cm^{-1} comes from the EG.
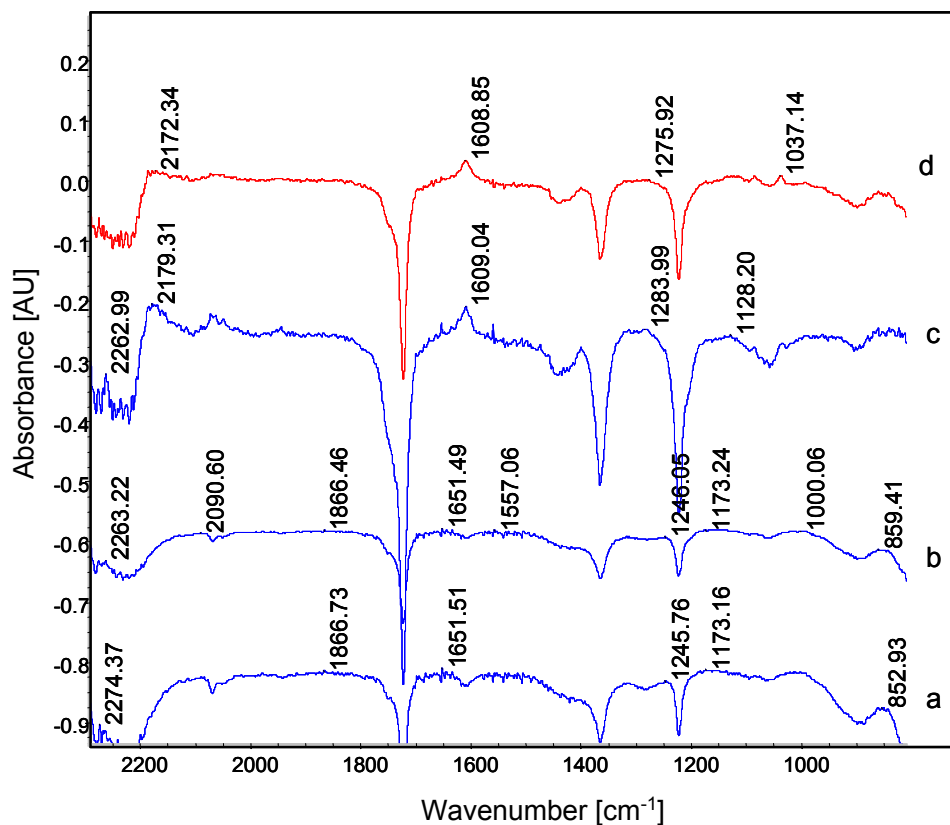

Figure 5-4: IR spectrum during extraction with scCO$_2$: (a) 0 min, (b) 30 min, (c) 60 min, (d) 120 min.

The low intensity of the peaks are because of the low concentration of the EG and ECH in the polymer (ppm level). The interactions of these impurities are though to be through the OH present in both compounds and the carbonyl group of CO$_2$. This is possible because of the capacity of CO$_2$ to acts as a Lewis acid or electron acceptor (8, 12).

5.3 Removal of EG and ECH with scCO$_2$ and Cosolvents

A convenient characteristic of the cosolvent addition is that in some cases the

operational conditions (e.g., pressure and temperature) can be reduced.

The addition of small amounts of a cosolvent with intermediate volatility can increase the solvent capacity of the primary solvent (e.g., CO_2), while retaining the favorable mass transport properties (high molecular diffusivities and low viscosities) for which SCFs are well known. Non-polar cosolvents were the first ones to be used. Although, they increase the solute solubility by increasing the dispersion forces in the solution; there is not an improvement in the selectivity, because those forces are not selective. The addition of polar cosolvents (such as, ethanol or methanol), increases the polarity, and dielectric constant (i.e., the dielectric constant of $scCO_2$ was doubled when 12v% of ethanol was added). There is a greater increase in solubility and improvement in selectivity, because the forces between the cosolvent and solute are more specific.

Liu et al. (9), have determined that the addition of cosolvents can reduce the cloud point of the systems, in aadition to increasing solute solubility. Those favorable conditions are promoted when pressure and concentration, rather than temperature, are increased. They reported that cosolvents with an aromatic ring (i.e., benzyl alcohol) do not reduce the cloud point and improve the solute solubility. In addition of the solvation behavior of supercritical fluids, the presence of a cosolvent able to form HB generates a different type of system (free non-hydrogen bonded solutes establish an equilibrium with aggregates of hydrogen-bonded solute clusters of various stoichiometric sizes).

There are many studies that use cosolvents to increase the solvating power of CO_2. Koga et al. (19) measured the influence of certain cosolvents (i.e., ethanol, and octane) on solubilities of fatty acids and higher alcohols, concluding that ethanol is more effective on the solubility enhancement for fatty acids in $scCO_2$. Even though there has been an extensive amount of research, done in the use of cosolvents, the mechanisms of these entrainer effects has not been clarified yet. Thus a more reasonable choice of entrainer may be possible by understanding the microscopic structure in $scCO_2$. Walsh et al. (18) demonstrated the different types of HB interactions that can occur in cosolvent systems and showed spectroscopic and modeling techniques that can be used to understand them.
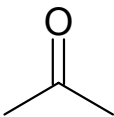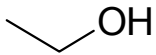
Fulton et al. (5), and Yee et al. (21), studied the intermolecular or intramolecular HB species of several alcohols in scCO$_2$ and ethane. They reported the aggregation of these alcohols in scCO$_2$. Gupta et al. (21), found that the self HB could be represented by a function of concentration. These and other studies suggest that the solubility enhancement by cosolvents relates to the amount of hydrogen bonding species.

The alcohols used as cosolvents have comparatively large α and β values in the liquid phase, and act as HB-donors as well as HB-acceptors. In that sense, they form HB bonds with organic compounds that often contain polar organic groups. The β and π* parameters for the scCO$_2$/n-alcohol system has been determined using solvatochromic probes. These studies determined that the π* values were insensitive to the length of the n-alkyl group in the alcohol molecules (3). However, the β value increased in accordance with the elongation of the n-alkyl chain. Thus, the donor ability of the alkyl group and a stabilization of the HB increase through inductive effects. It is known that the OH bond of the alcohol is very sensitive to hydrogen bonding and thus provides a measurement of the degree of hydrogen bonding, the size of the aggregate, and the enthalpy of hydrogen bonding. It is well established that in liquid phase the hydrogen bonding results in a large red shift of the ν(OH) bands (21). Also highly hydrogen bonding solvents (e.g., acetone, methanol) show strong deviation with a large red shift.

Cosolvents and cosurfactans can be used in reverse micelles to increase surfactant solubility and promote surfactant aggregation. McFann et al. (11), showed that alcohol of medium chain length can increase the size and solubilization capacity of the reverse micelle.

The properties of the cosolvents used are summarized in Table 5-5.

Table 5-5: Principal properties of the organic compounds used as cosolvents (13)

	Acetone	Acetonitrile	Ethanol
Chemical structure		$CH_3C\equiv N$	OH
Formula	C_3H_6O	C_2H_3N	C_2H_6O
Molecular weight	58.09	41.053	46.069
Critical temperature [K] [14]	508.1	548	516.2
Critical pressure [bar] [14]	47	48.3	63.8
Critical density [g/cm^3] [14]	0.278	0.237	0.276
Specific gravity	0.784	0.786	0.794
Boiling point [K]	329.22	354.75	351.54
Dielectric constant	20.56	36.6[16]	24.3[16]
Solubility parameter [cal/m^3]$^{1/2}$	10	11.9[17]	12.92[17]
Polarizability (α cm^3)	63.3[14]		
Permanent Dipole moment (μ D)	2.88[16]	3.94	1.70
Water solubility [mg/kg]	Inf	Miscible	Inf
Solvatochromic Parameters (7)			
α	0.08	0.19	0.83
β	0.48	0.31	0.77
π*	0.71	0.90	0.47

Even though they have similar properties, they posses different chemical nature, such as acetone is an aprotic solvent, ethanol is polar protic and acetonitrile is polar aprotic with very different functional groups. We used those solvents to provoke any interaction between the EG and CO_2 to increase the removal of impurities from HES. Only for reference, at 202.2 bar and 45°C the EtOH-scCO$_2$ system merely has π* and β value of -0.157 and 0.393 respectively (3).
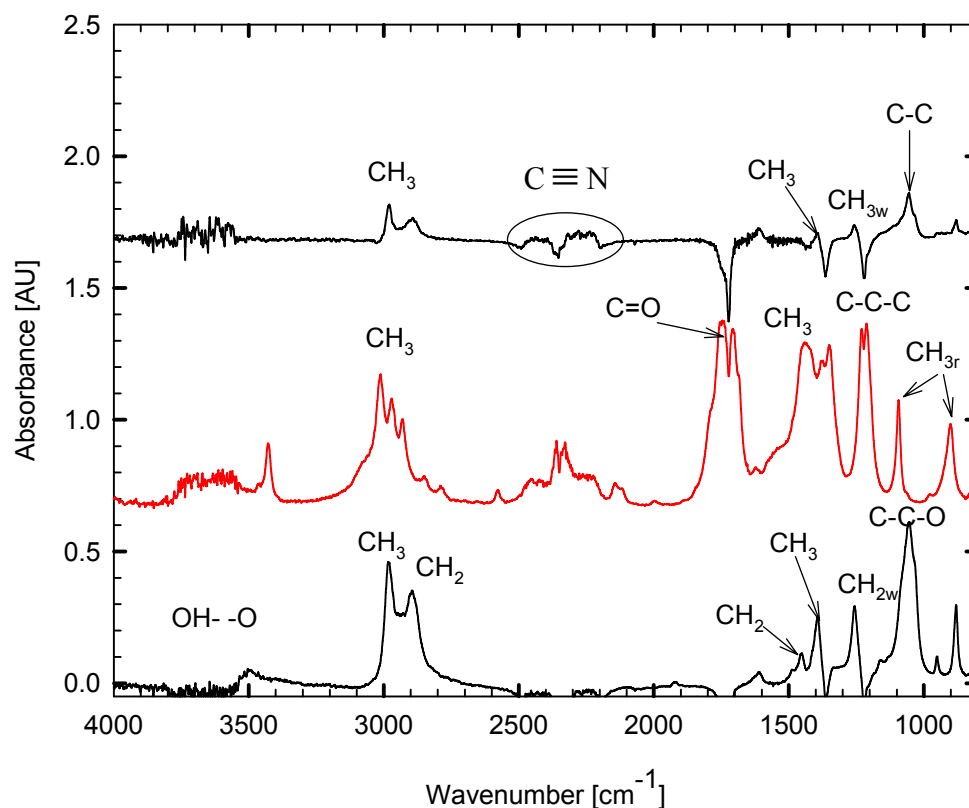
Figure 5-5: IR spectrum of ethanol (bottom), acetone (center), and acetonitrile (top) in scCO$_2$ (200 bar, 40°C).

After subtraction of scCO$_2$ spectrum, the cosolvent FTIR spectrums are seen in Figure 5-5 (from bottom to top: ethanol, acetone, and acetonitrile). Ethanol (EtOH) presents in the 3800-3500 cm^{-1} region, the ν(OH---O) hydrogen bonding; clearly the intensity of the band is decreased by the intensity of scCO$_2$. The asym ν(CH$_3$) and ν(CH$_2$) appear at 2984 and 2895 cm^{-1} respectively. The bending vibrations corresponding to CH$_2$ and CH$_3$ occur at 1452 and 1394 cm^{-1} respectively. The C–O vibration frequency occurs at 1053 cm^{-1}; this bond is especially sensitive to electronic and symmetry effects resulting in changes in force constants, hence in band positions. For acetone (ACE), the asym ν(CH$_3$) vibration appears at the region 3012–2900 cm^{-1}. Two peaks at 1442 cm^{-1} from

asym $\delta(CH_3)$ and 1374 cm^{-1} from sym $\delta(CH_3)$, the presence of the carbonyl group intensify the vibration. The analysis of these bands is important in studies of compounds containing structural elements capable of affecting the vibration of this group. Methyl rocking (CH_{3r}) (see Table 4-9) are mass sensitive and variable in position due to the interaction with skeletal stretching modes, frequencies at 1093 and 901 cm^{-1} are assigned to them. The asym stretching vibration C–C occurring at 1221 cm^{-1}. In the vapor phase, saturated alkylketone have a strong absorption at 1738-1742 cm^{-1}, generally in nonpolar solvents the frequency decreases by 20-25 cm^{-1}. The C=O vibration in the spectrum appears at 1740 cm^{-1} (1742 cm^{-1} in vapor phase, 1), and a peak at 1707 cm^{-1} indicates the existence of self associated ACE molecules. The polar character of the CO group enables the occurrence of weak electrostatic bonds between the more positive carbon of one carbonyl group and the negatively polarized oxygen of another. For acetonitrile (ACN), the IR absorption of saturated nitriles occurs in the region 2240-2300 cm^{-1}, specifically a strong band at 2273 cm^{-1}. The asym $\nu(CH_3)$ occurs at 2980 cm^{-1} and sym $\nu(CH_3)$ 2893 cm^{-1}. The sym $\delta(CH_3)$ vibration that occurs at 1393 cm^{-1} and the CH_{2w} at 1258 cm^{-1}. Finally, the C–C is seen at 1055 cm^{-1}.

5.3.1 Ethanol-scCO₂ System

The main differences with respect to pure scCO$_2$ system can be seen in Figure 5-6. In the $\nu(O{-}H)$ region the intensity is intensified. In the region 2400-2200 cm^{-1} the appearance of large peaks correspond to an intensification of the C=O broaden band. It may indicate the interaction of the carbonyl group from CO$_2$ with an electronegative group from the cosolvent or the solute. The peak at 1609 shifts to 1633 cm^{-1}; this peak corresponds to the $\delta(\text{--OH})$. The peak at 1388 cm^{-1} shift to 1397 cm^{-1}. The shoulder at 1159 cm^{-1} (spectrum of ethanol) is intensified corresponding to a peak at 1162 cm^{-1} and other peak approximately 1132 cm^{-1}. These peaks come from the solutes (EG or ECH). The peak at 1258 cm^{-1} initially shifts to 1284 cm^{-1}, this corresponds to the (CH_{2w}—OH). The CH_{2w} vibrations are intensified in CH_2Cl and are seen at 1250 cm^{-1} (1). The other peaks remain at the same frequency during extraction.

The peak at 1078 cm^{-1} corresponds to CH—OH, that increases during extraction, close appears a shoulder (around 1055 cm^{-1}) also the broaden of the peak occurs. This peak in EtOH appears at 1055 cm^{-1}, it has been shown that widen of the peak is produced by the increase of the rotational freedom of the alcohol that is loss when pressure is increased (5). The $\nu(CH_3)$ vibration is detected after some time of extraction at 2978 cm^{-1}, lesser frequency than in pure EtOH spectrum (2984 cm^{-1}), there is not much variation for $\nu(CH_2)$ that appear at 2893 cm^{-1}. The $\nu(CH_2)$ asym appears as a shoulder at 2944 cm^{-1}, maybe corresponding to CH$_2$ from EG. There is not much variation between the spectrum of Lot 1 and Lot 2 as we can observe in Figure 5-7. Not all the spectrums present the broaden bands corresponding to $\nu(O—H)$, it may indicates that the extraction of the solutes are not continuum with time.
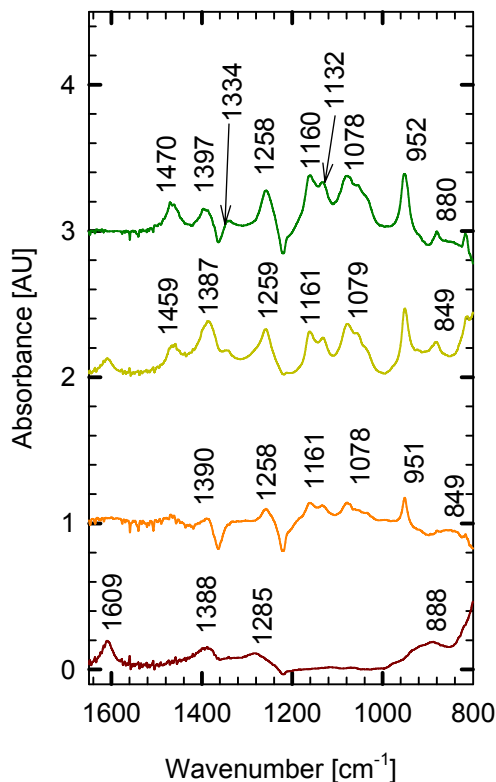

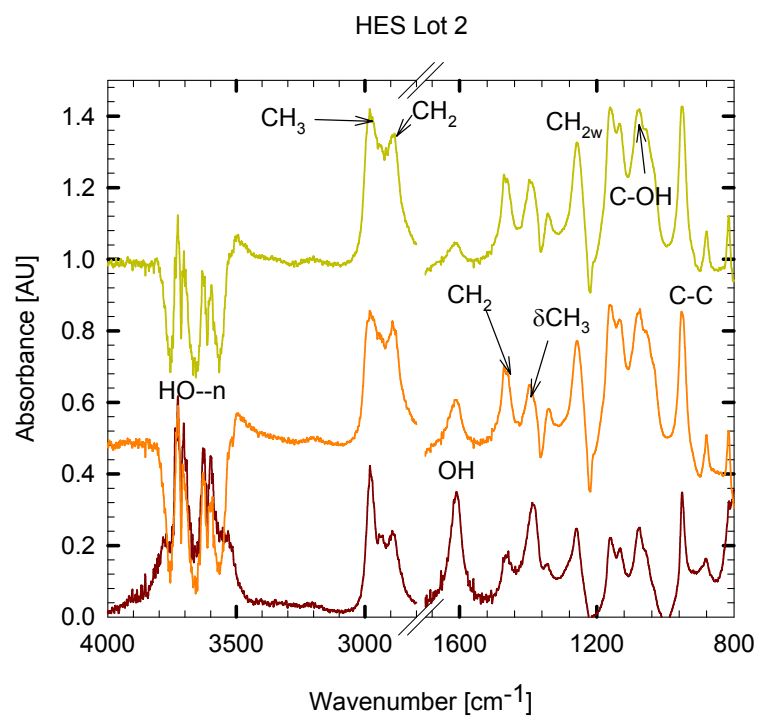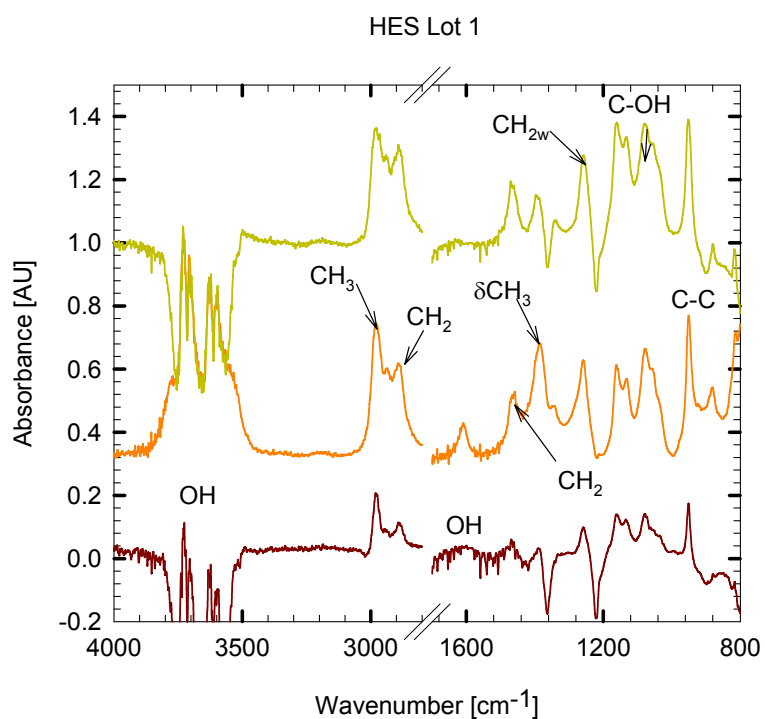Figure 5-6: Ethanol-scCO$_2$ spectrum (1600-800 cm^{-1} region).

Figure 5-7: HES treated with Ethanol-scCO$_2$ (200 bar, 40°C).

5.3.2 Acetone-scCO₂ System

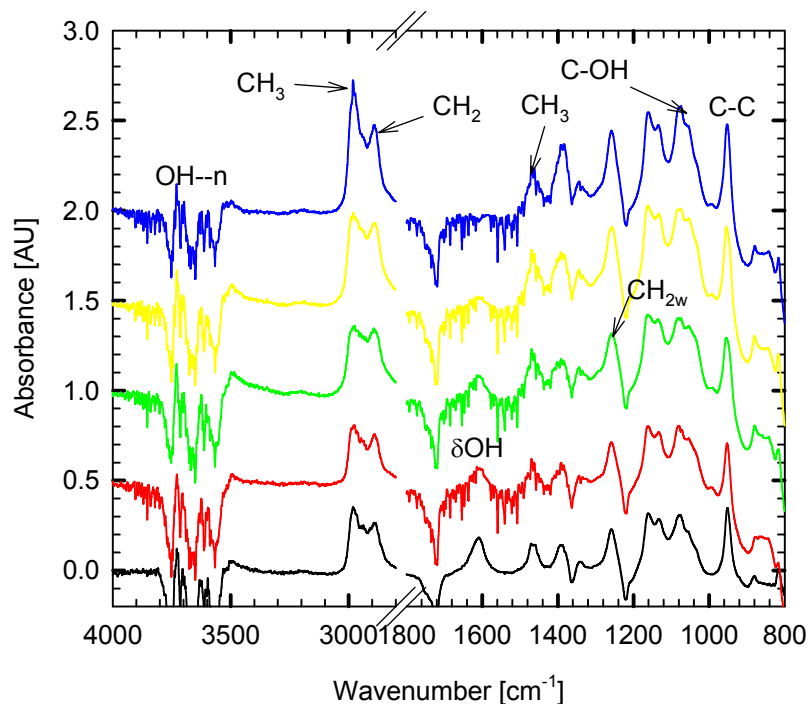For ACE the spectrum is shown in Figure 5-8.

Figure 5-8: HES treated with acetone-scCO$_2$ (200 bar, 40°C).

The principal features of the spectrum are the appearance of the ν(OH—O) stretching vibration denoting the presence of EG and H$_2$O. The ν(CH$_3$) asym of the ACE shifts to higher frequency 2980 cm^{-1} from 2970 cm^{-1}, and ν(CH) that appears in the range 2889-2894 cm^{-1}, the ν(CH$_2$) asym, that appears at 2931 cm^{-1} in ACE spectrum is not detected. A broad band of high intensity is verified in the region 2376-2309 cm^{-1}, perhaps from the interaction with the scCO$_2$. The peak corresponding to δ(OH) vibration initially at 1609 cm^{-1} shifts to 1620 cm^{-1} appearing a shoulder at 1613 cm^{-1}. Also, we can observe the saturation bands from H$_2$O, it is interesting to note that the intensity of this peak is decreasing along extraction, indicating that H$_2$O is being removed from the sample. The frequency of 1470 cm^{-1} is the δ(CH$_2$) from EG, its intensity slightly increases along

extraction, and the $\delta(CH_3)$asym from ACE that occurs at 1442 cm^{-1} shifts to 1454 cm^{-1}. The next peak is assigned to the interaction (HO—CH$_{2w}$) (range 1384-1392 cm^{-1}) this occurs in the EG at 1395 cm^{-1} and shifts to 1390 cm^{-1}. Close this peak, the $\delta(CH_3)$sym vibration of ACE shifted from 1351 cm^{-1} to 1343 cm^{-1}. The intensity of that peak is increased along the extraction process, as well. At 1258 cm^{-1} the high intensity peak, that may come from ECH corresponding to the interaction C-Cl. At 1161 cm^{-1} appears a new peak corresponding to the shifting of the vibration of EG occurring at 1174 cm^{-1}. The (CH$_3$) rocking occurring at 1093 cm^{-1} in pure ACE, it is shifted to lower frequency 1078 cm^{-1} approximately, this would suggest some interactions with other molecules able to form HB. The broad of the peak may indicate the existence of other vibrations modes that could arise from the coupling of C–C and C–O vibration modes. Finally, a peak at 951 cm^{-1} appears instead of the 901 assigned to $\delta(CH_3)$ rocking, its intensity increases initially, to keep constant after some time of extraction.

5.3.3 Acetonitrile-scCO$_2$ System

For ACN, the electronegative nitrogen atom makes the carbon atom more positive, and the polar CN group has an electron-attracting effect on the adjacent bond.
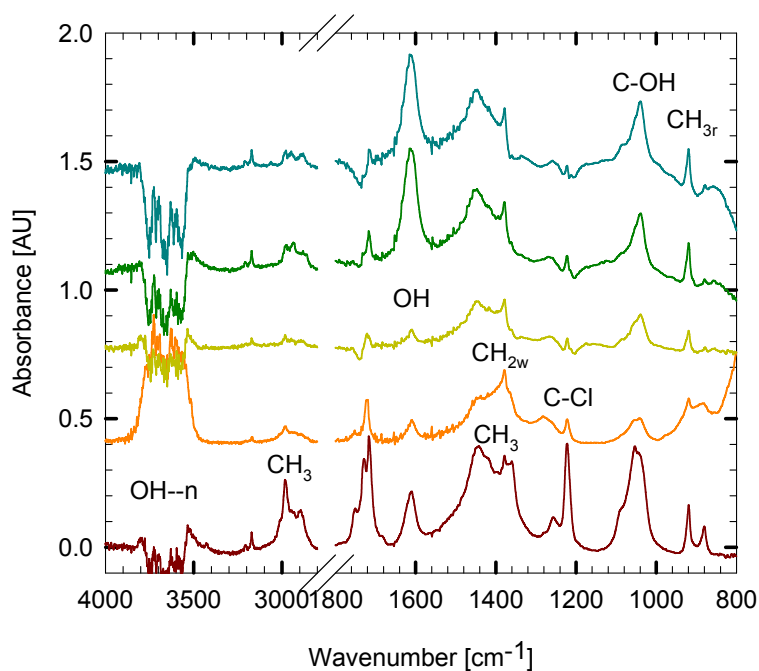
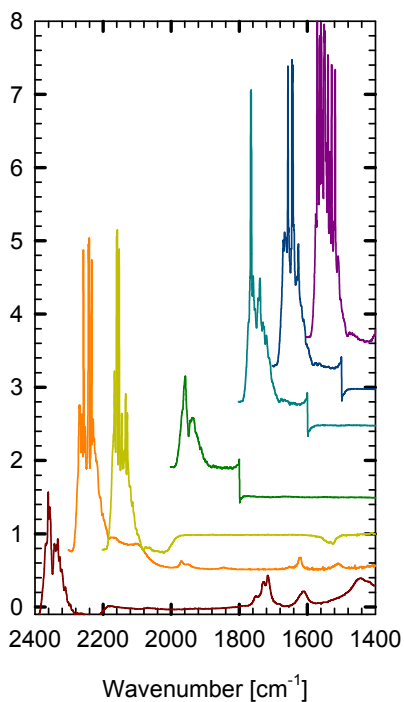Figure 5-9: HES treated with acetonitrile-scCO$_2$ (200 bar, 40°C).

Figure 5-10: Nitriles region

The spectrum of the extraction process using ACN can be seen in Figure 5-9. We can observe the $\nu(CH_3)$asym vibration at 2983 cm^{-1}. The $\delta(OH)$ vibration mode shift from 1609 cm^{-1} to 1615 cm^{-1} along extraction. The peak at 1222 cm^{-1} is assigned to C–Cl, and at 919 cm^{-1} corresponding to the interaction of the (CH$_2$—OH). The peak at 1055 cm^{-1} in pure ACN is shifted to 1039 cm^{-1} approximately in the extraction process. In the region 2400-2300 cm^{-1} the peaks are intensified, demonstrating variation along the extraction (Figure 5-10).

The results of the extraction of EG and ECH

using the co-solvents are summarized in Table 5-6 and the comparison of them can be seen in Figure 5-11.

Table 5-6: Results of extraction of EG and ECH with cosolvents (HES lot 1)

Acetone-scCO$_2$			
	Composition [mg/kg]	Solubility [mol/mol scCO$_2$-kg]	Extraction [%]
Ethylene Glycol	14658.80	0.2079	65
2-Chloroethanol	25.0	1.69E-05	10
Ethanol-scCO$_2$			
Ethylene Glycol	6187.99	0.1189	85
2-Chloroethanol	13.30	-----	-----
Acetonitrile-scCO$_2$			
Ethylene Glycol	5486.35	0.1199	87
2-Chloroethanol	13.30	-----	--------

Similar results were obtained for EtOH and ACN. The ECH was removed until limit detection, perhaps it is attributed to the polarity of ACN and EtOH, and the capacity to form HB between the OH—Cl.

Comparison among the FTIR spectrums of the cosolvent-scCO$_2$ systems are depicted in Figure 5-12. There are not differences in the frequencies of the asym $\nu(CH_3)$ and the (CH) vibrations which occur at

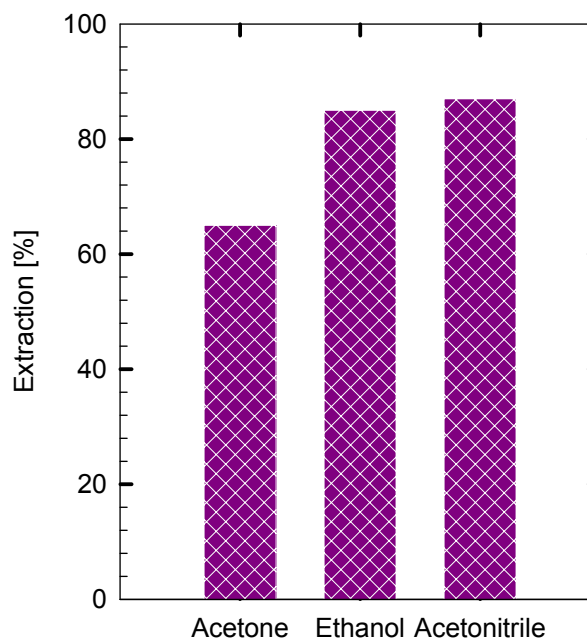Figure 5-11: Percentage of extraction.

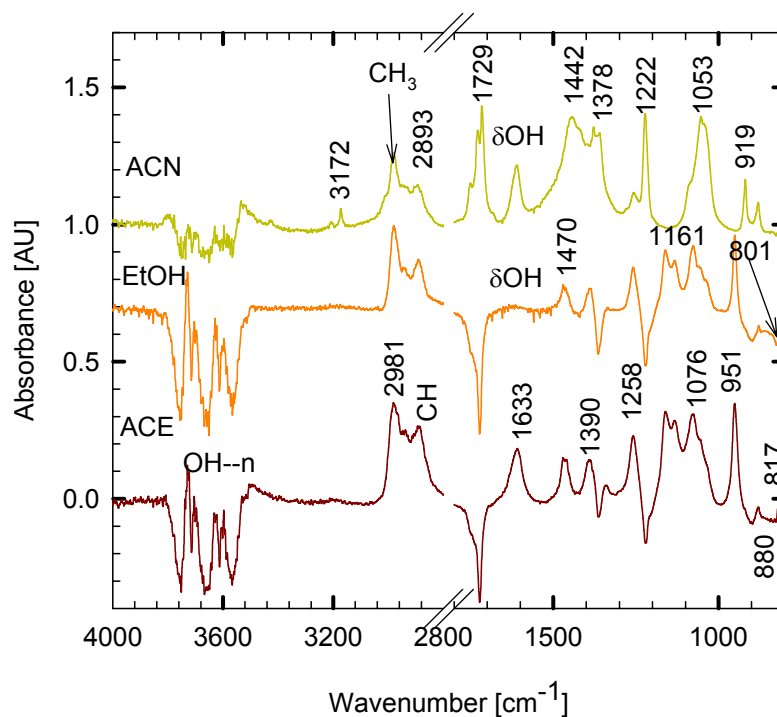2980 and 2890 cm^{-1}. In ACE the $\Delta v(CH_3)$ asym is 10, in ACN is 3, but in EtOH is only -4.

Figure 5-12: IR spectrum of EG and ECH extraction with scCO$_2$ and cosolvents.

In pure ACE the asym $v(CH_2)$ vibration appears at 2930 cm^{-1}, while in the spectrum from the extraction, instead of this vibration appears one at 2893 cm^{-1} corresponding to the CH vibration. It seems that one of the two free H of the methylene group is being attach, perhaps there is an intermolecular interaction with other molecules. If it is through a HB interaction this could be an oxygen atom from the OH or an electronegative molecule. The $v(CH_2)$ frequency for pure ACN-scCO$_2$ and ACN-scCO$_2$ in extraction is the same (2893 cm^{-1}). Surprisingly, the typical (C=O) vibration occurring at 1710 cm^{-1} in ACE is not detected in ACE-scCO$_2$ system when extraction is performed. This is because of the overlap of the peak occurring at this frequency coming from the impurity encountered in scCO$_2$ (see Appendix H) or the disappearance of monomeric ketone.

The vibration corresponding to $\delta(OH)$ does not undergo great variations, only for ACN ($\Delta\delta$=-5), the others remain the same. However, in the EtOH-scCO$_2$ system there is evidence of saturation bands denoting the existence of the hydroxyl group in different environments. At 1470 cm^{-1} the $\delta(CH_3)$ overlapped with $\delta(CH_2)$ vibration suggesting the it may come from EG that shifts from 1461 cm^{-1}. In pure EtOH-scCO$_2$ it occurs at 1452 cm^{-1}, and the $\Delta\nu$ is because of the presence of a rich HB environment (e.g., EG, H$_2$O, and ECH) that hindrance of the bending mode of the structure. The same occurs with the ACE-scCO$_2$ system, while the ACN-scCO$_2$ system shows a new peak at 1442 cm^{-1} that can be assigned to the vibration N≡C–CH$_2$. The evidence of this peak during extraction can be attributed to the interaction of a methyl group's hydrogen of the ACN with an electronegative molecule generating a HB interaction.

The region at 1374–1350 cm^{-1} that appears in pure ACE-scCO$_2$ corresponding to C–CH$_3$ shifts to 1390 cm^{-1} frequency. Perhaps, it is because of the dilution of the ACE in the supercritical phase, besides it is more intense due to the closeness to the carbonyl group. This vibration is sensitive to the electronegativity of the attached atom. In EtOH there is not variation of this vibration, however in ACN this vibration shifts to lower frequency approximately 1378 cm^{-1}, maybe because of the interaction with an electronegative atom. The three system shows a peak at 1257 cm^{-1} correspond to the CH$_{2w}$, only in ACN it appears as a shoulder that is overlapped with the intensity at 1222 cm^{-1} that come form Cl-CH$_2$.

As well as ACE-scCO$_2$ system, EtOH-scCO$_2$ system shows a peak at 1161 cm^{-1}, and a peak around 1132 cm^{-1}. For the ACN-scCO$_2$ system and the pure ACN-scCO$_2$, the peak at 1055 cm^{-1} remains invariable, but for the others the shift occurs in the opposite way. In ACE-scCO$_2$ system the frequency at 1093 cm^{-1} shift to lower frequency (1076 cm^{-1}). It frequency, assigned to interaction C-C, may be because of the rich HB environment that affects the carbon skeleton, provokes the bending vibration. Meanwhile in EtOH-scCO$_2$ system the shift occurs from 1053 to 1076 cm^{-1}, and in this system the environment could has a hindrance of the bending mode. In pure ACE-scCO$_2$ system the peak at 900 cm^{-1}

corresponding to (CH_{3r}) shifts to higher frequency 951 cm^{-1}. Meanwhile in EtOH-scCO$_2$ system remains invariable, and in ACN-scCO$_2$ system only a shoulder appears in this region. Only in ACN-scCO$_2$ system a peak at 919 cm^{-1} is detected. Finally, there is not change in the peak 880 cm^{-1} for both EtOH and ACN-scCO$_2$ systems.

The removal obtained from the extraction performed with the HES lot 2 is summarized in Table 5-7, and comparison with the results obtained with pure scCO$_2$ system can be seen in Figure 5-13. Two isotherms were obtained at 200 bar of pressure.

Table 5-7: Results of extraction of EG with cosolvents (HES lot 2)

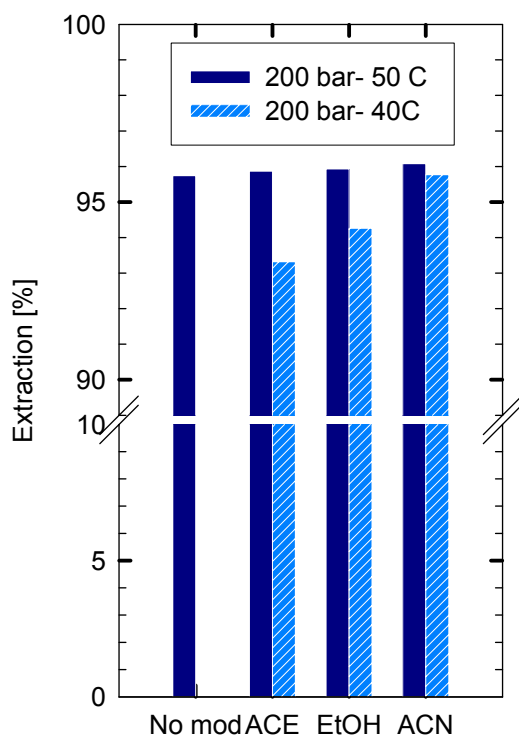|	EG [mg/kg]	Extraction [%]	Mw [Da]
200 bar – 50°C			
No modifier	33.61	95.74	199400
Acetone	32.54	95.87	200500
Ethanol	32.1	95.93	199700
Acetonitrile	30.89	96.08	198600
200 bar – 40°C			
Acetone	52.7	93.32	199100
Ethanol	45.24	94.26	197900
Acetonitrile	33.39	95.77	200200

Figure 5-13: Percentage of extraction (HES lot 2).

As we can observe there are not great differences among the cosolvents used in the extraction process. The higher percentage of extraction is when ACN is used at 200 bar and 50°C. One important characteristic of this lot is the low humidity of the polymer.

5.4 Removal of EG and ECH with scCO$_2$ and Surfactants

Pluronic surfactants (e.g., PL31 and P17R2), Gele and Zonyl, already widely described in chapter 2 have been used to extract EG and ECH from the HES polymer. The process intents to trap those polar molecules in the inner core of the aggregates formed in the scCO$_2$ media.

5.4.1 Pluronic-scCO$_2$ System

The IR spectrums of pluronic surfactants in the extraction process (e.g., PL31 and P17R2) are depicted in Figure 5-14 and Figure 5-15. There are not great differences in the IR spectrums. We can see that the vibration modes in the region 2300-2200 cm^{-1} are intensified when P17R2 is used rather than PL31. Both surfactants present broaden bands in the region 3400-3500 cm^{-1} corresponding to the existence of ν(OH), and therefore denoting the presence of intermolecular bonded OH.
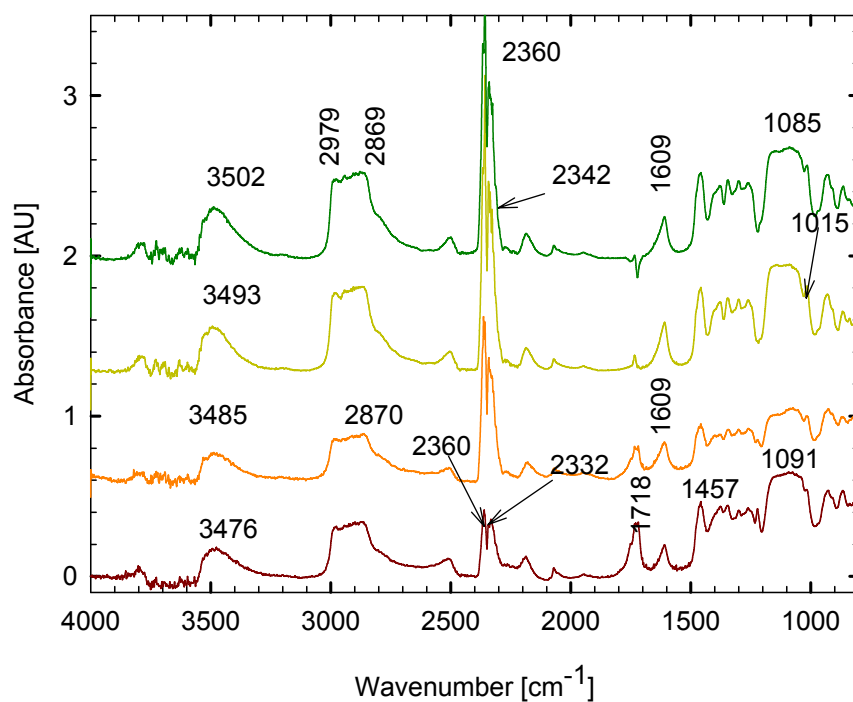
Figure 5-14: PL31-scCO$_2$ (200 bar, 40°C).
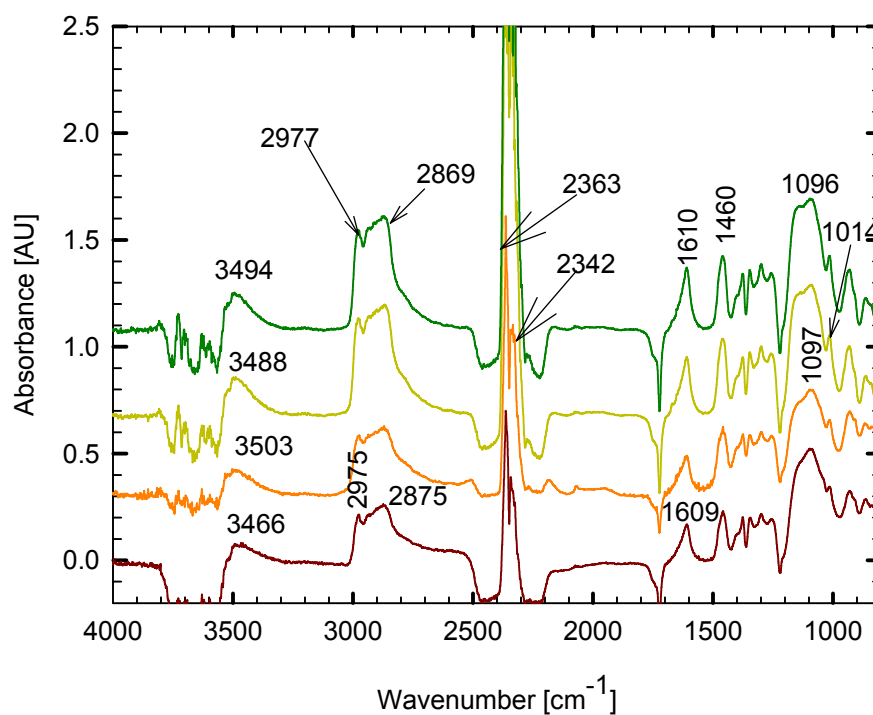
Figure 5-15: P17R2-scCO$_2$ (200 bar, 40°C).
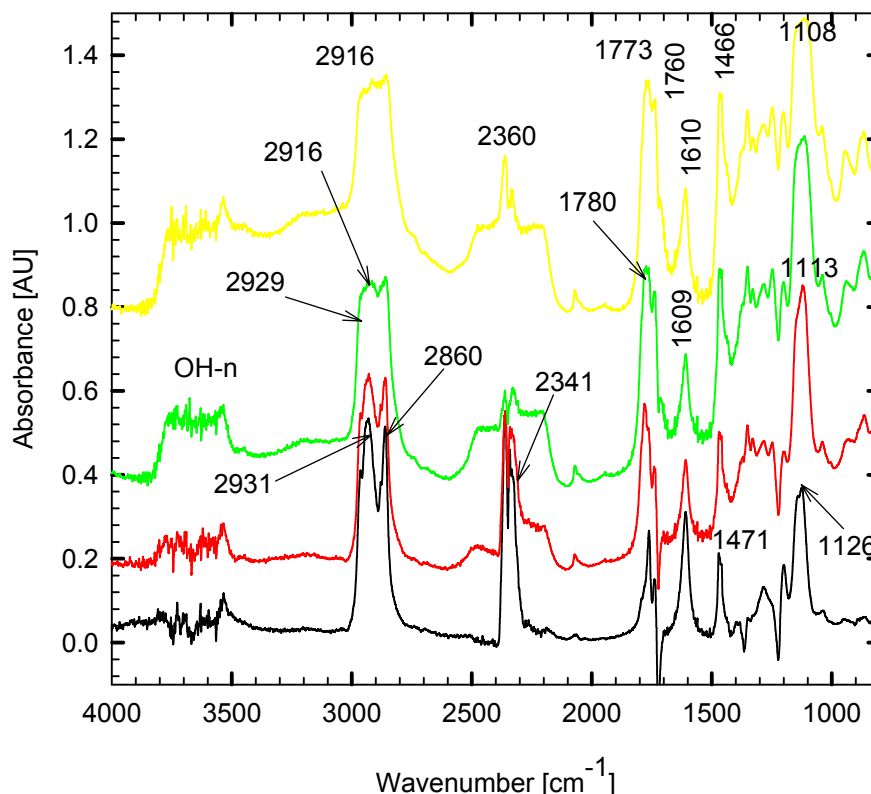
5.4.2 Gele-scCO₂ System

Figure 5-16: Removal with Gele-scCO₂ (200 bar, 40°C).

In the IR spectrum of Gele surfactant there are variations along extraction in some vibration modes, as can be seen in Figure 5-16. Shift of the $\nu(CH_3)$ asym from 2930 to 2916 cm^{-1}, the increase in intensity of the vibration $\nu(CH_2)$ asym at 2860 cm^{-1}. The peak at 1126 cm^{-1} shifts to 1108 cm^{-1} and broaden of the peak along extraction. There is a variation at the vibration C=O, from 1762 to 1773 cm^{-1}, also the appearance of shoulders at lower frequencies, denotes the interaction with other molecules or the formation of dimers. According the IR spectrum of Gele (chapter 4 section 4.4.2), the C=O peak is detected at 1780 cm^{-1}, with a shoulder at 1740 cm^{-1}. In the first spectrum shown in Figure 5-16, there is a peak at 1763 cm^{-1} and a shoulder at 1740 cm^{-1}. This shift $\Delta\nu$ equal 17 cm^{-1} could indicate the existence of formation of HB with some other species. According to

Yamamoto et al. (19), a shift equal to 23 cm^{-1} was detected in the system acetic acid monomer-EtOH-scCO$_2$, this peak was dependent on the EtOH concentration. In Figure 5-17, we can observe that the peak at 1763 cm^{-1} increases throughout the extraction, to finally overlap with the peak at 1780 cm^{-1}. This could be because of the presence of EG that initially is at high concentration generating the vibration at 1763 cm^{-1}, and as long as EG is being removed the monomer configuration is favored. Obviously the dimerization of the surfactant occurs through the extraction process, this can be observed through the increase of the peak at 1740 cm^{-1}. The appearance of peaks at lower frequencies suggest us the existence of another species. Those can be linear dimers, based on the behavior of scCO$_2$ to act as a Lewis acid, as well as Lewis base (2) or a dimer interacting with EG (19).
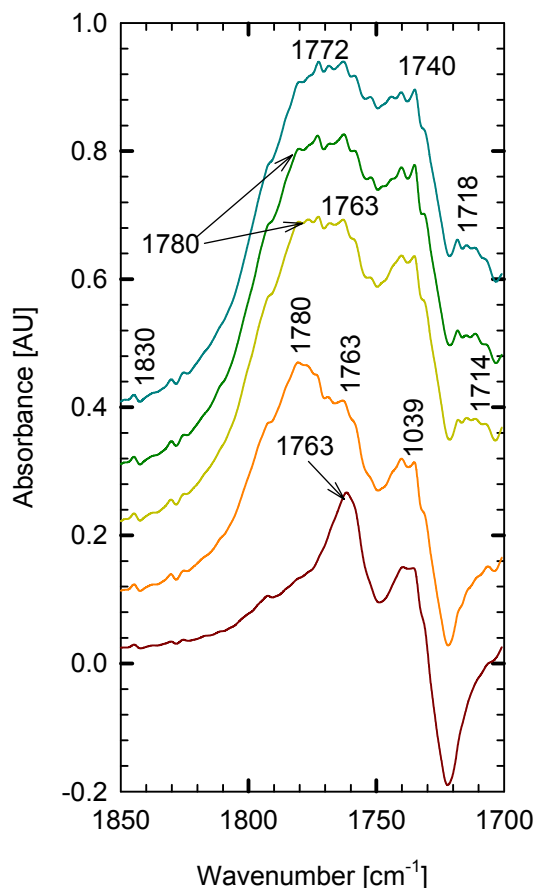

Figure 5-17: Carboxylic region. Gele-scCO$_2$ (200 bar, 40°C).

5.4.3 Zonyl-scCO$_2$ System

The Figure 5-18 shows the IR spectrum when Zonyl is used the principal feature of these spectrum are the presence of a broaden peak from the ν(OH) vibration at 3338 cm^{-1} approximately corresponding to H$_2$O and EG. At 2976 and 2893 cm^{-1} the symmetric and asymmetric ν(CH$_2$). In the region 2200-2400 cm^{-1} a very intense band is attributed to the interaction between stretching of the CO$_2$ and the fluorinated surfactant because of its high electron-donating capacity of the fluoroether functional groups (12). And at lower frequencies the region of C–F vibration modes are identified.
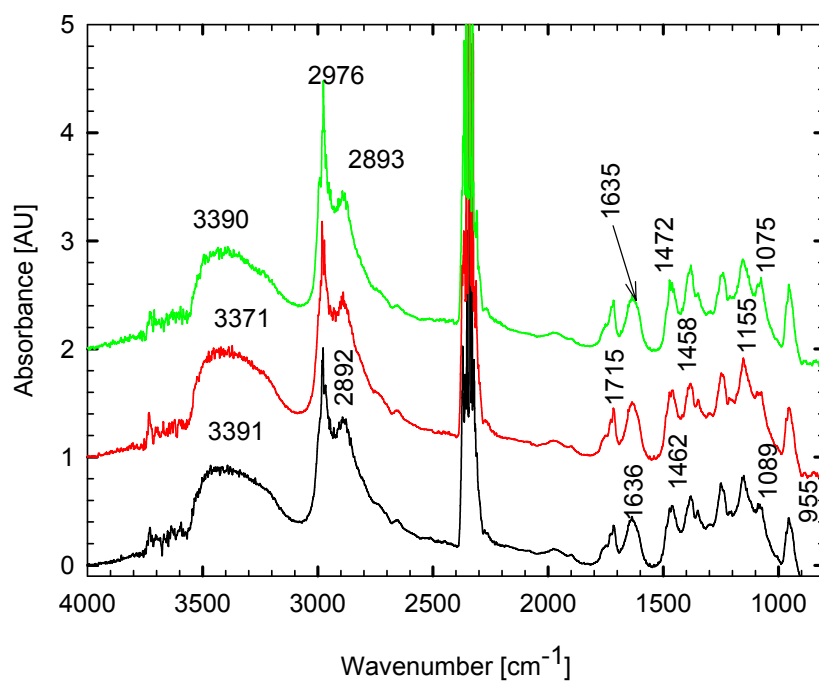
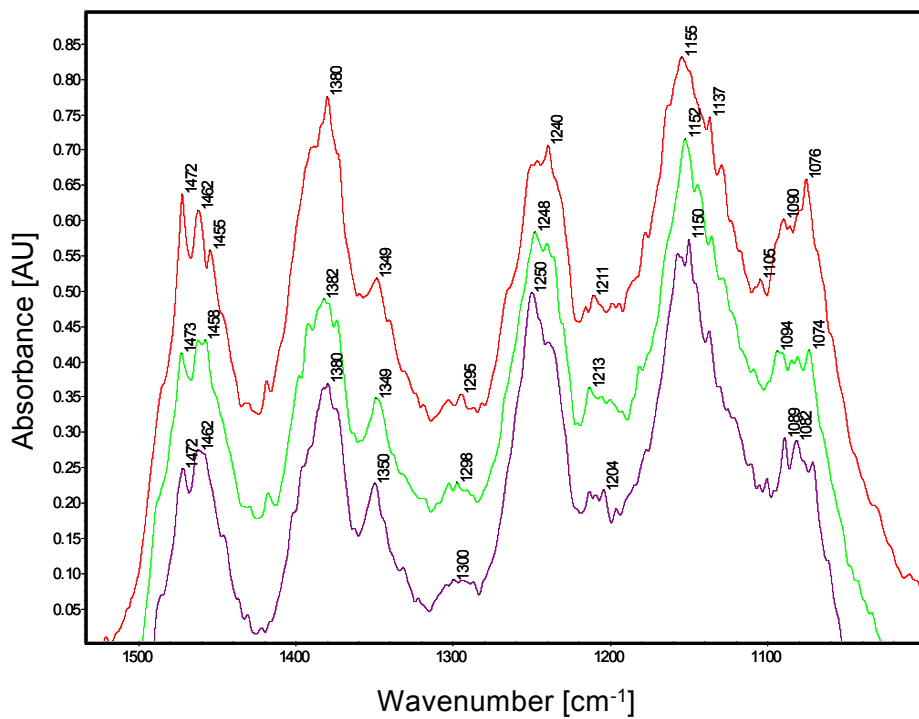Figure 5-18: Zonyl-scCO$_2$ (200 bar, 40°C).

Figure 5-19: Zonyl-scCO$_2$ (1600-800 region) (200 bar, 40°C).

Visible variations in the spectrums can be seen in Figure 5-19 and Figure 5-20. The region corresponding to C-F deformation around 1250 cm^{-1} which undergoes to red shift to 1240 cm^{-1} as extraction is performed, this will also may indicate a changing environment due to the removal of EG, CF$_3$ at 1340-1360 cm^{-1} and the high intensity at around 1000-1100 cm^{-1} that is overlapped with the CF$_2$ vibration. H$_2$O bonded in the system can be seen at 1635 cm^{-1} corresponding to the δ(OH) vibration.
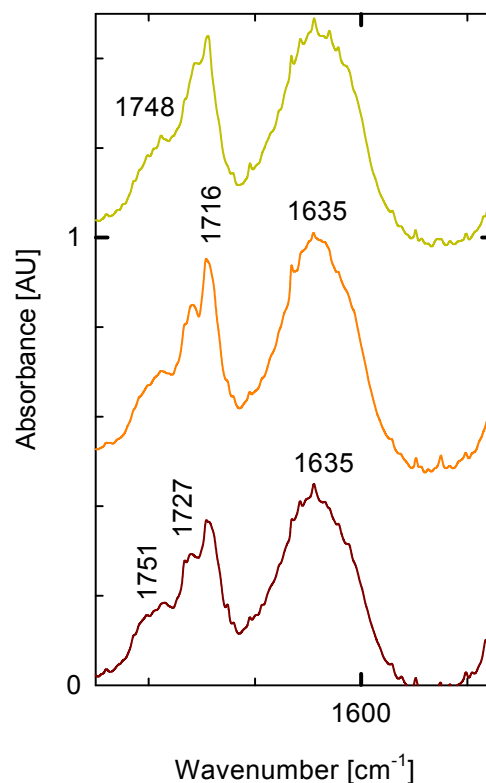
Results show that it was possible to

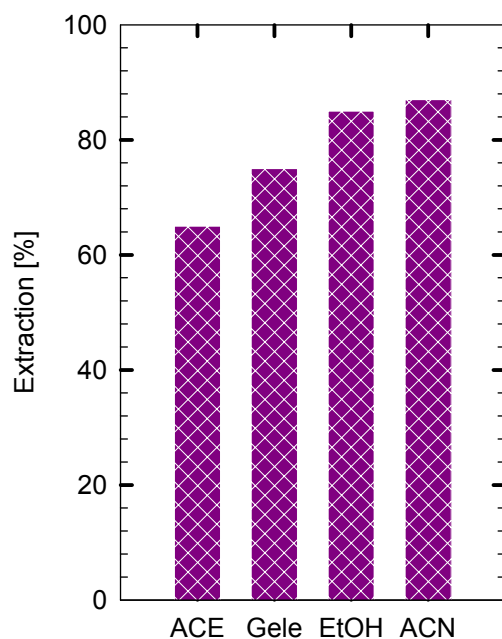

Figure 5-20: Zonyl-scCO$_2$ (1700-1500 cm^{-1} region).

remove EG with Gele surfactant. The concentration of EG was reduced from 42,236 to 10,500 ppm, approximately 75% of extraction. ECH was reduced until detection limit (13.30 ppm), and a molecular weigh of 271000 Da.

In general, comparing the results obtained among the surfactant and the cosolvents used can be observed in Figure 5-21.

Figure 5-21: Extraction with cosolvents and Gele.

The results of the investigation done to BBRAUN PR, lead as to the conclusions that the contents of H_2O in the HES polymer was crucial. That is why the removal of EG with the lot 2 was around 95%. A better extraction was obtained when HES Lot 1 was pretreated (e.g. drying). This main conclusion justified the used of surfactants to be able to trap H_2O.

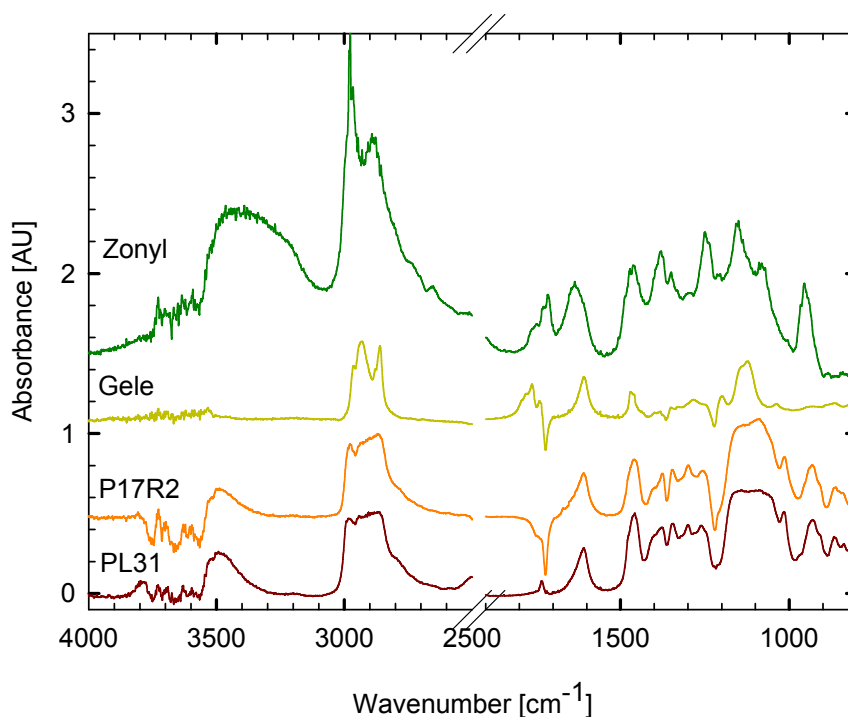In summary the comparison of the four surfactants is depicted in Figure 5-22.

Figure 5-22: IR spectrum of removal with surfactants-scCO$_2$.

As we can observe, the principal difference is at the $\nu(OH)$ vibration. Zonyl surfactant seems to have the major capacity to trap H_2O, followed by the pluronic surfactants and finally Gele that showed little evidence of HB bonding formation. The broaden peak in Zonyl also correspond to the $\nu(OH)$ vibration of EG, thus we can say that it will remove more EG.

References

1. Avram, M.; Mateescu, G.H. Infrared Spectroscopy. Applications in Organic Chemistry. Wiley-Interscience. **1972**

2. Bell, P. W.; Thote, A. J.; Park, Y.; Gupta, R. B.; Roberts, C. B. Strong Lewis Acid-Lewis Base Interactions Between Supercritical Carbon Dioxide and Carboxylic Acids: Effects on Self-association. *Ind. Eng. Chem. Res.* **2003**, 42 (25), 6280-6289.

3. Bulgarevich, D. S.; Sako, T.; Sugeta, T.; Otake, K.; Takebayashi, Y.; Kamizawa, C.; Horikawa, Y.; Kato, M. The Role of General and Hydrogen-Bonding Interactions in the Solvation Processes of Organic Compounds by Supercritical CO_2/n-Alcohol Mixtures. *Ind. Eng. Chem. Res.* **2002**, 41 (9), 2074-2081.

4. Daneshvar, M.; Gulari, E. Supercritical-Fluid Fractionation of Poly(ethylene glycols). *J. Super. Critical Fluids.* **1992**, (5), 143-150.

5. Fulton, J. L.; Yee, G. G.; Smith, R. D. Hydrogen Bonding of Methyl Alcohol-*d* in Supercritical Carbon Dioxide and Supercritical Ethane Solution. *J. Am. Chem. Soc.* **1991**, 113, 8327-8334.

6. Jou, F. Y.; Deshmukh, R. D.; Otto, F. D.; Mather, A. E. Vapor-Liquid Equilibria of H_2S and CO_2 and Ethylene Glycol at Elevated Pressures. *Chem. Eng. Comm.* **1990**, 87, 223-231.

7. Kamlet, M. J.; Abboud, J-L. M.; Abraham, M. H.; Taft, R. W. Linear Solvation Energy Relationships. 23. A Comprehensive Collection of the Solvatochromic Parameters, π*, α, and β, and Some Methods for Simplifying the Generalized Solvatochromic Equation. *J. Org. Chem.* **1983**, 48, 2877-2887.

8. Kazarian, S. G.; Vincent, M. F.; Bright, F. V.; Liotta, C. L.; Eckert, C. A. Specific Intermolecular Interaction of Carbon Dioxide with Polymers. *J. Am. Chem. Soc.* **1996**, 118, 1729-1736.

9. Liu, J.; Han, B.; Zhang, J.; Li, G.; Zhang, X.; Wang, J.; Dong, B. Effect of Cosolvent on the Phase Behavior of Non-Fluorous Ls-54 Surfactant in Supercritical CO_2. *Fluid Phase Equilib.* **2003**, 211, 265–271.

10. Loeker, F.; Marr, P. C.; Howdle, S. M. FTIR Analysis of Water in Supercritical Carbon Dioxide Microemulsions Using Monofunctional Perfluoropolyether Surfactants. *Colloids and Surfaces A: Physicochem. Eng. Aspects.* **2003**, 214, 143-150.

11. McFann, G. J.; Johnston, K. P.; Howdle, S. M. Solubilization in Nonionic Reverse Micelles in Carbon Dioxide. *AIChE J.* **1994**, 40 (3), 543-555.

12. Meredith, J. C.; Johnston, K. P.; Seminario, J. M.; Kazarian, S. G.; Eckert, C. A. Quantitative Equilibrium Constants Between CO_2 and Lewis Bases from FTIR Spectroscopy. *J. Phys. Chem.* **1996**, 100, 10837-10848.

13. NIST Webbook; http://www.Webbook.nist.gov/chemistry

14. Prausnitz, J. M.; Lichtenthaler, R. N.; Gomez de Azevedo, E. G. Molecular Thermodynamics of Fluid-Phase Equilibria. Second edition, Prentice-Hall Inc. **1986**.

15. Suleiman, D.; Jara-Morante, E. Removal of Ethylene Glycol from HES with Supercritical Fluid Carbon Dioxide. Technical report, **2003**.

16. Unknown; http://sdvdb.ncms.org/sdvdb.htm

17. Unknown; http://www.usm.maine.edu/~newton/Chy251_253/Lectures/Solvents/Solvents.html

18. Walsh, J. M.; Greenfield, M. L.; Ikonomou, G. D.; Donohue, M. D. An FTIR Spectroscopic Study of Hydrogen Bonding Competition in Entrainer-Cosolvent Mixtures. *Int. J. Thermophysics*. **1990**, 11 (1), 119-131.

19. Yamamoto, M.; Iwai, Y.; Nakajima, T.; Arai, Y. Fourier Transform Infrared Study on Hydrogen Bonding Species of Carboxylic Acids in Supercritical Carbon Dioxide with Ethanol. *J. Phys. Chem.* **1999**, 103 (18), 3525-3529.

20. Yee, G. G.; Fulton, J. L.; Smith, R. D. Fourier Transform Infrared Spectroscopy of Molecular Interactions of Heptafluoro-1-butanol or 1-Butanol in Supercritical Carbon Dioxide and Supercritical Ethane. *J. Phys. Chem*. **1992**, 96 (15), 6172-6181.

CHAPTER 6

Conclusions and Recommendations

6.1 Chapter 3: UV-Vis Spectroscopy Studies

1. *Changing microenvironment*

   The change in π^* suggests that a changing microenvironment is formed when surfactant, H_2O, and $scCO_2$ are mixed. The polarity values for the surfactant-H_2O-$scCO_2$ systems are closer to those of linear hydrocarbons, but have a lower polarizability than expected. This indicates that the indicator is mainly surrounded by CO_2 molecules and that the H_2O molecules that produce micellization are interacting strongly mainly with the EO groups of the surfactant.

2. *Dipolarity/polarizability values of the system is changing*

   The dipolarity of the system for temperature range 30-45°C is summarized in Table 6-1.

   Table 6-1: π^* values of PL92-Indicator system

System	Pressure range [bar]	π^* range
Indicator-$scCO_2$	72–92	(-0.37)–(-0.20)
Indicator- H_2O-$scCO_2$	72–125	(-0.45)–(-0.14)
PL92-Indicator- H_2O-$scCO_2$	71–121	(-0.58)–(-0.07)

   The dipolarity achieved with the surfactants used in the research is summarized in Table 6-2.

Table 6-2: π^* values of surfactants-Indicator systems

System	Pressure range [bar]	π^* range
PL31-Indicator- H_2O-scCO$_2$	83–153	(-0.24)–(-0.02)
P17R2-Indicator- H_2O-scCO$_2$	91–221	(-0.22)–(0.05)
Gele-Indicator- H_2O-scCO$_2$	75–107	(-0.34)–(-0.24)
Zonyl-Indicator- H_2O-scCO$_2$	171–239	(-0.17)–(-0.14)

Specifically, the higher polarizability value was achieved when P17R2 surfactant was used at 323.15 K. Perhaps, due to the PPO-EO-PPO structure that might have more stability and ability to attract H_2O. P17R2 has a central 10 EO groups that can interact with H2O strongly, and also this continuum EO structure would promotes the formation of hydrogen bonding H2O. Conversely, PL31 has only 2 non vicinal terminal EO groups, although it would be more polar by itself, the capacity of interact with H_2O is restricted.

3. *Stability of the systems PL92, PL31 and P17R2*

Among the pluronic surfactants used in this research, PL92 and P17R2 have proven to be the more stable, at the range of pressures studied. Even though the high cloud point pressure of PL92 compared with P17R2, it was possible to form a micro-domain with the former surfactant. PL31 has shown to be more unstable and unable to prevent coagulation of the hydrophilic groups. According to our results, the configuration PPO-EO-PPO (type R) was the more favorable for microemulsion formation because there is not an entropic barrier between the hydrophobic groups and the solvent and constrains related to the curving of the macromolecule's chain. These results are in agreement with what was stated in hydrophilic media, where the micellization was favored by the EO-PPO-EO configuration.

4. *Zonyl and Gele*

These surfactants are very unstable and few measurements were made. The results were worse when acetaminophen and imipramine HCl were used.

5. *Effect of the solute used in the micelle*

Aggregation of pluronic surfactants is very sensitive to additive (e.g., acetaminophen, imipramine HCl, indicator). This is because it might affect the critical micelle concentration/pressure. The performance of the surfactant is different when the drug instead of the indicator is used. Comparing PL31 and P17R2, there is an effect of the molecule used in the experiments and this can be observed in Figure 6-1. The polarities achieved when the indicator is used are lower compared when the drugs are used, and this is for PL31 and P17R2. Although, approximately the same polarities are accounted for PL31 and P17R2, the absorbance is lower for P17R2.
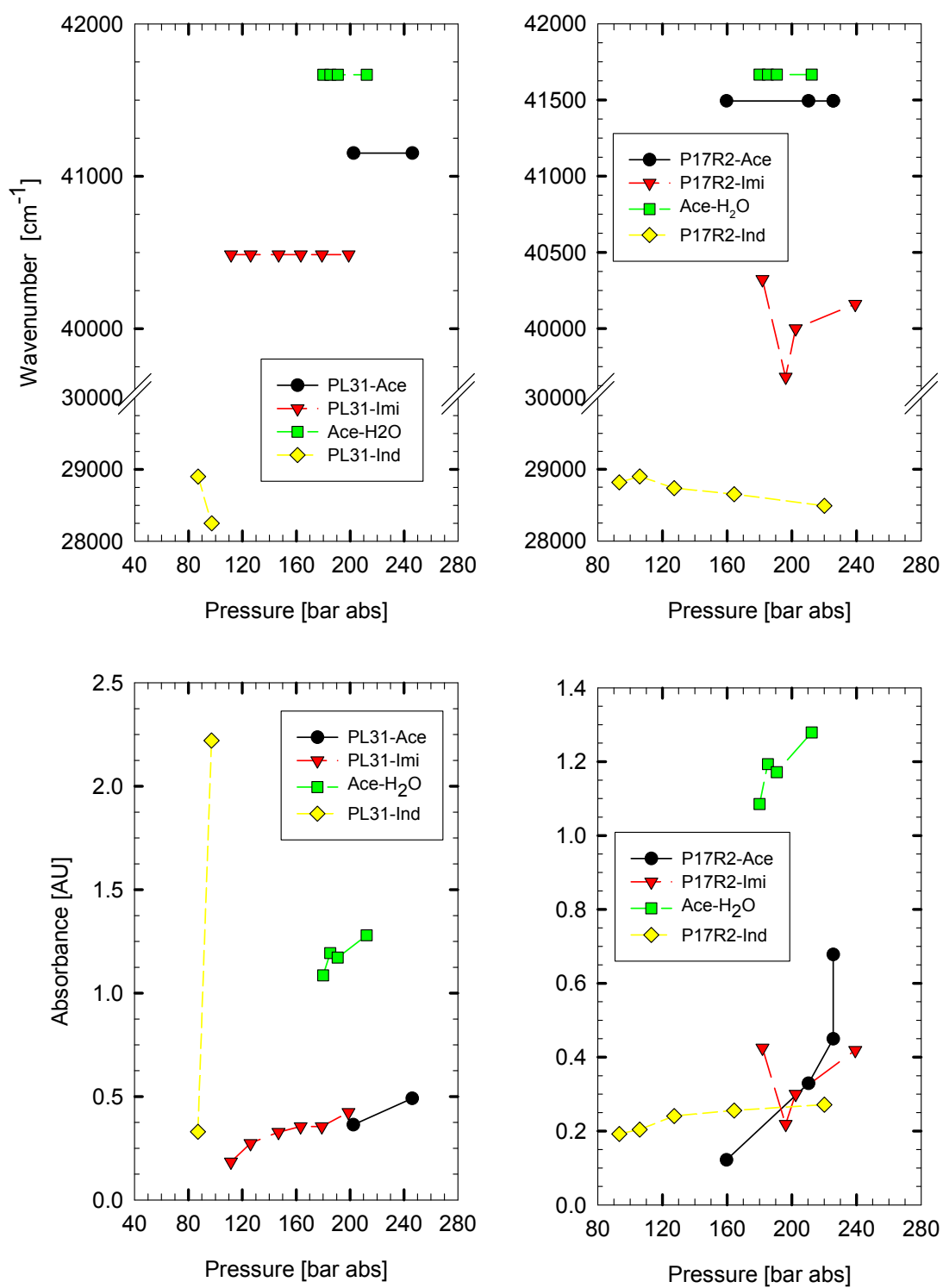
Figure 6-1: (Top) Shift according surfactant, (below) absorbance according surfactant.

The indicator shifts to higher wavelength (red shift) as the polarity of the solvent increases. It seems that the indicator presents a strong interaction with the $scCO_2$ rather than with H_2O molecules; this is also supported by the values of second virial coefficient calculated. In Figure 6-2 we can see that PL31 and PL92 have similar behavior and that the indicator interacts better with them rather than with P17R2.
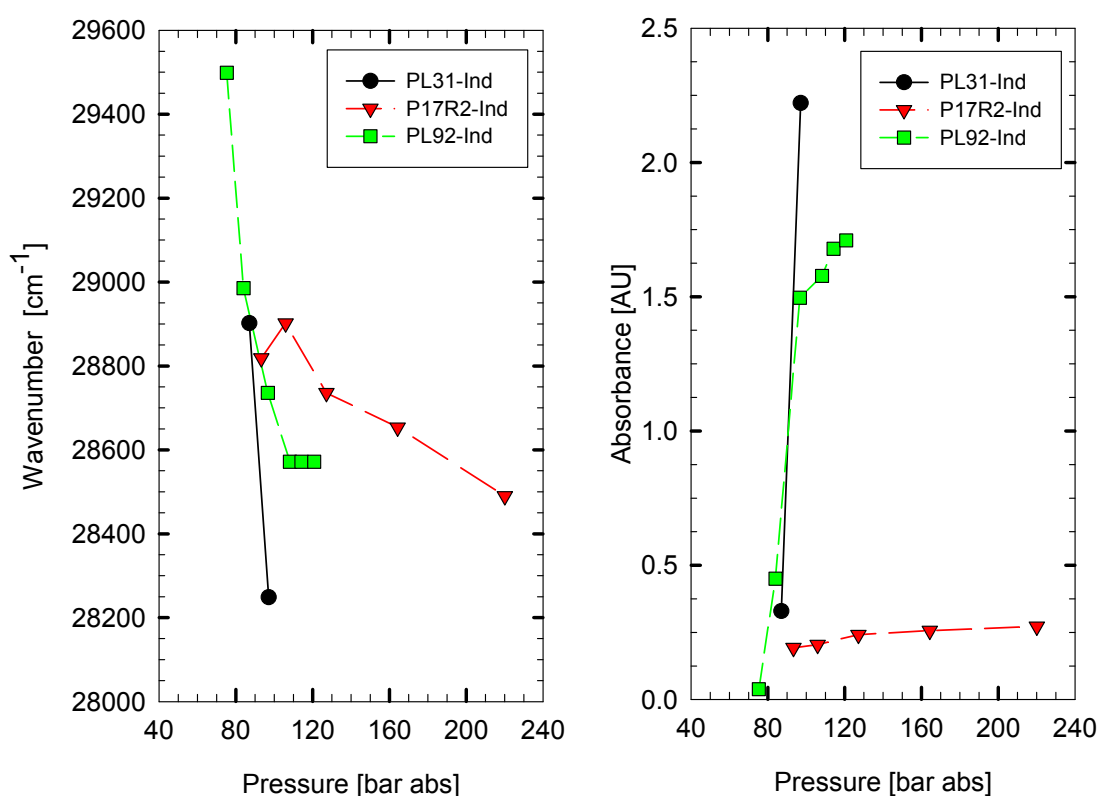

Figure 6-2: Behavior of the indicator with the surfactants.

Both drugs are surrounded by a polar environment, but their behavior is significantly different. Acetaminophen dissolved in a H_2O-$scCO_2$ media (Figure 6-3) presents a higher polarity and also higher absorbance, the addition of the pluronic decreases the polarity, the lowest account for PL31. At the highest pressure, the absorbance was high for P17R2; however, both surfactants produced

the precipitation of the drug from the fluid phase. This could indicate that acetaminophen does not promote aggregation by increasing the repulsive forces among the EO groups. But the configuration of PPO-EO-PPO is preferable to promote micellization.
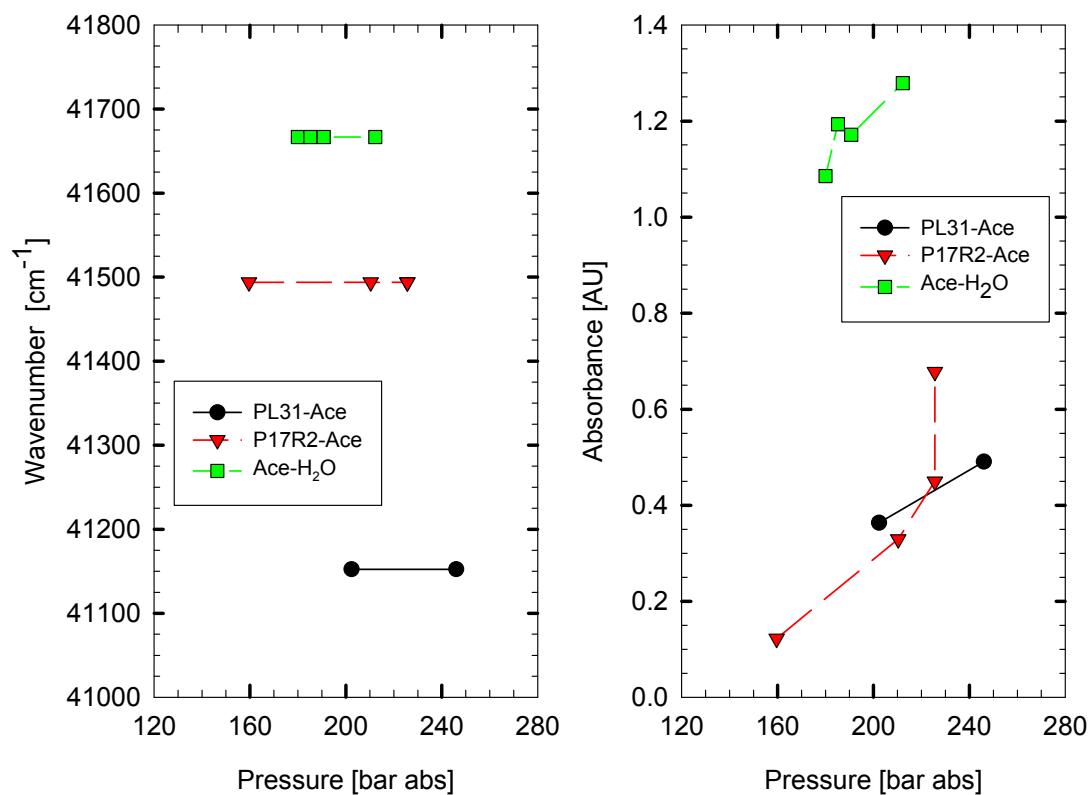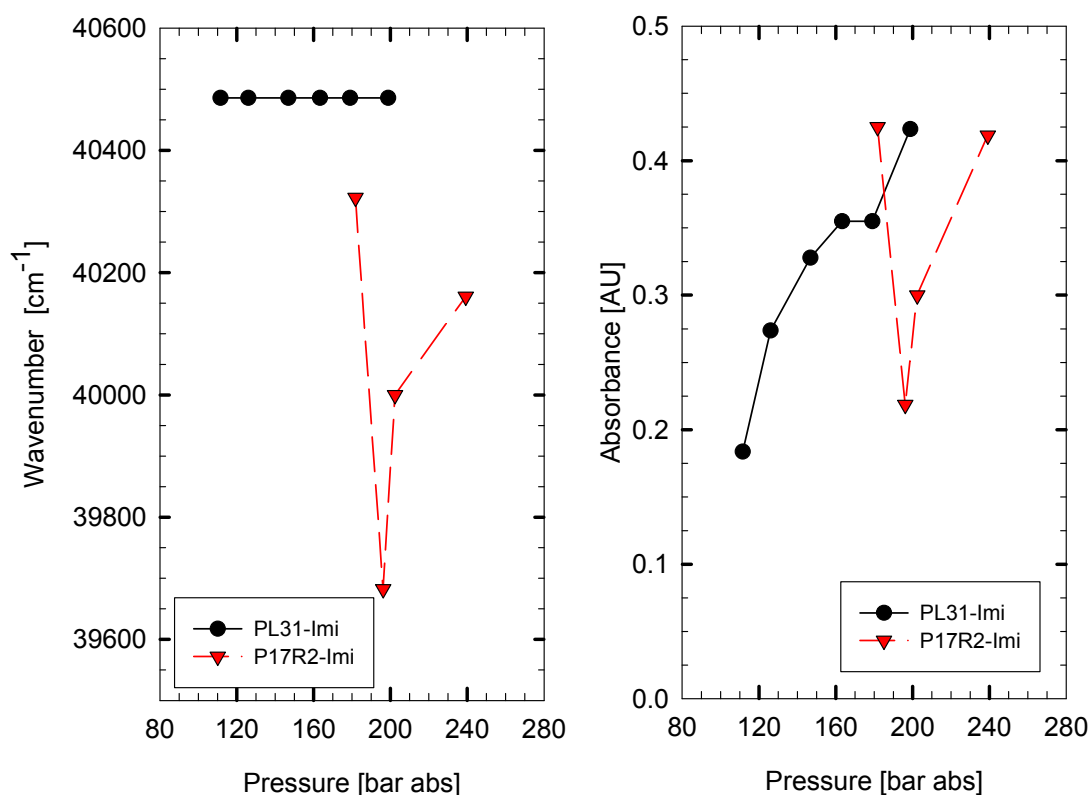

Figure 6-3: Behavior of acetaminophen.

Figure 6-4: Behavior of imipramine HCl.

Acetaminophen showed a blue shift, meaning that it shifts to shorter wavelength as the polarity of the solvents increases. Imipramine HCl did not show any variation representative of a non-changing microenvironment (Figure 6-4). The wavenumber determined in both surfactants resemble an environment closer to water-like surrounding. The absorbance values are also approximately similar, and the system was more stable than with the indicator.

It is known that the core of the microemulsion has a pH approximately near to 3 because of the formation of the ion HCO_3^-. Imipramine HCl is a salt that is ionized when dissolved in H_2O, obviously this will increase the acidic character of the microenvironment, and the effect of this pH value in the microemulsion formation was not determined.

6. *Local density augmentation*

The way in which local solvent density enhancement varies with bulk solvent density is important because it expresses local density inhomogeneities occurring around a solute in supercritical fluids. The existence of the local density enhancement and inhomogenieties in the fluid phase was demonstrated through many analysis methods. According to the results, the three systems described a decreasing trend indicating that the saturation of the solvation shell occurs at low pressures. Since the large value of the ratio ρ_{local}/ρ_{bulk} is located well below the critical density, the local density augmentation was a short range effect. The solute-solvent interactions are of the dipole-induced dipole nature.

7. *Microemulsion formation.*

According to the results, the system where P17R2 and PL92 surfactants were used resembled the formation of a micellar microenvironment.

8. *Conclusions of the technique used*

The UV-Vis spectroscopy demonstrated to be an adequate technique to study the microenvironment formed, around a solute. The indicator or solvatochromic probe used was in a concentration low enough to compromise the phase behavior, this is 1.21×10^{-3} molar percent.

Because the presence of the surfactant provoked the precipitation of the drug (e.g., acetaminophen), this system can be adequate for emulsion-extraction process, where the drug dissolved in an aqueous solution in a polar organic solvent can be separated through the extraction of the solvent and H_2O upon addition of the SCF.

It would be interesting to study surfactants with chains, thus the stability of the system can be improved and also performs studies of flocculation and steric hindrance. Another way to improve the performance of the surfactant it would be interesting to add co-surfactants (e.g., alkyl alcohol, surfactant).

6.2 Chapter 4: FT-IR Spectrocopy Studies

9. *Interactions of the surfactants with the scCO$_2$ and the formation of microemulsions*

The effect of H$_2$O in the formation of microemulsions was determined through the variation in the characteristic peaks corresponding to class of each surfactant.

With pluronic surfactants, there was a variation in the ratio CH$_2$ asym/CH$_3$ sym, deformation of the region around CH$_3$ asymmetric bending vibration or the CH$_2$ scissoring vibration, besides the shift of the peak corresponding to the stretching C–O vibration mode.

The deformation of the bending vibration indicates the increase of the rotational freedom of the molecular group. The C–O shift to shorter wavenumber may be attributed to the interaction of the molecule with rich hydrogen bonding neighboring molecule (e.g., EO).

In the case of Zonyl surfactant, the interactions can be seen in the region corresponding to the CH$_2$ scissoring deformation, and of the out of phase CH$_2$ wagging, as well as in the asymmetric vibration of C–O. In the CH$_2$ scissoring, the H$_2$O provokes a broad band that overlaps the peak corresponding the CH$_2$ wagging. This fact is characterized by the presence of saturation bands. The stretching C–O shift to lower frequencies (red shift) but since this is overlapped with another peak we can not assure that by itself the peak is shifting. The C-O asymmetric vibration in both cases (with acetaminophen and imipramine HCl) shifts to lower frequencies also.

With Gele surfactant, the interactions can be observed in the carboxylic region (1850-1700 cm^{-1}), when the appearance of others peaks with intermediate frequencies (of the monomer and dimer), denotes the hydrogen bonding interaction between the surfactant and the H$_2$O.

10. *Stability of the system*

In the range of our study, pluronic surfactants P17R2 showed to be more stable than PL31, this was concluded after stopping the stirring and observing a stable IR spectrum.

Zonyl is unstable upon heating and H_2O addition, phase separation occurs and also foaming. Even though it is able to trap H_2O the EO groups could not stabilize the formation of microemulsions. The type of drugs studied also affects the performance of the surfactant; it seems to be more unstable when imipramine HCl is used.

Gele was unstable and phase separation occurs after addition of 0.50% of H_2O.

11. *Effect of the drug in the phase equilibria*

It is not clear the effect of the drug in the phase equilibria. Obviously, in cases where an excess of solute was loaded to the cell, a two-phase system was formed, but how much the presence of it increased the cloud point it was not precised.

Acetaminophen and imipramine HCl behave similarly when Gele was used. The qualitative differences would denote that even the surrounding was polar enough to trap the drug there are interactions (eg., surfactant-H_2O, solute-H_2O, surfactant-solute, solute-solute) that promotes or hinder the solubilization of the drugs. Even the presence of CO_2 in the form of HCO_3^- would have some effect.

12. *Effect of H_2O in the micellization*

The independent information about possible components under a broad band in OH stretching region, was obtained. Different states of solubilized H_2O were identified, those are as follow:

-   OH stretch in a hydrogen-bonded polymeric chain, which is placed in the core of the reverse micelle. These molecules should be strongly hydrogen bonded to one another and their absorption appears at the lowest wavenumber.

- Hydrogen bonded dimers which usually bond at the interface. In this state two H_2O molecules can form hydrogen bonds to two vicinal oxygen atoms of the EO chain in such a manner that the two molecules themselves are linked by a hydrogen bond. The OH bond is weak and the absorption appears at a middle wavenumber (Figure 6-5).
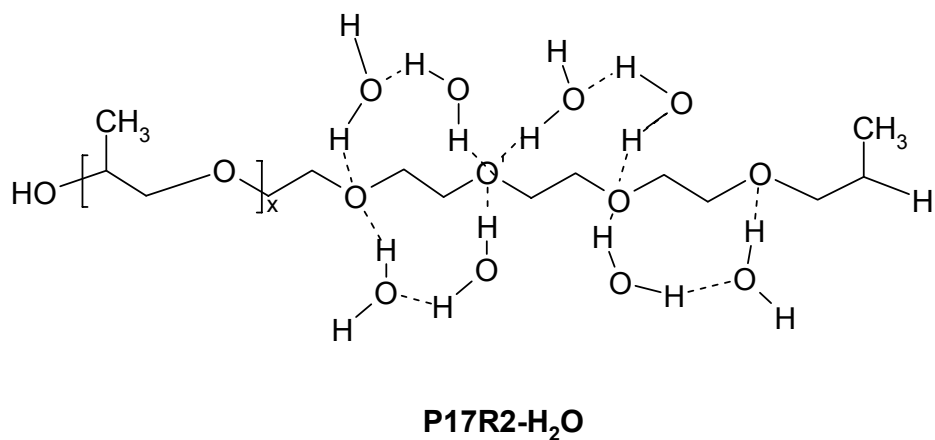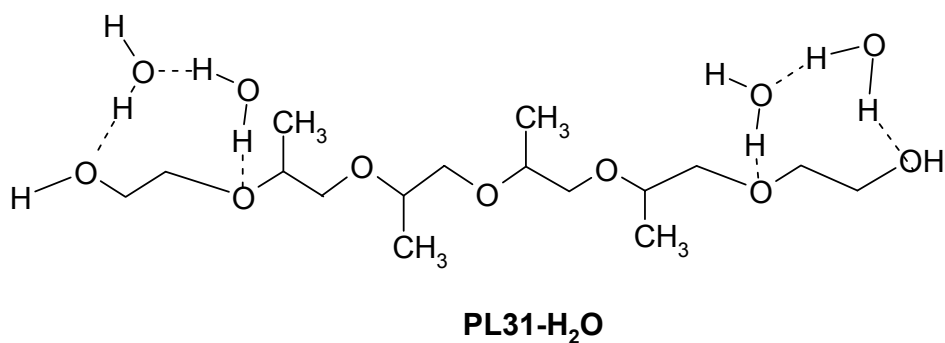
PL31-H$_2$O

P17R2-H$_2$O

Figure 6-5: Hydrogen bond H_2O type interacting with ethylene oxide groups.

- Non-hydrogen bonded H_2O molecules, which has penetrated into the surfactant layer. In this case one H_2O molecule forms hydrogen bond to two vicinal oxygen atoms of the EO chain (Figure 6-6).
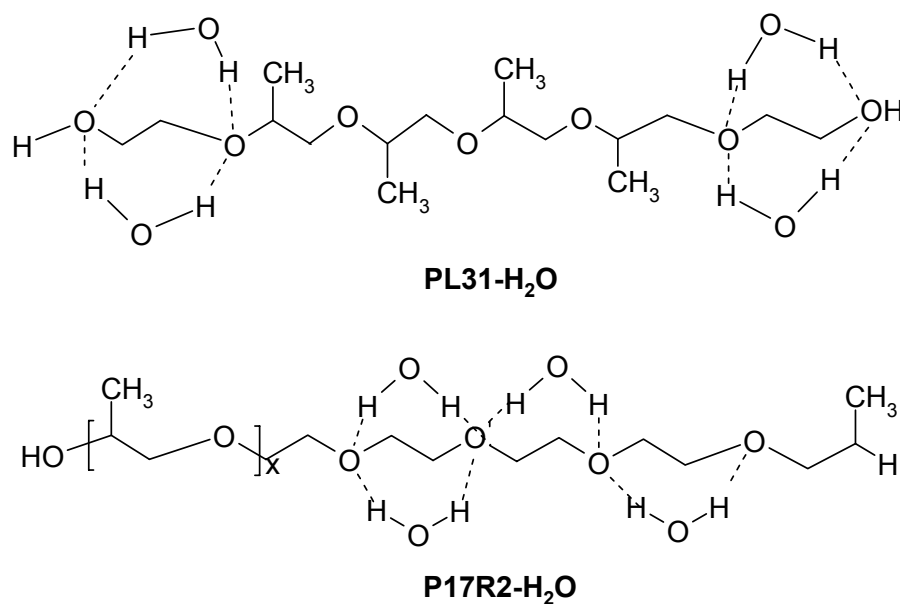
Figure 6-6: Non-hydrogen bonded H_2O interacting with ethylene oxide groups.

- The absorption band at the highest wavenumber is due to H_2O molecules that are trapped between surfactants. These H_2O molecules should behave as monomer-like isolated H_2O analogous to the gas phase spectrum of H_2O.

Using a Gaussian fitting method, the four peaks were found to center at 3245 ± 30, 3474 ± 35, 3588 ± 42, 3737 ± 29 for acetaminophen (Ace)-surfactant systems. The full widths at half height of were 144 ± 3, 70 ± 10, 55 ± 7, and 47 ± 6 respectively. For imipramine HCl-surfactant systems those were found to be 3210 ± 9, 3481 ± 23, 3585 ± 38, and 3725 ± 20. The full widths at half height of were 146 ± 3, 71 ± 9, 55 ± 8, and 52 ± 8, respectively.

The appearance of different hydrogen bonding environments coming from the stretching vibration mode of OH occurs at the compositions summarized in Table 6-3.

Table 6-3: Compositions of Acetaminophen-surfactants systems

System	W_0		Free H_2O	
	Min	Max	Min	Max
PL31-Ace	84.03	485.29	2.33	172.90
P17R2-Ace	168.90	2797.53	4.21	1273.59
Zonyl-Ace		199.92		73.39
Gele-Ace	11.67	29.17	1.17	11.60

For imipramine HCl we find the distribution for free H_2O type to be as follow (Table 6-4):

Table 6-4: Composition of Imipramine HCl-surfactants systems

System	W_0		Free H_2O	
	Min	Max	Min	Max
PL31-Imi	16.81	151.25	6.56	28.58
P17R2-Imi	169.10	338.19	24.18	132.76
Zonyl-Imi	290.28	399.83	31.45	47.25
Gele-Imi	11.67	40.84	3.47	9.92

The dependence of micellization with pressure was also studied, this is dependent on the quantity of H_2O used in the system. Table 6-5 summarizes the results.

Table 6-5: Effect of pressure over imipramine HCl-surfactants systems

System (W_0)	Pressure		Free H_2O	
	Min	Max	Min	Max
PL31-Imi (630)	110	216	16.59	71.91
P17R2-Imi (1194)	106	239	42.50	123.90
Zonyl-Imi (400)	207	224	47.25	88.32
Gele-Imi (195)	109	209	5.64	19.52

As we can see the pressures promotes the formation of different states of H_2O. In our study, the pressure achieved is limited by the windows IR cell. A peak at the

highest wavenumber, which was overlapped by the broad OH stretching region, was found by the deconvolution, and due to its frequency corresponding to amines this peak was assigned to the solute. This denotes the solubilization of the drug in the micro-domain formed and it is verified by detection of Acetaminophen and imipramine HCl in UV-Vis spectroscopy.

13. ***Which one is the best surfactant to form reverse micelles or microemulsions?***

There are many criteria to qualify the surfactants. According to the stability point of view, the P17R2 showed better performance, with the quantity of H_2O trapped in the core. Zonyl was also able to trap H_2O, however it tends to form foam and phase separation. In order to characterized these systems, there has been stated that system with $W_0 < 15$ are referred to as reverse micelles, whereas $W_0 > 15$ indicates larger H_2O droplets and are labeled as microemulsions. In this sense, according to our results, we can assume that Gele was able to form reverse micelles along the range of pressures and concentrations studied.

14. ***Should one monitor the fundamental bending mode of scCO$_2$ at 667 cm^{-1}.*** This peak gives us information about the interaction, but unfortunately this region was hindered to further study because of the windows used in the IR cell. An alternative is to used ZnSe windows that allow us to observe the v_2 spectral region (680-600 cm^{-1}), but this windows holds pressure less than 276 bar that is possible with our ZnS windows.

15. ***The IR spectroscopy studies demonstrated to be complementary to the UV-Vis spectroscopy studies.*** The results obtained reinforced the conclusions got in the previous chapter, about the polarizability and characterization of our micro-domains. Furthermore, the IR technique was able to identified the different environments formed (e.g., states of hydration of H_2O) which characterize the formation of microemulsions or reverse micelles.

6.3 Chapter 5: Extraction of Ethylene Glycol from HES: A practical Study of Supercritical Fluid Processing.

16. scCO$_2$ can remove polar organic compounds like EG and ECG

Pure scCO$_2$ was able to remove polar organic compounds like EG and ECH from the drug HES. Differences in extraction were found between the two lots of HES treated. For HES lot 1, the maximum extraction of 48% (reducing from 42 236 to 21 902 ppm) of EG was achieved at 200 bar and 50°C, in a 3 hours single extraction process. Meanwhile for HES Lot 2 it was about of 96% (reducing from 788 to 31 ppm). Although, the high polarity of EG, it was possible to establishes some intermolecular interaction with CO$_2$. This solubility can be attributed to a quadrupole/dipole interaction between the hydroxyl group and the CO$_2$. Because of the low tendency to accept protons of CO$_2$ the interaction through the carbonyl group of CO$_2$ and the non interacting oxygen of the glycol could occur.
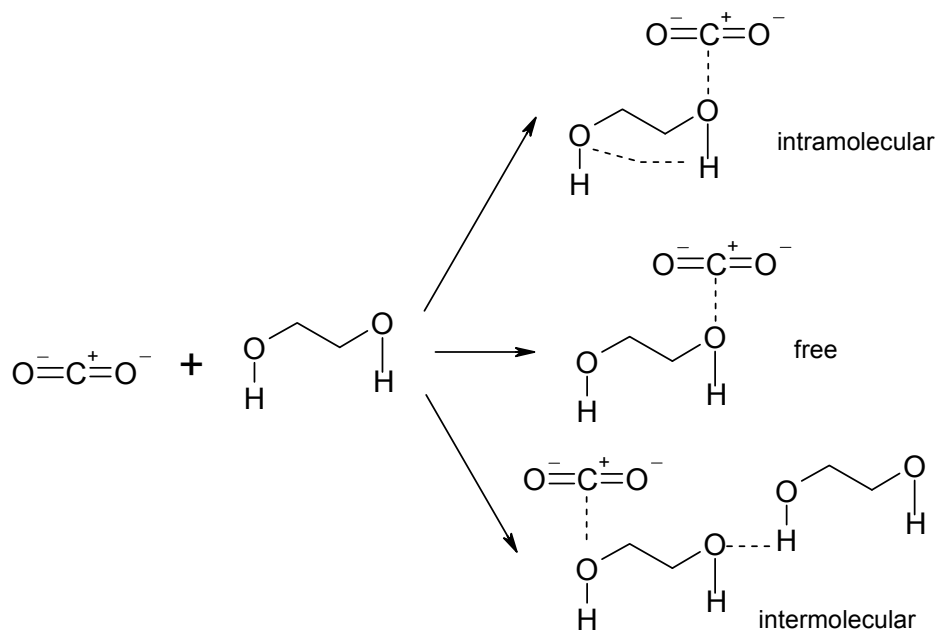
This could be proven if we were able to detect the asymmetric bending vibration (v$_2$) of CO$_2$, which occurs at a frequency 667 cm^{-1}, but we were limited by the IR windows range of transparency.

We can not discharge another mechanism where CO_2 acts as an HB acceptor, even its low capacity to behave like that.
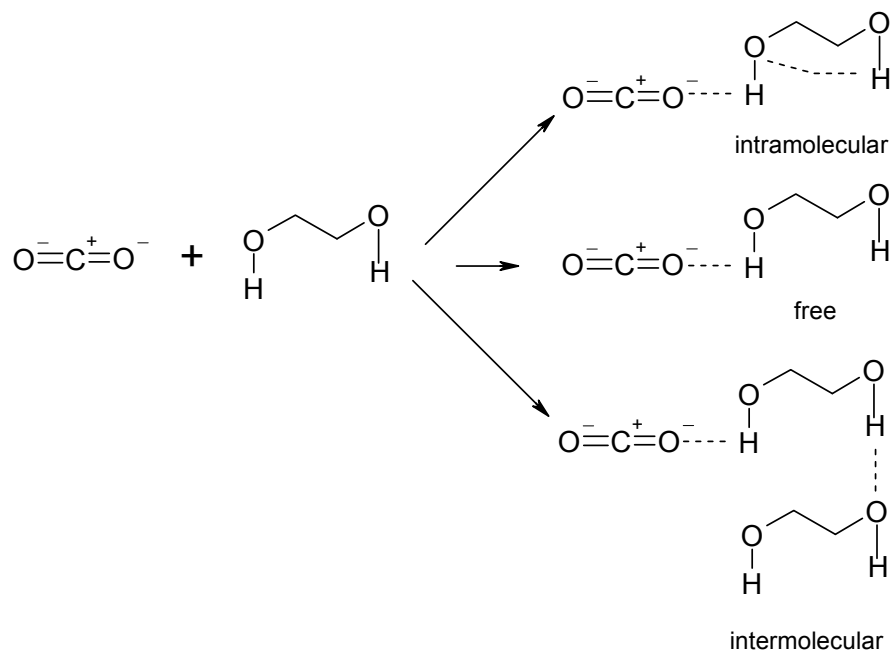
In both cases, the red shift of the frequency should be observed. In the same way the asymmetric stretching vibration of CO_2 is detected in the region 2200-2600 cm^{-1} and it is a broad intense band, where not precise conclusion could be made. Due to the low concentration of EG it was not possible to detect intermolecular bonded EG, thus, the interaction with intramolecular and free EG will be more appealing. Unfortunately these vibration modes are detected in the 3900-3400 cm^{-1} and overlapped with the broad band of scCO$_2$.

17. The presence of H$_2$O in HES

H_2O has an important effect in the extraction of EG. Because of EG has great affinity for H_2O, in a hydrated system the EG will prefer to interact with H_2O rather than CO_2. Thus, a competition between CO_2 and H_2O for EG association will limit the extraction. The extraction is not totally limited, because H_2O is partially soluble in CO_2. This can be observed in the red shift that the $\delta(OH)$

vibration mode (from 1652 to 1609 cm^{-1}) undergoes during extraction of EG upon hydrogen bonding interaction.

In previous works, it was found that when H_2O was removed by drying from the polymer, the extraction of EG with pure $scCO_2$ was about 79% (from 42 236 to 8 757 ppm). In the same way when HES lot 2 was used the extraction was 96% (from 788 to 31 ppm). It is important to point it out that HES lot 2 corresponds to a more treated product (e. g., drier and cleaner).

In any case, the stretching vibration $v(OH)$ was not possible to detect because it was overlapped with the overtone/combination bands of CO_2 in the region 3400-3900 cm^{-1}.

18. *What kind of interactions exists between cosolvents?*

CO_2 has different interactions with each cosolvent used in the present research. EtOH is hydrogen bonding donor as well as hydrogen bonding acceptor. It is obvious that the interaction for EG will be strong, because of its high polarity and infinite dilution in H_2O. The mechanism of interaction could be:

Hydrogen bond acceptor

Hydrogen bond donor
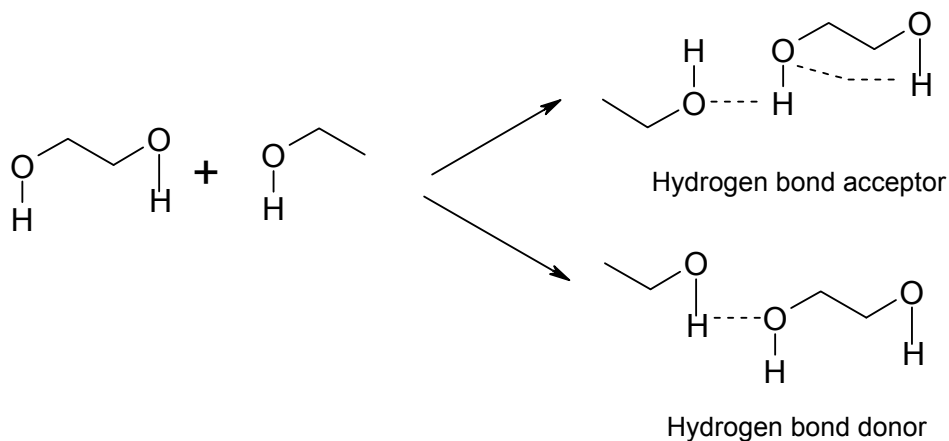
The blue shift of the peak at 1452 cm^{-1} to 1470 cm^{-1} corresponding to the asymmetric $\delta(CH_3)$ vibration overlapped with the $\delta(CH_2)$ scissoring, it could be attributed to the strengthening of electrostatic/dispersion or repulsive contribution due to compression. This also occurs with EG that shift from 1461 to 1470 cm^{-1} in

extraction. The symmetric $\delta(CH_3)$ vibration is slightly affected by the EG as well as the stretching C-O vibration mode that undergoes a blue shift (from 1053 to 1076 cm^{-1}). Because of this shift, we can state that the HB donor is preferred. Obviously, the presence of EtOH favors the solubility of EG increasing to a 85% (from 42 236 to 6 200 ppm) of extraction.

ACE is an aprotic solvent with hydrogen bonding acceptance capacity. The interaction with EG will be through

Hydrogen bond acceptor
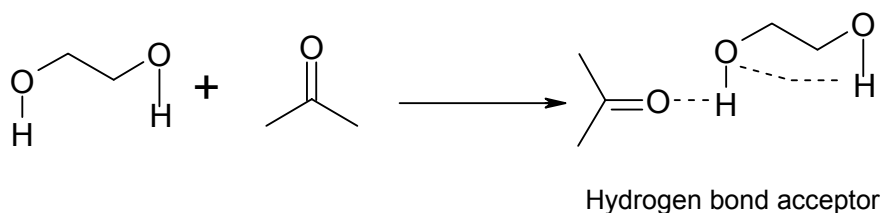
The shape of the region around the asymmetric $\delta(CH_3)$ vibration suggests an enhancement of the rotation freedom of the molecular group. Also, the blue shift is observed decreasing from 1442 to 1470 cm^{-1}. Conversely, to EtOH, the stretching C-O vibration mode undergoes to a red shift from 1093 to 1076 cm^{-1}, this would favor the mechanism stated above. The use of ACE increases the extraction of EG to 65% (from 42 236 to 14 275 ppm).

ACN is a hydrogen bonding acceptor, the interaction with EG could be through the nitrogen and the OH of the glycol.

Hydrogen bond acceptor
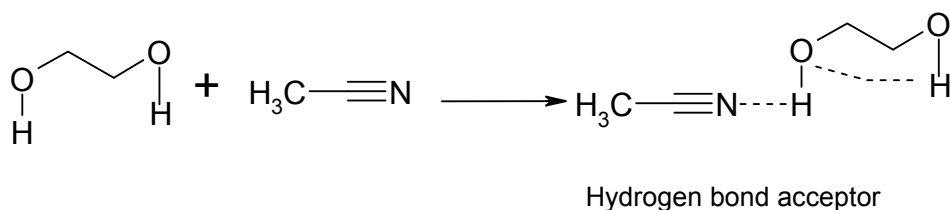
This interaction is detected in the strong intense band in the region 2200-2400 cm-1. We observe the increase in the asymmetric $\delta(CH_3)$ vibration as well as the symmetric $\delta(CH_3)$ vibration that undergoes to red shift from 1393 to 1378 cm-1. Also the shift of the stretching C-C vibration would support this mechanism.

The presence of ACN increases the removal of EG to 87% (from 42 236 to 5 490

ppm).

19. *Which cosolvent is the best?*

Based in the percentage of extraction we range the performance of the cosolvent from best to worst ACN > EtOH > ACE. Which agree with their dielectric constants. This is expected because ACN has a dielectric constant similar to EG (37 at 68°F). We can not separate the effect of H_2O from EG itself.

When HES lot 2 is treated, there is not difference in extraction for any of the cosolvents used. The extraction is comparable to the extraction with pure $scCO_2$.

20. *What kind of interaction exists between $scCO_2$ and the surfactants?*

The interactions between $scCO_2$ and the surfactants were studied in chapter 4. We mainly focused on the capacity of the surfactant to trap the organic compounds in the core on the microemulsion. This was verified in the stretching $\nu(OH)$ vibration of the glycol.

21. *Which surfactant is the best?*

According to the results we can see that the zonyl has the major ability to trap organic compounds.

22. *Which SCF system (cosolvent, surfactant-$scCO_2$) is the best?*

The surfactant approach seems to be adequate for the extraction of EG, or to system were the ppm-level concentration does not compromise the phase behavior of the system.
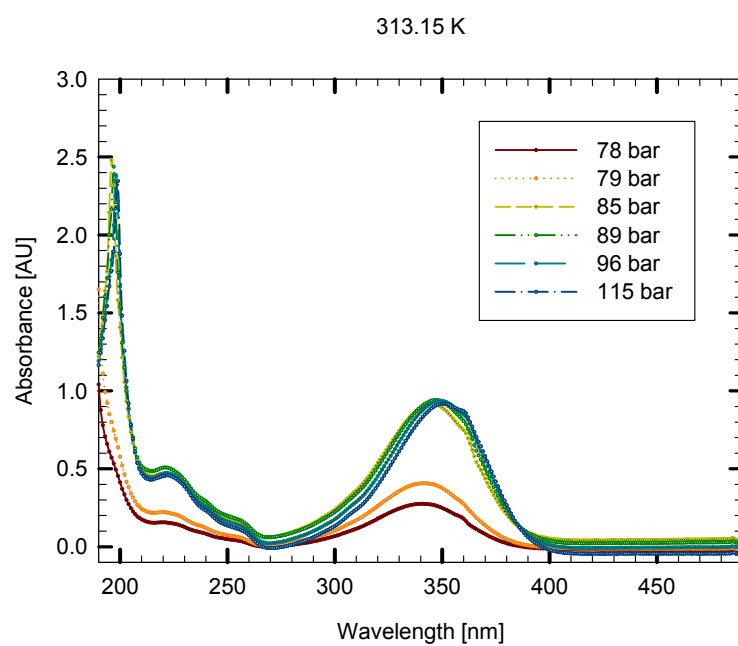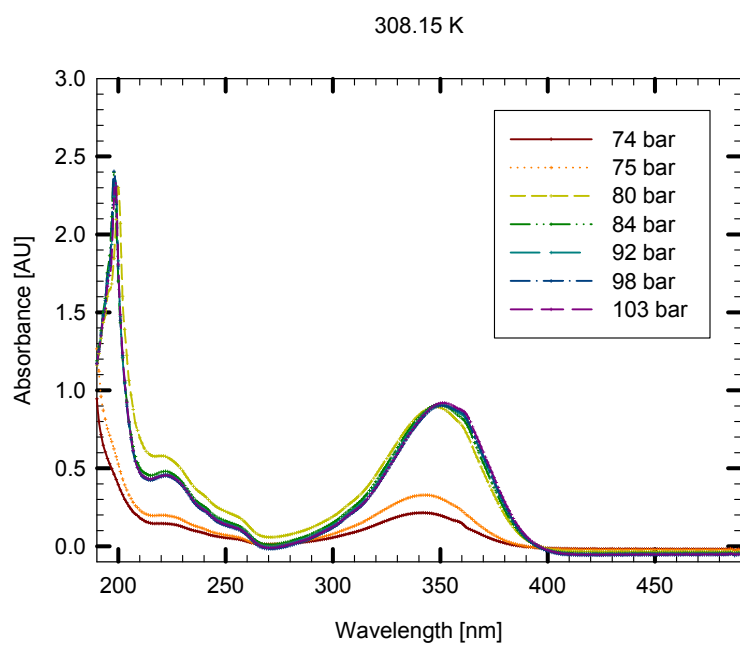
Appendix A

Indicator-scCO$_2$ System at 308.15, 313.15, and 318.15
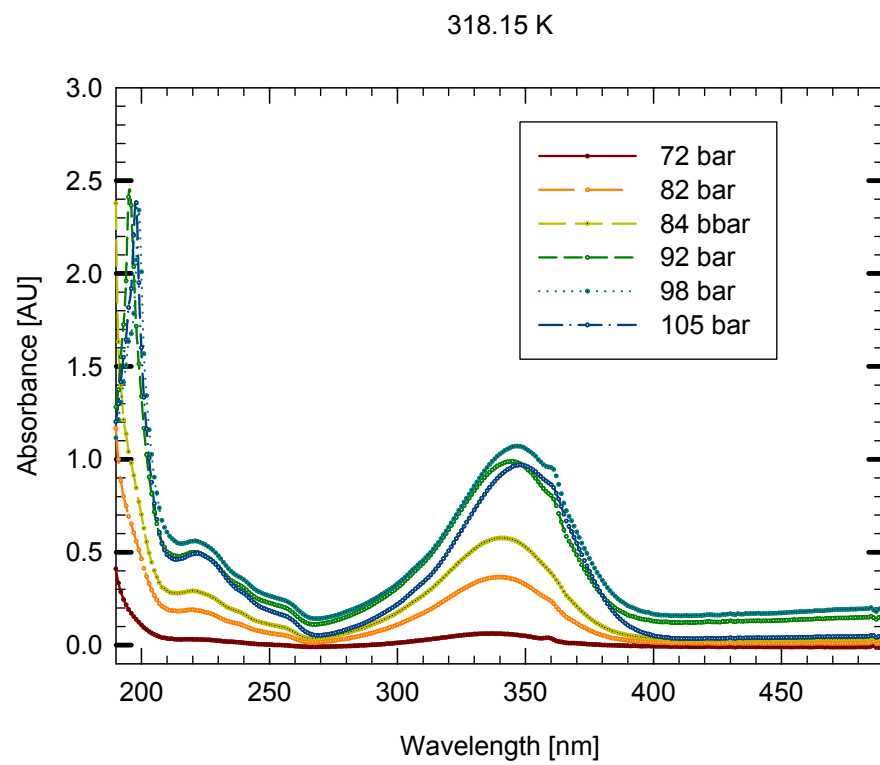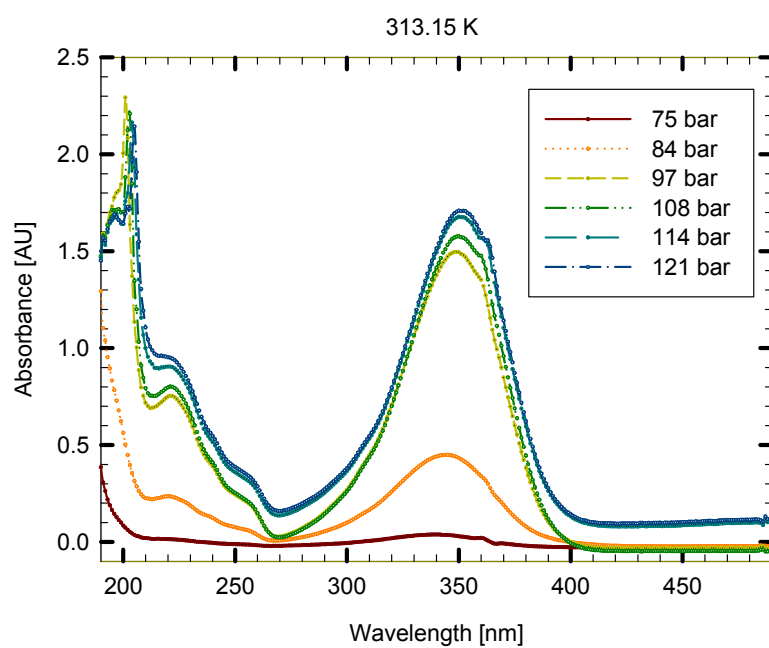
308.15 K
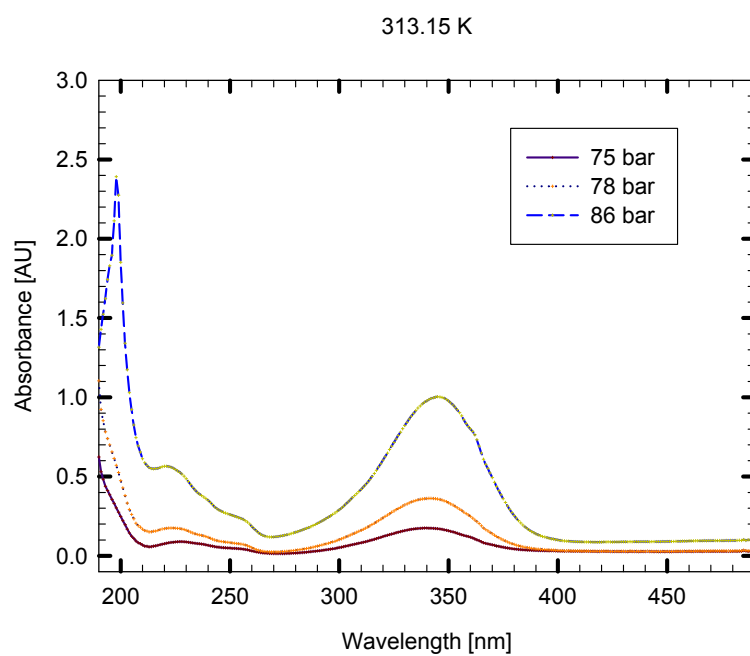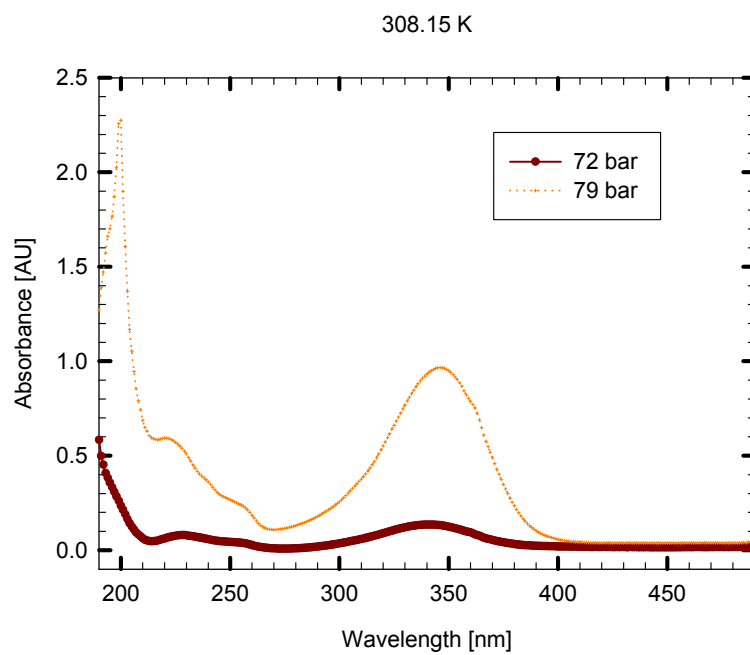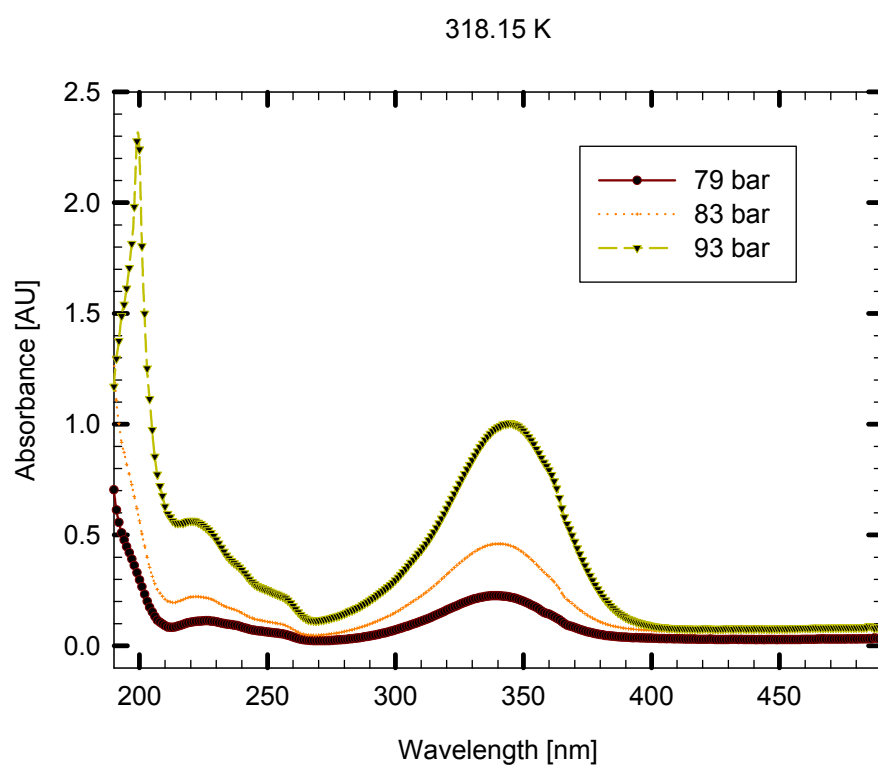
313.15 K

318.15 K

Appendix B

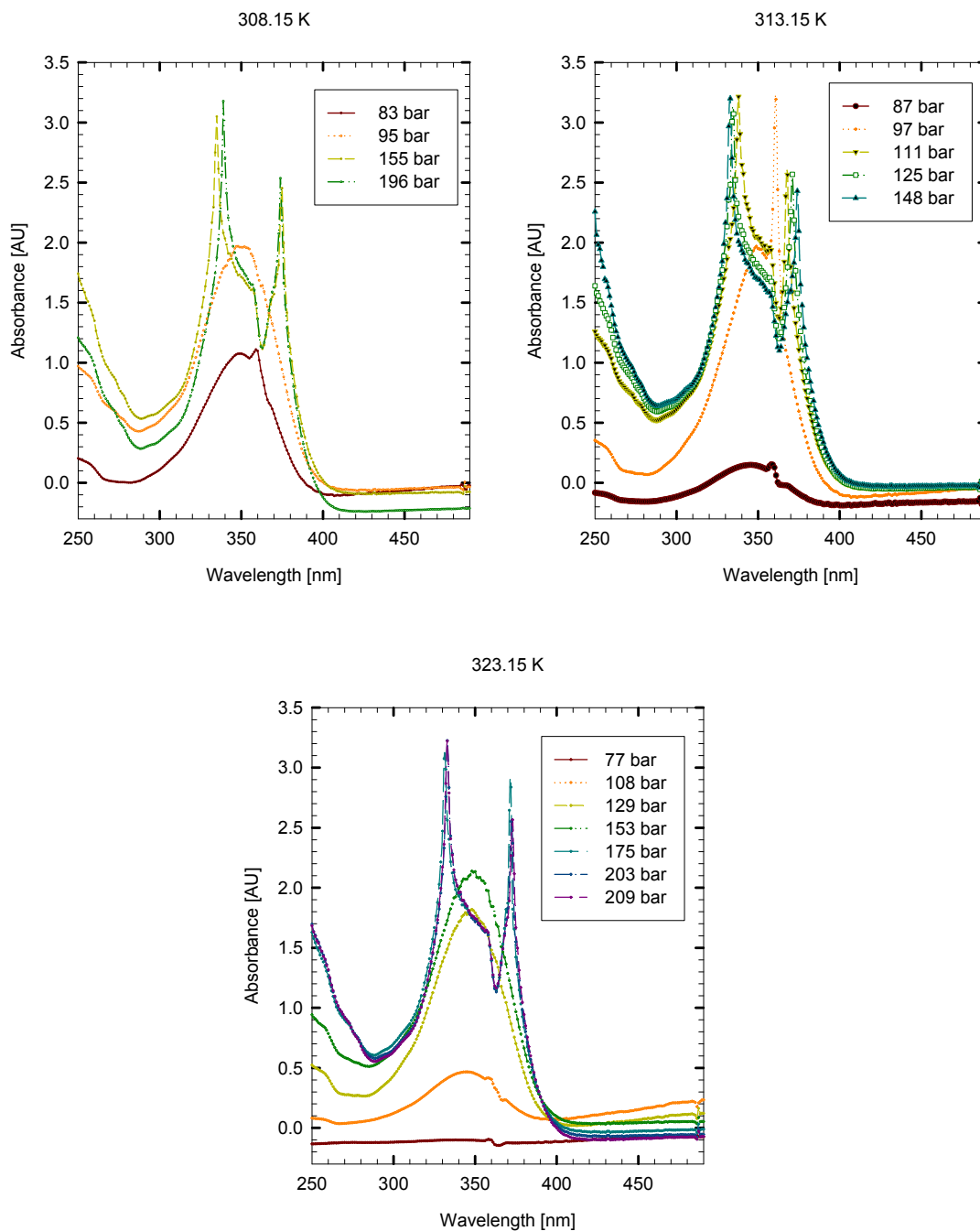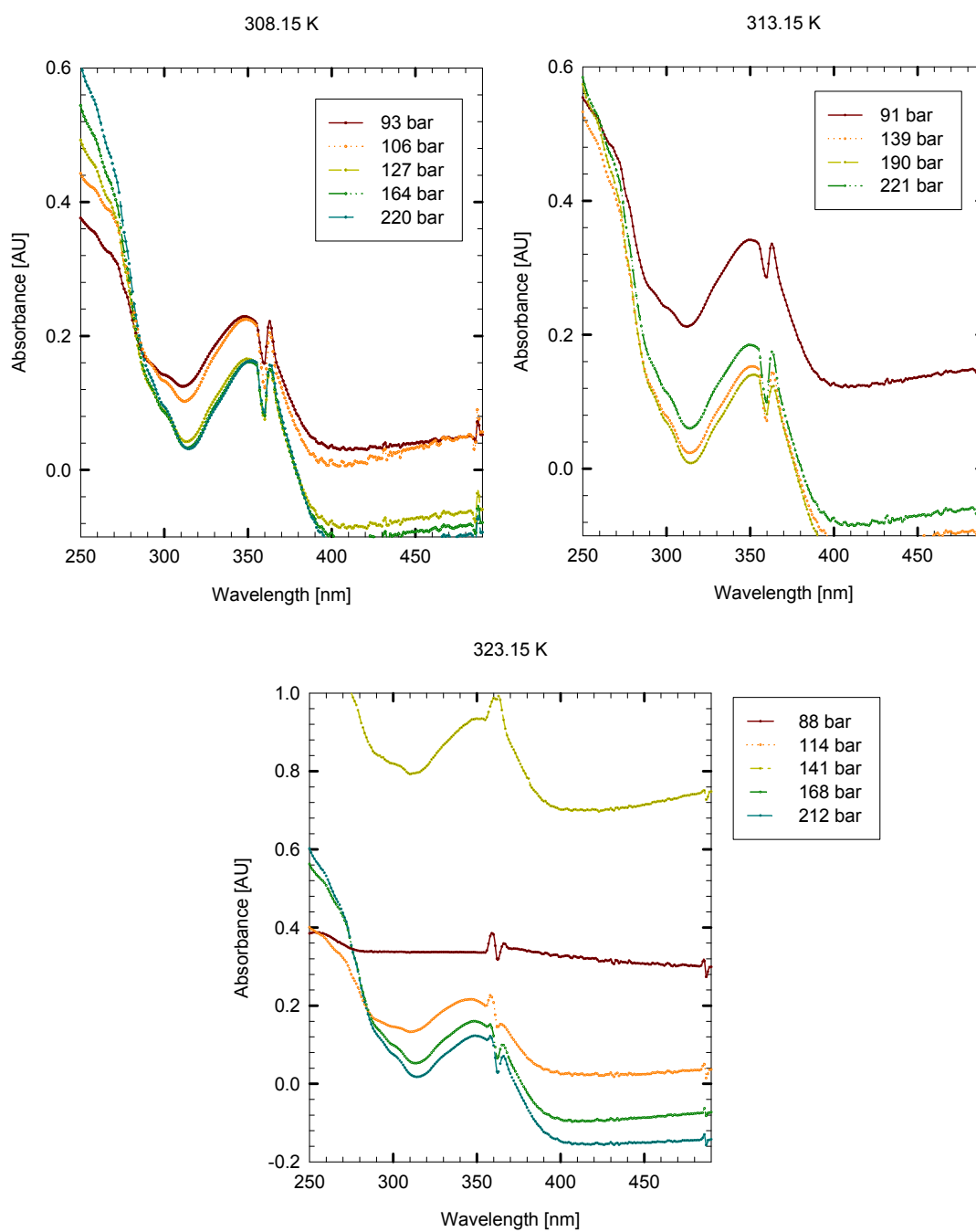## Indicator-H₂O-scCO₂ System at 308.15, 313.15, and 318.15 K

308.15 K

313.15 K

318.15 K

Appendix C

PL92-Indicator-H₂O-scCO₂ System at 308.15, 313.15, and 318.15 K

308.15 K

313.15 K
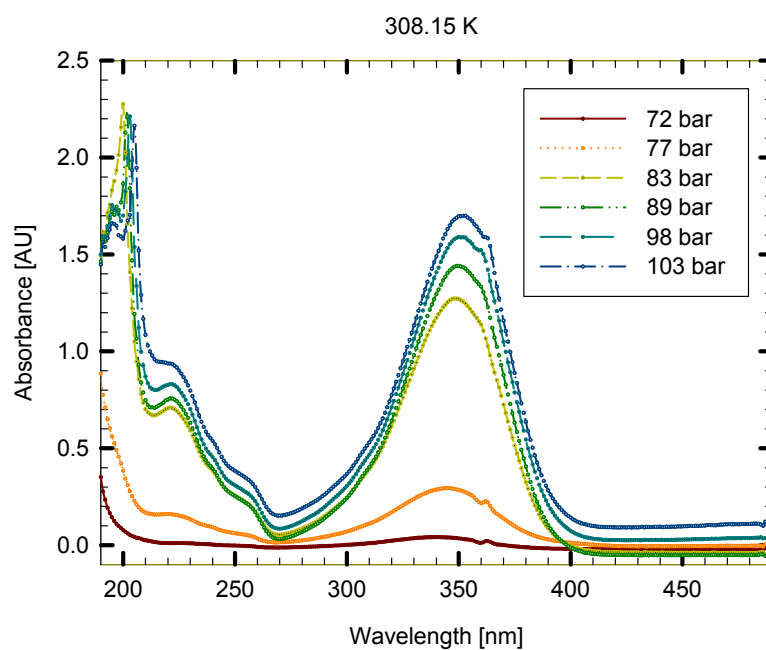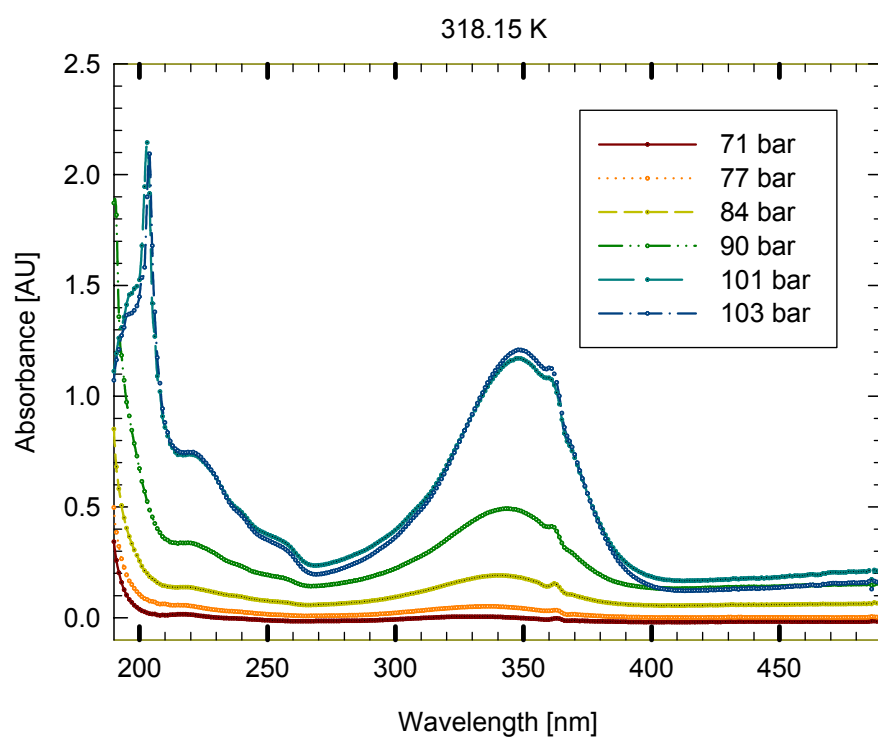
Appendix D

PL31-Indicator-H₂O-scCO₂

Appendix E

P17R2-Indicator-H₂O-scCO₂

308.15 K

313.15 K

323.15 K

Appendix F

Gele-Indicator-H₂O-scCO₂

308.15 K

313.15 K

323.15 K
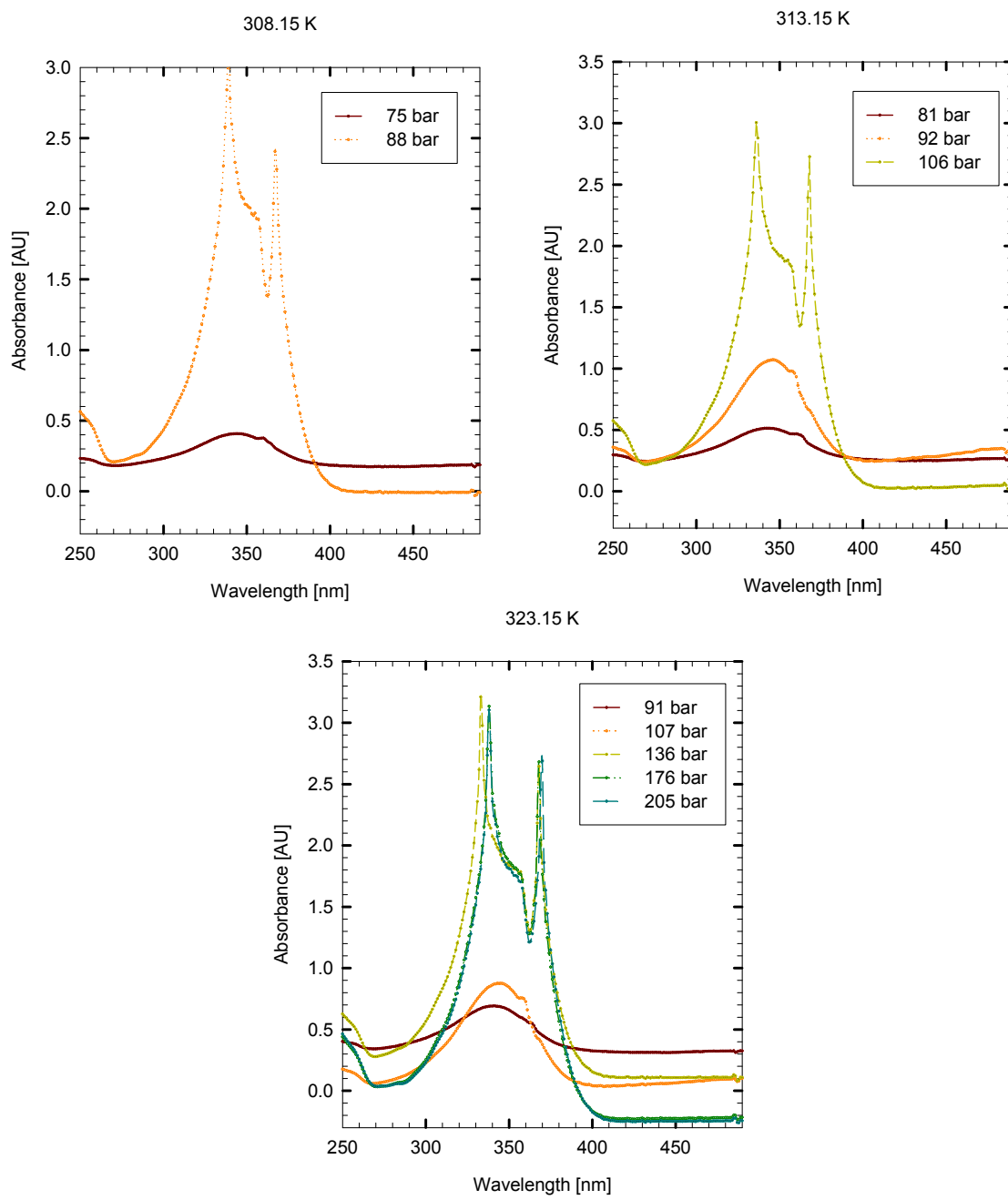
Appendix G

Zonyl-Indicator-H₂O-scCO₂
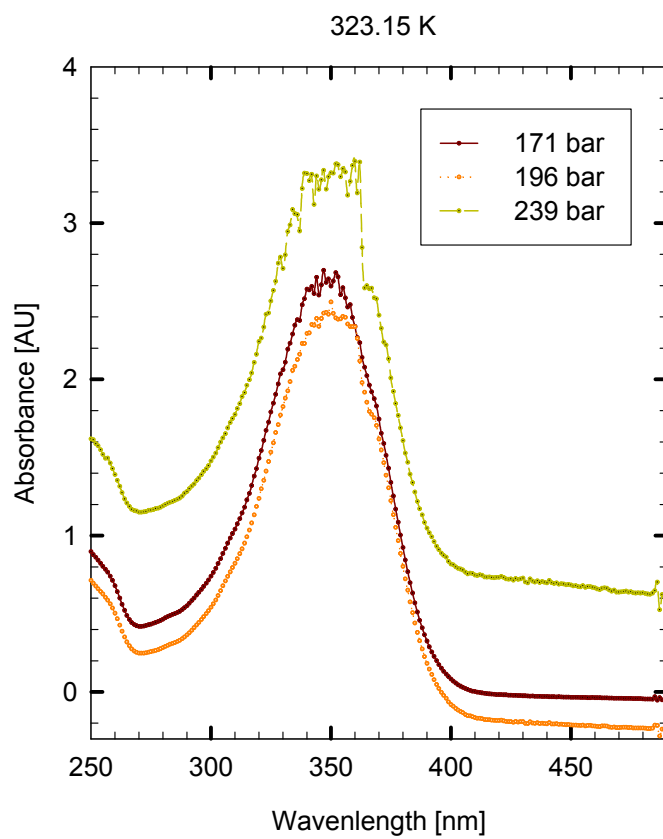
Appendix H

Spectrum of CO₂ Used in the Extraction of Ethylene Glycol

CO₂ (200 bar, 40C)